

---

# On the analytical and combinatorial structure of cosmological observables

Francisco Vicente Vazão

---



München 2025



---

# **On the analytical and combinatorial structure of cosmological observables**

**Francisco Vicente Vazão**

---

Dissertation  
der Fakultät für Physik  
der Ludwig-Maximilians-Universität  
München

vorgelegt von  
Francisco Vicente Vazão  
aus Leiria, Portugal

München, den 08.05.2025

Erstgutachter: Prof. Dr. Johannes M. Henn  
Zweitgutachter: Prof. Dr. Ivo Sachs  
Tag der mündlichen Prüfung: 23.06.2025



# Contents

<b>Summary</b>	<b>xiii</b>
<b>List of Publications</b>	<b>xvi</b>
<b>1 Introduction</b>	<b>1</b>
1.1 Inflation . . . . .	2
1.2 Cosmological Correlators . . . . .	6
1.3 Context and Results . . . . .	7
1.4 Outline . . . . .	12
<b>2 The Cosmological Wavefunction</b>	<b>15</b>
2.1 Definition . . . . .	16
2.2 Singularities of the Integrand . . . . .	23
2.3 Integrand from combinatorics . . . . .	25
2.4 Cosmological Correlators . . . . .	28
2.5 Parametrizing with Sub-polygons . . . . .	29
2.5.1 Flat Space $\rightarrow$ Cosmological Wavefunction . . . . .	33
<b>3 Perturbative Structure of Cosmological Observables</b>	<b>35</b>
3.1 Cosmological Integrals . . . . .	35
3.2 Examples . . . . .	40
3.3 The asymptotic structure of cosmological integrals . . . . .	45
3.3.1 The perturbative structure of the tree-level wavefunction . . . . .	52
3.3.2 The perturbative structure of the Loop-level wavefunction . . . . .	61
3.3.3 Example: The two-site one-loop graph . . . . .	66
3.4 $\lambda\phi^4$ examples at loop level . . . . .	69
3.5 Infrared Finite Computables . . . . .	74
3.5.1 Tree-level subtractions . . . . .	74
3.5.2 Loop-level subtractions . . . . .	77
3.5.3 Examples . . . . .	80
3.6 Discussion . . . . .	84

<b>4</b>	<b>Towards integrating cosmological integrals</b>	<b>87</b>
4.1	Differential Equations for Twisted Period Integrals . . . . .	87
4.1.1	Integral Identities and basis of <i>Master Integrals</i> . . . . .	88
4.1.2	Differential Equations for <i>Master Integrals</i> . . . . .	90
4.2	Differential equations for one loop cosmological integrals . . . . .	91
4.3	Integrals over the one-loop measure . . . . .	91
4.3.1	One-loop Two-site graph . . . . .	93
4.3.2	One-loop three-site graph . . . . .	97
4.4	Correlator versus Wavefunction . . . . .	102
4.5	Discussion . . . . .	102
<b>5</b>	<b>Combinatorial Structure of the Wavefunction</b>	<b>105</b>
5.1	Combinatorial Wavefunction . . . . .	105
5.1.1	Graph Associahedra . . . . .	105
5.1.2	The Cosmohedron . . . . .	109
5.2	Embedding . . . . .	112
5.3	Computing the Wavefunction from the Cosmohedron . . . . .	121
5.3.1	The geometry of recursive factorization . . . . .	121
5.3.2	Wavefunction from Geometry . . . . .	123
5.4	Loop Cosmohedron . . . . .	127
5.5	Cosmological correlahedra . . . . .	135
5.6	Discussion . . . . .	138
<b>6</b>	<b>Conclusion</b>	<b>141</b>
<b>A</b>	<b>The ABHY Associahedron</b>	<b>145</b>
	<b>Acknowledgments</b>	<b>168</b>

# List of Figures

1.1	The cosmic microwave background (CMB) [1]. . . . .	2
2.1	Examples of diagrams for the wavefunction. Gray line is the future boundary onto which we are projecting. Any lines attached to the boundary correspond to external states, in the integral they correspond to bulk-to-boundary propagators. Lines not attached to the boundary correspond to bulk-to-bulk propagators in the respective integral. The dots correspond to vertices (also called sites), and to each one we attribute a coupling $\lambda_k(\eta_s)$ in the respective integral. . . . .	19
2.2	Examples of singularity/tube correspondence. . . . .	23
2.3	(Top) Diagrammatic representation of the terms contributing to the three-site chain graph, in terms of tubings (collections of non-overlapping tubes). Here the graph has the external states amputated for simplicity. (Bottom) The representation of the five terms contributing to the four-site chain graph. Here we omitted the single site tubes and the total energy tube since every single term contains them. . . . .	26
2.4	The diagrammatic representation of all the six terms contributing to the four-site star graph. The graph has the external states amputated and we omitted the single site tubes as well as the total energy tube. . . . .	27
2.5	Momentum polygon for a six particle process. . . . .	30
2.6	Sub-polygons of the momentum polygon and their perimeters, below there is the direct correspondence in terms of tubings. . . . .	31
2.7	Five-point wavefunction in terms of russian dolls from sub-polygons. . . .	32
3.1	Examples of loop graphs. The associated loop integrals are $n_e$ -fold if $n_e < d$ , and the integration measure is proportional to the squared volume of a simplex in $\mathbb{P}^{n_s+n_e-2}$ . . . . .	40

- 3.2 *On the left:* Newton polytope associated to (3.42). Its facets are identified by  $\mathcal{W}'^{(1)} := (-\text{Re}\{s_1\}, -1, 0)^T$ ,  $\mathcal{W}^{(12)} := (\text{Re}\{s_1 + s_2 - \tau\}, 1, 1)$ ,  $\mathcal{W}'^{(2)} := (-\text{Re}\{s_2\}, 0, -1)$  and divide the region of integration in three sectors, each of which bounded by a pair of co-vectors associated to the facets. *On the right:* Decomposition into sectors of the domain of the integration in the original integration variables. The blue square is the sector identified by the pair  $(\mathcal{W}'^{(2)}, \mathcal{W}'^{(1)})$  – it is the only sector containing the possible infra-red divergences. The red and the green areas instead single out the sector identified by  $(\mathcal{W}'^{(1)}, \mathcal{W}'^{(12)})$  and  $(\mathcal{W}^{(12)}, \mathcal{W}'^{(2)})$ . . . . . 50
- 3.3 Newton polytope associated to a two-site graph  $\mathcal{G}$ . It is constructed as a Minkowski sum of the Newton polytopes associated to its subgraphs  $\mathfrak{g}$ , *i.e.* a triangle and two segments respectively for  $\mathfrak{g} = \mathcal{G}$  and the two subgraphs containing a single site only – see the triple of pictures on the left. The final Newton polytope can be realised as a truncation of the triangle based on the underlying graph and the tubings corresponding to the single-site graphs, and hence its facets are associated to tubings of the graph. . . . . 53
- 3.4 Newton polytope associated to the denominators of the three-site graph  $\mathcal{G}$ . It is constructed as a Minkowski sum of the simplices corresponding to all *connected subgraphs of  $\mathcal{G}$*  (*on the left*). It can be realised by truncating the top-dimensional simplex, based on all the allowed tubings, which corresponds to a subset of the facet of the simplex itself (*on the right*). . . 54
- 3.5 Newton polytope associated to the two integrals with numerator of degree 0 in which the three-site graph can represent, and their overlap. They both can be constructed via a truncation of the top-dimensional simplex via lower dimensional simplices associated to the underlying subgraphs in such a way that iteratively connected subgraphs are taken. Their overlap (*right*) represents the convergence of the full integral associated to the three-site tree graph, with its combinatorial structure identical to the nestohedron in Fig. 3.4. . . . . . 56
- 3.6 *On the left:* Newton polytope corresponding to the two-site tree graph. It has five possible divergent directions that divide the domain of integration in five sectors. *On the right:* Sectors in which the domain of integration is decomposed in the original site weights parametrisation. . . . . 60
- 3.7 Newton polytope associated to the edge weight integration only for a three-site one-loop graph. *On the left:* The simplices building blocks and their tubings. *On the right:* The Newton polytope is a nestohedron which can be realised by truncating the top-dimensional simplex (a tetrahedron) via the tubings associated to the underlying graph. . . . . 63

- 3.8 *On the left:* The Newton polytope associated to the edge weight integration for the two-site one-loop graph is a nestohedron whose facets are identified by certain tubings. They correspond to directions in which the integral might diverge. The number of tubings instead correspond to how these directions are approached. A subset of these directions are selected by the integration contour. *On the right:* The knowledge of compatible facets of the Newton polytope allows to decompose  $\mathbb{R}_+^2$  in sectors, which can be restricted onto the domain of integration via the non-negativity condition which defines it. 66
- 3.9 *On the left:* The one-site one loop graph. *Center:* the realisation of the Newton polytope for the integral (3.61) associated to the one-site one-loop graph in terms of tubings. *On the right:* Possible divergent directions for the integral (3.61). . . . . 70
- 3.10 Two-site two-loop graph. The associated Newton polytope is lives in  $\mathbb{P}^5$  and characterised by 16 facets. They signal the possible divergent direction, which are further limited by the non-negativity condition from the integration contour. . . . . 73
- 3.11 Nestohedron associated to the two-site tree graph. It shows divergences along the normal vectors  $\{\mathcal{W}^{(12)}, \mathcal{W}^{(j)}, \mathcal{W}'^{(j)}, j = 1, 2\}$  that identify its facets. The potential IR divergences are captured by the sectors containing  $\mathcal{W}^{(12)}, \mathcal{W}^{(1)}, \mathcal{W}^{(2)}$ . . . . . 81
- 3.12 Convergence polytope associated to the two-site tree thick graph. It is given the overlap of the Newton polytopes of the integrals in which it can be decomposed as a sum, with in this case is a square – it is indicated by the shaded blue region. *Left:* The integral is decomposed according to the monomials in the numerator. *Center:* The numerator is decomposed as  $\mathcal{X}_{g_2}x_1 + \mathcal{X}_{g_1}(x_2 + \mathcal{X}_{g_2})$ . *Right:* The numerator is decomposed as  $\mathcal{X}_{g_1}x_2 + \mathcal{X}_{g_2}(x_1 + \mathcal{X}_{g_1})$ . . . . . 82
- 4.1 One-loop two-site diagram. The corresponding integrand has 5 denominators, each corresponding to a connected subgraph of the above graph. Two subgraphs enclose each of the two sites, then two subgraphs enclose both sites and cut one edge twice and finally there is the full graph which corresponds to the total energy pole. . . . . 93
- 4.2 One loop three-site diagram. The corresponding integrand has 10 denominators, each corresponding to a connected subgraph of the above graph. Three subgraphs which enclose a single site, three which enclose two sites at a time, three which enclose all three sites but cut each edge twice and finally the full graph which corresponds to the total energy singularity. . . 99

4.3	Zero sector of the one-loop three-site-graph. The first four integrals form a $4 \times 4$ homogeneous diagonal block, corresponding to the one-loop three point function with denominator raised to half-integer powers, and each of the subsequent three integrals form a $1 \times 1$ diagonal block, and can be identified with one-loop two-point functions with denominators raised to half integer powers. . . . .	100
4.4	Homogeneous sector of the one-loop three-site graph with denominator $q_a$ . There are a total of 9 master integrals, which decouple in blocks of dimensions $1 \times 1, 2 \times 2, 2 \times 2, 4 \times 4$ . In the last block, the elliptic family appears. . . . .	101
5.1	5(left) and 6(right) point graph associahedron. When drawing the graph we omit the external legs to make manifest that for the purpose of the combinatorics of tubings what matters is the topology of the graph with just the internal edges. . . . .	106
5.2	(Left) 7-point graph associahedra for triangulations from the cyclic classes $\{(1, 3), (1, 4), (4, 6), (1, 6)\}, \{(1, 3), (3, 5), (1, 5), (1, 6)\}$ . (Right) 7-point graph associahedra for triangulations from the cyclic classes $\{(1, 3), (1, 4), (1, 5), (1, 6)\}, \{(1, 3), (1, 4), (1, 5), (5, 7)\}, \{(1, 3), (1, 4), (4, 7), (5, 7)\}, \{(1, 3), (3, 7), (3, 6), (4, 6)\}$ . . . . .	108
5.3	associahedron (left) and cosmohedron (right) at 6-points . . . . .	109
5.4	(Left) associahedron (pentagon) and cosmohedron (decagon) at 5-points. (Right) 5-point cosmohedron with respective labelling of facets in terms of relevant sub-polygons. . . . .	110
5.5	Cosmo <sub>6</sub> with labelling of different codimension facets in terms of relevant subpolygons . . . . .	111
5.6	(Left) "Cosmologizing" the $n = 6$ associahedron fan to obtain the Cosmo <sub>6</sub> fan. In light blue, we highlight the cone corresponding to the non-simple vertex. (Right) Labelling of the four-facets meeting at the non-simple vertex, as well as the two possible "blow up"s into simple vertices. In both cases, we create a new edge (marked in red) that is already labelled by a full russian doll. . . . .	112
5.7	(Left) Fan of the 6-point associahedron. (Right) Fan of the 6-point cosmohedron that can be obtained by "cosmologizing" the associahedron one. . .	114
5.8	Realizations of cosmohedra. (Left) Embedding of Cosmo <sub>6</sub> with pentagonal facets highlighted in pink and hexagonal ones highlighted in yellow. (Right) Embedding of the Cosmo <sub>3</sub> <sup>1-loop</sup> . The purple facets correspond to partial triangulations, and the pink and yellow facets correspond to full triangulations. . . . .	117
5.9	(Left) Set of facets corresponding to partial triangulations with a single chord that by themselves contain <i>all</i> vertices of the cosmohedron. (Right) Set of facets corresponding to full triangulations that also touch <i>all</i> vertices. . . . .	122
5.10	Examples of $1/X_C$ for different faces of $n = 5$ and $n = 8$ cosmohedron. . .	125

5.11	(Left) cosmohedron 2-point 1-loop, edges are labelled by partial triangulations with a single curve (where we have two types of curves ending in the puncture, marked in red and blue), and vertices correspond to full triangulations. We can read off the russian doll at each vertex by taking the union of the subsurfaces entering on each edge. (Right) cosmohedron 3-point 1-loop. Highlighted in blue and green we have facets labeled by a single curve (squares, decagons and dodecagons); in gray facets labeled by two curves (squares); and in red and yellow faces labelled by full triangulations (pentagons and hexagons) – corresponding to the graph-associahedra for the loop graphs. . . . .	128
5.12	(Left) Graph associahedron for the triangle graph. (Right) Graph associahedron for the box graph. . . . .	129
5.13	(Left) Fan of the cosmological correlahedron for $n = 4$ . In dashed, we represent the underlying associahedron fan. (Right) 4-points cosmological correlahedron. . . . .	136
5.14	(Left) Projection of the $n = 5$ cosmological correlahedron fan. In dashed we represent the underlying associahedron fan with rays $(3, 5)$ , $(1, 3)$ , $(1, 4)$ and $(2, 4)$ marked in gray, with the added dimension corresponding to $E_t$ . Shaded in red we highlight the pentagonal facet which is touching the base $\text{Cosmo}_5$ , and in blue the hexagonal facet which is touching the top $\text{Assoc}_5$ . (Right) 3-dimensional projection of the $\text{Corr}_6$ fan, coming from the underlying 3-dimensional associahedron cone containing rays $(1, 3)$ , $(1, 4)$ , $(1, 5)$ . In green, we highlight a square pyramid corresponding to a non-simple vertex of $\text{Corr}_6$ . . . . .	137
5.15	(Left) Embedding of the $\text{Corr}_5$ . (Right) Embedding of the $(1, 4)_T$ facet of $\text{Corr}_6$ . . . . .	139
5.16	The top figure shows the combinatorial structure of the three-dimensional $n = 5$ cosmological correlahedron, looked at from above. We see the top pentagon facet as the $n = 5$ associahedron, and the bottom decagon as the $n = 5$ cosmohedron. A number of other facets, edges and vertices are labelled by collections $(C, P)$ of non-overlapping chords and subpolygons. There are 30 vertices. The top 5 vertices (marked in blue) all correspond to triangulations of the associahedron, the rest of the vertices are all the terms in the correlator. The bottom figure shows exactly the same for the $n = 2$ , 1-loop correlator. As for the amplitude polytopes, there are two kinds of “loop” variable, touching the puncture. The top facet is the hexagon familiar from the amplitude. The bottom is the dodecagon for the cosmohedron. The vertices not on the top facet all correspond to the terms in the correlator. . . . .	140





# List of Tables

5.1	The $\mathcal{F}$ -vector of Cosmohedra up to 9-points. . . . .	119
5.2	The $\mathcal{F}$ -vector of Associahedra up to 9-points. . . . .	119



# Summary

The cosmological wavefunction is one of the central objects when one is considering the formulation and computation of cosmological observables in inflation. In recent years, the wavefunction has gained further interest when it was found that its diagrammatic expansion, at each order in perturbation theory, can be understood combinatorially in terms of geometric objects, cosmological polytopes. To each Feynman diagram in the wavefunction there is one correspondent polytope whose volume form is the integrand of the associated Feynman integral (cosmological integrals).

In this thesis, we explore the analytic properties of these integrals by developing a framework to compute their divergences. This framework is heavily dependent on mathematical objects, Newton polytopes, which capture the asymptotic structure of the integrand; as well as, the understanding of the geometry of the loop measure for a general cosmological integral. This allows us to understand the divergent structure of any loop cosmological integral. As well as computing their leading and sub-leading divergences in terms of a series expansion in an analytic regulator. This, in turn, permitted the development of a diagrammatic scheme that constructs infrared safe computables. Furthermore, we were able to explore computational methods for the one loop wavefunction, having computed the one loop two-site wavefunction and showed that the function space for the one-loop three-site wavefunction consists of Elliptic iterated integrals. Finally, we discuss the relevance of these tools to tackle a long standing issue in inflationary cosmology, the existence of infrared divergences for light scalar fields in expanding backgrounds. As well as possible phenomenological applications.

Afterwards, we turn to the combinatorial structure of the wavefunction. We start by providing an alternative combinatorial picture for each graph in the wavefunction, the graph associahedron. This new combinatorial picture has the advantage of being able to easily combine every single graph associahedron to build a new polytope, the Cosmohedron. This encodes all the contributions to the wavefunction. We describe how to obtain the wavefunction from the cosmohedron. And we further show the generalisation of the Cosmohedron for the loop wavefunction. Additionally, we use the same ideas to construct the polytope for the correlator. Finally, we discuss how the cosmohedron may provide a path towards a stringy formulation of cosmological correlators.



# Zusammenfassung

Die kosmologische Wellenfunktion ist eines der zentralen Objekte, wenn es um die Formulierung und Berechnung kosmologischer Observablen in der Inflation geht. In den letzten Jahren hat die Wellenfunktion weiter an Interesse gewonnen, als man herausfand, dass ihre diagrammatische Ausdehnung bei jeder Ordnung in der Störungstheorie kombinatorisch in Form von geometrischen Objekten, den kosmologischen Polytopen, verstanden werden kann. Zu jedem Feynman-Diagramm in der Wellenfunktion gibt es ein entsprechendes Polytop, dessen Volumenform der Integrand des zugehörigen Feynman-Integrals ist (kosmologische Integrale). In dieser Arbeit erforschen wir die analytischen Eigenschaften dieser Integrale, indem wir einen Rahmen entwickeln, um ihre Divergenzen zu berechnen. Dieser Rahmen ist stark abhängig von mathematischen Objekten, Newton-Polytopen, die die asymptotische Struktur des Integranden erfassen, sowie vom Verständnis der Geometrie des Schleifenmaßes für ein allgemeines kosmologisches Integral. Dies ermöglicht es uns, die divergente Struktur jedes kosmologischen Schleifenintegrals zu verstehen. Außerdem können wir ihre führenden und untergeordneten Divergenzen in Form einer Reihenentwicklung in einem analytischen Regulator berechnen. Dies wiederum ermöglichte die Entwicklung eines diagrammatischen Schemas, das infrarotsichere berechenbare Größen konstruiert. Darüber hinaus waren wir in der Lage, Berechnungsmethoden für die Ein-Schleifen-Wellenfunktion zu erforschen, indem wir die Ein-Schleifen-Zwei-Seiten-Wellenfunktion berechneten und zeigten, dass der Funktionsraum für die Ein-Schleifen-Drei-Seiten-Wellenfunktion aus elliptischen iterierten Integralen besteht. Schließlich diskutieren wir die Relevanz dieser Werkzeuge, um ein seit langem bestehendes Problem in der inflationären Kosmologie zu lösen: die Existenz von Infrarot-Divergenzen für leichte Skalarfelder in expandierenden Hintergründen. Außerdem diskutieren wir mögliche phänomenologische Anwendungen. Danach wenden wir uns der kombinatorischen Struktur der Wellenfunktion zu. Wir beginnen mit einem alternativen kombinatorischen Bild für jeden Graphen in der Wellenfunktion, dem Graphen-Assoziahedron. Dieses neue kombinatorische Bild hat den Vorteil, dass jedes einzelne Graphenassoziaeder leicht kombiniert werden kann, um ein neues Polytop, das Kosmoeder, zu bilden. Dieses kodiert alle Beiträge zur Wellenfunktion. Wir beschreiben, wie man die Wellenfunktion aus dem Kosmoeder erhält. Außerdem zeigen wir die Verallgemeinerung des Kosmoeders für die Schleifenwellenfunktion. Außerdem verwenden wir die gleichen Ideen, um das Polytop für den Korrelator zu konstruieren. Schließlich diskutieren wir, wie das Kosmoeder einen Weg zu einer stringy Formulierung kosmologischer Korrelatoren bieten kann.



# List of Publications

This thesis is based on the author's work conducted at the Max Planck Institute for Physics in Munich from March 2022 to April 2025. Parts of this work have already been presented in the following publications:

## **Cosmohedra**

Nima Arkani-Hamed, Carolina Figueiredo and Francisco Vazão.

arXiv:2412.19881, *Submitted to JHEP*.

## **On one-loop corrections to the Bunch-Davies wavefunction of the universe**

Paolo Benincasa, Giacomo Brunello, Manoj K. Mandal, Pierpaolo Mastrolia and Francisco Vazão.

arXiv:2408.16386. *Published in Phys.Rev.D 111 (2025) 8, 085016*

## **Cosmological Infrared Subtractions & Infrared-Safe Computables**

Paolo Benincasa and Francisco Vazão.

arXiv:2405.19979, *Submitted to SciPost*.

## **The Asymptotic Structure of Cosmological Integrals**

Paolo Benincasa and Francisco Vazão.

arXiv:2402.06558, *Submitted to SciPost*.

Part of this work was also presented in the workshop *S-Matrix Marathon* at the Institute for Advanced Study in Princeton, and collected in the proceedings:

## **Records from the S-Matrix Marathon: Observables in Expanding Universes**

Paolo Benincasa, Mathieu Giroux, Holmfridur S. Hannesdottir, Sebastian Mizera, Celina Pasiecznik and Francisco Vazão

arXiv:2409.14947 *To be published in: "Records from the S-Matrix Marathon: Selected Topics on Scattering Amplitudes. Springer Lecture Notes in Physics, 2025."*





# Chapter 1

## Introduction

Over the past century, the understanding of the beginning of the universe has rapidly improved. Guided by a deep understanding of particle physics, through the Standard Model, and of gravity, through general relativity, cosmologists have a beautifully working picture of the evolution of the universe from the first  $10^{-10}$  seconds until the present day, which we call the  $\Lambda$ CDM model. One key catalyzer for this revolution in our understanding of the universe was Einstein's paper on general relativity in 1916. This new theory of gravity was crucial to the first proposal of the Big Bang model a few years later in 1927 by Lemaître, which was further developed over the next decades. In the Big Bang model the universe started in hot dense state nearly 13.8 billion years ago, and expanded (and cooled) until its current state. Strong evidence of this expansion quickly appeared when, in 1929, Edwin Hubble experimentally verified what later became known as Hubble-Lemaître's law. He demonstrated that galaxies are moving away from us at speeds proportional to their distance [2]. This was a crucial piece of evidence that the universe was expanding in concordance with Lemaître's model. Further evidence for the Big Bang model came in 1964, when Arno Penzias and Robert Wilson first discovered the cosmic microwave background (CMB) [3], which is pictured in figure 1.1. The CMB is the light emitted at the surface of last scattering. This is the period when photons decoupled from matter, and travelled freely across spacetime until they reach us today. Thus, it is one of the experimental cornerstones of modern cosmology, as it is one of the strongest evidences of the Big Bang model. However, at this point there were a few puzzles in this model, namely the Horizon problem, the flatness problem, the super-horizon correlations in the CMB and the magnetic monopole abundance problem in grand unified theories (in the next section we will explain these problems in more detail). This led to the proposal of the inflationary universe in the beginning of the decade of 1980, by Guth [4], and later it was further developed by Linde [5], Albrecht and Steinhardt [6] and Starobinski [7], among many others. The theory of inflation describes the beginning of the universe as being a period of exponentially fast expansion of spacetime where the quantum fluctuations of a scalar field get stretched to super-horizon scales and seed the initial conditions for the early universe. These perturbations are in principle related to the temperature perturbations we see in the CMB, which later evolve to form the distribution of galaxies as we observe

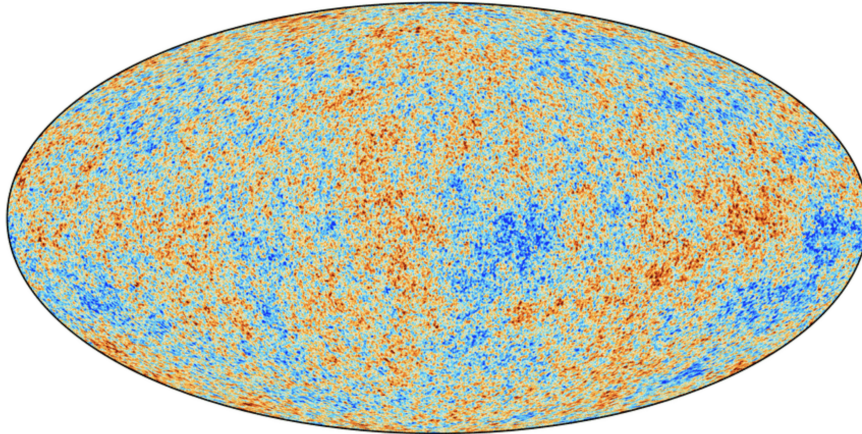


Figure 1.1: The cosmic microwave background (CMB) [1].

today in the large scale structure. Furthermore, we will see later that inflation resolves the puzzles mentioned above. At around the same time, observations of the large scale structure of universe led to the proposal that besides baryonic matter (matter described by the standard model of particle physics), there was a much bigger abundance of dark matter, and dark energy. This led to the formulation of the  $\Lambda$ CDM model [1] which parametrises the abundance of the different forms of energy/matter in the universe, and thus correctly models the evolution of the universe from the period after inflation until the present day. Since then more accurate measurements of the CMB, for example the experiments COBE, WMAP and Planck [1, 8–12], supported the  $\Lambda$ CDM model predictions of the composition and geometry of the universe.

In this thesis, we will focus in the study of several aspects related to the quantum fluctuations during the inflationary period. To understand how these fluctuations arise, it is first important to understand why inflation is needed and what is the basic underlying physics that describes it, in what follows we will have a qualitative discussion about this. For more detailed discussions on this topic we refer the reader to [13–19].

## 1.1 Inflation

Recent observations of the early universe exhibit three problems that, without inflation, had been left unaddressed - the Horizon problem, the flatness problem, and the super-horizon correlations. Starting with the Horizon problem, the key concept is the co-moving particle horizon,  $d_h$ . This is the co-moving distance that light can travel in the period  $t - t_i$ , and determines the region that the observer has causal contact with. We can define it as:

$$d_h = \int_{t_i}^t \frac{dt}{a(t)} = \int_{a_i}^a d \log a \frac{1}{aH}, \quad (1.1)$$

where the function  $a(t)$  is the scale factor that usually defines a FLRW (Friedmann-Lemaître-Robertson-Walker) spacetime, which has a metric of the type:  $ds^2 = -dt^2 + a(t)d\mathbf{x}^2$ . The parameter  $H = \frac{\dot{a}}{a}$  is the *Hubble parameter*, and it is the physical energy scale that characterises a FLRW spacetime. The quantity  $(aH)^{-1}$  is the co-moving Hubble radius, and in the literature, is often referred to as the horizon, due to the fact that, in standard cosmological settings,  $d_h \sim (aH)^{-1}$ . Thus the Hubble radius provides the region that is causally connected within one expansion time,  $H^{-1}$ .

Given this, the horizon problem stems from the fact that one can find patches of the CMB whose particle horizons (considering a standard matter or radiation dominated cosmology) do not overlap at the big bang singularity. Yet, we find that the temperature of the CMB is extremely homogeneous. Fluctuations around the average temperature have magnitudes of  $10^{-5}$ . This is hard to explain if we believe that these patches have never come into causal contact, and defines the horizon problem. The flatness problem of the early universe is related to the fact that our measurements of the curvature of the early universe, yield that the universe was essentially flat, to a great accuracy. However, when we consider a standard cosmological model consistent with our universe, we find that equations of state lead to value zero of the curvature to be an unstable fixed point. We would require an extreme amount of fine tuning in order to have a flat spacetime. Finally, in the CMB we find that the density fluctuations in different points in the CMB are correlated, in fact they are correlated even at different points which are in principle causally disconnected.

Inflation addresses these problems by providing a mechanism in which the Hubble radius shrinks for a certain period in the very beginning of the universe, and thus at the time of the CMB the particle horizon is much larger than the Hubble radius. This provides an explanation to all the problems mentioned above. It resolves the horizon problem because at the beginning of inflation the Hubble radius was much larger and then shrank during the inflationary period. Thus regions which are not in causal contact at the CMB time, could have been before during the initial stages of inflation. Similarly, one can understand super-horizon correlations in the same way, during the period where the Hubble radius was larger there could have been processes that were causally allowed, yet as their length scale became larger than the Hubble radius (since this shrank, this is usually referred to as exiting the horizon) they can be observed today as super-horizon correlations.

One fundamental idea in inflation is that the Hubble radius shrinks during this period, so in practice, we want that:

$$\frac{d}{dt} \left( \frac{1}{aH} \right) = -\frac{1}{a} \left( 1 + \frac{\dot{H}}{H} \right) < 0, \quad (1.2)$$

where we define  $\varepsilon \equiv -\frac{\dot{H}}{H}$ . For the inequality to hold true, we need that  $\varepsilon < 1$ . Furthermore current observations of scale invariance of the power-spectrum require that  $\varepsilon \ll 1$  [1]. Thus the expansion factor  $H$  must be nearly constant and this means that  $a \approx e^{Ht}$ , which is the de Sitter scale factor. In other words, we need that the inflationary background is described by a quasi-de Sitter spacetime.

In order to realize this, in inflation one usually considers a scalar field,  $\phi$ , with an action:

$$\mathcal{S} = \int dt d\mathbf{x} \sqrt{-g} \left( \frac{M_{\text{Pl}}^2}{2} R - \frac{1}{2} (\partial\phi)^2 - V(\phi) \right), \quad (1.3)$$

this action leads to the following equation of motion and Friedmann equation, respectively:

$$\begin{aligned} \ddot{\phi} + 3H\dot{\phi} + \frac{dV}{d\phi} &= 0 \\ H^2 &= \frac{1}{3M_{\text{Pl}}^2} \left( \frac{1}{2} \dot{\phi}^2 + V \right). \end{aligned} \quad (1.4)$$

From these equations we can find  $\varepsilon$ :

$$\varepsilon = \frac{\dot{\phi}^2}{2M_{\text{Pl}}^2 H^2}. \quad (1.5)$$

Therefore, in order to obtain our condition  $\varepsilon \ll 1$ , we must have that the potential energy must be much larger than the kinetic energy. And, for inflation to continue for a sufficient amount of time, we must have that the kinetic energy does not increase very fast, thus the second derivative of the field must be small. These conditions pose constraints on the type of potential that is allowed, however there are still infinitely many choices for potentials.

We discussed how this scalar field can drive the exponentially fast expansion of space-time, and thus driving inflation, which can provide an explanation for the horizon and flatness problems. However, we still have not fully addressed the super-horizon correlations, namely we have to understand how the fluctuations in the CMB were created in the first place. The answer comes from the fact that the scalar field can have quantum fluctuations which are stretched by the expansion and become of the scale of the universe. To understand these fluctuations, we will consider a quantum field theory for a massive scalar in a fixed power-law FLRW spacetime. That is, a spacetime background with metric:

$$ds^2 = -dt^2 + a(t)^2 d\mathbf{x}^2 = a(\eta)^2 (-d\eta^2 + d\mathbf{x}^2), \quad (1.6)$$

where  $\eta = \int_0^{t'} \frac{dt}{a(t)}$  is conformal time. By power-law FLRW we mean that  $a(\eta) = -\frac{1}{(H\eta)^\gamma}$ , for example  $\gamma = 1$  is de Sitter spacetime and  $\gamma = 0$  is Minkowski. And by fixed background we mean that we will not be considering a dynamical gravity setup, and it is simply a scalar field in an expanding background with at most self-interactions. This is the underlying setup of the entire thesis.

Then, before we delve into the complexities of interacting quantum field theory, it is necessary to understand the quantization of the free theory first. With that in mind, let us consider the action for a massive scalar field in a power-law FRW background, given by

$$\mathcal{S}[\varphi] = \int d\eta d^3x \sqrt{-g} \left( -\frac{1}{2} (\partial\varphi)^2 - \frac{1}{2} (m^2 + \xi R) \varphi^2 \right). \quad (1.7)$$

Note that our mass term has an additional term  $(\xi R)$  when compared to Minkowski space-time actions for scalar fields, which denotes the coupling to the background. Henceforth,

we will re-define the mass to be  $\mu^2 \equiv m^2 + \xi R$ . There will be two particular values of interest throughout this thesis, the massless minimally coupled scalar field ( $\mu = 0$ ), and the conformally coupled scalar field ( $\mu^2 = 2H^2$  for dS). From the action we can derive the equations of motion:

$$\partial_\eta^2 \varphi_{\mathbf{k}} + \frac{\dot{a}}{a} \partial_\eta \varphi_{\mathbf{k}} + (k^2 + \mu^2 a(\eta)^2) \varphi_{\mathbf{k}} = 0, \quad (1.8)$$

where we have already performed a spatial Fourier transform. Specializing the form for the scale factor,  $a(\eta) = -\frac{1}{(H\eta)^\gamma}$ , we then obtain a differential equation for general massive states in general power law FLRW cosmologies. We will solve it in two limits, for a massless field for general power  $\gamma$ , and the massive field in de Sitter ( $\gamma = 1$ ). Of course, in the Minkowski limit we obtain the standard Klein-Gordon equation. In these limits, the equation (1.8) can be transformed into a Bessel equation, and we can write the solution in the following form:

$$\varphi_{\mathbf{k}}(\eta) = H\sqrt{k}\eta^{\frac{1}{2}+\gamma} \left( c_1 H_\nu^{(1)}(-k\eta) + c_2 H_\nu^{(2)}(-k\eta) \right). \quad (1.9)$$

And:

$$\begin{aligned} \nu &= \frac{1}{2} + \gamma, \quad (\mu = 0, \text{FRW}), \\ \nu &= \sqrt{\frac{9}{4} - \frac{\mu^2}{H^2}}, \quad (\mu, \gamma = 1). \end{aligned} \quad (1.10)$$

Now, we need to fix the constants  $c_1$  and  $c_2$ . In order to do that, we will pick the vacuum of the theory to be Bunch-Davies [20]. This vacuum is de Sitter invariant for massive states [21], and it implies that the mode functions for very short wavelengths or very far away from the future boundary ( $\eta \rightarrow 0$ ) reduce to a standard Minkowski mode function. This adheres to our naive expectations that very short wavelength modes do not feel the curvature. Using the known behavior of Hankel functions when  $-k\eta \rightarrow \infty$ , we find that the mode functions become:

$$\varphi_{\mathbf{k}}(\eta) = H\sqrt{\frac{\pi}{4}} e^{-\frac{i}{4}\pi(1+2\nu)} (-\eta)^{\frac{1}{2}+\gamma} H_\nu^{(2)}(-k\eta). \quad (1.11)$$

An interesting exercise to consider is to take the limit of the mode functions when  $\eta \rightarrow 0$ , in a de Sitter spacetime, for example. Physically, this means that the fields are approaching the future boundary of de Sitter. We find that the massive fields all vanish in this limit, and only massless fields reach the boundary. This has very interesting implications, since it means when considering correlation functions in inflation, massless fields are more relevant external states since in principle those are the ones that reach the boundary and produce observables.

As mentioned above, we will be particularly interested in massless conformally coupled scalars in de Sitter. For these, the mode functions are simpler, taking the limit:

$$\varphi_{\mathbf{k}}(\eta) = H \frac{(-\eta)}{\sqrt{2}} e^{ik\eta}, \quad \mu^2 = 2H^2, \quad (1.12)$$

as you can see the mode functions are very similar to plane waves. This is an extremely useful observation, since as we will see later on it allows connecting the flat space observables to FLRW observables with conformally coupled scalars, which can then be related to states with different masses in FLRW.

## 1.2 Cosmological Correlators

Cosmological observable is an all-encompassing term, but the natural first observable to consider is a correlation function of fields at different points in the future boundary of inflation [22–28], henceforth called cosmological correlator. Here, we will have a quick overview of how to compute this correlation functions.

Cosmology is an observational science, since all the experiments have already happened. To measure any inflationary observable, all we have access to, is a space-like surface at the future boundary of inflation. Therefore, unlike in particle physics where we can prepare the incoming states and measure the asymptotic out-going states, in inflation we can only assume that the state evolved from the vacuum at past infinity to a some state on the boundary. Computationally, this means that, instead of in-out correlation functions, we are interested in evolving a state from the vacuum until the boundary and then evolve it back to the vacuum. This is called the Schwinger-Keyldish contour [29, 30], and the correlators are *in-in* correlation functions. In practice, we can write

$$\langle \phi(t, \vec{x}_1) \cdots \phi(t, \vec{x}_n) \rangle := \langle 0 | \bar{T} \{ e^{i \int_{-\infty}^0 dt' H_I} \} \phi(t, \vec{x}_1) \cdots \phi(t, \vec{x}_n) T \{ e^{-i \int_{-\infty}^0 dt' H_I} \} | 0 \rangle, \quad (1.13)$$

where  $H_I$  stands for the interaction Hamiltonian, and  $\bar{T}$  is the anti-time ordering operator. In principle, one can use this picture to compute the expectation value for any operator, not just  $n$ -point correlation functions. This is referred to in the literature as *in-in* formalism.

However, in this thesis we will focus on a different way to compute correlation functions. As we are used to, from quantum mechanics, we can compute expectation values of operators by integrating against the norm square of the wavefunction

$$\langle \Phi(\vec{x}_1) \cdots \Phi(\vec{x}_n) \rangle = \frac{\int \mathcal{D}\Phi \Phi(\vec{x}_1) \cdots \Phi(\vec{x}_n) |\Psi[\Phi]|^2}{\int \mathcal{D}\Phi |\Psi[\Phi]|^2}, \quad (1.14)$$

where the wavefunction  $\Psi[\Phi]$  is the solution to the functional Schrödinger's equation. And it is simply the transition amplitude from the Bunch-Davies vacuum to a field configuration at the future boundary of inflation. It is defined in terms of the Feynman path integral:

$$\Psi[\Phi] = \int_{\phi(-\infty(1-i\epsilon))=0}^{\phi(0)=\Phi} \mathcal{D}\phi e^{iS[\phi]}. \quad (1.15)$$

Naturally, unlike the correlator, it is not invariant under field redefinitions. Nevertheless, as we will see it has a remarkably simple structure. In the next chapter of the thesis we will

go further in this formalism, but for now we will just write the saddle point approximation of the above integral:

$$\log \Psi [\Phi, t_f] = \sum_{n=2} \frac{1}{n!} \int \frac{d^3 k_1 \cdots d^3 k_n}{(2\pi)^{3n}} \Phi_{\vec{k}_1} \cdots \Phi_{\vec{k}_n} (2\pi)^3 \delta(\vec{k}_1 + \cdots + \vec{k}_n) \psi_n(\vec{k}_N) . \quad (1.16)$$

Where here we are considering the Fourier transforms of the fields in position space,  $\psi_n(\vec{k}_N)$  are called wavefunction coefficients, and as we will see, we can generally write them as integrals over rational functions of the kinematics. It turns out that these rational functions have a very interesting combinatorial and mathematical structure, as shown in [31]. This is the main reason why we solely focus on the wavefunction formalism to compute cosmological observables.

The correlation functions can be computed in terms of wavefunction coefficients (we will show the derivation in more detail in the next section), for example the three-point function:

$$\langle \Phi_{\vec{p}_1} \Phi_{\vec{p}_2} \Phi_{\vec{p}_3} \rangle = \delta(\vec{p}_1 + \vec{p}_2 + \vec{p}_3) \frac{\text{Re } \psi_3(\vec{p}_1, \vec{p}_2, \vec{p}_3)}{\text{Re } \psi_2^{\text{free}}(\vec{p}_1) \text{Re } \psi_2^{\text{free}}(\vec{p}_2) \text{Re } \psi_2^{\text{free}}(\vec{p}_3)} . \quad (1.17)$$

At present, our best measurements of the CMB [1, 11, 12], and large scale structure surveys [32] are only able to probe the two-point function. The observation of a scale invariant and gaussian power-spectrum is in full agreement with a weakly coupled theory in a quasi de Sitter background, which is the underlying setup of inflation. Nevertheless, inflation predicts a small deviation from gaussianity by having a non-vanishing three-point function and beyond. Therefore, future more accurate measurements of the CMB perturbations that could actually probe these non-gaussianities could provide key evidence for inflation [33]. On the other hand, and even though we do not go into detail on this, besides the scalar perturbations parameterized by the field  $\phi^1$ , we also have tensor perturbations of the metric. These induce a special polarization pattern in the CMB radiation, the so-called B-mode pattern [34], which if measured, allows us to probe the tensor perturbations which are a key prediction of the inflationary model.

Therefore, the main subject of this thesis is the study these correlation functions that can be computed when considering a scalar field with polynomial interactions in a quasi-de Sitter background. In particular, we will be studying their combinatorial and analytic properties.

## 1.3 Context and Results

The study of mathematical structures, and the computation of cosmological observables has a interesting theoretical motivation, as we will discuss in this section. Understanding how simple physical concepts must be imprinted in cosmological observables is a natural

---

<sup>1</sup>One can use a gauge transformation to parametrize the scalar perturbations with the scalar mode of the metric

question if one is looking for a more fundamental picture that governs inflation than that of a quantum field theory in a curved background. In particular, here we look for combinatorial and geometric formulations that could help us understand what this picture looks like. On the other hand, understanding the analytical properties of these observables, either by computing them directly, or through a regulated expansion, can help us connect the perturbative picture of inflation, with the non-perturbative regime, tied with large super-horizon fluctuations. This is a natural concern from the perspective of a self-consistent theory, but can also provide us with new phenomenological predictions to test. In the next paragraphs, we discuss these ideas in more detail, and how the results obtained in this thesis tie into them.

**A bootstrap approach to scattering amplitudes and cosmology** In inflationary physics, when it comes to experimental verifications, all we have access to are correlation functions on the CMB, which, in principle, we can relate to correlation functions at the final boundary of inflation. If we go back in time, starting at the boundary, we will reach a singularity in time, the big bang. Therefore, it is reasonable to think that we should construct a theory which avoids time evolution altogether, since we expect this concept to breakdown at very early times. The expectation is that all the physics of our theory is somehow imprinted in the correlation functions that we can measure at the future boundary of inflation. Assuming that our observables must satisfy basic physical principles that we are familiar with, such as symmetries, locality, unitarity and causality, one can, in principle, fix the correlation functions for various processes. For the study of scattering amplitudes this approach has been carried out with great success [35–63], allowing the computation of higher loop Feynman diagrams, as well as bootstrapping the full amplitude.

Unfortunately, in de Sitter physics these concepts are much less well understood. We do understand the unitary irreducible representations of the de Sitter isometry group,  $SO(1, 4)$ , and since it is isomorphic to the Euclidean conformal group one can import ideas from Anti-de Sitter to bootstrap cosmological correlators in de Sitter [64–74]. However, as we have seen an inflationary background is not exactly de Sitter, and therefore we expect these symmetries to be approximate.

For the case of locality, where for scattering amplitudes we expect that they will have only poles and branch cuts which directly correspond to the local exchange of a particle. This stems directly from cluster decomposition, from which we expect that the correlation functions in position space are suppressed by the increasing distance between the different points. For sufficiently light states in de Sitter, cluster decomposition does not hold globally, instead two-point correlation functions grow logarithmically with the distance. On the other hand, we can still demand that a theory with a local interaction cannot have singularities in the external energies. This is the Manifest locality test [75].

For the case of unitarity, we can comprehend it in terms of the Cosmological Optical theorem [76], which is really a perturbative statement since its precise form has to be derived for each order individually. A non-perturbative formulation of unitarity is still elusive, but recent developments in constructing a S-matrix for de Sitter may help shed



some light on this [77, 78].

Causality is the least well understood of the three, and it is clear why, since typically we see it from the non-vanishing of commutation relations of fields at time-like or null distances. Since we can only have access to equal time correlation functions, then we can't access this information. One way in which we can understand causality at the level of scattering amplitudes is that their singularity structure obey the Steinmann relations. At the level of the wavefunction, these Steinmann relations do exist, however it is unclear how these conditions relate back to causality [79, 80]. However, very recently in [81], the authors have shown that imposing causal propagation on the co-moving curvature perturbation in the EFT of inflation, imposes significant constraints on Wilson coefficients of the theory.

Understanding these principles is very useful for scattering amplitudes, where locality and unitarity allow us to predict the poles and factorization structure of tree-level scattering amplitudes, and generalized unitarity allowed understanding the branch cut structure of one-loop amplitudes, and gives some insights at higher loops. For the wavefunction, or cosmological correlators, we know what poles and factorization properties to expect, see for example [82–91]. We know that the singularities of the wavefunction correspond to the total energy of the process, or partial energies of sub-processes. Additionally, the residue of the total energy singularity is the corresponding flat-space scattering amplitude. For other singularities the residue is a factorization of the corresponding lower-point scattering amplitude and a linear combination of wavefunctions (this will be described in detail later). Indeed, this knowledge can be used to bootstrap the wavefunction and cosmological correlators [82, 87–90]. However, we do not fully understand how these structures relate to the basic physical principles described above.

**A combinatorial and geometric approach to cosmology** A different way in which we can see how the singularity structure entirely defines the integrand of the wavefunction, was formulated in terms of cosmological polytopes [83]. A polytope can be defined in terms of the linear inequalities that bound it, the definition of cosmological polytope is that the singularities (which are linear in the kinematics) of the wavefunction form hyperplane inequalities that bound a polytope. To this polytope we can associate a volume form (also referred to as canonical form) which matches the rational integrand of a wavefunction coefficient (defined in the previous section). This statement is very powerful since it provides a first principle formulation of the integrand of the wavefunction which avoids any reference to time evolution. Again, this follows the approaches undertaken for scattering amplitudes where discoveries such as the Amplituhedron [92], the ABHY Associahedron [93], among many others [94–104]. However, these examples are typically for the sum of Feynman diagrams, unlike a graph-by-graph description. Studying the sum of graphs directly has been known to lead to remarkable simplifications. The most notorious example being in the study of tree-level gluon amplitudes. When summing over all Feynman diagrams in the appropriate parameterization (in this case the spinor-helicity formalism), the answer becomes incredibly simple when compared to the Feynman diagram approach, as was shown by the Parke-Taylor formula [35]. Hence, the motivation to find a picture that deals with

the full amplitude.

For example, the Amplituhedron is a positive geometry whose canonical form gives us the scattering amplitude of  $\mathcal{N} = 4$  Supersymmetric Yang-Mills (at tree-level, and the integrand at loop level), and physical principles such as locality and unitarity are emergent from the geometry.

Additionally, let us consider the ABHY associahedron for  $\text{Tr}[\phi^3]$  for example. Here the full scattering amplitude of a given process in  $\text{Tr}[\phi^3]$  (at tree level, or the integrand at loop-level) emerges as the canonical form associated to the respective polytope. Furthermore, the polytope contains the full information on the factorization properties of the amplitude when one takes one of the internal particles on-shell. But the particularly interesting feature of the ABHY associahedron is that its canonical form can be obtained from a *stingy* integral (which called this way as it shares many important properties of string amplitudes) [105,106]. This provided a direct connection between particle and string amplitudes. Recently, in [107–111], the authors showed that different deformations of this stringy integral representation of  $\text{Tr}[\phi^3]$ , allow obtaining amplitudes for non-supersymmetric gluons, and scattering amplitudes of the non-linear sigma model.

In cosmology, as explained above, there is still only a graph-by-graph combinatorial description, not for the full wavefunction, or the correlator. In this thesis, we solve this problem. We develop a novel combinatorial formulation for the Bunch-Davies wavefunction of the universe. It turns out, the integrand of the wavefunction can be fully encoded in a polytope, which we called the *Cosmohedron*, and it is fully described in the chapter 5. We show that the Cosmohedron can be obtained by the ABHY associahedron by “blowing-up” its faces. The Cosmohedron also provides a natural formulation of new geometry for individual graphs, the graph associahedron, as well as a recursive formulation for the full wavefunction. We also find the polytope which encodes the full correlator. Given the close connection between the Cosmohedron and the associahedron, it is natural to speculate whether a stringy representation of the cosmological wavefunction is attainable, and from here, whether we can establish similar connections with other realistic theories beyond  $\text{Tr}[\phi^3]$ .

**Computing cosmological correlators** The previous discussion was mostly centred around obtaining the integrand of the wavefunction, or correlator, from physical principles or deeper geometric ideas. Indeed, it is possible in some cases to also obtain the integrated object, but that is a much more difficult task [112–117]. In this thesis, we also devote a lot of effort in the direct computation of the integrated function, which being generally a divergent function needs to be analytically regulated, and then computed in terms of a series expansion of the regulator. Also, here we will import ideas from the study of Feynman integrals, in chapter 3 we will use ideas developed in the context of algebraic geometry to identify and compute the leading and subleading divergences in the integrals appearing in the wavefunction, or correlator. In chapter 4, we will use the method of differential equations [118] to compute the one loop bubble integral and identify the function space of the one loop triangle integral.

**Large fluctuations and infrared divergences** Besides the phenomenological applications of computing cosmological correlators, the understanding of loops in inflation is deeply tied with the emergence of infrared divergences in the perturbative structure of cosmological observables in general. This issue has been noted decades ago and the literature on the subject is vast [119–165]. In inflation divergences coming from the long-wavelength spectrum have contributions from different effects. When one has minimally coupled massless states in a fixed de Sitter background<sup>2</sup>, the correlators not only have an infrared divergence coming from the loop integration. But they also have a secular growth coming from the time integration, which at late times leads to a breakdown of the perturbative expansion, where each order contributes with the same magnitude. This second effect comes from the accumulation of super-horizon modes (long wavelength) at late times.

Therefore, understanding the infrared effects in inflation is of great relevance to have a self consistent theory. And although it is unclear to what extent they can also be relevant from a phenomenological perspective, since the length scales of these contributions can be larger than the observable universe, these effects are physical and can have measurable contributions to the correlator [166–169]. Then, the framework used to deal with these long wavelength modes, stochastic inflation, forms the basis to describe eternal inflation [170–173]. Finally, we expect that the dynamics of the sub-leading contributions from the infrared spectrum contain interesting information relative to the de-coherence of the quantum fluctuations. The literature on the subject is long, and over the years several ways of re-summing the infrared effects have been discussed. It was shown to be possible to re-sum the secular effects, through a dynamical renormalisation group [163], or using the  $\delta N$  formula [174–180]. On the other hand, the infrared divergences coming from the loop integration could also be re-summed in Euclidian de Sitter [132, 141], and one expects this to be analytically continued to Lorentzian de Sitter.

But in recent years, it was shown in a variety of ways that all of these effects get re-summed through the formalism of stochastic inflation [7, 177, 181, 182]. By treating the long wavelengths as a system in a thermal bath (similar physical systems are described by Brownian motion for example), then it is known that the probability distribution function governing these modes follows a Fokker-Planck equation. From this regime it is possible to compute the probability distribution function, which in turn one can obtain correlation functions of the modes. It has been shown that this formalism correctly reproduces the leading order logarithms that appear in perturbative computations [147–150, 164]. Typically, this is done by formulating an effective description of the long-wavelength modes by integrating out modes which are inside a co-moving scale which is larger than the de Sitter horizon. These different field-theoretic approaches have since then been extended to compute corrections to the Fokker-Planck equation, see for example [147, 153, 154].

All of this progress clearly shows that perturbation theory in a fixed de Sitter background is well defined at least in some cases. However, these formalisms usually restrict to de Sitter space, and most of the time  $\phi^4$  interactions. It would be interesting to understand

---

<sup>2</sup>These effects arise in more general scenarios, here we are focusing on massless fields in fixed backgrounds.

the resummation of infrared effects on a more general setting, for example general polynomial interactions in quasi-de Sitter spacetimes, and have a systematic computational formalism to obtain the sub-leading corrections to Stochastic inflation.

In this thesis, we take a step in this direction [165, 183], in chapter 3 we take the general parameterization of the wavefunction/correlators in terms of cosmological integrals, provide a formalism to split the integration region into different regions (sectors) and extract the divergences as a series expansion in analytic regulators coming from the different sectors. Our formalism has several interesting features. Firstly, the parameterisation of cosmological integrals allows studying different power-law FRW cosmologies, and different states including a discrete set of massive states. We find that it makes obvious the effects which are contributing to the divergences, where it either is a secular divergence, a loop divergence, or a mix. In fact, we can identify the same regions proposed in [184]. The fact that our parameterisation is so general, allows putting the wavefunction and the correlators on the same footing, and even different types of observables. At the end of chapter 3 we discuss the formulation of infrared finite computables, akin to similar formulations in the quantum field theory literature [185]. Furthermore, it becomes also very obvious to show that the disconnected parts of the correlator are the ones that carry the leading order infrared effects which are re-summed by stochastic inflation, as was proved in [156]. The question that remains, which we leave for future work, is how our computational framework can be incorporated in the current re-summation formalisms mentioned earlier, or whether it makes natural the construction of a different way in which the re-summation can be formulated.

## 1.4 Outline

The outline of this thesis is as follows:

**In chapter 2** we introduce the derivation of the cosmological wavefunction, and our preferred parametrisation of cosmological integrals for different states, both massless and massive. We then discuss the singularity and factorization structure of the wavefunction, introduce cosmological polytopes which is the graph-by-graph combinatorial formulation of the wavefunction, and introduce graphical rules to compute the correlators from the wavefunction. We conclude the section by describing a different parametrisation of the wavefunction in terms of the momentum polygon.

**In chapter 3** we discuss the computation of infrared divergences, in tree and loop integrals of cosmological observables, as well as formulating an infrared finite computable. This work is based on the papers [165, 183, 186].

**In chapter 4** we discuss the integration of cosmological integrals using the method of differential equations, this chapter heavily relies on the preceding chapters. This work is heavily based on [187].

---

**In chapter 5** we discuss a novel combinatorial formulation of the full wavefunction, the cosmohedron, and the correlator. This work is heavily based on [188].

**In the conclusion** we go over in more detail the main results of the thesis, and the future directions which naturally arise from them.



## Chapter 2

# The Cosmological Wavefunction

Usually, in particle physics where the quantum field theory sits in a Minkowski background we are interested in in-out correlation functions, and ultimately the S-matrix (related through the LSZ reduction formula) and cross-sections of scattering processes, which is what we actually measure. As motivated previously, in inflationary cosmology we want to compute correlation functions at the future boundary of inflation, since in principle we are able to connect them to correlations of temperature at the CMB. Earlier, we learned that we can compute these correlation functions using the interaction picture and the Schwinger-Keyldish contour. Already from quantum mechanics we know that we can compute correlation functions of observables, by integrating them against a probability distribution function given by the norm squared of the wavefunction. The wavefunction is simply the transition amplitude from the vacuum at very early times to a state  $\Phi$  at the spacelike boundary of inflation, at some fixe time  $t^*$ . This makes it clear that this object loses explicit Lorentz invariance due to breaking time translation invariance, and keeps only spatial translation invariance. Obviously, this means that energy is not conserved, only spatial momentum. Here we will focus on theories of scalars in FLRW backgrounds, where the wavefunction has shown to have very interesting features. Remarkably, we will see explicitly later in this section that the wavefunction contains the amplitude of the corresponding process, as a residue of a singularity given by the sum of all external energies in the process. Which we refer to as total energy singularity. We will also see that, for a certain class of scalar theories, the singularity structure of the wavefunction entirely defines it, allowing us to bypass the usual lagrangian formulation of the theory, and instead we can define the wavefunction purely with boundary information. This new formulation also allows us to obtain the integrand of the wavefunction in a more efficient form, without needing to do the time integration in the Feynman integrals every time. These features make the wavefunction, albeit being a more primitive object than the correlator, a particularly interesting object to study, at least for scalar theories. Therefore, we will devote this section to discuss the wavefunction, both in flat-space as well as power-law FLRW cosmologies, and for different massive scalars. We will begin by defining the wavefunction in these different theories, and then discuss the properties of the integrand. Afterwards, we will discuss a combinatorial formulation of the integrand, and how to compute cosmo-

logical correlators from the wavefunction. Finally, we will end with a discussion on a new parameterization of the wavefunction which will become very useful in the later sections of the thesis.

## 2.1 Definition

In this section, we go in detail on the cosmological wavefunction and its properties [31, 84, 90, 189–192]. The wavefunction here discussed is the solution to the functional Schrödinger's equation, and can be defined in terms of Feynman path integrals as follows:

$$\Psi[\Phi] = \int_{\phi(-\infty(1-i\epsilon))=0}^{\phi(0)=\Phi} \mathcal{D}\phi e^{i\mathcal{S}[\phi]},$$

where the lower boundary is chosen such that we pick the Bunch-Davies vacuum state (see section 1). And the upper boundary defines the state onto which we are projecting. It is the transition amplitude between the vacuum state at past infinity, and the state  $\Phi$  at the space-like boundary at  $\eta = 0$ . Given the wavefunctional, we can compute  $n$ -point correlation functions in the future space-like boundary by integrating the fields against a probability distribution function given by the square of the wavefunction, this is simply the Born rule:

$$\langle \Phi(\vec{x}_1) \cdots \Phi(\vec{x}_n) \rangle = \frac{\int \mathcal{D}\Phi \Phi(\vec{x}_1) \cdots \Phi(\vec{x}_n) |\Psi[\Phi]|^2}{\int \mathcal{D}\Phi |\Psi[\Phi]|^2}. \quad (2.1)$$

Throughout this thesis, we will be considering scalar theories with polynomial self couplings in a fixed background, not necessarily flat, for example in inflation one expects the background to be quasi-de Sitter. Therefore, the action can be written in conformal time  $\eta$ , as:

$$\mathcal{S}[\phi] = \int_{-\infty}^0 d\eta \int d\vec{x} \sqrt{-g} \left[ \frac{1}{2} g^{\mu\nu} (\partial_\mu \phi) (\partial_\nu \phi) - \frac{1}{2} m^2 \phi^2 - \xi R \phi^2 + \sum_{k \geq 3} \lambda_k \phi^k \right]. \quad (2.2)$$

Upon a field redefinition:

$$g_{\mu\nu} \rightarrow a(\eta)^2 g_{\mu\nu}, \quad \phi \rightarrow a(\eta)^{-\frac{d-1}{2}} \phi, \quad (2.3)$$

the action becomes,

$$\mathcal{S}[\phi] = \int_{-\infty}^0 d\eta \int d\vec{x} \left[ \frac{1}{2} (\partial\phi)^2 - \frac{1}{2} \mu(\eta)^2 \phi^2 + \sum_{k \geq 3} \lambda_k(\eta) \phi^k \right]. \quad (2.4)$$

Where the mass and couplings are now time dependent, with the following relations:

$$\begin{aligned} \mu(\eta) &= m^2 a(\eta)^2 + 2d \left( \xi - \frac{d-1}{4d} \right) \left[ \partial_\eta \left( \frac{\dot{a}}{a} \right) + \frac{d-1}{2} \left( \frac{\dot{a}}{a} \right)^2 \right], \\ \lambda_k(\eta) &= \lambda_k(a(\eta))^{2 + \frac{(d-1)(k-2)}{2}}. \end{aligned} \quad (2.5)$$



For conformally coupled scalars,  $\xi = \frac{d-1}{4d}$ , the action becomes conformally equivalent to that of a massless scalar in flat space. In this thesis, we will be interested in power law cosmologies for which the scale factor is  $a(\eta) = \frac{1}{(H\eta)^\gamma}$ , where  $\gamma = 1$  is for de Sitter, and  $\gamma = 0$  is for Minkowski.

If we split the action into a free and interacting part, such as:

$$S[\phi] = S_{\text{free}}[\phi] + S_{\text{I}}[\phi], \quad (2.6)$$

then, in general, our equations of motion do not have a closed analytic solution, but we can still write the formal solution:

$$\phi(\mathbf{x}, \eta) = \int d\mathbf{x}' \sqrt{\tilde{g}} G_{B,\partial}(\mathbf{x}, \mathbf{x}', \eta) \Phi(\mathbf{x}', \eta) + i \int d\mathbf{x}' d\eta' G_{B,B}(\mathbf{x}, \mathbf{x}', \eta, \eta') \left. \frac{dS_{\text{I}}}{d\phi} \right|_{\phi=\Phi}, \quad (2.7)$$

where  $\tilde{g}$  is the spatial metric. Therefore, we can apply the above solution recursively and obtain the saddle point approximation for an interacting theory. After performing a spatial Fourier transform, this allows us to write the wavefunction into the following form:

$$\log \Psi[\Phi, \eta_f] = \sum_{n=2} \frac{1}{n!} \int \frac{d^3 k_1 \cdots d^3 k_n}{(2\pi)^{3n}} \Phi_{\vec{k}_1} \cdots \Phi_{\vec{k}_n} (2\pi)^3 \delta(\vec{k}_1 + \cdots + \vec{k}_n) \psi_n(\vec{k}_N), \quad (2.8)$$

where  $\psi_n$  are the wavefunction coefficients, and can be organised diagrammatically in terms of Feynman graphs:

$$\psi_n = \sum_{\mathcal{G}} \psi_{\mathcal{G}},$$

where each coefficient  $\psi_{\mathcal{G}}$  corresponds to an integral. To obtain the construction of the respective Feynman integrals, the usual rules apply. For each vertex (also referred to as site) in the corresponding diagram we attribute a coupling constant,  $\lambda_k(\eta)$ . For each external state we attribute a bulk-to-boundary propagator, which is just the solution of the free equations of motion,  $G_{B,\partial}(E_k, \eta)$ , with  $E_k$  being the norm of the momentum in the external propagator. And for each internal edge we have a bulk-to-bulk propagator,  $G_{B,B}(y_e, \eta, \eta')$ , with  $y_e$  is the norm of the momentum running in the propagator, which is a solution to the free two-point correlation function. For example, for a massless scalar in flatspace it obeys the following differential equation:

$$(\partial_\eta^2 - y_e^2) G_{B,B}(y_e, \eta, \eta') = \delta(\eta - \eta').$$

Then,

$$\psi_{\mathcal{G}} = \int_{-\infty(1-i\epsilon)}^0 \prod_{s \in \mathcal{V}} \left[ d\eta_s \lambda(\eta_s) \prod_{\vec{k}_i} G_{B,\partial}(E_{k_i}, \eta_s) \right] \prod_{e \in \mathcal{E}} G_{B,B}(y_e; \eta_s, \eta_{s'}),$$

where  $\mathcal{V}$  denotes the set of sites  $s$  in the graph  $\mathcal{G}$  (dots in the diagrams in figure 2.1), and  $\mathcal{E}$  denotes the set of edges  $e$  in the graph (lines not attached to the boundary, gray line, in figure 2.1). The product over  $\vec{k}_i$  is over all the external states attached to the site  $s$  (lines attached from the dots to the boundary, gray line, in figure 2.1). However, here we are

only doing the saddle point approximation which is valid in the  $\hbar \rightarrow 0$  limit. Therefore, our derivation will only produce tree level contributions, and not closed loops (like the rightmost graph in figure 2.1). In order to obtain loop contributions, which will concern us a lot in this thesis, we need to expand around the classical value,

$$\phi = \phi_o + \varphi, \quad (2.9)$$

where  $\phi_o$  is the solution of the free classical equations of motion, with boundary value  $\phi_o(\eta = 0) = \Phi$ , and  $\varphi$  is the fluctuation around the classical value with vanishing boundary value, so it does not satisfy the equations of motion. Then, the action after integration by parts becomes:

$$\mathcal{S}[\phi] = \int d^3x \Phi(\partial_\eta \phi)|_{\eta=0} + \int_0^\infty d\eta \int d^3x \phi(\square - \mu^2)\phi + \mathcal{S}_I[\phi], \quad (2.10)$$

notice that the first term is a non-vanishing boundary term that comes from using integration by parts in the  $\eta$  integral. After plugging-in (2.9), the action becomes:

$$\mathcal{S}[\phi] = \int d^3x \Phi(\partial_\eta \phi)|_{\eta=0} + \int_0^\infty d\eta \int d^3x \varphi(\square - \mu^2)\varphi + \mathcal{S}_I[\phi_o, \varphi]. \quad (2.11)$$

As we mentioned,  $\phi_o$  is the solution to the free equations of motion, and imposing the correct boundary values it becomes:

$$\phi_o(\vec{k}_i, \eta) = \Phi_{\vec{k}_i} G_{B,\partial}(|\vec{k}_i|, \eta). \quad (2.12)$$

Now that we have a specific form for the action we can write the wavefunction to be:

$$\Psi[\Phi] = e^{\frac{i}{2} \int d^3x \Phi(\partial_\eta \phi)|_{\eta=0}} \int \mathcal{D}\varphi e^{\frac{i}{2} \int_0^\infty d\eta \int d^3x \varphi(\square - \mu^2)\varphi} \left( \sum_{n=0}^\infty \frac{S_I[\phi_o, \varphi]^n}{n!} \right). \quad (2.13)$$

Now that we factorized the boundary terms we can treat the path integral over  $\varphi$  in the usual way, we insert a source terms and act with functional derivatives in order to generate the terms downstairs in the sum of powers of  $S_I$ . This will bring down powers of the inverse of the operator  $(\square - \mu^2)$ , which is our bulk-to-bulk propagator defined in (2.1). This will turn (2.13) into the infinite sum:

$$\Psi[\Phi] = e^{\frac{1}{2} \int d^3\vec{k}_1 d^3\vec{k}_2 \psi_2^{\text{free}} \Phi_{\vec{k}_1} \Phi_{\vec{k}_2}} \left( 1 + \sum_{n=2}^\infty \prod_{j=1}^n \int \frac{d^3k_j}{(2\pi)^3} \Phi_{\vec{k}_j} (2\pi)^3 \frac{\delta(\vec{k}_1 + \dots + \vec{k}_n)}{n!} \sum_{L=0}^\infty \psi_n^{(L)} \right), \quad (2.14)$$

where again we performed a spatial Fourier transform. The wavefunction has exactly the same form as the saddle point expression if we were to expand around a Gaussian distribution in the weak coupling limit, except now we have to sum over all loop contributions to  $\psi_n$ , which now can be written as:

$$\psi_n = \sum_{L=0}^\infty \psi_n^{(L)} = \sum_{L=0}^\infty \sum_{\mathcal{G}^{(L)}} \psi_{\mathcal{G}^{(L)}}. \quad (2.15)$$

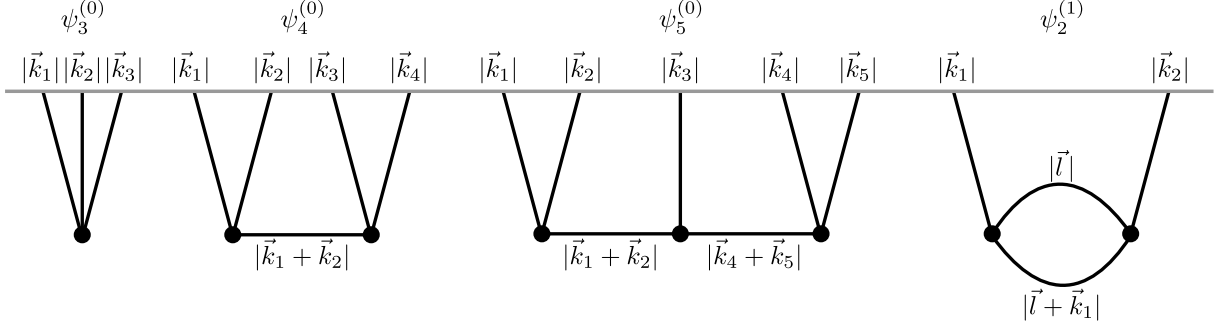


Figure 2.1: Examples of diagrams for the wavefunction. Gray line is the future boundary onto which we are projecting. Any lines attached to the boundary correspond to external states, in the integral they correspond to bulk-to-boundary propagators. Lines not attached to the boundary correspond to bulk-to-bulk propagators in the respective integral. The dots correspond to vertices (also called sites), and to each one we attribute a coupling  $\lambda_k(\eta_s)$  in the respective integral.

The Feynman rules are essentially the same but now we have to integrate over the loop momentum for graphs with closed loops. And the free two-point wavefunction is given by:

$$\psi_2^{\text{free}} = i(\partial_\eta G_{B,\partial}(|\vec{k}_i|, \eta))_{\eta=0}. \quad (2.16)$$

Now that we established how to derive the wavefunction, we can compute the correlators. The formula for correlators is given by the Born rule (2.1). In order to obtain the concrete form for the correlators we insert a source term in (2.14), and act with functional derivatives to lower  $\Phi$ . Then, it is clear that the inverse propagators that are lowered this time are simply  $(2 \text{Re } \psi_2^{\text{free}})^{-1}$ . And in the numerator we will obtain the linear combinations of higher point wavefunction coefficients. For example, the three point correlator is:

$$\langle \Phi_{\vec{p}_1} \Phi_{\vec{p}_2} \Phi_{\vec{p}_3} \rangle = \delta(\vec{p}_1 + \vec{p}_2 + \vec{p}_3) \frac{\text{Re } \psi_3(\vec{p}_1, \vec{p}_2, \vec{p}_3)}{\text{Re } \psi_2^{\text{free}}(\vec{p}_1) \text{Re } \psi_2^{\text{free}}(\vec{p}_2) \text{Re } \psi_2^{\text{free}}(\vec{p}_3)}. \quad (2.17)$$

In section 2.4 we discuss general diagrammatic rules to obtain the form of the correlators.

For the moment, let us consider that a flat-space background, then the mode functions are plane waves, and we can write:

$$G_{B,\partial}(E_k, \eta) = e^{iE_k \eta},$$

$$G_{B,B}(y_e, \eta, \eta') = \frac{1}{2y_e} \left( e^{iy_e(\eta' - \eta)} \Theta(\eta - \eta') + e^{iy_e(\eta - \eta')} \Theta(\eta' - \eta) - e^{iy_e(\eta + \eta')} \right), \quad (2.18)$$

where the last term in the bulk-to-bulk propagator is to ensure it vanishes when taking one of the edges to the boundary. And the coupling parameters are constant,  $\lambda_k(\eta) \equiv \lambda_k$ . With this we can compute the wavefunction coefficients in flat-space, for example the three-point contact diagram (see the first graph in figure 2.1), is given by:

$$\psi_3^{(0)}(E_1, E_2, E_3) = -i\lambda_3 \int_{-\infty(1-i\epsilon)}^0 d\eta e^{i(E_1 + E_2 + E_3)\eta} = \frac{\lambda_3}{E_1 + E_2 + E_3}, \quad (2.19)$$

where the lower boundary term is killed by the  $i\epsilon$ -prescription. The four-point exchange diagram can be computed as follows:

$$\begin{aligned}
\psi_4^{(0)} &= \lambda_3^2 \int d\eta_1 d\eta_2 e^{i(E_1+E_2)\eta_1} e^{i(E_3+E_4)\eta_2} \times \\
&\quad \times \frac{1}{2y} \left( e^{iy(\eta_2-\eta_1)} \Theta(\eta_1 - \eta_2) + e^{iy(\eta_1-\eta_2)} \Theta(\eta_2 - \eta_1) - e^{iy(\eta_1+\eta_2)} \right) \\
&= \frac{\lambda_3^2}{2y(E_1 + E_2 + E_3 + E_4)(E_3 + E_4 + y)} + \frac{\lambda_3^2}{2y(E_1 + E_2 + E_3 + E_4)(E_1 + E_2 + y)} - \\
&\quad - \frac{\lambda_3^2}{2y(E_1 + E_2 + y)(E_3 + E_4 + y)} \\
&= \frac{\lambda_3^2}{(E_1 + E_2 + E_3 + E_4)(E_1 + E_2 + y)(E_3 + E_4 + y)}, \tag{2.20}
\end{aligned}$$

where  $E_i = |\vec{k}_i|$  and  $y = |\vec{k}_1 + \vec{k}_2| = |\vec{k}_3 + \vec{k}_4|$ . More complex diagrams will simply have more bulk-to-boundary propagators, and more bulk-to-bulk propagators, but in essence the time integration can be easily done as it one is just integrating over simple exponential functions. Further examples, are given by the five-point exchange diagram (in a cubic theory):

$$\begin{aligned}
\psi_5^{(0)} &= \frac{1}{(|\vec{k}_1| + |\vec{k}_2| + |\vec{k}_3| + |\vec{k}_4| + |\vec{k}_5|) (|\vec{k}_1| + |\vec{k}_2| + |\vec{k}_1 + \vec{k}_2|) (|\vec{k}_3| + |\vec{k}_1 + \vec{k}_2| + |\vec{k}_4 + \vec{k}_5|)} \times \\
&\quad \times \frac{1}{|\vec{k}_4| + |\vec{k}_5| + |\vec{k}_4 + \vec{k}_5|} \left( \frac{1}{|\vec{k}_3| + |\vec{k}_4| + |\vec{k}_5| + |\vec{k}_1 + \vec{k}_2|} + \frac{1}{|\vec{k}_1| + |\vec{k}_2| + |\vec{k}_3| + |\vec{k}_4 + \vec{k}_5|} \right),
\end{aligned}$$

and by the two-point one-loop diagram:

$$\begin{aligned}
\psi_2^{(1)} &= d\vec{l} \frac{1}{(|\vec{k}_1| + |\vec{k}_2|) (|\vec{k}_1| + |\vec{l}| + |\vec{k}_1 + \vec{l}|) (|\vec{k}_2| + |\vec{l}| + |\vec{k}_1 + \vec{l}|)} \times \\
&\quad \times \left( \frac{1}{|\vec{k}_1| + |\vec{k}_2| + |\vec{l}|} + \frac{1}{|\vec{k}_1| + |\vec{k}_2| + |\vec{k}_1 + \vec{l}|} \right)
\end{aligned}$$

The previous examples are for the flat-space wavefunction, if on the other hand we want to consider an expanding background, like FLRW, then our coupling parameter will be time dependent (see (2.5)). As such, our mode functions will, in general, be Hankel functions, and performing the time integration becomes much more cumbersome,

$$G_{B,\partial}(E_p, \eta) = \sqrt{-E_p \eta} H_\nu^{(2)}(-E_p \eta),$$

where for massless conformally coupled scalars  $\nu = 1/2$ , and for massless minimally coupled scalars,

$$\nu = \frac{1}{2} + \frac{d-1}{2}\gamma,$$

of course for general massive states in de Sitter we recover the result  $\nu = \sqrt{d^2/4 - m^2/H^2}$ .

In our discussion, we will be mainly concerned with states identified by  $\nu = l + 1/2$  with  $l \in \mathbb{Z}_+ \cup \{0\}$ . The mode function of such states with arbitrary positive integers  $l$  is related to the plane wave, corresponding to  $l = 0$ , via a differential operator:

$$G_{B,\partial}(E_p, \eta) = \frac{1}{(-E_p \eta)^l} \hat{\mathcal{O}}_l(E_p) e^{iE_p \eta}, \quad \hat{\mathcal{O}}_l(E_p) := \prod_{r=1}^l \left[ (2r-1) - E_p \frac{\partial}{\partial E_p} \right] \quad (2.21)$$

It is easy to see that for massless states in de Sitter ( $l = 1$ ) this operator acting on the exponential will yield the correct mode function:  $(1 + iE_p \eta) e^{iE_p \eta}$ . This allows to derive processes involving these states from massless scalars with time-dependent couplings in flat-space. Using the relation (2.21) between the states with order parameter  $\nu = l + 1/2$  and the conformally coupled one ( $l = 0$ ) and rescaling the bulk-to-bulk propagator via

$$G_{B,B}(y_e, \eta, \eta') \longrightarrow (-y_e \eta)^{-l_e} (-y_e \eta')^{-l_e} G_{B,B}(y_e; \eta, \eta') \quad (2.22)$$

the wavefunction  $\psi_{\mathcal{G}}^{\{l_j, l_e\}}$  for internal and external states parameterized by an integer order parameter,  $l_j$  and  $l_e$  respectively, can be written as [189]

$$\psi_{\mathcal{G}}^{\{l_j, l_e\}} = \prod_{j=1}^n \left[ \frac{1}{E_j^{l_j}} \hat{\mathcal{O}}_{l_j}(E_j) \right] \prod_{e \in \mathcal{E}} \left[ \frac{1}{y_e^{2l_e}} \right] \psi_{\mathcal{G}}^{\{l_e\}} \quad (2.23)$$

with

$$\psi_{\mathcal{G}}^{\{l_e\}} = \int_{-\infty}^0 \prod_{s \in \mathcal{V}} \left[ d\eta_s \frac{\lambda_k(\eta_s)}{(-\eta_s)^{\rho_s}} e^{iX_s \eta_s} \prod_{e \in \mathcal{E}} G_{B,B}(y_e; \eta_{s_e}, \eta_{s'_e}) \right] \quad (2.24)$$

where  $\{l_e\}$  indicates that each edge  $e$  has a state with order parameter  $l_e$  associated to it. And  $\psi_{\mathcal{G}}^{\{l_e\}}$  indicates the re-scaled wavefunction coefficient with internal states with parameter  $l_e$ , below we will see how it is recursively related to  $\psi_{\mathcal{G}}^{l_e-1, \{l_e\}}$  (where the edge  $e$  has its parameter  $l_e$  shifted by one unit).  $X_s$  is the sum of the external energies at the site  $s$ ,  $\rho_s$  is a function of the order parameters of both external and internal states at the site  $s$

$$X_s := \sum_{j=1}^{k_s} E_j, \quad \rho_s := \sum_{j=1}^{k_s} l_j + \sum_{e \in \mathcal{E}_s} l_e, \quad (2.25)$$

where  $k_s$  is the number of external states at the site  $s$ ,  $\mathcal{E}_s \subset \mathcal{E}$  the subset of edges incident at the site  $s$ , while  $l_j$  and  $l_e$  are the integer order parameters associate to the  $j$ -th external state and to the edge  $e$  respectively.

Due to the time dependence of the couplings  $\lambda_{k_s}(\eta_s)$ , as well as the additional  $1/(-\eta_s)^{\rho_s}$ , the time integration cannot be performed as for the flat-space counterpart. In order to obtain a rational integrand, first one needs to perform a Fourier transformation on the whole function  $\lambda_{k_s}(\eta_s)/(-\eta_s)^{\rho_s}$ , as follows

$$\frac{\lambda_k(\eta_s)}{(-\eta_s)^{\rho_s}} = \int_{-\infty}^{+\infty} dz_s e^{iz_s \eta_s} f(z_s). \quad (2.26)$$

The time-dependent coupling constant is given by

$$\lambda_k(\eta_s) = \lambda_k [a(\eta_s)]^{\gamma[2 - \frac{(k-2)(d-1)}{2}]} \quad (2.27)$$

and for cosmologies described via the warp factor  $a(\eta) = -(1/H\eta)^\gamma$ , (2.26) becomes

$$\frac{\lambda_k(\eta_s)}{(-\eta_s)^{\rho_s}} = i^{\beta_{ks,l}} (i\lambda_k) H^{-\gamma[2 - \frac{(k-2)(d-1)}{2}]} \int_{-\infty}^{+\infty} dz_s e^{iz_s \eta_s} z_s^{\beta_{ks,l}-1} \theta(z_s) \quad (2.28)$$

where  $\beta_{ks,l} := \rho_s + \gamma[2 - (k-2)(d-1)/2]$ . Hence, the wavefunction coefficient  $\tilde{\psi}_{\mathcal{G}}^{\{l_e\}}$  associated to a graph  $\mathcal{G}$  can be written as

$$\begin{aligned} (\psi_{\mathcal{G}}^{\{l_e\}})^{\text{FLRW}} &= \int_{X_s}^{+\infty} \prod_{s \in \mathcal{V}} [dx_s f(x_s - X_s)] \psi_{\mathcal{G}}^{\{l_e\}}, \\ \psi_{\mathcal{G}}^{\{l_e\}} &:= (i\lambda_k)^{n_s} \int_{-\infty}^0 \prod_{s \in \mathcal{V}} [d\eta_s e^{ix_s \eta_s}] \prod_{e \in \mathcal{E}} G_{B,B}(y_e; \eta_{s_e}, \eta_{s'_e}) \end{aligned} \quad (2.29)$$

where  $n_s$  is the number of sites of the graph. And here we set  $z_s = x_s - X_s$ . This representation allows encoding the details of the specific cosmology into the measure of integration  $f(x_s - X_s)$  and single out the information which is common to all cosmologies and encoded into  $\psi_{\mathcal{G}}^{\{l_e\}}$ , which we refer to as *wavefunction universal integrand*. Then, from the wavefunction with general internal states, parameterized by  $l_e$ , one can simply shift the sum of external energies entering a site  $s$  by  $x_s$ , and then integrate over the shift, providing the kernel  $f(x_s - X_s)$ , one can obtain the wavefunction in power-law cosmologies in a very simple fashion. To obtain the wavefunction integrand for general internal states, of integer parameter  $l_e$ , it turns out that there is a simple recursion relation between the integrand and an integrand with one internal state with one edge shifted by one unit,  $l_e - 1$ . The proof of this recursion relation can be found in [189], and it is of the following form:

$$\psi_{\mathcal{G}}^{\{l_e\}} = \sum_{\substack{e, \bar{e} \in \mathcal{E} \\ \bar{e} \neq e}} \hat{\mathcal{O}}_e \psi_{\mathcal{G}}^{l_e - 1, \{l_e\}}, \quad \hat{\mathcal{O}}_e := \frac{2(l_e - 1)}{\sum_{s \in \mathcal{V}} x_s} \left( \frac{\partial}{\partial x_{s_e}} + \frac{\partial}{\partial x_{s'_e}} \right) - \frac{\partial^2}{\partial x_{s_e} \partial x_{s'_e}}. \quad (2.30)$$

Therefore, one can obtain the integrand for a process with all massless internal states from the integrand with conformally coupled internal states by acting with the above operator for each edge in the corresponding graph.

Note that  $\psi_{\mathcal{G}}^{\{l_e\}}(x_s, y_e)$  is a function of  $\{x_s, s \in \mathcal{V}\}$  and  $\{y_e | e \in \mathcal{E}\}$ , which parametrise the kinematic space as well as the loop space in case of graphs with loops. It is then possible to associate a weighted reduced graph to  $\psi_{\mathcal{G}}^{\{l_e\}}(x_s, y_e)$  by simply suppressing the lines representing the external states and attaching a weight  $x_s$  to each site  $s \in \mathcal{V}$  and the pair  $(y_e, l_e)$  to each edge  $e \in \mathcal{E}$ .

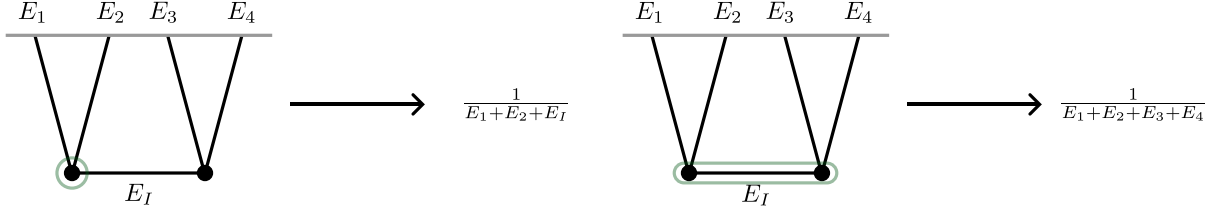


Figure 2.2: Examples of singularity/tube correspondence.

At this point, we find it instructive to give an example of the integral we have in power-law FRW cosmologies. Let us consider the four point function at tree level in theory with cubic interactions, for conformally coupled scalars:

$$(\psi_{2\text{-chain}}^{\{0\}})^{\text{FLRW}} = \int_0^\infty dx_1 \int_0^\infty dx_2 x_1^\alpha x_2^\alpha \left( \frac{1}{(x_1 + x_2 + X_1 + X_2)(x_1 + X_1 + y)(x_2 + X_2 + y)} \right), \quad (2.31)$$

where  $X_1 = E_1 + E_2$ , and  $X_2 = E_3 + E_4$ , and we can similarly use the second graph in 2.1 to represent it. Then, the integrand (which is function in parenthesis in (2.31)) for an all massless minimally coupled scalar process is obtained by acting on the integrand of (2.31) with the operator  $\frac{\partial^2}{\partial x_1 \partial x_2}$ , dividing it by  $1/y^2$ , changing the value of  $\alpha$  accordingly, and finally acting with the operator (2.21) four times, one for each of the external energies.

## 2.2 Singularities of the Integrand

If we consider a general diagram,  $\mathcal{G}$ , then we can identify all the singularities of the integrand of  $\psi_{\mathcal{G}}$  from the diagram. Each singularity has a one-to-one correspondence with a sub-diagram of  $\mathcal{G}$ , and is given by the sum of external energies in the sub-diagram. It is useful to find a suitable representation of these sub-diagrams, and we can do this by drawing *tubes* on the original diagram, see for example figure 2.2. Then, by drawing every possible tube in the diagram,  $\mathcal{G}$ , one can find the denominator of the integrand for the wavefunction coefficients.

One interesting question about the integrand is, what happens when we localise in one of the singularities of the integrand. From our knowledge of quantum field theory, we know that scattering amplitudes factorize in products of lower-point scattering amplitudes when we localize in a singularity. However, the wavefunction does not have such a simple behaviour, in general, the residue of a singularity is the scattering amplitude of sub-diagram corresponding to the singularity, times a linear combination of lower-point wavefunctions. In particular, let us consider a general graph and divide it into a left and right component connected by an edge. If we take the singularity of the left sub-process then the factorization is as follows:

$$\lim_{E_L \rightarrow 0} \psi_n(E_1, \dots, E_n) = \frac{\mathcal{A}_{k+1} \tilde{\psi}_{n-k+1}(E_L, E_{k+1}, \dots, E_n)}{E_L}, \quad (2.32)$$

where  $E_L = E_1 + \dots + E_k + E_I$ , and

$$\tilde{\psi}_{n-k+1}(E_I, E_{k+1}, \dots, E_n) = \frac{\psi_{n-k+1}(-E_I, E_{k+1}, \dots, E_n) - \psi_{n-k+1}(E_I, E_{k+1}, \dots, E_n)}{2E_I}. \quad (2.33)$$

For more general set ups, where there is no left and right sub-processes, but something more intricate, the above formula generalizes accordingly (see for example [80]). For the case of the total energy singularity the residue is the full scattering amplitude (corresponding to the process represented by  $\mathcal{G}$ ):

$$\lim_{E_t \rightarrow 0} \psi_n(E_1, \dots, E_n) = \frac{\mathcal{A}_n}{E_t}, \quad (2.34)$$

this can be seen as restoring energy conservation, leads to a Lorentz invariant object. In this sense, the wavefunction contains the information about the amplitude of the corresponding process, as well as lower point processes.

Finally, in the above discussion we only addressed how to obtain the denominator of the wavefunction from the tubes of the graph. To obtain the full integrand one can just compute the time integral as discussed in the previous sub-section, but it is also possible to obtain it from reading the tubes of the graph as well. The rule is simple, we consider all maximal sets of tubes which are non-overlapping (where two tubes overlap if there is partial overlap, and do not overlap if they are disjoint or one is fully contained by the other), then the rational integrand is the sum of terms where each term corresponds to one such set, its denominator is given by the singularities of the set, and the numerator is one. To a maximal set of non-overlapping tubes we designate as a *tubing*, or colloquially a *Russian Doll*. This representation is known as *old-fashioned perturbation theory*. To understand this representation, let's consider the time integral representation of a given graph contributing to  $\Psi$ :

$$\psi_{\mathcal{G}} = \int_{-\infty(1-i\epsilon)}^0 \left[ \prod_{v \in \mathcal{V}} d\eta_v \right] \left[ \prod_{v \in \mathcal{V}} e^{i \left( \sum_{i_v \in \mathcal{E}'_v} E_{i_v} \right) \eta_v} \right] \left[ \prod_{e \in \mathcal{E}} G(E_{k_e}; \eta_e, \eta_{e'}) \right], \quad (2.35)$$

where  $\mathcal{V}$  is the set of vertices in the graph,  $\mathcal{E}$  is the set of internal edges of the graph,  $\mathcal{E}'_v$  is the set of external states attached to the vertex  $v$  (and  $E_{i_v}$  are the respective moduli of the momenta), and  $E_{k_e}$  is the momentum flowing in the edge  $e$ . We now consider the action of the operator:

$$\Delta = -i \sum_{v \in \mathcal{V}} \partial_{\eta_v},$$

on the integrand of (2.35). We can start by applying integration-by-parts. The total derivative vanishes, since the bulk-to-bulk propagators vanish at the upper boundary (see (2.18) when sending  $\eta_1$  or  $\eta_2$  to zero), and on the other hand the  $i\epsilon$  prescription (Bunch-Davies condition) ensures the integrand vanishes in the lower boundary. Then we consider the action of  $\Delta$  separately in the external propagators, and in the product of bulk-to-bulk



propagators,  $G(y_e; \eta_e, \eta_{e'})$ . It is clear that,

$$\Delta \left[ \prod_{v \in \mathcal{V}} e^{i \left( \sum_{i_v \in \mathcal{E}'_v} E_{i_v} \right) \eta_v} \right] = \left( \sum_{v \in \mathcal{V}} \sum_{i_v \in \mathcal{E}'_v} E_{i_v} \right) \left[ \prod_{v \in \mathcal{V}} e^{i \left( \sum_{i_v \in \mathcal{E}'_v} E_{i_v} \right) \eta_v} \right],$$

where the quantity in parentheses is the total energy of  $\psi_{\mathcal{G}}$ . Then the action of  $\Delta$  on the bulk-to-bulk propagators is essentially only the action on the boundary term, since when acting on the time-ordered terms, these vanish. This is true because  $\Delta$  is the time-translation operator, and the time-ordered terms are time translation invariant. Practically, one can simply see that by acting with  $\partial_{\eta_1} + \partial_{\eta_2}$  on the time ordered terms in (2.18), that the derivatives of the exponentials in  $\eta_1$  and  $\eta_2$  will cancel each other. Therefore, we can say that:

$$\Delta \left[ \prod_{e \in \mathcal{E}} G(y_e; \eta_e, \eta_{e'}) \right] = - \left( \sum_{\tilde{e} \in \mathcal{E}} e^{i E_{k_{\tilde{e}}} (\eta_{\tilde{e}} + \eta_{\tilde{e}'})} \left[ \prod_{e \in \mathcal{E} / \{\tilde{e}\}} G(E_{k_e}; \eta_e, \eta_{e'}) \right] \right).$$

Putting everything together, the exponentials in the expression above will be just like bulk-to-boundary propagators. Then, we can write,

$$E_t \psi_{\mathcal{G}}(E_1, \dots, E_n) = \sum_{e \in \mathcal{E}_{\text{Tree}}} \psi_{\mathcal{G}_L}(\mathcal{E}_{L_e}; E_{k_e}) \psi_{\mathcal{G}_R}(\mathcal{E}_{R_e}; E_{k_e}) + \sum_{e \in \mathcal{E}_{\text{Loop}}} \psi_{\tilde{\mathcal{G}}}(E_1, \dots, E_n, E_{k_e}, E_{k_e}). \quad (2.36)$$

Where in the first term we are summing over every edge that is not in a loop (the set  $\mathcal{E}_{\text{Tree}}$ ), and  $\mathcal{G}_L$  and  $\mathcal{G}_R$  correspond to the subgraphs to the left and right of the edge  $e$ .  $\mathcal{E}_{L_e}$  are the external states of the left subgraph, and similarly for the right subgraph. Additionally, both  $\mathcal{G}_L$  and  $\mathcal{G}_R$  also have an external state with the momentum of the edge  $e$  in  $\mathcal{G}$ . In the second term, we are summing over the remaining edges, which are part of a loop (the set  $\mathcal{E}_{\text{Loop}}$ ).  $\tilde{\mathcal{G}}$  stands for the graph obtained by cutting the edge  $e$  in the graph  $\mathcal{G}$ . It will have all the  $n$  external states plus two more, both with momentum of the edge  $e$ . Equation (2.36), when applied recursively, allows us to construct the OFPT representation of the wavefunction. In [193], the authors showed that there is one triangulation of the dual of the cosmological polytope which yields the OFPT representation.

From (2.36), we have that in the sum on the right-hand side, each term will be a product of singularities corresponding to tubes that do not overlap, either are fully inside one another, or are disjoint. Applying this formula recursively, we can see that this property will hold in the expansion of the different terms. Therefore, it becomes clear that we can write the wavefunction as a sum of russian dolls.

## 2.3 Integrand from combinatorics

We have seen in the previous section, from the Russian doll rule, that the integrand of the wavefunction can be entirely defined from the its singularity structure. In this section, we will learn about a combinatorial formulation of the integrand, which is completely defined

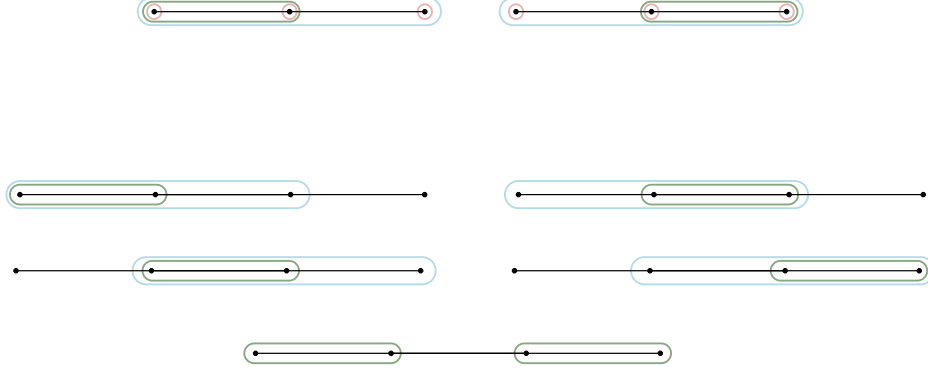


Figure 2.3: (Top) Diagrammatic representation of the terms contributing to the three-site chain graph, in terms of tubings (collections of non-overlapping tubes). Here the graph has the external states amputated for simplicity. (Bottom) The representation of the five terms contributing to the four-site chain graph. Here we omitted the single site tubes and the total energy tube since every single term contains them.

by its singularities. This formulation is given by (generalised) cosmological polytopes for the Bunch-Davies wavefunction [80, 83, 189], or by the weighted cosmological polytopes for cosmological correlators [194]. Here we give a brief description of these objects.

Let us consider a graph  $\mathcal{G}$  endowed with its sets of site- and edge- weights,  $\{x_s, s \in \mathcal{V}\}$  and  $\{y_e, e \in \mathcal{E}\}$  respectively. It is possible to associate a linear polynomial  $q_{\mathfrak{g}}(\mathcal{Y})$  to each subgraph  $\mathfrak{g} \subseteq \mathcal{G}$  defined as the sum over the weights associated to the sites in  $\mathfrak{g}$  and the weights of the edges departing from it. Let us consider both the site and edge weights as the local coordinates in projective space  $\mathbb{P}^{n_s+n_e-1}$ , so that a generic point in it can be written as  $\mathcal{Y} := (x, y)$ ,  $x$  and  $y$  being a shorthand notation for  $x := (x_1, \dots, x_{n_s})$  and  $y := (y_{e_1}, \dots, y_{e_{n_e}})$  and  $n_s, n_e$  being the number of sites and edges respectively. The polynomials

$$\left\{ q_{\mathfrak{g}}(\mathcal{Y}) = \sum_{s \in \mathcal{V}_{\mathfrak{g}}} x_s + \sum_{e \in \mathcal{E}_{\mathfrak{g}}^{\text{ext}}} y_e, \mathfrak{g} \subseteq \mathcal{G} \right\}$$

can be written as  $q_{\mathfrak{g}}(\mathcal{Y}) = \mathcal{Y}^I \mathcal{W}_I^{(\mathfrak{g})}$  where  $\mathcal{W}^{(\mathfrak{g})}$  is a vector in the dual space of  $\mathbb{P}^{n_s+n_e-1}$ , which is still indicated as  $\mathbb{P}^{n_s+n_e-1}$  – we will refer to it as a co-vector. Then the inequalities  $\{q_{\mathfrak{g}}(\mathcal{Y}) \geq 0\}$  define a cosmological polytope  $\mathcal{P}_{\mathcal{G}}$ , with the co-vector  $\mathcal{W}^{(\mathfrak{g})}$  identifying a hyperplane that intersects the cosmological polytope along its boundary only, containing a facet (*i.e.* a codimension-1 face)  $\mathcal{P}_{\mathcal{G}} \cap \mathcal{W}^{(\mathfrak{g})}$ . This means that a vertex  $\mathcal{Z}^I$  of the polytope  $\mathcal{P}_{\mathcal{G}}$  on the facet  $\mathcal{P}_{\mathcal{G}} \cap \mathcal{W}^{(\mathfrak{g})}$  satisfies the condition  $\mathcal{Z}^I \mathcal{W}^{(\mathfrak{g})} = 0$ . Given a cosmological polytope  $\mathcal{P}_{\mathcal{G}} \subset \mathbb{P}^{n_s+n_e-1}$  there is a unique rational function  $\Omega(\mathcal{Y}, \mathcal{P}_{\mathcal{G}})$  – up to an overall constant –, named *canonical function* associated to it, such that:

- its only singularities are simple poles along the boundaries of the polytope  $\mathcal{P}_{\mathcal{G}}$ ;
- its residue of a given pole is a canonical function of a codimension-1 polytope associated to the boundary identified by the pole;

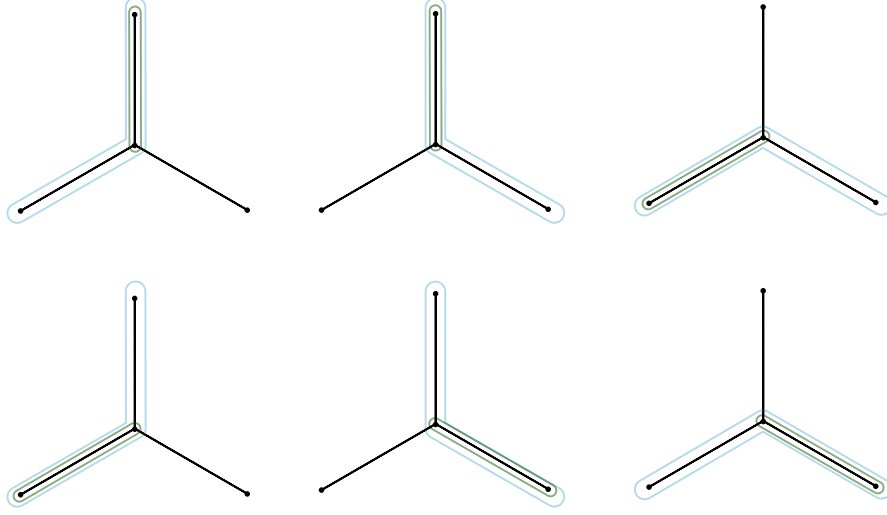


Figure 2.4: The diagrammatic representation of all the six terms contributing to the four-site star graph. The graph has the external states amputated and we omitted the single site tubes as well as the total energy tube.

- all its highest codimension singularities have the same normalisation, up to a sign;

It turns out that the canonical function  $\Omega(\mathcal{Y}, \mathcal{P}_{\mathcal{G}})$  is the wavefunction universal integrand associated to the graph  $\mathcal{G}$ :

$$\Omega(\mathcal{Y}, \mathcal{P}_{\mathcal{G}}) = \psi_{\mathcal{G}}(x, y). \quad (2.37)$$

Then the boundaries of  $\mathcal{P}_{\mathcal{G}}$  are associated to the residues of  $\psi_{\mathcal{G}}(x, y)$ . As the boundaries of  $\mathcal{P}_{\mathcal{G}}$  are identified by the co-vectors  $\mathcal{W}^{(\mathfrak{g})}$ , the canonical function  $\Omega(\mathcal{Y}, \mathcal{P}_{\mathcal{G}})$  can be generically written as

$$\Omega(\mathcal{Y}, \mathcal{P}_{\mathcal{G}}) = \frac{\mathbf{n}_{\delta}(\mathcal{Y})}{\prod_{\mathfrak{g} \subseteq \mathcal{G}} q_{\mathfrak{g}}(\mathcal{Y})} \quad (2.38)$$

where  $\mathbf{n}_{\delta}(\mathcal{Y})$  is a homogeneous polynomial in  $\mathcal{Y}$  of degree  $\delta$ . From a geometrical perspective, it provides the locus of the intersection of the hyperplanes  $\{\mathcal{W}^{(\mathfrak{g})}, \mathfrak{g} \subseteq \mathcal{G}\}$  *outside* of  $\mathcal{P}_{\mathcal{G}}$  [79, 195]. Said differently, it is determined by the set of vanishing multiple residues of (2.38), which determine the compatibility condition from the facets (*i.e.* which intersection among the facets form a higher codimension face), and, from a physics perspective, they determine Steinmann-like relations [79, 193]. The degree of the numerator is fixed by projectivity: the differential form defined by equipping the canonical function (2.38) with the canonical measure of  $\mathbb{P}^{n_s+n_e-1}$ , *i.e.*  $\langle \mathcal{Y} d^{n_s+n_e-1} \mathcal{Y} \rangle$ , is invariant under  $\text{GL}(1)$  rescaling, fixing the degree  $\delta$  of  $\mathbf{n}_{\delta}$  in terms of the number of facets  $\tilde{\nu}$  of  $\mathcal{P}_{\mathcal{G}}$  and the dimension of projective space:  $\delta = \tilde{\nu} - n_s - n_e$ . The locus  $\mathbf{n}_{\delta} = 0$  is the *adjoint* of  $\mathcal{P}_{\mathcal{G}}$ , and its *maximal subspaces* identified by the intersections of the hyperplanes containing the facets of  $\mathcal{P}_{\mathcal{G}}$  outside  $\mathcal{P}_{\mathcal{G}}$  such that *no vertex* of  $\mathcal{P}_{\mathcal{G}}$  lies on the intersection, can be used to triangulate  $\mathcal{P}_{\mathcal{G}}$  via a collection of polytopes  $\{\mathcal{P}_{\mathcal{G}}^{(i)}, i = 1, \dots, m\}$  whose elements' facets are all facets

of  $\mathcal{P}_{\mathcal{G}}$  [195]. In terms of the canonical function, this reflects into its partial fractioning into the sum of the canonical functions of all the elements of the collection  $\{\mathcal{P}_{\mathcal{G}}^{(i)}, i = 1, \dots, m\}$ , without introducing spurious poles<sup>1</sup>:

$$\Omega(\mathcal{Y}, \mathcal{P}_{\mathcal{G}}) = \sum_{j=1}^m \Omega(\mathcal{Y}, \mathcal{P}_{\mathcal{G}}^{(j)}) = \prod_{\mathfrak{g} \in \mathcal{G}_o} \left[ \frac{1}{q_{\mathfrak{g}}(\mathcal{Y})} \right] \sum_{\{\mathcal{G}_c\}} \prod_{\mathfrak{g}' \in \mathcal{G}_c} \left[ \frac{1}{q_{\mathfrak{g}'}(\mathcal{Y})} \right], \quad (2.39)$$

where  $\mathcal{G}_o$  is one of the maximal subspaces of the adjoint,  $\mathcal{G}_c$  is a set of compatible graphs – *i.e.* graphs that identifies singularities such that the sequential residue of the canonical function along them is non-zero – disjoint from  $\mathcal{G}_o$ , and the sum runs over all possible of these subsets. Such triangulations, triangulate a cosmological polytope using an external lower-dimensional hyperplane, identified by the intersections of the codimension-1 hyperplanes corresponding to the elements of  $\mathcal{G}_o$ , without introducing spurious boundaries. Triangulations that only use the vertices of  $\mathcal{P}_{\mathcal{G}}$ , introduce spurious boundaries, translating into spurious poles in the partial fraction of the canonical function [83, 86, 196].

There is a generalisation of this construction – the *generalised cosmological polytopes* – which has a rational function associated to it with multiple poles [189, 197]: this rational function has still the form (2.38) but with multiple poles, and its singularities are still associated to subgraphs.

A further generalisation – the *weighted cosmological polytope*  $\mathcal{P}_{\mathcal{G}}^{(w)}$  – has additional boundaries, with the special feature that both the half-planes identifies by the polynomial associated to it,  $q_{\mathfrak{g}_e}(\mathcal{Y})$  intersect the geometry [194]. This type of boundary is named *internal boundary* [194, 198]. In the system of local coordinates associated to the weights of the graph, the internal boundaries are given by  $\{q_{\mathfrak{g}_e}(\mathcal{Y}) := \mathcal{Y}^I \widetilde{\mathcal{W}}^{(\mathfrak{g}_e)} = y_e, e \in \mathcal{E}\}$ . The canonical function associated to a weighted cosmological polytope  $\mathcal{P}_{\mathcal{G}}^{(w)}$  provides the universal integrand for the cosmological correlator associated to the graph  $\mathcal{G}$ :

$$\Omega(\mathcal{Y}, \mathcal{P}_{\mathcal{G}}^{(w)}) = \mathcal{C}_{\mathcal{G}}(x, y) \quad (2.40)$$

We will not go into any further details for any of these constructions. But ultimately it should be clear that the cosmological polytope, being defined as the region bounded by the hyperplane inequalities that are given directly by the singularities, in turn corresponding to the sum of energies entering a sub-process of the diagram in question, fully defines the integrand of the wavefunction. Later in the thesis we will see a different combinatorial formulation of the integrand, which encompasses the full wavefunction at once.

## 2.4 Cosmological Correlators

The perturbative expansion of the Bunch-Davies wavefunction (2.8), and its diagrammatic rules, together with the Born rule, allow extracting diagrammatic rules for the correlation

---

<sup>1</sup>Recall that the singularities are associated to the facets of the polytope: if the facets of each  $\mathcal{P}_{\mathcal{G}}^{(i)}$  are facets of  $\mathcal{P}_{\mathcal{G}}$ , then each of the terms of the partial fraction shows only singularities which are also singularities of the wavefunction.

functions in terms of wavefunction graphs [80, 194]. First, a  $n$ -point cosmological correlator at  $L$ -loops can be written as

$$\langle \prod_{j=1}^n \Phi(\vec{p}_j) \rangle = \prod_{j=1}^n \frac{1}{2\text{Re}\{\psi_2(E_j)\}} \sum_{\mathcal{G} \in \mathcal{G}_n^{(L)}} \tilde{\mathcal{C}}_{\mathcal{G}}, \quad (2.41)$$

where  $\mathcal{G}_n^{(L)}$  is the set of graphs at  $L$ -loops with  $n$  external states, and  $\mathcal{C}_{\mathcal{G}}$  is computed by summing (twice the real part of) the wavefunction coefficient  $\psi_{\mathcal{G}}$  associated to the graph  $\mathcal{G}$  with the contribution coming from all the possible ways of the edges and replacing them with the inverse of the real part of two-point wavefunction  $\psi_2$ . The edge deletion operation and replacement by  $\psi_2$ , can be graphically represented as a dash on the relevant edge  $\text{---}|$ : then a cosmological correlator can be obtained by summing over all the possible graph topologies with a fixed number of external states  $n$  and at a given loop order  $L$  as well as over all the possible ways of dashing the edges of each of these graphs. The function  $\tilde{\mathcal{C}}_{\mathcal{G}}$ , which we will refer to simply as *correlator*, can then be written in terms of wavefunction graphs as

$$\tilde{\mathcal{C}}_{\mathcal{G}} = \sum_{j=0}^{n_e} \sum_{\{\mathcal{G}_j\}} \psi_{\mathcal{G}_j} \quad (2.42)$$

where  $\mathcal{G}_j$  is the graph  $\mathcal{G}$  with  $j$  edges deleted<sup>2</sup>,  $\{\mathcal{G}_j\}$  is the set whose elements are given by all the possible ways of deleting  $j$  edges from  $\mathcal{G}$ , and  $\psi_{\mathcal{G}_j}$  are the wavefunction coefficients associated to  $\mathcal{G}_j$  – as  $\mathcal{G}_j$  can be either connected or disconnected,  $\psi_{\mathcal{G}_j}$  can represent either contributions coming from connected and disconnected graphs.

We can now compute the contribution of the second diagram in figure 2.1 to the respective four point correlator for the massless field in flatspace is:

$$\langle \Phi_1 \Phi_2 \Phi_3 \Phi_4 \rangle = \frac{\lambda_3^2}{8k_1 k_2 k_3 k_4} \left( \psi_4^{(0)} + \frac{\psi_3^{(0)}(k_1, k_2, |\vec{k}_1 + \vec{k}_2|) \psi_3^{(0)}(k_3, k_4, |\vec{k}_1 + \vec{k}_2|)}{|\vec{k}_1 + \vec{k}_2|} \right) \quad (2.43)$$

where the wavefunction coefficients corresponding  $\psi_3^{(0)}$ , and  $\psi_4^{(0)}$  have been computed in (2.19) and (2.20), respectively. Here we are considering only the  $s$ -channel contribution, the other contributions follow the same structure, and we dropped the momentum conserving delta function.

## 2.5 Parametrizing with Sub-polygons

In this section, we discuss an alternative way to tubes and tubings for the representation of the singularities of the wavefunction. In order to do this we need to introduce the concept of momentum polygon. In general, in many of the systems one is considering in quantum field theory there is momentum conservation. For scattering amplitudes we have four-momentum conservation, and for the wavefunction we have spatial momentum conservation

<sup>2</sup>Hence  $\mathcal{G}_0 = \mathcal{G}$  and  $\mathcal{G}_{n_e}$  is the disconnected graph given by the union of all the sites of  $\mathcal{G}$

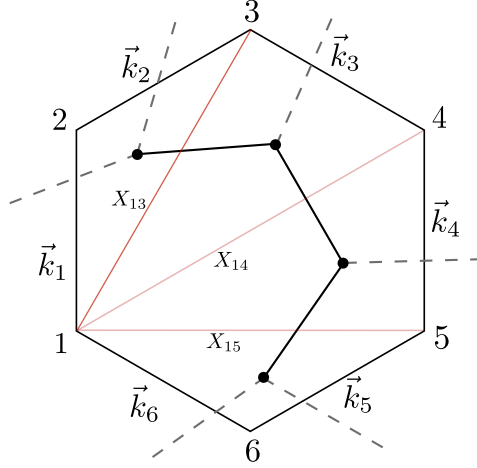


Figure 2.5: Momentum polygon for a six particle process.

(3-momentum). Then, a very trivial exercise one can make is to draw all momenta vector as a sum of vectors. It is clear that this sum should close in a polygon, which we will call momentum polygon. This object is useful since we can say that its triangulations are dual to a Feynman graph with cubic vertices. In general, by considering poly-angulations one can get the dual representation to Feynman graphs with general polynomial interactions. For our purposes, we will just consider cubic theories when discussing the momentum polygon. To see this duality, one simply needs to triangulate the momentum polygon and associate a node to each triangle, connect the nodes between themselves and finally, draw a line from the node that crosses the external cords of the triangles (cords which are part of the original momentum polygon). An example of this is in figure 2.5.

Now that we have established the definition of the momentum polygon, and in what sense it is dual to a Feynman graph, we can see that it tells us about natural variables to parametrize the wavefunction. These variables are the perimeters of the sub-polygons in the momentum polygons. If we label a sub-polygon by the numbers of the vertices it contains (see fig. 2.5), the perimeter will be  $\mathcal{P}_{i\dots j}$ . For example, the triangle sub-polygons in figure 2.5, will be:

$$\begin{aligned} \mathcal{P}_{123} &= |\vec{k}_1| + |\vec{k}_2| + |\vec{k}_1 + \vec{k}_2|, & \mathcal{P}_{134} &= |\vec{k}_1 + \vec{k}_2| + |\vec{k}_3| + |\vec{k}_1 + \vec{k}_2 + \vec{k}_3|, \\ \mathcal{P}_{145} &= |\vec{k}_1 + \vec{k}_2 + \vec{k}_3| + |\vec{k}_4| + |\vec{k}_5 + \vec{k}_5|, & \mathcal{P}_{1345} &= |\vec{k}_5| + |\vec{k}_6| + |\vec{k}_5 + \vec{k}_6|. \end{aligned}$$

But we can keep going, and consider larger sub-polygons, for example squares and pentagons:

$$\mathcal{P}_{1345} = |\vec{k}_1 + \vec{k}_2| + |\vec{k}_3| + |\vec{k}_4| + |\vec{k}_5 + \vec{k}_6|, \quad \mathcal{P}_{12345} = |\vec{k}_1| + |\vec{k}_2| + |\vec{k}_3| + |\vec{k}_5| + |\vec{k}_5 + \vec{k}_6|.$$

At this point, it should be clear that the perimeters precisely match the singularities of the integrand of the wavefunction. This is generally true, to each singularity of the wavefunction one can find a representation in terms of a perimeter of sub-polygon in the

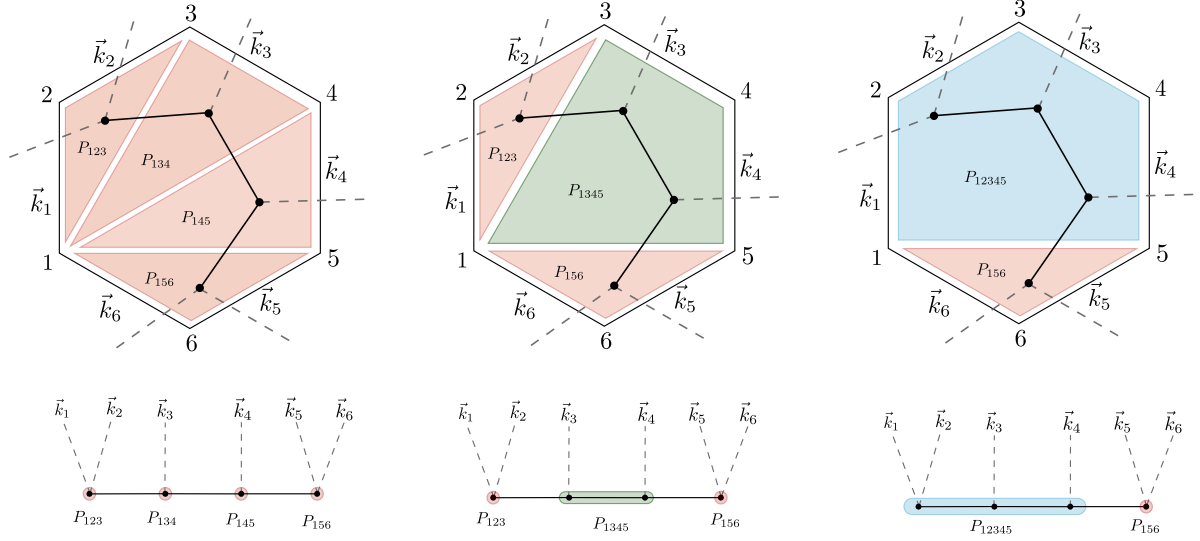


Figure 2.6: Sub-polygons of the momentum polygon and their perimeters, below there is the direct correspondence in terms of tubings.

momentum polygon of interest. Therefore, there is also a direct correspondence between tubes of the graph and perimeters of sub-polygons. This is illustrated in figure 2.6. The triangles are equivalent to single site tubes, squares are equivalent to tubes which enclose two nodes, pentagons equivalent to tubes which enclose three nodes, and so on. Naturally, one can then re-define the concept of tubings/russian-dolls. Now a tubing is now defined to be a maximal set of non-overlapping sub-polygons (where non-overlapping has the same definition as before, two polygons are either disjoint or one is fully contained in the other). And the full wavefunction is defined to be the sum over all of these sets (see figure 2.7). Mathematically, we can write:

$$\Psi = \sum_{\mathbf{P}} \prod_{P \in \mathbf{P}} \frac{1}{\mathcal{P}_P}. \quad (2.44)$$

So far we have given more emphasis to the tree-level case, but all of the above discussion extends to all loops. Already at tree-level, we can replace the momentum  $n$ -gon by a disk with  $n$  marked points on the boundary (following the appropriate color-ordering), and where each boundary component is assigned a momentum  $\vec{k}_i$ . The subpolygons were then defined by collections of boundary edges and internal chords, whose perimeter was just the sum of the length of each of these. In the disk case, the subpolygons correspond to subsurfaces bounded by boundary components as well as internal curves going from marked points to marked points. We can determine the perimeter of the subsurfaces as the sum of the absolute values of the curves/boundary components bounding the subsurface, where the momentum associated to a given curve is read by *homology*. But as with the story of “surface kinematics” [107] for amplitudes on surfaces, it is fruitful to think of more general kinematic variables associated with the curve on the surface (in general, up to *homotopy*),

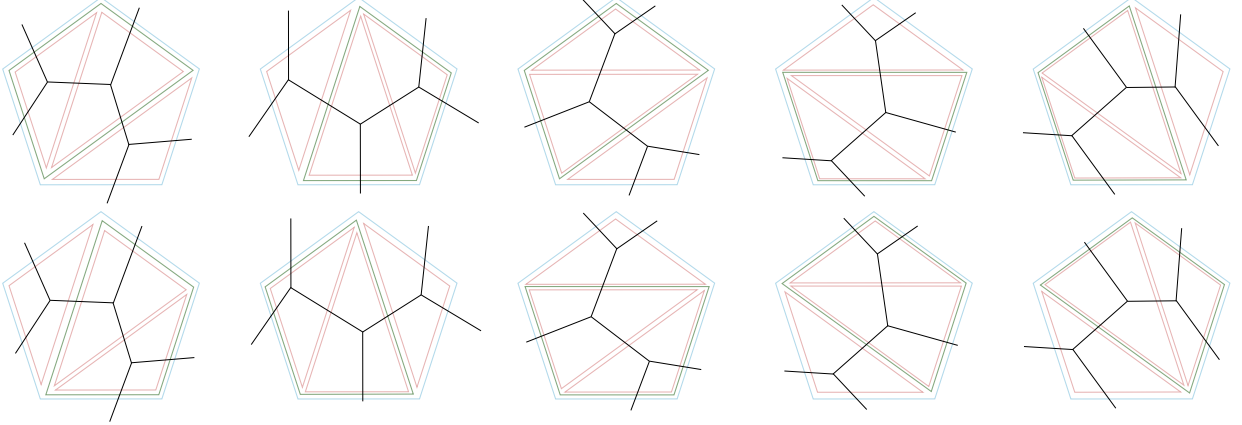


Figure 2.7: Five-point wavefunction in terms of russian dolls from sub-polygons.

instead of relating it to a set of momenta. In the context of the wavefunction at tree-level, this means that we can think of the perimeters of each subpolygon as independent variables.

At  $n$ -points one-loop, the surface we get is instead a punctured disk with  $n$ -marked points. In this case, to provide a basis of homology on top of assigning momentum to the boundary components of the disk, we also have to give momentum to one of the curves starting in a boundary marked point and ending on the puncture – this corresponds to the spatial *loop momentum*. Once we have done this, we can again read off the momentum of any curve,  $\vec{k}_C$ , on the surface by homology. Finally, just like at tree-level, we can list all possible cubic graphs by considering all the possible triangulations of the punctured disk, and the wavefunction is then given as a sum over all russian dolls – which are now maximal collections of non-overlapping subsurfaces – where to each subsurface we get a factor of its perimeters – the sum of  $|\vec{k}_C|$  for each curve  $C$  bounding the subsurface. The same picture holds at all orders in the topological expansion, where for each order we have a different surface. And again, we will consider more general kinematic variables for the wavefunction as being labelled by subsurfaces of the surface bounded by curves up to homotopy, which can be specialized to the perimeters when written in terms of momenta determined by homology. Most of this note will focus on the tree-level wavefunction, but in section 5.4 we explain how our results extend to loop-level.

Finally, there is an obvious recursive expression for the wavefunction [199], trivially generalizing the recursive expression as a sum over cuts for single graphs given in [31]. We can phrase this at any loop order in terms of the perimeters  $\mathcal{P}_S$  for any surface  $S$ , as

$$\Psi_S = \frac{1}{\mathcal{P}_S} \sum_{\text{curves } C} \Psi_{S/C} \quad (2.45)$$

where we sum over all curves  $C$ , and  $S/C$  is the simpler surface obtained by cutting  $S$  along  $C$ . Since every  $\mathbf{P}$  includes the triangles of a triangulation, we can also write this as a sum over all diagrams/triangulations  $T$ , together with a sum over all the “russian dolls”



associated with the diagram  $R_T$ , as

$$\Psi = \sum_T \sum_{R_T} \prod_{P \subset R_T} \frac{1}{\mathcal{P}_P}. \quad (2.46)$$

It should be clear the advantage of defining singularities in terms of sub-polygons instead of tubes, the momentum polygon provides a platform to discuss different graphs. Later in the thesis this will allow us to find combinatorial structures for the sum of graphs.

### 2.5.1 Flat Space $\rightarrow$ Cosmological Wavefunction

As explained above, for the case where the cubic coupling has some general time-dependence  $\lambda_3(\eta)$ , it is useful to analyze each Fourier mode,  $\lambda_3(\varepsilon)$ , separately. In which case, for each cubic vertex,  $\lambda_3(\varepsilon)$  produces a shift in the energies entering the vertex by  $\varepsilon$ . So, for a general graph, we have that the energies associated to each cubic vertex are shifted by the energies  $\varepsilon_i$  associated to the couplings. This can be rephrased in terms of the perimeters of subpolygons as follows: the perimeters associated to the triangles,  $t_i$  entering the triangulation are shifted by the respective energy,  $\mathcal{P}_{t_i} \rightarrow \mathcal{P}_{t_i} + \varepsilon_i$ , and for a generic subpolygon,  $P$ , we have  $\mathcal{P}_P \rightarrow \mathcal{P}_P + \sum_{t_i \subset P} \varepsilon_i$ .

Therefore, having obtained the wavefunction for a single graph,  $G$ , it is easy to obtain the corresponding cosmological wavefunction, in the following way

$$\Psi_G^{\text{Cosm}} = \int_{-\infty}^{\infty} \left( \prod_{\text{triangles } t_i} d\varepsilon_i \lambda_3(\varepsilon_i) \right) \Psi_G^{\text{Flat}} \left( \mathcal{P}_P \rightarrow \mathcal{P}_P + \sum_{t_i \subset P} \varepsilon_i \right), \quad (2.47)$$

where we associate a shift  $\varepsilon_i$  with all the  $(n-2)$  triangles  $t_i$  in the triangulation, and shift every perimeter  $\mathcal{P}_P$  of a sub-polygon  $P$  by the sum of the  $\varepsilon_i$  for all the triangles  $t_i$  contained in  $P$ , as described earlier. The precise form of  $\lambda_3(\varepsilon)$  depends on the time-dependence that we are interested in studying, but already here we see that the combinatorics associated to the flat-space wavefunction coefficients port literally to those of the cosmological wavefunction, with the difference that for the latter we need to further perform this shift and integral.

We can now describe the same procedure for the full wavefunction, given by the sum over all graphs. The obvious challenge is that the shifts  $\varepsilon_i$  seem to be different from graph-to-graph, and this doesn't give us a universal  $(n-2)$  dimensional " $\varepsilon$  integrand" we simply integrate to get the cosmological wavefunction.

Fortunately, there is a beautiful solution to this problem, which also arose in labeling general interactions for colored Lagrangians in [200]. Let us choose a base triangulation that defines our surface, and label the triangles in this base triangulation as  $(t_1, \dots, t_N)$ . Then, as explained in [200], *every other triangle* on the surface is canonically associated with *one* of these  $t_i$ . In a similar way, any subpolygon  $P$  is associated with a collection of triangles,  $T_i$ , that triangulate it, that can ultimately map it to a collection of triangles in the base triangulation. Therefore, having made a choice of base triangulation, we can

unambiguously associate a  $\varepsilon_i$  shift to every subpolygon, and we find

$$\Psi^{\text{Cosm}} = \int_{-\infty}^{\infty} \left( \prod_{\text{triangles } t_i} d\varepsilon_i \lambda_3(\varepsilon_i) \right) \Psi^{\text{Flat}} \left( \mathcal{P}_P \rightarrow \mathcal{P}_P + \sum_{T_i \subset P} \lambda_i \right) \quad (2.48)$$

where here we can choose any triangulation of the subpolygon  $P$  we like, as the sum  $\sum_{T_i \subset P} \lambda_i$  will be the same for all of them.

# Chapter 3

## Perturbative Structure of Cosmological Observables

In this chapter we develop a formalism to compute cosmological observables as an expansion in the appropriate analytic regulator. We start by defining cosmological integrals as large class of integrals where the integrand is given by the canonical form of the cosmological polytope, defined in the previous chapter, and a measure which is where we turn most of our attention in the beginning of the chapter. In particular, with this formalism we are interested in the leading terms of the expansion, which account for the divergent parts. We make use of this formalism in order to find infrared finite computables, which is described towards the end of the chapter.

### 3.1 Cosmological Integrals

In this section, we define cosmological integrals. We have shown in the previous section how the wavefunction can be computed perturbatively in terms of wavefunction coefficients, which in turn are integrals over rational functions. We have also seen that cosmological correlators, which are the objects closest to our observables, can be computed as functions of these wavefunction coefficients. Therefore, there is a large class of integrals which are important in the study of cosmological observables in inflation, we call them *cosmological integrals*. Most of the examples so far, have been focused on the integrand of cosmological integrals, and also mostly up to tree level. However, when we want to consider loop level contributions, we need to parameterize these integrals, and it turns out the measure and integration region require some careful attention. Thus, the next sub-section is focused on describing in full generality this class of integrals, both at tree- and loop-level.

A general graph  $\mathcal{G}$  contributing to the perturbative observables has associated an integral, whose general form – irrespectively of the topology of  $\mathcal{G}$  – is given by

$$\mathcal{I}_{\mathcal{G}}[\alpha, \beta; \mathcal{X}] = \int_{\mathbb{R}_+^{n_s}} \prod_{s \in \mathcal{V}} \left[ \frac{dx_s}{x_s} x_s^{\alpha_s} \right] \int_{\Gamma} \prod_{e \in \mathcal{E}^{(L)}} \left[ \frac{dy_e}{y_e} y_e^{\beta_e} \right] \mu_d(y_e; \mathcal{X}) \frac{\mathbf{n}_{\delta}(z, \mathcal{X})}{\prod_{\mathfrak{g} \subseteq \mathcal{G}} [q_{\mathfrak{g}}(z, \mathcal{X})]^{\tau_{\mathfrak{g}}}} \quad (3.1)$$

where  $z := (x, y)$  is a vector whose entries are given by the integration variables  $x := (x_s)_{s \in \mathcal{V}}$  and  $y := (y_e)_{e \in \mathcal{E}^{(L)}}$ ;  $\mathcal{X}$  indicates the set of rotational invariants parametrising the kinematic space;  $\mathcal{E}^{(L)} \subseteq \mathcal{E}$  is the subset of the edges of the graph  $\mathcal{G}$  associated to loops<sup>1</sup>, the integrations over  $\{y_e | e \in \mathcal{E}^{(L)}\}$  parametrise the loop integration in terms of, at most,  $n_e^{(L)} := \dim\{\mathcal{E}^{(L)}\}$   $y$ -variables,  $\mu_d(y_e)$  is the measure of integration which turns out to be always positive within the domain of integration  $\Gamma$  and zero at its boundaries; the set of parameters,

$$\left\{ \sigma := (\alpha, \beta) \in \mathbb{R}^n \mid \alpha := (\alpha_s)_{s \in \mathcal{V}}; \beta := (\beta_e)_{e \in \mathcal{E}^{(L)}}, n := n_s + n_e^{(L)} \right\}$$

depend on the cosmology as well as on the states at the site  $s_j$  (for  $\alpha$ ), and on those propagating along the loop edges (for  $\beta$ );  $q_{\mathbf{g}}(z, \mathcal{X})$  is a linear polynomial associated to the subgraph  $\mathbf{g}$ ,

$$q_{\mathbf{g}}(z, \mathcal{X}) = \sum_{s \in \mathcal{V}_{\mathbf{g}}} x_s + \sum_{e \in \mathcal{E}_{\mathbf{g}, L}^{\text{ext}}} y_e + \mathcal{X}_{\mathbf{g}}, \quad \mathcal{X}_{\mathbf{g}} := \sum_{s \in \mathcal{V}_{\mathbf{g}}} X_s + \sum_{e \in \mathcal{E}_{\mathbf{g}, 0}^{\text{ext}}} y_e, \quad (3.2)$$

$\tau_{\mathbf{g}}$  is generally an integer number associated to the subgraph  $\mathbf{g}$  whose value depends on the states propagating along the edges;  $\mathbf{n}_{\delta}(z, \mathcal{X})$  is a polynomial of degree  $\delta < \tau := \sum_{\mathbf{g} \subseteq \mathcal{G}} \tau_{\mathbf{g}} - i.e.$  the integrand vanishes as  $z^{-(\tau-\delta)}$  as  $z \rightarrow +\infty$  – which is fixed by compatibility conditions among the subgraphs  $\mathbf{g}$  [193].

An important aspect of cosmological integrals is that the integrand is always non-negative in the integration contour. The rational function which comes from the cosmological polytope, where the singularities,  $q_{\mathbf{g}}$ , are linear polynomials with positive coefficients. This clearly never becomes singular unless the integration variables are either made to be very large, or very small, since from the contour of integration they are always non-negative as well. The measure  $\mu_d$  turns out to also be always positive by definition, as we will see below, since the region of integration will be defined to be the region where  $\mu_d$  is positive. And as we will see,  $\mu_d$  is just the volume of a simplex raised to a half-integer power, and the region of integration  $\Gamma$ , is given by demanding that the volume is non-negative. So at most, our integrand will become singular at the boundaries of the region of integration. This is a very important point, as we will see it allows us to use Newton polytopes to fully capture the divergent regions of a cosmological integrals. Then, natural regularisation parameters for the integral (3.1) are given by suitably analytic continuing the parameters  $(\alpha, \beta, \tau)$  in the spirit of analytic regularisation [201]<sup>2</sup>.

In the next sections, we will be concerned with the study of the infra-red/ultraviolet behaviour of the class of integrals (3.1), which need to be regularised. Such a regularisation is implemented by analytically continuing the parameter vector  $\sigma$ , as well as  $\tau_{\mathbf{g}}$ , to arbitrary complex values [201], and also consider the suitable  $i\epsilon$ -prescription – for an extended discussion, see [202]. The infrared regions for physical kinematics are obtained for large

<sup>1</sup>Said differently, there is no integration over the  $y$ -variables associated to purely tree subgraph. These  $y$ -variables instead parametrise the angles among external states.

<sup>2</sup>This usually comes with the introduction of a regularisation scale. We will be sloppy with it, as we will just focus on the analysis itself of the asymptotic behaviour of the cosmological integrals.

$x_s$ 's and/or small  $y_e$ 's – importantly, as we will see later on, at most  $L$  edge variables, associated to different loops, can be taken to be simultaneously small.

Before digging into the infra-red/ultraviolet behaviour of (3.1), there is one more ingredient that deserves a bit of discussion: the loop integration measure  $\mu_d(y, \mathcal{X})$  and the loop integration contour  $\Gamma$ . They turn out to have a beautiful geometrical interpretation.

A cosmological integral of the form (3.1) is the Mellin transform<sup>3</sup> over the  $x$ -variables, and the integral over the space of loop  $y$ -variables of a rational function, which is the canonical function of a cosmological polytope [83], generalised cosmological polytope [197] or a weighted cosmological polytope [194]. Its numerator  $\mathbf{n}_\delta(z, \mathcal{X})$  being the adjoint surface of the relevant geometry, and the denominators  $\{q_{\mathfrak{g}}(z, \mathcal{X}), \mathfrak{g} \subseteq \mathcal{G}\}$  identify their boundaries and are associated to the subgraphs  $\{\mathfrak{g}, \mathfrak{g} \subseteq \mathcal{G}\}$ . It turns out that the loop measure  $\mu_d(y_e, \mathcal{X})$  and the loop contour of integration have an interesting geometrical interpretation.

Let us begin with considering  $\mathcal{G}$  to be a one-loop graph. For  $d \geq n_e^{(1)}$ , the standard measure  $d^d l$  in loop space can be then written in terms of  $\vec{l}^2$  as well as  $n_e^{(1)} - 1$  scalar products  $(\vec{l} \cdot \vec{q}_j)$ , where the vectors  $\vec{q}_j$ 's are a basis in the space spanned by the  $n_e^{(1)} - 1$  linearly independent momenta at each site of the graph. This decomposition can be obtained by splitting the loop momentum vector,  $\vec{l}$ , into a component which is parallel to the vector space generated by the external momenta,  $\vec{q}_i$ , and another component which is perpendicular to this space. Then, the measure relative to the perpendicular component can be treated in terms of spherical coordinates, where the norm of the perpendicular component can be given as the square root of the ratio of the volume of the simplex formed by the full loop momentum vector and the external momenta vectors, and the volume of the simplex formed just by the external momenta vectors. These volumes can be computed in terms of Gram determinants. The measure of the parallel part can be computed by changing variables into the axes formed by the external momenta vectors. These axes, in general, do not form an orthonormal basis of the vector space they generate, thus the measure requires a normalisation given as a volume of the simplex formed by the vectors of the external momenta. This is again given by a Gram determinant. Then, our integration variables are thus the scalar products of loop momenta and the external momenta, which can be linearly related to the square of the  $y$ -variables in the loop. Thus, the full Jacobian of this change of variable is given in terms of a Gram-determinant in momentum space

$$d^d l = dV_{d-n_e^{(1)}} \prod_{e \in \mathcal{E}^{(1)}} [dy_e^2] [G(\vec{q}_1, \dots, \vec{q}_{n_e^{(1)}-1})]^{-\frac{1}{2}} \left[ \frac{G(\vec{l}, \vec{q}_1, \dots, \vec{q}_{n_e^{(1)}-1})}{G(\vec{q}_1, \dots, \vec{q}_{n_e^{(1)}-1})} \right]^{\frac{d-n_e^{(1)}-1}{2}}, \quad (3.3)$$

where  $dV_{d-n_e^{(1)}}$  is the volume form for a  $(d - n_e^{(1)})$ -dimensional sphere, and  $G(\vec{v}_1, \dots, \vec{v}_n)$  is the Gram determinant whose  $(i, j)$ -entry is given by  $\vec{v}_i \cdot \vec{v}_j$ . The contour integration  $\Gamma$  can

<sup>3</sup>Let us stress that the appearance of an  $n_s$ -dimensional Mellin transform is just a consequence of the choice of focusing on power-law cosmologies – the measure of integration is related to the choice of cosmologies

be expressed as a positivity condition on the Gram determinants

$$\Gamma = \frac{G(\vec{l}, \vec{q}_1, \dots, \vec{q}_{n_e^{(1)}-1})}{G(\vec{q}_1, \dots, \vec{q}_{n_e^{(1)}-1})} \geq 0. \quad (3.4)$$

As a basis for the space spanned by the external momenta at the sites of  $\mathcal{G}$ , let us take

$$\left\{ \vec{q}_j = \vec{P}_{2\dots j+1} := \sum_{k=2}^{j+1} \vec{p}_k, j = 1, \dots, n_e^{(1)} - 1 \right\}. \quad (3.5)$$

Interestingly, the integration variables in  $\mathcal{I}_{\mathcal{G}}$  parametrise precisely the scalar products among the loop momentum and the external ones, and allow writing each Gram determinant in terms of a Cayley-Menger determinant

$$G(\vec{l}, \vec{q}_1, \dots, \vec{q}_{n_e^{(1)}-1}) = (-1)^{n_e^{(1)}+1} \text{CM}(y_{i,i+1}^2, P_{2\dots j+1}^2) \quad (3.6)$$

where,

$$\text{CM}(y_{i,i+1}^2, P_{2,j+1}^2) = \begin{vmatrix} 0 & 1 & 1 & 1 & \dots & 1 & \dots & 1 \\ 1 & 0 & y_{12}^2 & y_{23}^2 & \dots & y_{i,i+1}^2 & \dots & y_{n_e^{(1)},1}^2 \\ 1 & y_{12}^2 & 0 & P_2^2 & \dots & P_{2\dots i}^2 & \dots & P_{2\dots n_e^{(1)}}^2 \\ 1 & y_{23}^2 & P_2^2 & 0 & \dots & P_{3\dots i}^2 & \dots & P_{3\dots n_e^{(1)}}^2 \\ \vdots & \vdots & \vdots & \vdots & \dots & \vdots & \dots & \vdots \\ 1 & y_{n_e^{(L)},1}^2 & P_{2\dots n_e^{(1)}}^2 & P_{3\dots n_e^{(1)}}^2 & \dots & P_{i+1\dots n_e^{(1)}}^2 & \dots & 0 \end{vmatrix}, \quad (3.7)$$

with  $P_{s_j} = X_{s_j}$  if there is just one external state at the site  $s_j$ . The Gram determinant is given by  $G(\vec{q}_1, \dots, \vec{q}_{n_e^{(1)}-1}) = (-1)^{n_e^{(1)}} \text{CM}^{(2,2)}$ , where the index indicates the  $(2,2)$ -minor of the Cayley-Menger determinant (3.7). The condition (3.4) is just the statement that the space is Euclidean. From the perspective of the Cayley-Menger determinant, the Euclidean space condition is reflected into the matrix (3.7) being a matrix with non-negative entries which can be associated to Euclidean distances. The determinant (3.7) is therefore proportional to the squared volume of a  $n_e$ -dimensional simplex  $\Sigma_{n_e^{(1)}}$  whose squared side lengths are given by the non-zero entries, with the condition that the squared volume is positive [203]

$$(-1)^{n_e^{(1)}+1} \text{CM}(y_{i,i+1}^2, P_{2\dots j+1}^2) = (n_e^{(1)}!)^2 \text{Vol}^2\{\Sigma_{n_e^{(1)}}\} \geq 0 \quad (3.8)$$

Another way of stating that the space is Euclidean, is that the distance matrix  $D$ , defined as  $D := \{D_{ij}, i, j = 1, j = 1, \dots, n_e + 1 \mid D_{ij} := \sqrt{\text{CM}_{ij}^{(1,1)}} \geq 0\}$ , is embeddable in Euclidean space. Let  $\mathcal{I}_k$  and  $\mathcal{J}_k$  be a set of  $n_e^{(1)} - k$  rows and a set of  $n_e^{(1)} - k$  columns of CM in (3.7), then a necessary and sufficient condition for the associated matrix  $D$  to be embeddable in Euclidean space is that for all sets  $\mathcal{I}_k$  and  $\mathcal{J}_k$  and for all  $k = 1, \dots, n_e^{(L)}$  then

$$(-1)^{k+1} \text{CM}^{(\mathcal{I}_k, \mathcal{J}_k)} \geq 0 \quad (3.9)$$

$\text{CM}^{(\mathcal{I}_k, \mathcal{J}_k)}$  is the minor of CM obtained from the latter erasing the rows in  $\mathcal{I}_k$  and the columns in  $\mathcal{J}_k$  [203]. Recalling that  $G(\vec{q}_1, \dots, \vec{q}_{n_e^{(1)}}) = (-1)^{n_e^{(1)}} \text{CM}^{(2,2)}$ , then the embeddability of  $D$  in Euclidean space guarantees (3.4). Said differently, the integration region is given by the non-negativity condition on the volume of a  $n_e$ -simplex with side lengths given by the non-zero entries of the distance matrix  $D$ .

The boundary of the integration region is given by the vanishing of the Cayley-Menger determinant, *i.e.* by the condition that the volume of  $\Sigma_{n_e}$  vanishes. This implies that the vertices of  $\Sigma_{n_e^{(1)}}$  lie in a proper affine subspace of  $\mathbb{R}^{n_e^{(1)}}$  [203]. The Cayley-Menger determinant is in general an irreducible multivariate polynomial, except for  $n_e^{(1)} = 2$  [204]. The integral (3.1) can then be rewritten as

$$\mathcal{I}_{\mathcal{G}} = \mathbf{c}_{d, n_e^{(1)}} \int_{\mathbb{R}^{n_s} \cup \Sigma_{n_e^{(1)}}} \left[ \frac{dz}{z} \right] \left[ \frac{\text{Vol}^2\{\Sigma_{n_e^{(1)}}(y, P_{2\dots j})\}}{\text{Vol}^2\{\Sigma_{n_e^{(1)}-1}(P_{2\dots j})\}} \right]^{\frac{d-n_e^{(1)}-1}{2}} \frac{\mathbf{n}_{\delta}(z, \mathcal{X})}{\prod_{\mathfrak{g} \subseteq \mathcal{G}} [q_{\mathfrak{g}}(z, \mathcal{X})]^{\tau_{\mathfrak{g}}}} \quad (3.10)$$

where the overall factor  $\mathbf{c}_{d, n_e^{(1)}}$  is a function of the external data  $P_{2\dots j}^2$  and its explicit expression is given by

$$\mathbf{c}_{d, n_e^{(1)}} = \mathbf{c}_{d, n_e^{(1)}}(P_{2\dots j}^2) := 2^{n_e^{(1)}} (n_e^{(1)})^{d-n_e^{(1)}-2} (n_e^{(1)}!) \frac{\pi^{\frac{d-n_e^{(1)}}{2}}}{\Gamma\left(\frac{d-n_e^{(1)}+1}{2}\right)} \text{Vol}\left\{\Sigma_{n_e^{(1)}-1}(P_{2\dots j})\right\}^{-1}. \quad (3.11)$$

Let us now move to the measure for the multi-loop integrals. Proceeding as before, for each loop momentum  $\{l_l \mid l = 1, \dots, L\}$  we can write:

$$d^d l_l = dV_{d-n_{e_l}-L+l} \prod_{e \in \mathcal{E}_l^{(L)}} [dy_e^2] [\text{CM}(Q_{i\dots j}^2)]^{-\frac{1}{2}} \frac{[\text{CM}(y_e^2, Q_{2\dots j}^2)]^{\frac{d-n_s-1-L+l}{2}}}{[\text{CM}(Q_{i\dots j}^2)]^{\frac{d-n_{s_l}-L+l}{2}}} \quad (3.12)$$

where the  $Q$ 's appearing in the Cayley-Menger determinants refer to the moduli of the momenta external to the  $l$ -th loop, *i.e.* some of them can be related to actual external momenta,  $Q_{2\dots j} = P_{2\dots j}$ , while others can depend on the edge weights associated with other loops (or, which is the same, on momenta running in the other loops). Thus, a  $L$ -loop integral  $\mathcal{I}_{\mathcal{G}}$  associated to a graph  $\mathcal{G}$  acquires the form

$$\mathcal{I}_{\mathcal{G}} = \prod_{l=1}^L \left[ \frac{\pi^{\frac{d-n_{s_l}-L+l}{2}}}{\Gamma\left(\frac{d-n_{s_l}-L+l}{2}\right)} \int_{\Gamma_l} \prod_{e_l \in \mathcal{E}_l^{(1)}} [dy_{e_l}^2] \frac{[\text{CM}(y_{e_l}^2, Q_{i\dots j}^2(y_{\not{e}_l}))]^{\frac{d-n_{s_l}-1-L+l}{2}}}{[\text{CM}(Q_{i\dots j}^2(y_{\not{e}_l}))]^{\frac{d-n_{s_l}-L+l}{2}}} \right] \frac{\mathbf{n}_{\delta}(y_e)}{\prod_{\mathfrak{g} \subseteq \mathcal{G}} q_{\mathfrak{g}}(y_e)} \quad (3.13)$$

where  $y_{\not{e}_l}$  is associated to an edge which is not in  $\mathcal{E}_l$ , and the contour  $\Gamma_l$  for the  $l$ -th loop is given by

$$\Gamma_l := \left\{ \frac{\text{CM}(y_{e_l}^2, Q_{i\dots j}^2(y_{\not{e}_l}))}{\text{CM}(Q_{i\dots j}^2(y_{\not{e}_l}))} \leq 0 \right\}. \quad (3.14)$$

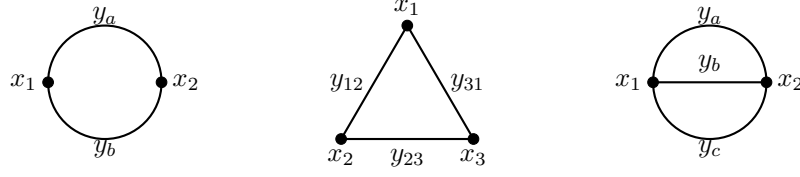


Figure 3.1: Examples of loop graphs. The associated loop integrals are  $n_e$ -fold if  $n_e < d$ , and the integration measure is proportional to the squared volume of a simplex in  $\mathbb{P}^{n_s+n_e-2}$ .

Such an expression can be further manipulated to get

$$\mathcal{I}_{\mathcal{G}} = \mathbf{c}_{d,n_e^{(L)},L} \int_{\mathbb{R}_+^{n_s} \cup \Gamma} \left[ \frac{dz}{z} z^{\sigma-1} \right] \left[ \frac{\text{Vol}^2(y_e, P_{i\dots j}^2)}{\text{Vol}^2(P_{i\dots j}^2)} \right]^{\frac{d-n_s-L}{2}} \frac{\mathbf{n}_{\delta}(z, \mathcal{X})}{\prod_{\mathbf{g} \subseteq \mathcal{G}} q_{\mathbf{g}}(z, \mathcal{X})} \quad (3.15)$$

where the integration region  $\Gamma$  is determined by the intersection among all the contours  $\Gamma_l$ .

$$\Gamma = \bigcap_{l=1}^L \Gamma_l \quad (3.16)$$

and the coefficient  $\mathbf{c}_{d,n_e,L}$  is given by

$$\mathbf{c}_{d,n_e^{(L)},L} := \frac{\pi^{\frac{d-n_s+L(L-1)}{2}}}{\prod_{l=1}^L \Gamma\left(\frac{d-n_{s_l}-L+l}{2}\right)} 2^{n_e^{(L)}} (n_e^{(L)})^{d-n_e-L-2} (n_e^{(L)}!) \text{Vol}\{\tilde{\Sigma}(P_{i\dots j})\}^{-1} \quad (3.17)$$

As a final remark, the representation of the measure of integration in terms of the Cayley-Menger determinant allows for a geometrical interpretation in terms of volumes of a simplex in  $\mathbb{P}^{n_e}$ , with all the edge weights and the moduli  $\{p_s, s \in \mathcal{V}\}$  of the momenta of the external states<sup>4</sup> at each site  $s$  associated to the edges of the simplex, and the boundaries of the region of integration determined by projecting its vertices on a lower-dimensional hyperplane.

## 3.2 Examples

**Two-site one-loop graph** – Let us begin with the simplest non-trivial one-loop example, the two-site one-loop graph – see Figure 3.1. Let  $\mathcal{P} := \{\vec{p}_j, j = 1, \dots, n\}$  be the set of external spatial momenta. The external kinematics can be parametrised via

$$X_1 := \sum_{\vec{p} \in \mathcal{P}_1} |\vec{p}|, \quad X_2 := \sum_{\vec{p} \in \mathcal{P}_2} |\vec{p}|, \quad P := \left| \sum_{\vec{p} \in \mathcal{P}_1} \vec{p} \right| = \left| \sum_{\vec{p} \in \mathcal{P}_2} \vec{p} \right| \quad (3.18)$$

<sup>4</sup>Importantly, if at a site  $s$  more than one external state is attached, then  $P_s$  parameterise the angle among them. If instead just a single external state is attached to it, then  $P_s = X_s$ .



where  $\mathcal{P}_1, \mathcal{P}_2 \subset \mathcal{P}$  such that  $\mathcal{P}_1 \cup \mathcal{P}_2 = \mathcal{P}$  and  $\mathcal{P}_1 \cap \mathcal{P}_2 = \emptyset$  — *i.e.*  $\mathcal{P}_1$  and  $\mathcal{P}_2$  are the sets of external momenta at the two vertices of the graph. The loop space can instead be parametrised as

$$y_a := |\vec{l}|, \quad y_b := |\vec{l} + \vec{P}|, \quad \vec{P} := \sum_{\vec{p} \in \mathcal{P}_1} \vec{p}. \quad (3.19)$$

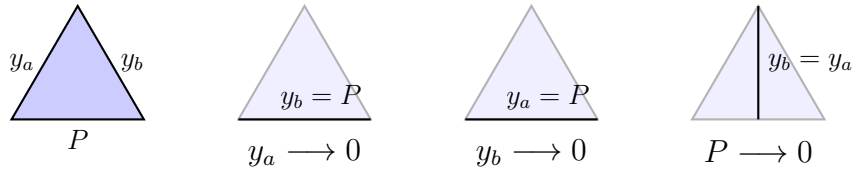
For  $d \geq 2$ , *i.e.* the number of spatial dimension greater than the number of edges of the graph, then the loop integration is a two-fold integral in  $y_a$  and  $y_b$ . From (3.10), the measure can be written in terms of the squared volume of a triangle in  $\mathbb{P}^2$ , whose boundaries' volumes are given by the triple  $(y_a, y_b, P)$  and that is proportional to (minus) the Cayley-Menger determinant  $\text{CM}(y^2, P^2)$ :

$$\text{Vol}^2\{\Sigma_2(y, P)\} \sim -\text{CM}(y^2, P^2) = - \begin{vmatrix} 0 & 1 & 1 & 1 \\ 1 & 0 & y_a^2 & y_b^2 \\ 1 & y_a^2 & 0 & P^2 \\ 1 & y_b^2 & P^2 & 0 \end{vmatrix} = [(y_a + P)^2 - y_b^2] [y_b^2 - (y_a - P)^2] \quad (3.20)$$

The proportionality factor in the measure depends on the  $(2, 2)$ -minor of (3.20), which returns the volume of the codimension-1 boundary of the triangle that purely depends on the external kinematics, *i.e.*  $\text{CM}^{(2,2)}(y^2, P^2) = 2P^2$ . The case (3.20) is the only one in which the Cayley-Menger determinant is factorisable. The non-negativity of (3.20) as well as of the individual integration variables  $y_a$  and  $y_b$  as well as of the external kinematic parameter  $P$  defines the contour of integration  $\Gamma$  to be,

$$\Gamma_2 := \left\{ [(y_a + P)^2 - y_b^2] [y_b^2 - (y_a - P)^2] \geq 0, \quad y_a \geq 0, \quad y_b \geq 0 \right\}. \quad (3.21)$$

This geometrical picture also allows to straightforwardly understand the behaviour of the measure as certain limits are taken. For example, as any of the elements of the triple  $(y_a, y_b, P)$  are taken to zero, the triangle associated to the measure gets mapped into a segment by collapsing two of its vertices onto each other:



If the graph is characterised by just an external state for each site, then spatial momentum conservation implies that  $X := X_1 = X_2$  and  $P = X$ . In this case, as  $y_a \sim \rho X$ <sup>5</sup>, the triangle volume also vanishes.

The full integral corresponding to the 2-site 1-loop graph then acquires the form

$$I_2^{(1)} = \frac{\pi^{\frac{d-2}{2}}}{\Gamma\left(\frac{d-2}{2}\right)} \int_0^{+\infty} \frac{dx_1}{x_1} x_1^\alpha \int_0^{+\infty} \frac{dx_2}{x_2} x_2^\alpha \int_{\Gamma_2} dy_a^2 dy_b^2 \frac{[(y_a + P)^2 - y_b^2](y_b^2 - (y_a - P)^2)^{\frac{d-3}{2}}}{P^{d-2}} \Omega(x, y) \quad (3.22)$$

<sup>5</sup>This is nothing but the collinear limit  $\vec{l} \rightarrow \rho \vec{P}$ .

where  $\Omega(x, y)$  is the universal integrand provided by the combinatorial picture of standard / generalised / weighted cosmological polytopes. Note that for  $d = 2$  – when the number of spatial dimensions is the same as the number of edges of the graph, the squared volume of the triangle appears in the denominator and its vanishing – that typically occurs at the boundary of the integration region – might imply the appearance of a singularity from the measure which does not appear for  $d > n_e = 2$ . However, this is not the case, as the factor  $y_a y_b$  cancels such potential divergence.

For  $d < n_e = 2$ , *i.e.*  $d = 1$ , then the edge weights are not independent, and the loop space is parameterised by one of them only. In the simple case under discussion, such a space is 1-dimensional and can be parameterised by any of the two edge weights. Without loss of generality, it is possible to take  $y_a$ . Then  $y_b = y_a + P$  and  $dl = dy_a$ , with the integration region being just the positive real axis  $\mathbb{R}_+$ . The integral associated to two-site one-loop in  $d = 1$  can then be written as

$$I_2^{(1)} \Big|_{d=1} = \delta(X_2 - X_1) \int_0^{+\infty} \frac{dx_1}{x_1} x_1^\alpha \int_0^{+\infty} \frac{dx_2}{x_2} x_2^\alpha \int_0^{+\infty} dy_a \int_0^{+\infty} dy_b \delta(y_b - y_a - P) \Omega(x, y), \quad (3.23)$$

where the overall delta function simply enforces the two external states to have the same energy, and we kept the integration over  $y_b$  but constrained by the delta function in such a way that the integrand can be still written in terms of the canonical function of the relevant polytope – then integrating it out is geometrically equivalent to a covariant restriction <sup>6</sup> of the relevant geometry on to the hyperplane  $y_b - y_a - P = 0$ .

**Three site, one loop graph** – Let us turn now to the next-to-simplest case, the three-site one-loop graph – see Figure 3.1. The external kinematics is parametrised as

$$X_j := \sum_{\vec{p} \in \mathcal{P}_j} |\vec{p}|, \quad P_j := \left| \sum_{\vec{p} \in \mathcal{P}_j} \vec{p} \right|, \quad j = 1, 2, 3 \quad (3.24)$$

where  $\{\mathcal{P}_j, j = 1, 2, 3\}$  are such that  $\mathcal{P}_1 \cup \mathcal{P}_2 \cup \mathcal{P}_3 = \mathcal{P}$  and  $\{\mathcal{P}_i \cap \mathcal{P}_j = \emptyset, \forall i \neq j, i, j = 1, 2, 3\}$  – they are the sets of momenta at the vertices 1, 2, 3. Notice that in case the graph has one momentum for each vertex, then  $\{X_j = P_j, \forall j = 1, 2, 3\}$ . The loop momentum can be parametrised in terms of

$$y_{12} := |\vec{l}|, \quad y_{23} := |\vec{l} + \vec{P}_2|, \quad y_{31} := |\vec{l} - \vec{P}_1|, \quad (3.25)$$

where

$$\vec{P}_j := \sum_{\vec{p} \in \mathcal{P}_j} \vec{p}, \quad j = 1, 2, 3. \quad (3.26)$$

For  $d \geq 3$ , the loop momentum is a three-fold integral over the variables (3.25). The loop

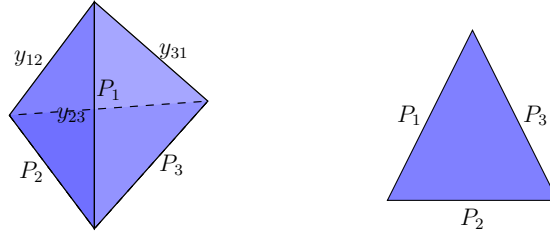
---

<sup>6</sup>For a general definition and discussion of the covariant restriction, see [197].

integration measure is now given in terms of the squared volume of a tetrahedron in  $\mathbb{P}^3$ :

$$\text{Vol}^2 \left\{ \Sigma_3(y^2, P^2) \right\} = +\text{CM}(y^2, P^2) = \begin{vmatrix} 0 & 1 & 1 & 1 & 1 \\ 1 & 0 & y_{12}^2 & y_{23}^2 & y_{31}^2 \\ 1 & y_{12}^2 & 0 & P_2^2 & P_1^2 \\ 1 & y_{23}^2 & P_2^2 & 0 & P_3^2 \\ 1 & y_{31}^2 & P_1^2 & P_3^2 & 0 \end{vmatrix} \quad (3.27)$$

As for the previous case, the proportionality factor depends on the volume of the simplex in one dimension less give by the  $(2, 2)$ -minor of (3.27), *i.e.* a triangle whose sides' volumes are given by the triple  $(P_1, P_2, P_3)$



The contour of integration is then given by

$$\Gamma_3 := \left\{ (-1)^{k+1} \text{CM}^{(\mathcal{I}_k, \mathcal{J}_k)} \geq 0, \forall (\mathcal{I}_k, \mathcal{J}_k) \ k = 1, \dots, 3 \right\} \quad (3.28)$$

where  $\mathcal{I}_k$  and  $\mathcal{J}_k$  are sets of  $3 - k$  rows and  $3 - k$  columns respectively. In words, all the minors of  $\text{CM}(y_{j,j+1}^2, P_j^2)$ , including the full Cayley-Menger determinant, with the appropriate  $(-1)$  factors have to be non-negative, with the equality for  $(-1)^4 \text{CM}(y_{j,j+1}^2, P_j^2) = 0$  establishing the boundary of the region of the integration. The Cayley-Menger determinant  $(-1)^4 \text{CM}(y_{j,j+1}^2, P_j^2)$  proportional to the squared volume of a tetrahedron whose sides have lengths  $\{y_{12}, y_{23}, y_{31}, P_1, P_2, P_3\}$ . The boundary of the contour of integration implies that the four vertices of the tetrahedron become co-planar. As in the previous case, this geometrical picture makes manifest the behaviour of the measure as several limits are taken. In particular, as any of the  $\{y_{i,i+1}, i = 1, 2, 3\}$  is taken to zero, the tetrahedron is mapped into a triangle.

The full integral corresponding to the 3-site 1-loop graph then acquires the form

$$I_3^{(1)} = \frac{2\pi^{\frac{d-3}{2}}}{\Gamma\left(\frac{d-3}{2}\right)} \prod_{j=1}^3 \left[ \int_0^{+\infty} \frac{dx_j}{x_j} x_j^\alpha \right] \int_{\Gamma_3} \prod_{e \in \mathcal{E}} dy_e^2 \frac{[(-1)^4 \text{CM}(y^2, P^2)]^{\frac{d-4}{2}}}{[(-1)^3 \text{CM}^{(2,2)}(P^2)]^{\frac{d-3}{2}}} \Omega_{\mathcal{G}}(x, y) \quad (3.29)$$

For  $d < n_e = 3$ , not all the edge weights are independent and, hence, the integral is  $d$ -fold integral.

**Two-site, two-loop graph** – Let us conclude with a two-loop example, the two-site two-loop graph – see Figure 3.1. Its kinematics can be parametrised as

$$X_1 := \sum_{\vec{p} \in \mathcal{P}_1} |\vec{p}|, \quad X_2 := \sum_{\vec{p} \in \mathcal{P}_2} |\vec{p}|, \quad P := \left| \sum_{\vec{p} \in \mathcal{P}_1} \vec{p} \right| = \left| \sum_{\vec{p} \in \mathcal{P}_2} \vec{p} \right| \quad (3.30)$$

where  $\mathcal{P}_1, \mathcal{P}_2 \subset \mathcal{P}$  such that  $\mathcal{P}_1 \cup \mathcal{P}_2 = \mathcal{P}$  and  $\mathcal{P}_1 \cap \mathcal{P}_2 = \emptyset$ . The edge weights of the graph instead parametrise the loop space via

$$y_a := |\vec{l}_1|, \quad y_b := |\vec{l}_1 + \vec{l}_2 + \vec{P}|, \quad y_x := |\vec{l}_2|. \quad (3.31)$$

Let us proceed one loop at a time, as described in the main text, focusing on the loop subgraph with edge weights  $y_a$  and  $y_b$ . It can be taken to have external kinematics to be given by  $y_d = |\vec{l}_2 + \vec{P}|$  – from a graph perspective this is equivalent to open up one of the sites into two:



with white site not carrying any weight. Then, a measure  $\mu_d^{(1)}(y_a, y_b, y_d)$  gets associated to the 2-site 1-loop subgraph being constituted by the white site and the black one with weight  $x_2$ . A second measure is associated to the graph obtained by replacing the previous 1-loop subgraph by an edge with weight  $y_d$  (*i.e.* the modulus of the momentum flowing through the deleted subgraph):



The measure associated to the 2-site 2-loop graph can be written as

$$\mu_d^{(2)}(y, P) := \int dy_d^2 \mu_d^{(1)}(y_a, y_b, y_d) \mu_d^{(1)}(y_d, y_c, P) \quad (3.32)$$

with  $\mu_d^{(1)}$  being the measure for the 2-site 1-loop graph computed earlier. The contour of integration is then given by  $\Gamma = \Gamma_1 \cap \Gamma_2$  where

$$\begin{aligned} \Gamma_1 &= \left\{ (-1)^{k+1} \text{CM}^{(\mathcal{I}_k, \mathcal{J}_k)}(y_a, y_b, y_d) \geq 0, \quad \forall (\mathcal{I}_k, \mathcal{J}_k), \quad k = 1, 2 \right\}, \\ \Gamma_2 &= \left\{ (-1)^{k+1} \text{CM}^{(\mathcal{I}_k, \mathcal{J}_k)}(y_d, y_c, P) \geq 0, \quad \forall (\mathcal{I}_k, \mathcal{J}_k), \quad k = 1, 2 \right\} \end{aligned} \quad (3.33)$$

The integral associated to 2-site 2-loop graph acquires the form

$$I_2^{(2)} \sim \int_0^{+\infty} \frac{dx_1}{x_1} x_1^\alpha \int_0^{+\infty} \frac{dx_2}{x_2} x_2^\alpha \int_\Gamma \prod_{e \in \mathcal{E} \cup \{e_d\}} dy_e^2 \mu_d^{(1)}(y_a, y_b, y_d) \mu_d^{(1)}(y_d, y_c, P) \Omega_{\mathcal{G}}(x, y) \quad (3.34)$$

where  $\sim$  indicates the omission of factors which are irrelevant to the present discussion, and  $e_d$  is the edge with weight  $y_d$ . Note that the integrand  $\Omega_{\mathcal{G}}(x, y)$  does not depend on the additional variable  $y_d$  which, consequently, can be integrated out returning a measure that depends only on the edge weights of the original graph as well as its external kinematics.

### 3.3 The asymptotic structure of cosmological integrals

It is useful to summarise the salient features of the general cosmological integral (3.1) associated to a given graph  $\mathcal{G}$ :

- its integrand  $\Omega_{\mathcal{G}}(x, y)$  is a rational function whose denominator is a degree- $\tilde{\nu}$  factorisable polynomial, whose factors are  $\tilde{\nu}$  linear polynomials which are in 1 – 1 correspondence with subgraphs of  $\mathcal{G}$  and individually identifies a facet of the relevant polytope;
- the numerator of  $\Omega_{\mathcal{G}}(x, y)$  is a polynomial of degree  $\tilde{\nu} - n_s - n_e$  that identifies the adjoint surface of the relevant polytope, and it's fixed by compatibility conditions among singularities [79, 193] and, in the case of a correlation function, by additional conditions on the residues [?];
- the integral (3.1) can be seen as a Mellin transform of  $\Omega_{\mathcal{G}}(x, y)$  over the site weights, and over  $\prod_{l=1}^L \min\{n_e^{(l)}, d\}$ -dimensional edge-weight space whose measure can be expressed in terms of squared volume of simplices;
- the integration measure in the edge-weight space is always positive in the interior of the integration region, and vanishes just on its boundary.

Because of all these features, the integral (3.1) can show divergences when the graph weights become large or small. Such a behaviour is controlled by the powers in the site and edge weights in the integrand  $\Omega_{\mathcal{G}}(x, y)$  and in the weight integration measure. It is in turn codified in the combinatorics of the *Newton polytope* associated to it, which controls the convergence of the integral [205, 206], allow identifying the divergences and isolate them via sector decomposition [207–213].

**Newton polytopes and asymptotic behaviour** – In order to fix the ideas, let us consider the following toy integral

$$\mathcal{I}[\sigma] := \int_{\mathbb{R}_+^n} \left[ \frac{dz}{z} z^\sigma \right] \frac{\mathbf{n}_\delta(z)}{[p_m(z)]^\tau} \quad (3.35)$$

where  $z := (z_1 \dots z_n) \in \mathbb{R}_+^n$ ,  $\sigma := (\sigma_1, \dots, \sigma_n) \in \mathbb{C}^n$ . While  $p_m(z)$  and  $\mathbf{n}_\delta(z)$  are multivariate polynomials in  $z$  of degrees  $m \in \mathbb{Z}_+$  and  $\delta \in \mathbb{Z}_+$  respectively. Such an integral falls into the class of cosmological integrals given in (3.1), in particular all tree-level cosmological integrals are of this form. Let us begin with the case for which the numerator is a degree-zero polynomial. The integral (3.35) will diverge when  $p_m(z)$  vanishes for  $z$  inside the integration region,  $\mathbb{R}_+^n$ , or when the integration variables  $z$  either become very large or very small, in other words when some of them go to infinity or to zero, respectively.

Therefore, when the polynomial  $p_m(z)$  does not vanish inside the integration region, for some domain in the space of exponents  $\sigma \in \mathbb{C}^n$ , the integral will converge. For polynomials with real coefficients (which is our case of interest) this will happen when the coefficients are positive. This region in  $\sigma$ -space is bounded in the real directions and unconstrained in the imaginary directions, thus we can call it a tube domain. Then, the integral can only have singularities when  $z$  becomes very large, or very small. And this singular behaviour is determined by the powers  $\sigma$ ,  $\tau$  and the exponents in each monomial of  $p_m(z)$ . A geometric object which encodes this asymptotic behaviour of polynomials like  $p_m(z)$  (with real, positive coefficients) is the *Newton polytope*. It is simply defined by considering the space  $\rho \in \mathbb{R}^n$  of the powers of the monomials in  $p_m(z)$ , assigning a point  $(\rho_1, \dots, \rho_n)$  for the monomial  $z_1^{\rho_1} \dots z_n^{\rho_n}$ , then the *Newton polytope* is the convex hull of the set of points we have from  $p_m(z)$ . Intuitively, the faces of this polytope tell us which monomials are leading when we take certain  $z$ 's to be very large or very small. Thus, we can learn the possible divergent directions of the integral. Then, we say that the region in  $\sigma$ -space where the integral converges and defines an analytic function in  $\sigma$  is obtained by requiring that  $(\text{Re}\sigma_1, \dots, \text{Re}\sigma_n)$  lies in the interior of the *Newton polytope* of  $p_m(z)$  [205]. Let's consider a simple example to better understand the above discussion. Take the integral,

$$\mathcal{I}[\sigma_1, \sigma_2] = \int_{\mathbb{R}_+^2} \frac{dz_1}{z_1} \frac{dz_2}{z_2} z_1^{\sigma_1} z_2^{\sigma_2} \frac{1}{1 + z_1 + z_2}.$$

The polynomial  $p_m(z) \equiv p_1(z_1, z_2) = 1 + z_1 + z_2$ , and we can identify the points in  $\rho$ -space to be  $(0, 0)$ ,  $(1, 0)$ , and  $(0, 1)$ , and therefore the Newton polytope is a triangle, with these points as the vertices. This example provides us with a simple intuition on how the Newton polytope encodes the asymptotic structure of the polynomial  $p_m(z)$ . If we consider the limit  $z_1 \rightarrow \infty$ , then the leading monomial in  $p_1$  is  $z_1$ , and is identified with the vertex  $(1, 0)$ . If we were to consider the direction  $z_1 \rightarrow \infty$ , and  $z_2 \rightarrow \infty$ , then  $p_1 \rightarrow z_1 + z_2$  and is identified with the boundary line with vertices  $(1, 0)$ , and  $(0, 1)$ . On the other hand, by looking into the direction  $z_1 \rightarrow 0$ , and  $z_2 \rightarrow 0$ , then  $p_1 \rightarrow 1$ , and we can identify this limit with the vertex  $(0, 0)$ . From this quick analysis, we see how the boundaries of the Newton polytope inform us of the behaviour of the respective polynomial, in the asymptotic directions of its variables. In turn, this makes it very clear how to identify the domain of convergence of the integral  $\mathcal{I}[\sigma_1, \sigma_2]$ . In the lower boundary of the integral,  $(z_1 = 0, z_2 = 0)$ , for the integral to converge we need  $\{\text{Re}\sigma_1 > 0, \text{Re}\sigma_2 > 0\}$  since in this limit  $p_1(z_1, z_2) \rightarrow 1$  and for non-positive values of  $\sigma$  we would have logarithmic singularities in  $\mathcal{I}[\sigma_1, \sigma_2]$ . These two inequalities in  $\sigma$  are precisely two of the boundaries of the Newton polytope. Similarly, we can perform the same analysis on the third boundary to find that  $\text{Re}\sigma_1 + \text{Re}\sigma_2 - 1 < 0$ , and thus we find the bounded region of the real values of  $\sigma$ , and in turn the tube domain of convergence of  $\mathcal{I}[\sigma_1, \sigma_2]$ .

Now that we have looked at a simple example that illustrates the usefulness of the Newton polytope in identifying the convergence region of integrals of the type (3.35), lets

consider a more general setup. Take the multivariate polynomial  $p_m(z)$  written as,

$$p_m(z) := \sum_{\substack{\rho_1 \dots \rho_n = 0 \\ \rho_1 + \dots + \rho_n \leq m}}^m a_{\rho_1 \dots \rho_n} \prod_{j=1}^n z_j^{\rho_j} \equiv \sum_{\substack{\rho \in \mathbb{Z}^n \\ \rho_1 + \dots + \rho_n \leq m}} a_{\rho} z^{\rho}$$

where  $z := (z_1, \dots, z_n)$ ,  $\rho := (\rho_1, \dots, \rho_n)$ , and  $a_{\rho_1 \dots \rho_n} \in \mathbb{C}^n$ . It is possible to associate a collection of vertices,

$$\left\{ \mathcal{Z} := (1, \text{Re}\{\rho\}) \in \mathbb{P}^n \mid \text{Re}\{\rho\} \in \mathbb{Z}^n, \sum_{j=1}^n \rho_j \leq m \right\}$$

in  $\mathbb{P}^n$ . Then, the convex hull of the set of points defined above is the Newton polytope  $\mathcal{N}[p_m(z)]$  associated to  $p_m(z)$ . If the polynomial  $p_m(z)$  is factorisable, *i.e.*  $p_m(z) = p_{m_1}(z) \cdots p_{m_t}(z)$  with  $m_1 + \dots + m_t = m$ , then the Newton polytope  $\mathcal{N}[p_m(z)]$  is given by the *Minkowski sum* of the Newton polytopes associated to each  $\{p_{m_j}(z), j = 1, \dots, t, m_1 + \dots + m_t = m\}$ :

$$\mathcal{N}[p_m(z)] = \bigoplus_{j=1}^t \mathcal{N}[p_{m_j}(z)]. \quad (3.36)$$

with  $\bigoplus$  indicating the Minkowski sum. The Minkowski sum between two polytopes can be computed by summing every vertex in one polytope, with every vertex in the other polytope, then the convex hull of the resultant set of points is the Minkowski sum of the two polytopes. Finally, if the polynomial factorises as  $p_m(z) := [p_{m_1}(z)]^{\tau_1} \cdots [p_{m_t}(z)]^{\tau_{m_t}}$ , with  $\tau_1 m_1 + \dots + \tau_{m_t} m_t = m$  and  $\{\tau_j \in \mathbb{C} \mid j = 1, \dots, t\}$ , then its Newton polytope can be written as the *weighted Minkowski sum* of the individual polynomials  $\{p_{m_j}(z), j = 1, \dots, t\}$  with the weights given by  $\{\text{Re}\{\tau_j\} \geq 0, j = 1, \dots, t\}$ :

$$\mathcal{N}[p_m(z)] = \bigoplus_{j=1}^t \text{Re}\{\tau_j\} \mathcal{N}[p_{m_j}(z)]. \quad (3.37)$$

Interestingly, the combinatorial structure of (3.37) does not depend on the weights.

Note that the monomial  $z^{\sigma}$  appearing in the measure of the Mellin transform in (3.35) can be included in the definition of Newton polytope:

$$\mathcal{N}[\mathcal{I}(\sigma)] := -\sigma \bigoplus_{j=1}^t \text{Re}\{\tau_j\} \mathcal{N}[p_{m_j}(z)].$$

As it just identifies a point in the space of powers, its only effect would be a translation of the polytope  $\mathcal{N}[p_m(z)]$  that depends on  $\text{Re}\{\sigma\}$ . Thus, the combinatorial structure of  $\mathcal{N}[\mathcal{I}(\sigma)]$  is the same as  $\mathcal{N}[p_m(z)]$ .

What occurs when the numerator is a polynomial of degree greater than zero? The convergence of the integral (3.35) can be effectively analyzed by expanding the numerator  $\mathbf{n}_{\delta}(z)$  in terms of monomials. This allows us to transform (3.35) into a series of integrals

that all share the same denominator  $[p_m(z)]^\tau$ . Each integral has a numerator equal to one, differing only in their Mellin transform parameters, which are shifted in distinct ways. The nature of these shifts is determined by the powers present in the monomials of  $\mathbf{n}_\delta(x, y)$ :

$$\mathcal{I}[\sigma] = \sum_{\substack{r=0 \\ r_1+\dots+r_n \leq \delta}} \mathbf{a}_r^{(n)} \mathcal{I}[\sigma + r] = \sum_{\substack{r=0 \\ r_1+\dots+r_n \leq \delta}} \mathbf{a}_r^{(n)} \int_0^{+\infty} \left[ \frac{dz}{z} z^{\sigma+r} \right] \frac{1}{[p_m(z)]^\tau} \quad (3.38)$$

The asymptotic behavior of the entire integral is still defined by the Newton polytope linked to the denominator, which is common across all integrals in the sum (3.38), albeit with different shifts for each integral. It turns out that each separate integral (3.38) converges if the point  $(1, \text{Re}\{\sigma\} + r)$  resides within the interior of the pertinent Newton polytope. Additionally, the overall integral (3.35) converges in the region where these Newton polytopes overlap [205].

The condition for each individual integral can be alternatively verified by examining the facets of the corresponding Newton polytope along with the co-vectors in the dual space that define them. It is important to note that this set  $\{\mathcal{W}_I^{(j)}\}$  of co-vectors in the dual space <sup>7</sup> is represented by,

$$\mathcal{W}_I^{(j)} = (-1)^{j(n-1)} \epsilon_{IK_1 \dots K_n} \mathcal{Z}_{a_{j+1}}^{K_1} \dots \mathcal{Z}_{a_{j+n1}}^{K_n},$$

where  $\epsilon_{IK_1 \dots K_n}$  denotes the anti-symmetric  $(n+1)$ -dimensional Levi-Civita symbol. Since the vectors that define the vertices are of the form  $\mathcal{Z} = (1, \rho)$  with  $\rho \in \mathbb{Z}^n$ , the co-vectors  $\mathcal{W}$  exhibit the structure  $\mathcal{W} = (\lambda, \omega)$ . Here,  $\lambda = \lambda(\text{Re}\{\sigma\}, \text{Re}\{\tau\})$  is dependent on the parameters  $\text{Re}\{\sigma\}$  and  $\text{Re}\{\tau\}$ , while  $\omega$  is an  $n$ -vector that does not depend on these parameters. The function  $\lambda$  can be expressed explicitly as

$$\lambda(\sigma, \tau; \omega) = \text{Re}\{\sigma\} \cdot \omega - \text{Re}\{\tau\} \sum_{\{\rho\}} \max\{\rho \cdot \omega\} \quad (3.39)$$

and indicates how the direction pointed by  $\omega$  is approached <sup>8</sup>. Moreover, understanding the co-vectors enables the tiling of the integration region into sectors  $\Delta_{\mathcal{W}_c}$  [207–213], each characterized by a set of adjacent co-vectors  $\mathcal{W}_c$ ,

$$\mathbb{R}_+^n = \bigcup_{\{\mathcal{W}_c\}} \Delta_{\mathcal{W}_c}, \quad (3.40)$$

and the integral (3.35), with a degree  $\delta = 0$  numerator, can then be written as

$$I[\sigma] = \sum_{\{\mathcal{W}_c\}} \int_{\Delta_{\mathcal{W}_c}} \left[ \frac{dz}{z} z^\sigma \right] \frac{\mathbf{n}_\delta(z)}{[p_m(z)]^\tau} \equiv \sum_{\{\mathcal{W}_c\}} I_{\Delta_{\mathcal{W}_c}}[\sigma].$$

<sup>7</sup>The dual space will still be denoted as  $\mathbb{P}^n$ .

<sup>8</sup>In the context of Feynman integrals where tropical geometry techniques are applied, the function  $\lambda(\sigma, \tau_o; \omega)$  is known as a *tropical function*, often denoted as *Trop* – see [105, 213–217]



The knowledge of the co-vectors identifying a given sector  $\Delta_{\mathcal{W}_c}$  also provides a change of variables to suitably parametrise the integral  $I_{\Delta_{\mathcal{W}_c}}[\sigma]$

$$z_j \longrightarrow \prod_{\omega \in \omega_c} \zeta_\omega^{-\mathbf{e}_j \cdot \omega}, \quad \zeta_\omega \in [0, 1], \quad \forall \omega \in \omega_c \quad (3.41)$$

$\forall j \in [1, n]$ , where  $\{\mathbf{e}_j \in \mathbb{R}^n, j = 1, \dots, n\}$  represents the canonical basis in  $\mathbb{R}^n$ , and  $\omega_c$  denotes the set of  $n$ -vectors in  $\mathcal{W}$  that are part of the collection of compatible facets identified by  $\mathcal{W}_c$ . With this change of variables, the integral  $I_{\Delta_{\mathcal{W}_c}}[\sigma]$  takes on the form

$$I_{\Delta_{\mathcal{W}_c}} = \int_0^1 \left[ \frac{d\zeta}{\zeta} \zeta^{-\lambda} \right] \frac{1}{[p_m(\zeta)]^\tau}$$

where  $\zeta := (\zeta_\omega)_{\omega \in \omega_c}$  and  $\lambda := (\lambda_\omega)_{\omega \in \omega_c}$ . In this way, the divergences can be isolated from one another, and the Laurent expansion of one of the  $\lambda_\omega$  receives contribution from just a subset of integrals. Notably, it was demonstrated in [213] that if the complete  $\lambda$  is set to zero, for instance by rescaling it with a smallness parameter  $\epsilon$  ( $\lambda \rightarrow \epsilon\lambda$ ), then as  $\epsilon \rightarrow 0$ , all sectors will contribute, and the leading divergence coefficient corresponds to the canonical function of the Newton polytope associated with  $p_m(z)$ .

To consolidate the above discussion, we can illustrate the ideas with an example. Let us consider a example of an integral of the type (3.35)

$$I[\sigma] := \int_0^{+\infty} \frac{dx_1}{x_1} x_1^{s_1} \int_0^\infty \frac{dx_2}{x_2} x_2^{s_2} \frac{1}{(X_{\mathcal{G}} + x_1 + x_2)^\tau} \equiv \int_0^{+\infty} \left[ \frac{dz}{z} z^\sigma \right] \frac{1}{(X_{\mathcal{G}} + \mathbf{e}_{12} \cdot z)^\tau} \quad (3.42)$$

where  $z := (x_1, x_2)$ ,  $\sigma := (s_1, s_2) \in \mathbb{C}^2$  and  $\mathbf{e}_{12} := (1, 1) \in \mathbb{R}^2$ . The potential asymptotic divergent directions, along with the manner in which they are approached, are represented by the Newton polytope associated with the polynomial  $1 + \mathbf{e}_{12} \cdot z$ , shifted by  $-\text{Re}\{\sigma\}$ . This polytope takes the form of a simple triangle, with its facets defined by the co-vectors:

$$\mathcal{W}'^{(1)} = \begin{pmatrix} -\text{Re}\{s_1\} \\ -\mathbf{e}_1 \end{pmatrix}, \quad \mathcal{W}'^{(2)} = \begin{pmatrix} -\text{Re}\{s_2\} \\ -\mathbf{e}_2 \end{pmatrix}, \quad \mathcal{W}^{(12)} = \begin{pmatrix} \text{Re}\{s_1\} + \text{Re}\{s_2\} - \text{Re}\{\tau\} \\ \mathbf{e}_{12} \end{pmatrix} \quad (3.43)$$

where, as before,  $\{\mathbf{e}_j \in \mathbb{R}^2, j = 1, 2\}$  is the canonical basis for  $\mathbb{R}^2$ . Being a triangle, all its facets are compatible with each other, and thus, the region of integration can be tiled into three sectors, identified by the three pairs of co-vectors (3.43).

The behaviour in each sector is made manifest via the change of variables

$$\begin{aligned} (\mathcal{W}'^{(2)}, \mathcal{W}'^{(1)}) : \quad & x_1 = (\zeta'_2)^{-\mathbf{e}_1 \cdot \omega'_2} (\zeta'_1)^{-\mathbf{e}_1 \cdot \omega'_1} = \zeta'_1, \quad x_2 = (\zeta'_2)^{-\mathbf{e}_2 \cdot \omega'_2} (\zeta'_1)^{-\mathbf{e}_2 \cdot \omega'_1} = \zeta'_2, \\ (\mathcal{W}'^{(1)}, \mathcal{W}^{(12)}) : \quad & x_1 = (\zeta'_1)^{-\mathbf{e}_1 \cdot \omega'_1} (\zeta_{12})^{-\mathbf{e}_1 \cdot \omega_{12}} = \frac{\zeta'_1}{\zeta_{12}}, \quad x_2 = (\zeta'_1)^{-\mathbf{e}_2 \cdot \omega'_1} (\zeta_{12})^{-\mathbf{e}_2 \cdot \omega_{12}} = \frac{1}{\zeta_{12}}, \\ (\mathcal{W}^{(12)}, \mathcal{W}'^{(2)}) : \quad & x_1 = (\zeta_{12})^{-\mathbf{e}_1 \cdot \omega_{12}} (\zeta'_2)^{-\mathbf{e}_1 \cdot \omega'_2} = \frac{1}{\zeta_{12}}, \quad x_2 = (\zeta_{12})^{-\mathbf{e}_2 \cdot \omega_{12}} (\zeta'_2)^{-\mathbf{e}_2 \cdot \omega'_2} = \frac{\zeta'_2}{\zeta_{12}} \end{aligned} \quad (3.44)$$

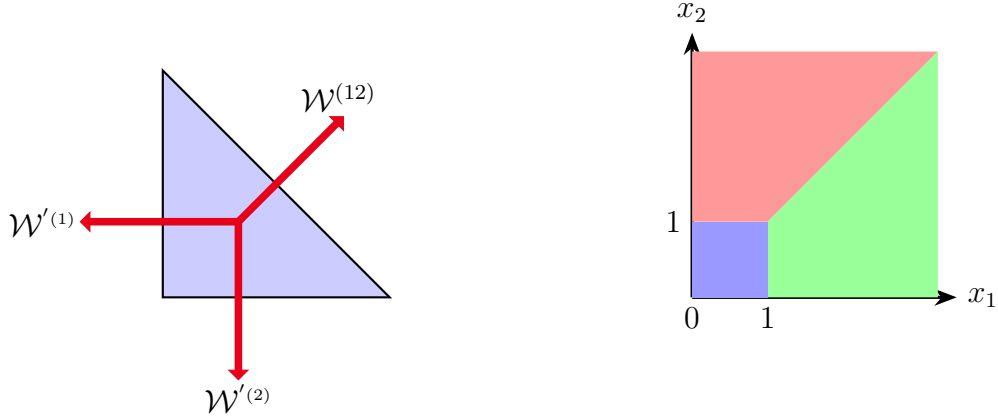


Figure 3.2: *On the left:* Newton polytope associated to (3.42). Its facets are identified by  $\mathcal{W}'^{(1)} := (-\text{Re}\{s_1\}, -1, 0)^T$ ,  $\mathcal{W}^{(12)} := (\text{Re}\{s_1 + s_2 - \tau\}, 1, 1)$ ,  $\mathcal{W}'^{(2)} := (-\text{Re}\{s_2\}, 0, -1)$  and divide the region of integration in three sectors, each of which bounded by a pair of co-vectors associated to the facets. *On the right:* Decomposition into sectors of the domain of the integration in the original integration variables. The blue square is the sector identified by the pair  $(\mathcal{W}'^{(2)}, \mathcal{W}'^{(1)})$  – it is the only sector containing the possible infra-red divergences. The red and the green areas instead single out the sector identified by  $(\mathcal{W}'^{(1)}, \mathcal{W}^{(12)})$  and  $(\mathcal{W}^{(12)}, \mathcal{W}'^{(2)})$ .

and the integral (3.42) can be written as

$$\begin{aligned} \mathcal{I}[\sigma] = & [\mathcal{X}_{\mathcal{G}}]^{s_1+s_2-\tau} \int_0^1 \frac{d\zeta'_1}{\zeta'_1} (\zeta'_1)^{s_1} \int_0^1 \frac{d\zeta'_2}{\zeta'_2} (\zeta'_2)^{s_2} \frac{1}{(1+\zeta'_1+\zeta'_2)^\tau} + \\ & + [\mathcal{X}_{\mathcal{G}}]^{s_1+s_2-\tau} \int_0^1 \frac{d\zeta'_1}{\zeta'_1} (\zeta'_1)^{s_1} \int_0^1 \frac{d\zeta_{12}}{\zeta_{12}} (\zeta_{12})^{\tau-s_1-s_2} \frac{1}{(1+\zeta'_1+\zeta_{12})^\tau} + \\ & + [\mathcal{X}_{\mathcal{G}}]^{s_1+s_2-\tau} \int_0^1 \frac{d\zeta_{12}}{\zeta_{12}} (\zeta_{12})^{\tau-s_1-s_2} \int_0^1 \frac{d\zeta'_2}{\zeta'_2} (\zeta'_2)^{s_2} \frac{1}{(1+\zeta'_2+\zeta_{12})^\tau} \end{aligned} \quad (3.45)$$

where the three integrals correspond to three sectors as in (3.44) – it is straightforward to check that, upon the change of variables in (3.44), the region of integration  $\mathbb{R}^2$  is split into the domains  $\Delta' := \{x_1 \in [1, +\infty[, x_2 \in [1, +\infty]\}$ ,  $\Delta_{1'2} := \{x_1 \in [0, x_2], x_2 \in [1, +\infty]\}$  and  $\Delta_{12'} := \{x_1 \in [1, +\infty[, x_2 \in [0, x_1]\}$  as shown in Figure 3.3, where they respectively correspond the blue, red and green regions. The three integrals in (3.45) are convergent for different values of the parameters  $(s_1, s_2, \tau)$ , concretely:  $(\text{Re}\{s_1\} > 0, \text{Re}\{s_2\} > 0)$ ,  $(\text{Re}\{s_1\} > 0, \text{Re}\{\tau - s_1 - s_2\} > 0)$  and  $\text{Re}\{\tau - s_1 - s_2\} > 0, (\text{Re}\{s_1\} > 0)$ .

Let us examine the limit in which both  $s_1$  and  $s_2$  approach zero. This is equivalent to allowing both directions  $\mathcal{W}^{(1)}$  and  $\mathcal{W}^{(2)}$  to diverge. In this case, the leading contribution is provided solely by the first integral in (3.45):

$$\mathcal{I}_{\Delta'}[\sigma] \sim \int_0^1 \frac{d\zeta'_1}{\zeta'_1} (\zeta'_1)^{s_1} \int_0^1 \frac{d\zeta'_2}{\zeta'_2} (\zeta'_2)^{s_2} + \dots = \frac{1}{s_1 s_2} + \dots, \quad (3.46)$$

where  $\mathcal{I}_{\Delta'}[\sigma]$  is the integral in the first line of (3.45), without the pre-factor  $[\mathcal{X}_G]^{s_1+s_2-\tau}$ . In order to extract all subleading divergences, one can rewrite  $(1 + \zeta'_1 + \zeta'_2)^{-\tau}$  as a double Mellin-Barnes integral

$$\frac{1}{(1 + \zeta'_1 + \zeta'_2)^\tau} = \frac{1}{\Gamma(\tau)} \int_{-i\infty}^{+i\infty} d\xi_1 (\zeta'_1)^{\xi_1} \int_{-i\infty}^{+i\infty} d\xi_2 (\zeta'_2)^{\xi_2} \Gamma(-\xi_1) \Gamma(-\xi_2) \Gamma(\tau + \xi_1 + \xi_2)$$

such that the integrations over  $\{\zeta'_j, j = 1, 2\}$  take the same form as (3.46), but with shifted powers,  $(s_1, s_2) \rightarrow (s_1 + \xi_1, s_2 + \xi_2)$ . These integrals can be evaluated, yielding the factor  $[(s_1 + \xi_1)(s_2 + \xi_2)]^{-1}$ . The contour integral can then be computed by closing both integration contours in the positive half-plane, resulting in a series representation for  $\mathcal{I}_{\Delta'}$ , which can safely be expanded as  $(s_1, s_2) \rightarrow (0, 0)$  to produce:

$$\mathcal{I}_{\Delta'}(\sigma) \sim \frac{1}{s_1 s_2} - \frac{\tau(2\tau^2 - 3\tau + 31)}{36} \left( \frac{1}{s_1} + \frac{1}{s_2} \right) + \dots$$

Indeed, contributions to the subleading divergences are given by the other two sectors as well

$$\begin{aligned} \mathcal{I}_{\Delta_{1'2}}[\sigma] &\sim \frac{1}{s_1} \times \int_0^1 \frac{d\zeta_{12}}{\zeta_{12}} (\zeta_{12})^\tau \frac{1}{(1 + \zeta_{12})^\tau}, \\ \mathcal{I}_{\Delta_{12'}}[\sigma] &\sim \frac{1}{s_2} \times \int_0^1 \frac{d\zeta_{12}}{\zeta_{12}} (\zeta_{12})^\tau \frac{1}{(1 + \zeta_{12})^\tau} \end{aligned}$$

with the leftover integral which evaluate to a Gaussian hypergeometric function.

A similar treatment can be carried out in the other limits. In particular, the infra-red behaviour of  $\mathcal{I}[\sigma]$  is encoded into the direction  $\mathcal{W}^{(12)}$ . It becomes divergent for  $\tau - s_1 - s_2 \rightarrow 0$  and receives contribution from both  $\mathcal{I}_{\Delta_{1'2}}[\sigma]$  and  $\mathcal{I}_{\Delta_{12'}}[\sigma]$ . Indicating both of them as  $\mathcal{I}_{\Delta_{1'2'}}[\sigma]$ , their leading behaviour can be written as,

$$\begin{aligned} \mathcal{I}_{\Delta_{1'2'}}[\sigma] &\sim \int_0^1 \frac{d\zeta_{12}}{\zeta_{12}} (\zeta_{12})^{\tau-s_1-s_2} \times \int_0^1 \frac{d\zeta'_j}{\zeta'_j} (\zeta'_j)^{s_j} \frac{1}{(1 + \zeta'_j)^\tau} = \\ &= \frac{1}{\tau - s_1 - s_2} \times \int_0^1 \frac{d\zeta'_j}{\zeta'_j} (\zeta'_j)^{s_j} \frac{1}{(1 + \zeta'_j)^\tau} \end{aligned}$$

with the integral evaluating to a Gaussian hypergeometric function. In the infra-red limit, the integral factorises into two integrals, one containing the divergence, which manifests itself as the pole in  $\tau - s_1 - s_2$  – signalling a logarithmic divergence – and the other integral is finite.

With this understanding of how the asymptotic structure of the integrals is encoded in the combinatorial properties of the Newton polytopes, the following subsection will focus on the explicit analysis of the cosmological integrals. Although the overarching concept remains unchanged regardless of the topology of the graphs, we find it beneficial to address tree and loop graphs separately. Mainly, because in loop integrals the measure associated with the loop integration introduces considerable complexity into the problem, and we build on the analysis done at tree level to tackle it.

### 3.3.1 The perturbative structure of the tree-level wavefunction

In this section, we will use the ideas discussed in the previous section, namely the Newton polytope and sector decomposition, in order to compute the tree level cosmological integrals as Laurent series in the analytic regulators  $\alpha_s$ . In practice, we are interested in extracting the leading and sub-leading divergences of these integrals. In general, we can write a tree-level integral associated to a graph  $\mathcal{G}$  as follows:

$$I_{\mathcal{G}}^{(0)}[\alpha, \tau, \mathcal{X}] = \int_0^{+\infty} \prod_{s \in \mathcal{V}} \left[ \frac{dx_s}{x_s} x_s^{\alpha_s} \right] \frac{\mathbf{n}_{\delta}(x, \mathcal{X})}{\prod_{\mathfrak{g} \subseteq \mathcal{G}} [q_{\mathfrak{g}}(x, \mathcal{X})]^{\tau_{\mathfrak{g}}}} \equiv \int_{\mathbb{R}_+^n} \left[ \frac{dz}{z} z^{\alpha} \right] \frac{\mathbf{n}_{\delta}(z, \mathcal{X})}{\prod_{\mathfrak{g} \subseteq \mathcal{G}} [q_{\mathfrak{g}}(z, \mathcal{X})]^{\tau_{\mathfrak{g}}}} \quad (3.47)$$

where  $x := (x_s)_{s \in \mathcal{V}}$ ,  $\alpha := (\alpha_s)_{s \in \mathcal{V}}$ , while  $\mathbf{n}_{\delta}(x)$  and  $\{q_{\mathfrak{g}}(x), \forall \mathfrak{g} \subseteq \mathcal{G}\}$  are inhomogeneous polynomials in  $x$  of degree  $\delta = \tilde{\nu} - n_s - n_e$  and 1 respectively. It is useful to recall the explicit expression for the linear polynomial  $q_{\mathfrak{g}}$

$$q_{\mathfrak{g}}(x) := \sum_{s \in \mathcal{V}_{\mathfrak{g}}} x_s + \mathcal{X}_{\mathfrak{g}}$$

where  $\mathcal{V}_{\mathfrak{g}}$  denotes the set of sites in  $\mathfrak{g}$ , and  $\mathcal{X}_{\mathfrak{g}}$  parameterizes the kinematic invariant associated with  $\mathfrak{g}$ . As previously mentioned, the asymptotic behavior of the integral (3.47) is encoded in the Newton polytope related to the denominator factors  $q_{\mathfrak{g}}(x)$ . For a generic tree graph with  $n_s$  sites, it resides in  $\mathbb{P}^{n_s}$ . As discussed earlier, the convergence of the integral (3.47) can be examined by considering the weighted Minkowski sum of the Newton polytopes  $\mathcal{N}[\mathfrak{g}]$  corresponding to the individual factors  $q_{\mathfrak{g}}(x)$ , shifted by the vector  $\mathcal{Z}_{\alpha, r} := (1, \text{Re}\{\alpha\} + r)$ , which is associated with the Mellin transform and the monomials of the numerator  $\mathbf{n}_{\delta}(x)$ . We will revisit this shift later:

$$\mathcal{N}_{\mathcal{G}}^{(\mathcal{Z}_{\alpha, r})} = -\mathcal{Z}_{\alpha, r} \oplus \mathcal{N}_{\mathcal{G}} \quad \mathcal{N}_{\mathcal{G}} := \bigoplus_{\mathfrak{g} \subseteq \mathcal{G}} \text{Re}\{\tau_{\mathfrak{g}}\} \mathcal{N}[\mathfrak{g}]$$

where  $\text{Re}\{\tau_{\mathfrak{g}}\} > 0$ . As emphasised earlier, the vector  $\mathcal{Z}_{\alpha, r}$ , and the positive weights  $\text{Re}\{\tau_{\mathfrak{g}}\}$  do not affect the combinatorial structure of  $\mathcal{N}_{\mathcal{G}}^{(\mathcal{Z}_{\alpha, r})}$ , however they determine the asymptotic behaviour.

In order to do a general analysis of the Newton polytope associated to the tree-level integrand, it is useful to organize the connected subgraphs  $\mathfrak{g}$  of  $\mathcal{G}$  in different sets,  $\mathcal{K}(n_s^{\mathfrak{g}})$ , where each set contains only subgraphs with the same number of sites. Then, it is clear that the union of the sets  $\mathcal{K}(n_s^{\mathfrak{g}})$  is equal to the set which contains all the connected subgraphs  $\mathfrak{g}$ ,

$$\{\mathfrak{g}, \mathfrak{g} \subseteq \mathcal{G}\} = \bigcup_{k=1}^{n_s} \mathcal{K}(k) \quad (3.48)$$

with  $\mathcal{K}(n_s) = \{\mathcal{G}\}$ , *i.e.* it contains a single element which is the whole graph  $\mathcal{G}$ ,  $\mathcal{K}(2)$  containing  $n_e = n_s - 1$ <sup>9</sup> elements given by all the 2-site subgraphs constituting  $\mathcal{G}$ , and

<sup>9</sup>This relation between number of edges and sites of a graph holds at for tree graphs only.

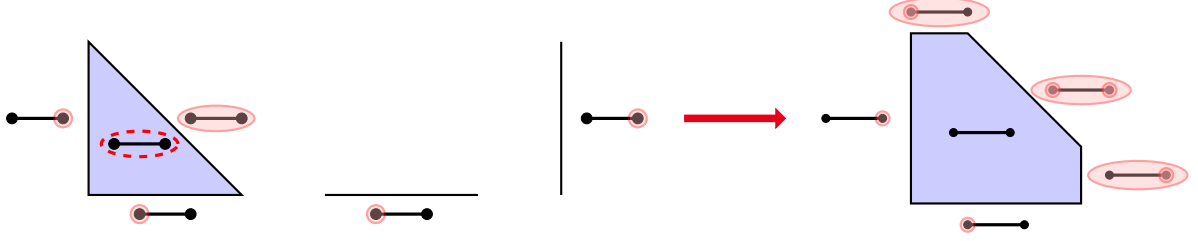


Figure 3.3: Newton polytope associated to a two-site graph  $\mathcal{G}$ . It is constructed as a Minkowski sum of the Newton polytopes associated to its subgraphs  $\mathbf{g}$ , *i.e.* a triangle and two segments respectively for  $\mathbf{g} = \mathcal{G}$  and the two subgraphs containing a single site only— see the triple of pictures on the left. The final Newton polytope can be realised as a truncation of the triangle based on the underlying graph and the tubings corresponding to the single-site graphs, and hence its facets are associated to tubings of the graph.

$\mathcal{K}(1)$  containing the  $n_s$  graphs constituted by a single site. Furthermore, as  $q_{\mathbf{g}}(x)$  is a linear polynomial dependent on all the site weights  $\{x_s, s \in \mathcal{V}_{\mathbf{g}}\}$ , the associated Newton polytope  $\mathcal{N}[\mathbf{g}]$  is a simplex  $\Sigma[\mathbf{g}]$  in  $\mathbb{P}^{n_s^{\mathbf{g}}} \subseteq \mathbb{P}^{n_s}$ . This should be clear since we have seen already that the polynomial which we associate to each singularity of the graph is linear in the  $x$ - and  $y$ -variables. So the set of points generated to build the Newton polytope are all of the form where only one component is non-zero, and that component is one. This is obviously a simplex.

The sum in (3.48) then becomes a Minkowski sum over simplices in  $\mathbb{P}^{n_s^{\mathbf{g}}}$  ( $n_s^{\mathbf{g}} = 1, \dots, n_s$ ) embedded into  $\mathbb{P}^{n_s}$ :

$$\mathcal{N}_{\mathcal{G}} := \bigoplus_{\mathbf{g} \subseteq \mathcal{G}} \text{Re}\{\tau_{\mathbf{g}}\} \Sigma[\mathbf{g}] \quad (3.49)$$

Because of (3.49), these polytopes constitute a special class of *nestohedra*, with the latter being introduced in [218, 219]. The combinatorial structure of (3.49) does not depend on the choice of the powers  $\text{Re}\{\tau_{\mathbf{g}}\}$  [219]. The Minkowski sum (3.49) is performed by starting with the highest dimension simplex, which corresponds to the Newton polytope of the full graph  $\mathcal{N}[\mathcal{G}]$ , then the other terms in the sum will be some of the faces of  $\mathcal{N}[\mathcal{G}]$ , given that also these are simplices which can be identified with the Newton polytopes of smaller subgraphs. These lower dimensional simplices will be faces of co-dimension  $n_s - n_s^{\mathbf{g}}$  [220, 221].

Let us denote the graph as  $\mathbf{g} = \mathcal{G}$  and consider the associated simplex  $\Sigma_{\mathcal{G}}$ . This simplex has facets that correspond to certain tubings of the graph, one of them being the full graph and the other facets can be identified with tubings which include  $n_s - 1$  sites. Keep in mind that a tubing can be composed of several tubes, so in figure 3.4 the bottom facet of the simplex on the top left is identified with a tubing made of two single site tubes.

When we refer to a site  $\not s$ , we mean the one site that is not included in a particular tubing configuration. This means that all the vertices on the facet of  $\Sigma_{\mathbf{g}}$  corresponding to this tubing will have a zero value for their  $\not s$  component. As a result, these vertices lie on a hyperplane of codimension-1, which is defined by the co-vector  $\mathcal{W}^{(\not s)}$ . This co-vector has

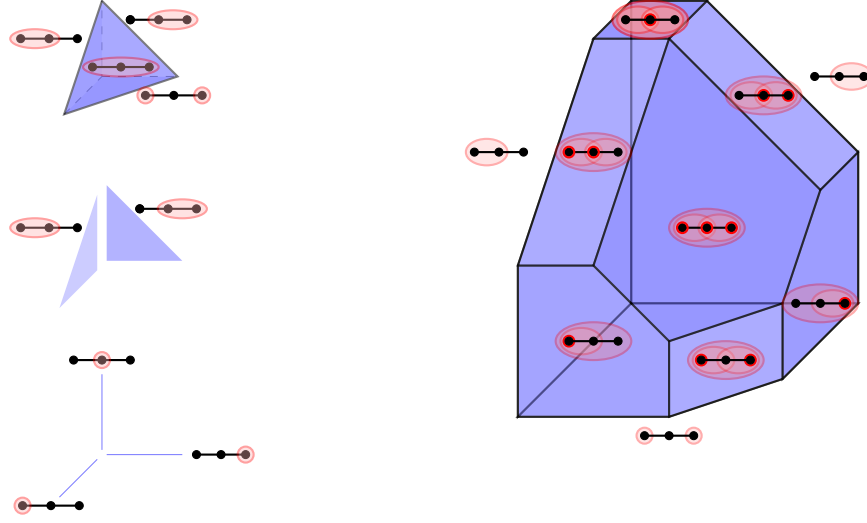


Figure 3.4: Newton polytope associated to the denominators of the three-site graph  $\mathcal{G}$ . It is constructed as a Minkowski sum of the simplices corresponding to all *connected subgraphs* of  $\mathcal{G}$  (on the left). It can be realised by truncating the top-dimensional simplex, based on all the allowed tubings, which corresponds to a subset of the facet of the simplex itself (on the right).

all components equal to zero except for the  $\not{j}$  component, which is set to  $-1$ .<sup>10</sup>

The facet that corresponds to the tube including all sites is represented by a vector where all components are equal to 1.

In the context of the Minkowski sum (3.49), the other simplices that appear are the codimension- $k$  faces of  $\Sigma_{\mathcal{G}}$  for  $k \in [1, n_e - 1]$ . These faces are identified by connected tubes that relate to the higher-dimensional faces of the simplex.

To construct the Newton polytope associated with the entire graph  $\mathcal{G}$ , one can iteratively truncate the top-dimensional simplex  $\Sigma_{\mathcal{G}}$  using the lower codimension simplices that correspond to connected subgraphs. The new facets that arise from this process are labeled by overlapping among the tubes related to the simplices contributing to the overall structure. This iterative truncation process retains the original facets of  $\Sigma_{\mathcal{G}}$  while adding new ones.

The original facets are characterized by the co-vectors  $\{\mathcal{W}^{(j)} := (0, -\mathbf{e}_j)^T, j = 1, \dots, n_s\}$  and  $\mathcal{W}^{(j_1 \dots j_{n_s})} := (\lambda^{(j_1 \dots j_{n_s})}, \mathbf{e}_{1 \dots n_s})^T$ . Here,  $\{\mathbf{e}_j \in \mathbb{R}^{n_s}, j = 1, \dots, n_s\}$  represents the canonical basis in  $\mathbb{R}^{n_s}$ , and  $\mathbf{e}_{1 \dots n_s}$  is a vector with all entries equal to 1.

As the new facets are derived from truncating the top-dimensional simplex  $\Sigma_{\mathcal{G}}$  through

<sup>10</sup>The minus sign is just a consequence of the convention that the co-vectors  $\mathcal{W}$  that identify the facets are directed outwards with respect to the polytope. It is possible to equivalently choose the opposite convention. In this case, the expression (3.39) would change as well, with the minimum replacing the maximum.

its codimension-1 allowed tubings, they are represented by co-vectors of a specific form:

$$\mathcal{W}^{(j_1 \dots j_{n_s^{(g)}})} = \begin{pmatrix} \lambda^{(j_1 \dots j_{n_s^{(g)}})} \\ \mathbf{e}_{j_1 \dots j_{n_s^{(g)}}} \end{pmatrix},$$

where the set  $\{\mathbf{e}_{j_1 \dots j_{n_s^{(g)}}}, j_k \in [k, n_s - n_s^{(g)} + k], k \in [1, n_s^{(g)}]\}$ . The entries of  $\mathbf{e}_{j_1 \dots j_{n_s^{(g)}}}$  are all zero except in the components labeled by the indices (*e.g.* if we are considering a three-site graph then a possible vector is  $\mathbf{e}_{12} = (1, 1, 0)$ ). And each of these non-zero components corresponds directly to one of the single site tubes of the corresponding facet. From the perspective of the graph, these entries are linked to the overlaps between different tubes. For a fixed value of  $n_s^{(g)}$ , these entries specifically identify the overlaps that contain  $n_s^{(g)}$  single-site tubes. This relationship is illustrated in Figures 3.3 and 3.4.

Additionally, the function  $\lambda^{(j_1 \dots j_{n_s^{(g)}})}$  is defined as (minus) the number of overlapping tubes that correspond to the facet identified by  $\mathcal{W}^{(j_1 \dots j_{n_s^{(g)}})}$ .

This formulation clarifies that the total number of facets of the Newton polytope  $\mathcal{N}_{\mathcal{G}}$  can be counted as

$$\tilde{\nu}[\mathcal{N}_{\mathcal{G}}] = 2n_s + \sum_{n_s^{(g)}=2}^{n_s} \binom{n_s}{n_s^{(g)}} = 2n_s + n_s - 1,$$

with the first term providing the dimension of the collection  $\{\mathcal{W}^{(j)}, \mathcal{W}'^{(j)} \in \mathbb{P}^{n_s}, j = 1, \dots, n_s\}$ , while each term in the sum counts the number of co-vectors  $\{\mathcal{W}^{(j_1 \dots j_{n_s^{(g)}})}\}$  for fixed  $n_s^{(g)} \in [2, \dots, n_s]$ . Interestingly, the number of facets  $\tilde{\nu}[\mathcal{N}_{\mathcal{G}}]$  is independent on the topology of the graph  $\mathcal{G}$  for a fixed number of sites  $n_s$ . Finally, two facets identified by any two of the co-vectors  $\{\mathcal{W}^{(j_1 \dots j_{n_s^{(g)}})}, n_s^{(g)} = 1, \dots, n_s\}$  of the Newton polytope  $\mathcal{N}_{\mathcal{G}}$  turn out to be compatible if they correspond to tubings that can be mapped into each other by erasing or adding a single tube or nested tubings (but not erase and add simultaneously).

The knowledge of the compatible facets, allows dividing the domain of integration into sectors  $\Delta_{\mathcal{W}_c}$ ,  $\mathcal{W}_c$  being a given set of compatible facets:

$$\mathbb{R}_+^{n_s} := \bigcup_{\{\mathcal{W}_c\}} \Delta_{\mathcal{W}_c}.$$

Besides for the two-site line graph contributing to the wavefunction for conformally coupled scalars, the rational integrand in (3.47) has a numerator which is a polynomial of degree higher than zero. As discussed earlier, for such cases, it is useful to consider the integral  $\mathcal{I}_{\mathcal{G}}^{(0)}$  as a sum of integrals that are a Mellin transform, whose parameters are shifted, of a rational function whose denominator is the same as the original integral, while its numerator is a constant. Alternatively, it is convenient to express the integrand via one of the triangulations of the underlying cosmological-type polytope in such a way that no spurious boundary is added [189, 193], *e.g.*

$$\mathcal{I}_{\mathcal{G}}^{(0)}[\alpha, \tau', \mathcal{X}] = \sum_{\{\mathcal{G}_c\}} \int_{\mathbb{R}_+^{n_s}} \left[ \frac{dz}{z} z^\alpha \right] \prod_{\mathbf{g}' \in \mathcal{G}_c} \frac{1}{[q_{\mathbf{g}'}(z, \mathcal{X}_{\mathbf{g}'})]^{\tau'_{\mathbf{g}'}}} \prod_{\mathbf{g} \in \mathcal{G}_o} \frac{1}{[q_{\mathbf{g}}(z, \mathcal{X}_{\mathbf{g}})]^{\tau_{\mathbf{g}}}}, \quad (3.50)$$

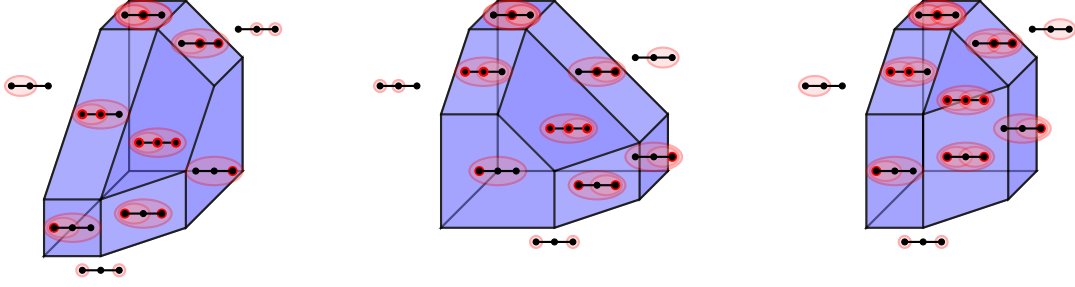


Figure 3.5: Newton polytope associated to the two integrals with numerator of degree 0 in which the three-site graph can represent, and their overlap. They both can be constructed via a truncation of the top-dimensional simplex via lower dimensional simplices associated to the underlying subgraphs in such a way that iteratively connected subgraphs are taken. Their overlap (*right*) represents the convergence of the full integral associated to the three-site tree graph, with its combinatorial structure identical to the nestohedron in Fig. 3.4.

where  $\mathcal{G}_o$  is a set of  $k$  subgraphs that identifies a subspace of the adjoint surface, while  $\mathcal{G}_c$  is a set of  $(n_s + n_e - k)$  compatible subgraphs which are not in  $\mathcal{G}_o$ . One of these representations can be expressed as a sum of all the possible ways of taking connected subgraphs [83, 189]<sup>11</sup> and hence the Newton polytope associated to each term is still a nestohedron: it can be realised as a truncation of the top-dimensional simplices via lower-dimensional ones associated to these nested subgraphs – see Figure 3.5.

The representation (3.50) has the virtue of guaranteeing that no spurious possible divergent directions are added, and the intersection of the different Newton polytopes provides the convergence of the full integral.

As described above, once the compatible co-vectors are identified, the integral in each sector defined by them can be conveniently parametrised as

$$\mathcal{I}_{\mathcal{G}}|_{\Delta_{\mathcal{W}_c}} := \mathcal{I}_{\Delta_{\mathcal{W}_c}} = \int_0^1 \prod_{\mathcal{W} \in \mathcal{W}_c} \left[ \frac{d\zeta_{\mathcal{W}}}{\zeta_{\mathcal{W}}} \zeta_{\mathcal{W}}^{-\lambda_{\mathcal{W}}} \right] \frac{\mathbf{n}_{\delta}(\zeta, \mathcal{X})}{\prod_{\mathfrak{g} \subseteq \mathcal{G}} [q_{\mathfrak{g}}(\zeta, \mathcal{X})]^{\tau_{\mathfrak{g}}}}, \quad (3.51)$$

with the variables  $\zeta_{\mathcal{W}}$  defined according to (3.41) as

$$x_j \longrightarrow \prod_{\mathcal{W} \in \mathcal{W}_c} \zeta_{\mathcal{W}}^{-\epsilon_j \cdot \omega_{\mathcal{W}}}.$$

The infra-red behaviour is encoded in those sectors which are bounded by the co-vectors

$$\left\{ \mathcal{W}^{(j_1 \dots j_{n_s(\mathfrak{g})})}, n_s^{(\mathfrak{g})} = 1, \dots, n_s \right\}.$$

<sup>11</sup>Such a recursion relation was found in the context of the Bunch-Davies wavefunction [83, 189], it is still applicable for the cosmological correlators: one of the triangulation of the weighted cosmological polytope provides a representation in terms of wavefunction graphs [194], to which the above-mentioned recursion relation can be applied.



Which sectors actually contribute depend on which  $\lambda_{\mathcal{W}} \geq 0$ . Note that as the actual value of lambda is related to the number of tubings that identify the associated facet of the Newton polytope, there is a hierarchy among the directions, with  $\lambda^{(j_1 \dots j_{n_s^{(\mathfrak{g})})})} > \lambda^{(j_1 \dots j_{\tilde{n}_s^{(\mathfrak{g})})})}$  for  $n_s^{(\mathfrak{g})} > \tilde{n}_s^{(\mathfrak{g})}$ . Hence,  $\lambda^{(1 \dots n_s)}$  is the highest possible value.

**Logarithmic divergences** – For  $\lambda^{(1 \dots n_s)} \rightarrow 0$ , then the sectors contributing to the divergence are all those containing  $\mathcal{W}^{(1 \dots n_s)}$  – all the other sectors contains co-vectors such that the related  $\lambda$  is negative. In this case, the divergence is logarithmic and the integral in one of the divergent sector can be written as

$$\mathcal{I}_{\Delta_{\mathcal{W}_c}}^{(0)} \sim \int_0^1 \frac{d\zeta_{\mathcal{W}^{(1 \dots n_s)}}}{\zeta_{\mathcal{W}^{(1 \dots n_s)}}} \zeta_{\mathcal{W}^{(1 \dots n_s)}}^{-\lambda^{(1 \dots n_s)}} \times \int_0^1 \prod_{\mathcal{W} \in \mathcal{W}_c \setminus \{\mathcal{W}^{(1 \dots n_s)}\}} \left[ \frac{d\zeta_{\mathcal{W}}}{\zeta_{\mathcal{W}}} \right] \frac{\mathbf{n}_{\delta}(\zeta)}{\prod_{\mathfrak{g} \subseteq \mathcal{G}} [q_{\mathfrak{g}}(\zeta)]^{\tau_{\mathfrak{g}}}} + \dots \quad (3.52)$$

The first integration decouples and provides a pole in  $\lambda^{(1 \dots n_s)}$ , while the remaining integrations show an integrand which is nothing but the original integrand computed at  $\zeta_{\mathcal{W}^{(1 \dots n_s)}} = 0$ . As this behaviour is common to all sectors sharing  $\mathcal{W}^{(1 \dots n_s)}$  and all the other sectors are well-behaved, the integral  $\mathcal{I}_{\mathcal{G}}^{(0)}$  can be written in terms of the original site weights as

$$\mathcal{I}_{\mathcal{G}}^{(0)} \sim \frac{1}{-\lambda^{(1 \dots n_s)}} \int_{\mathbb{R}_+^{n_s}} \prod_{s \in \mathcal{V}} \left[ \frac{dx_s}{x_s} x_s^{\alpha_s} \right] \frac{1}{\text{Vol}\{\text{GL}(1)\}} \frac{\mathbf{n}_{\delta}(x, \mathcal{X} = 0)}{\prod_{\mathfrak{g} \subseteq \mathcal{G}} [q_{\mathfrak{g}}(x, \mathcal{X}_{\mathfrak{g}} = 0)]^{\tau_{\mathfrak{g}}}} + \dots \quad (3.53)$$

This integral is truly a  $(n_s - 1)$ -dimensional integral – as from (3.52), it decouples into a one-dimensional integral, that provides the divergences, and the remaining integrations. However, it is possible to write it in a  $n_s$ -dimensional fashion by introducing a  $\text{GL}(1)$ -redundancy, which is specified by  $\text{Vol}\{\text{GL}(1)\}$ .

It is important to note that the subgraphs  $\{\mathfrak{g}_{s_j}, j = 1, \dots, n_s\}$  containing a single site contributes via  $q_{\mathfrak{g}_{s_j}}(x_{s_j}, \mathcal{X} = 0) := x_{s_j}$ . Hence, the divergent part in (3.53) can be written as,

$$\mathcal{I}_{\mathcal{G}}^{(0)} \sim \frac{1}{-\lambda^{(1 \dots n_s)}} \int_{\mathbb{R}_+^{n_s}} \prod_{s \in \mathcal{V}} \left[ \frac{dx_s}{x_s} x_s^{\alpha_s - \tau_{\mathfrak{g}_s}} \right] \frac{1}{\text{Vol}\{\text{GL}(1)\}} \frac{\mathbf{n}_{\delta}(x, \mathcal{X} = 0)}{\prod_{\mathfrak{g} \subseteq \mathcal{G} \setminus \{\mathfrak{g}_s\}} [q_{\mathfrak{g}}(x, \mathcal{X} = 0)]^{\tau_{\mathfrak{g}}}} + \dots$$

where the integrand can be interpreted as coming from the original graph by iteratively contracting the pairs of sites onto each other and assigning the sum of their weights to the site obtained from such a contraction [183]. From a combinatorial-geometrical point of view, the integrand can be seen as being:

- for a (generalised) cosmological polytope  $\mathcal{P}_{\mathcal{G}}$ , the covariant restriction [197] of its canonical function  $\Omega(\mathcal{Y}, \mathcal{P}_{\mathcal{G}})$  onto the hyperplane  $\mathcal{H} := \bigcap_{e \in \mathcal{E}} \widetilde{\mathcal{W}}^{(\mathfrak{g}_e)}$  defined as the intersection of the hyperplanes  $\{\widetilde{\mathcal{W}}^{(\mathfrak{g}_e)}, e \in \mathcal{E}\}$  containing the building blocks of the

construction – *i.e.* the triangles associated to the 2-site tree graphs in which a general graph can be decomposed:

$$\Omega^{(n_s)}(\mathcal{Y}_{\mathcal{H}}, \mathcal{P}_{\mathcal{G}} \cap \mathcal{H}) = \oint_{\mathcal{H}} \frac{\langle \mathcal{Y} d^{n_s+n_e-1} \mathcal{Y} \rangle}{(2\pi i)^{n_e}} \frac{\Omega(\mathcal{Y}, \mathcal{P}_{\mathcal{G}})}{\prod_{e \in \mathcal{E}} (\mathcal{Y} \cdot \widetilde{\mathcal{W}}^{(\mathfrak{g})})} \quad (3.54)$$

- for a weighted cosmological polytope  $\mathcal{P}_{\mathcal{G}}^{(w)}$ , the hyperplane  $\mathcal{H}$  defined above contains a codimension- $n_e$  face [194], and hence the integrand – that will still be indicated as  $\Omega^{(n_s)}(\mathcal{Y}, \mathcal{P}_{\mathcal{G}}^{(w)})$  is encoded in the canonical function of such a face  $\mathcal{P}_{\mathcal{G}}^{(w)} \cap \mathcal{H}$ :

$$\Omega^{(n_s)}(\mathcal{Y}_{\mathcal{H}}, \mathcal{P}_{\mathcal{G}} \cap \mathcal{H}) = \frac{1}{\prod_{e \in \mathcal{E}} (\mathcal{Y} \cdot \widetilde{\mathcal{W}}^{(\mathfrak{g}_e)})} \Omega(\mathcal{Y}_{\mathcal{H}}, \mathcal{P}_{\mathcal{G}}^{(w)} \cap \mathcal{H})$$

This provides a clear geometrical interpretation for the leading logarithmic infra-red divergences, which can now be directly extracted from the cosmological-like polytope description.

**Power-law divergences** – If  $\lambda^{(1 \dots n_s)} > 0$ , then all the sectors defined via  $\mathcal{W}^{(j_1 \dots j_{n_s^{(\mathfrak{g})})})}$  such that  $\lambda^{(j_1 \dots j_{n_s^{(\mathfrak{g})})})} \geq 0$  contribute to the divergences. Said differently, as  $\lambda^{(j_1 \dots n_s^{(\mathfrak{g})})} > \lambda^{(j_1 \dots \tilde{n}_s^{(\mathfrak{g})})}$  for  $n_s^{(\mathfrak{g})} > \tilde{n}_s^{(\mathfrak{g})}$ , all the sectors defined via (some of) the co-vectors  $\{\mathcal{W}^{(j_1 \dots j_{n_s^{(\mathfrak{g})})})}, n_s^{(\mathfrak{g})} \in [\tilde{n}_s^{(\mathfrak{g})} + 1, n_s]\}$ , with  $\tilde{n}_s^{(\mathfrak{g})}$  being the highest value for which  $\lambda^{(j_1 \dots j_{\tilde{n}_s^{(\mathfrak{g})})})} < 0$ . Let  $\mathcal{W}_{\text{div}}$  be the collection of co-vectors satisfying such a condition. From the structure of the integral (3.51) in a given sector  $\Delta_{\mathcal{W}_c}$ , it is straightforward to see that the leading divergence is given by the sectors containing the highest number, namely  $\tilde{\nu}_{\text{div}}$ , of elements of  $\mathcal{W}_{\text{div}}$ . Then, the integrals in these sectors develop a pole of multiplicity  $\tilde{\nu}_{\text{div}}$  and its coefficient is a  $(n_s - \tilde{\nu}_{\text{div}})$ -fold integral. The subleading divergences, instead, will take contribution from a higher number of sectors: at order  $\tilde{\nu}_{\text{div}} - k$  ( $k \in [0, \tilde{\nu}_{\text{div}} - 1]$ ), the sectors contributing are all those with a number of elements of  $\mathcal{W}_{\text{div}}$  greater or equal to  $\tilde{\nu}_{\text{div}} - k$ .

For each sector, the leading and subleading divergences can be conveniently organised by expressing the integrand in terms of a (multiple) Mellin-Barnes representation, and mapping the integral in a (multiple) sum whose argument shows the poles in the  $\lambda^{(j_1 \dots j_{n_s^{(\mathfrak{g})})})}$ s.

**Summary:** At this point, we can summarise the procedure to obtain the leading and sub-leading divergences from any tree-level cosmological integral:

- Begin by identifying all possible tubings which encode facets of the Newton polytope of your respective graph. These can be divided in two categories, first we have the tubings which identify with the original facets of the top dimensional simplex and they are all the tubes, and disconnected tubings, which enclose all but one site. The second category are the nested tubings which are composed by all tubes which enclose some subset of sites (this subset can contain any number of sites, from one to all of them).

- The respective co-vectors are then:  $\mathcal{W}'^{(j)}$  and  $\mathcal{W}^{(j_1 \dots j_{n_s^{(\mathfrak{g})})})}$ , respectively for each category. The first one has a  $\lambda$ -function which is zero, and the remaining components are given by a vector which is zero on all components except the  $j$ -component which is  $-1$  (the  $j$  component is the one corresponding to the site not enclosed by a tube). The second category has a  $\lambda$ -function given by (minus) the number of tubes in the tubing, and the remaining components are a vector that has entry 1 in all the components for which the tubing has single site tubes (given by the  $j_i$ 's in the label of the co-vector), and zero for all other components.
- From the tubings that correspond to each facet, one can list which facets are compatible with one another. Maximal sets of mutually compatible facets, mean these facets form a vertex, thus we say that the respective co-vectors associated with these sets form sectors. These sectors will tile the integration region.
- From the  $\lambda$ -function of each co-vector we can identify the divergent directions of the integral. Thus applying the change of variables (3.3.1) to each sector that has a divergent direction will make the computation of the Laurent series in the regulator a straightforward task.

**Example** – It is instructive to fix the ideas with a concrete example. Let us consider the cosmological integral associated to the two-site line graph:

$$\mathcal{I}_2^{(0)}[\alpha] := \int_0^\infty \frac{dx_1}{x_1} x_1^\alpha \int_0^\infty \frac{dx_2}{x_2} x_2^\alpha \frac{1}{(x_1 + x_2 + \mathcal{X}_{\mathcal{G}})(x_1 + \mathcal{X}_{\mathfrak{g}_1})(x_2 + \mathcal{X}_{\mathfrak{g}_2})}. \quad (3.55)$$

As discussed earlier, the asymptotic structure of  $\mathcal{I}_2^{(0)}$  is captured by a nestohedron in  $\mathbb{P}^2$  constructed from the triangle (the top-dimensional simplex in  $\mathbb{P}^2$ ) and truncating via the segments corresponding to two of its side and corresponding to one single tubing each – see Figure 3.3. Such a nestohedron is a pentagon whose facets are identified by the co-vectors

$$\mathcal{W}'^{(1)} = \begin{pmatrix} -\alpha_{\mathcal{R}} \\ -1 \\ 0 \end{pmatrix}, \quad \mathcal{W}'^{(2)} = \begin{pmatrix} -\alpha_{\mathcal{R}} \\ 0 \\ -1 \end{pmatrix}, \quad \mathcal{W}^{(1)} = \begin{pmatrix} \alpha_{\mathcal{R}} - 2 \\ 1 \\ 0 \end{pmatrix}, \quad \mathcal{W}^{(2)} = \begin{pmatrix} \alpha_{\mathcal{R}} - 2 \\ 0 \\ 1 \end{pmatrix}, \quad \mathcal{W}^{(12)} = \begin{pmatrix} 2\alpha_{\mathcal{R}} - 3 \\ 1 \\ 1 \end{pmatrix},$$

where  $\alpha_{\mathcal{R}} := \text{Re}\{\alpha\}$ . The region of integration  $\mathbb{R}_+^2$  can thus be divided into five sectors, each of which is determined by a pair of adjacent co-vectors – see Figure 3.6. The integral (3.55) is divergent along a given  $\mathcal{W}^{(j_1 \dots j_{n_s^{(\mathfrak{g})})})}$  if  $\lambda^{(j_1 \dots j_{n_s^{(\mathfrak{g})})})} \geq 0$ . Hence, depending on the divergences of interest, it is possible to focus on a subset of the sectors only. The integral (3.55) is divergent in the infra-red if  $\lambda^{(12)} := 2\alpha_{\mathcal{R}} - 3 \geq 0$  vel  $\lambda^{(j)} : 2 - \alpha_{\mathcal{R}} \geq 0$  – the equality signals a logarithmic divergence, while the strict positivity signals a power law divergence. If the divergence is logarithmic, it receives a contribution from two sectors, both of them sharing the co-vector  $\mathcal{W}^{(12)}$  and differing by  $\mathcal{W}^{(j)}$  ( $j = 1, 2$ ). Let  $\{\Delta_{\text{IR}}^{(j)}, j = 1, 2\}$  indicate these two sectors. In each of them, the integral can be parametrised as

$$\mathcal{I}_{\Delta_{\text{IR}}^{(j)}} = \int_0^1 \frac{d\zeta_j}{\zeta_j} (\zeta_j)^{-\lambda^{(j)}} \int_0^1 \frac{d\zeta_{12}}{\zeta_{12}} (\zeta_{12})^{-\lambda^{(12)}} \frac{1}{(1 + \zeta_j + \mathcal{X}_{\mathcal{G}}\zeta_{12}\zeta_j)(1 + \mathcal{X}_{\mathfrak{g}_{j+1}}\zeta_{12})(1 + \mathcal{X}_{\mathfrak{g}_j}\zeta_{12}\zeta_j)} \quad (3.56)$$

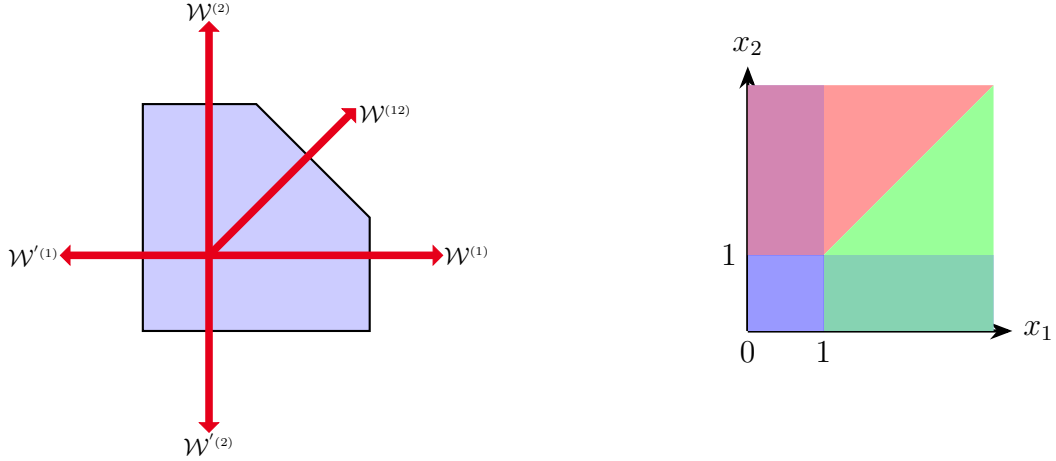


Figure 3.6: *On the left:* Newton polytope corresponding to the two-site tree graph. It has five possible divergent directions that divide the domain of integration in five sectors. *On the right:* Sectors in which the domain of integration is decomposed in the original site weights parametrisation.

with  $\{x_j := \zeta_{12}^{-\epsilon_j \cdot \omega_{12}} \zeta_j^{-\epsilon_j \cdot \omega_j}, j = 1, 2\}$ . If  $\lambda^{12} \rightarrow 0$ , then the integral over  $\zeta_j$  is finite and the divergence come just from the integration over  $\zeta_{12}$ . The divergent contribution is then given by,

$$\begin{aligned} \mathcal{I}_{\Delta_{\text{IR}}^{(j)}} &= \int_0^1 \frac{d\zeta_j}{\zeta_j} \frac{(\zeta_j)^{-\lambda^{(j)}}}{(1+\zeta_j)} \times \int_0^1 \frac{d\zeta_{12}}{\zeta_{12}} (\zeta_{12})^{-\lambda^{(12)}} + \dots \\ &= \frac{1}{2} \left[ \psi^{(0)} \left( \frac{-\lambda^{(j)} + 1}{2} \right) - \psi^{(0)} \left( \frac{-\lambda^{(j)}}{2} \right) \right] \times \frac{1}{-\lambda^{(12)}} + \dots \end{aligned}$$

where  $\psi^{(0)}(z)$  is the digamma function. As  $\lambda^{(12)} := 2\alpha_R - 3 \rightarrow 0$ , then  $\lambda^{(j)} := \alpha_R - 2 \rightarrow -1/2$ : the divergence is a simple pole and its coefficient becomes  $\pi/2$ . As discussed above, the integral can be recast as

$$\mathcal{I}_{\Delta_{\text{IR}}^{(j)}} = \frac{1}{-\lambda^{(12)}} \int_{\mathbb{R}_2^+} \prod_{s \in \mathcal{V}} \frac{1}{\text{Vol}\{\text{GL}(1)\}} \left[ \frac{dx_s}{x_s} x_s^{\alpha-1} \right] \frac{1}{x_1 + x_2}$$

where  $\alpha_R = -\lambda^{(j)} + 1 = 3/2$ . The integrand can be thought of a graph made of a single site with weight  $x_1 + x_2$ .

For power-law divergences, the divergences come from four out of the five sectors. Taking, for the sake of argument,  $\lambda^{(12)} \rightarrow 1$ , then  $\lambda^{(j)} \rightarrow 0$ . Two sectors defined by  $(\mathcal{W}^{(2)}, \mathcal{W}^{(12)})$  and  $(\mathcal{W}^{(12)}, \mathcal{W}^{(1)})$  shows both double and simple poles, while the other two just single poles: in order to correctly compute the subleading divergences, it is necessary to consider all these contributions. A way to organise them is via a Mellin-Barnes representation for the integrand  $\Omega(\zeta, \Delta_{\text{IR}}^{(j)})$  in (3.56):

$$\Omega(\zeta, \Delta_{\text{IR}}^{(j)}) = \int_{-i\infty}^{+\infty} \prod_{r=1}^3 [d\xi_r \Gamma(-\xi_r) \Gamma(1 + \xi_r)] (\mathcal{X}_{\mathcal{G}})^{\xi_1} (\mathcal{X}_{\mathfrak{g}_{j+1}})^{\xi_2} (\mathcal{X}_{\mathfrak{g}_j})^{\xi_3} \frac{(\zeta_j)^{\xi_3 + \xi_1} (\zeta_{12})^{\xi_1 + \xi_2 + \xi_3}}{(1 + \zeta_j)^{\xi_1}}$$

The integral  $\mathcal{I}_{\Delta_{\text{IR}}^{(j)}}$  then becomes

$$\begin{aligned} \mathcal{I}_{\Delta_{\text{IR}}^{(j)}} = & \frac{-\mathcal{X}_{\mathfrak{g}_{j+1}}}{(-\lambda^{(12)} + 1)(-\lambda^{(j)})} + \frac{1}{-\lambda^{(12)} + 1} \left[ -\mathcal{X}_{\mathcal{G}} \int_0^1 \frac{d\zeta_j}{\zeta_j} \frac{\zeta_j^{-\lambda^{(j)}+1}}{1 + \zeta_j} + \frac{-\mathcal{X}_{\mathfrak{g}_j}}{-\lambda^{(j)} + 1} \right] + \\ & + \frac{1}{-\lambda^{(j)}} \left[ \frac{1}{-\lambda^{(12)}} + \sum_{m \geq 2} \frac{(-\mathcal{X}_{\mathfrak{g}_j})^m}{\Gamma(1+m)(-\lambda^{(12)} + m)} \right] + \dots \end{aligned}$$

As a final comment, this approach is completely general and allows tackling leading and subleading divergences in arbitrary power-law FRW cosmologies. While this example as well as all the discussion in this section was devoted to tree-level, the combinatorics of the nestohedra turns out to encode the asymptotic behaviour of loop integral as well, as we will discuss in the next section. Despite it is possible to treat all divergences, what is still missing in this story is a full-fledge combinatorial understanding of the subleading divergences: while the leading one is understood as the restriction of the polytope associated to a given graph onto a special codimension- $n_e$  hyperplane, an understanding for the subleading ones along similar lines is still not available, and we leave it for future work.

### 3.3.2 The perturbative structure of the Loop-level wavefunction

The preceding analysis demonstrated how the asymptotic behavior of tree-level contributions to cosmological observables is governed by the combinatorial structure of a nestohedron. Its realization as sequential truncations of a top-dimensional simplex, formed by a collection of lower-dimensional simplices corresponding to a subset of its faces, facilitates the straightforward determination of all the directions along which they may diverge, as well as the degree of these divergences. The compatibility condition on the facets, formulated in terms of tubings on the underlying graph, enables the identification of the sectors in which, such directions partition the domain of integration. This, in turn, permits the extraction of all divergences in any of the aforementioned directions.

Let us turn now to the loop contributions to cosmological observables. Given an arbitrary graph  $\mathcal{G}$  with  $n_s$  sites,  $n_e$  edges – of which  $n_e^{(L)}$  are loop edges – and  $L$  loops, it has associated an integral  $\mathcal{I}_{\mathcal{G}}^{(L)}$  of the form

$$\mathcal{I}_{\mathcal{G}}^{(L)}[\alpha, \beta] := \int_{\mathbb{R}_+^{n_s}} \prod_{s \in \mathcal{V}} \left[ \frac{dx_s}{x_s} x_s^{\alpha_s} \right] \int_{\Gamma} \prod_{e \in \mathcal{E}^{(L)}} \left[ \frac{dy_e}{y_e} y_e^{\beta_e} \right] \mu_d(y_e, \mathcal{X}; n_s) \frac{\mathbf{n}_{\delta}(x, y; \mathcal{X})}{\prod_{\mathfrak{g} \subseteq \mathcal{G}} [q_{\mathfrak{g}}(x, y; \mathcal{X}_{\mathfrak{g}})]^{\tau_{\mathfrak{g}}}} \quad (3.57)$$

with:

- $\mathcal{E}^{(L)}$  being the set of loop edges;
- $\mu_d$  being the measure of the loop integration;
- $\Gamma$  being the contour of integration;

- $\mathcal{X}_{\mathfrak{g}}$  parametrising the external kinematics associated to the subgraph  $\mathfrak{g} \subseteq \mathcal{G}$ ;

This class of integrals is nearly Mellin-type: integration over  $x$ -variables acts as a Mellin transform, while integration over  $y$ -variables follows a contour defined by the non-negative volume of a top-dimensional simplex in  $\mathbb{R}^{n_e}$  and its faces. The integration boundary is set by the vanishing volume.

The rational integrand is determined by the combinatorics of cosmological polytopes, with linear polynomials  $q_{\mathfrak{g}}$  tied to subgraphs of  $\mathcal{G}$  and facets of the polytopes. The degree- $\delta$  polynomial  $\mathbf{n}_{\delta}$  provides the adjoint surface.

The integration measure, a polynomial related to the volume of simplices in  $y$ -space, introduces a new feature absent in tree graphs. Its power, dependent on spatial dimension and edge count, can be integer or half-integer. Integer powers theoretically allow expansion over measure monomials, but this is often impractical due to complexity.

For small  $y$ , the integration contour's non-negative condition requires only one  $y$  per loop to be arbitrarily small, simplifying divergence analysis and dictating infrared behavior. For large  $y$ , uniform largeness across loops simplifies ultraviolet behavior analysis.

Despite the complex integration domain, identifying divergences is straightforward. The integration measure's polynomial, derived from a determinant, has negative coefficients but remains positive in the integration region, vanishing only at boundaries. This allows unmodified asymptotic analysis.

With this information available, it is thus feasible to analyse the asymptotic behaviour of the integral in the same way we did for tree graphs, while keeping in mind the non-negative condition imposed by the previously described contour of integration.

Let us begin with the  $x$ -integration only. The Newton polytope associated to a loop graph  $\mathcal{G}$  then lives in  $\mathbb{P}^{n_s}$ , and still has the structure of a nestohedron. It can be obtained as the Minkowski sum of simplices, as in the tree case. The main differences with the latter are constituted by: *i*) the weight for the top-dimensional simplex as, for a loop graph, there are  $n_e + 1$  subgraphs which include all the sites of  $\mathcal{G}$ , *i.e.*  $\mathcal{G}$  itself and the  $n_e$  subgraphs obtaining by erasing one edges<sup>12</sup>; *ii*) the collection of simplices in co-dimension- $k$  ( $k \in [1, n_s - 1]$ ) on which the Minkowski sum runs, is larger than for the tree case. For the 2-site  $L$ -loop graphs ( $L \geq 1$ ), just *i*) holds, while *ii*) is as for the tree graphs – this implies that the set of co-vectors  $\{\mathcal{W}'^{(j_1)}, \mathcal{W}^{(j_1 \dots j_{n_s(\mathfrak{g})})} \in \mathbb{P}^{n_s}, j_{n_s(\mathfrak{g})} = 1, \dots, n_s, n_s^{\mathfrak{g}} = 1, \dots, n_s\}$  is the same, up to their component  $\lambda^{(j_1 \dots j_{n_s(\mathfrak{g})})}$  which is affected by the weights. Said differently, the divergent directions for all 2-site  $L$ -loop graphs are the same, and what changes is the way in which they are approached.

Let us now consider the  $y$ -integration only – this is relevant when either there is no site weight integration at all (*e.g.* a conformally-coupled scalar with conformal interactions), or when it can be replaced by a derivative operator (*e.g.* when the real part of the Mellin

<sup>12</sup>To be precise, the statement as formulated is valid for graphs such that all the edges are in a loop. If there are also tree edges, then the number of such subgraphs is  $n_e^{(L)}$

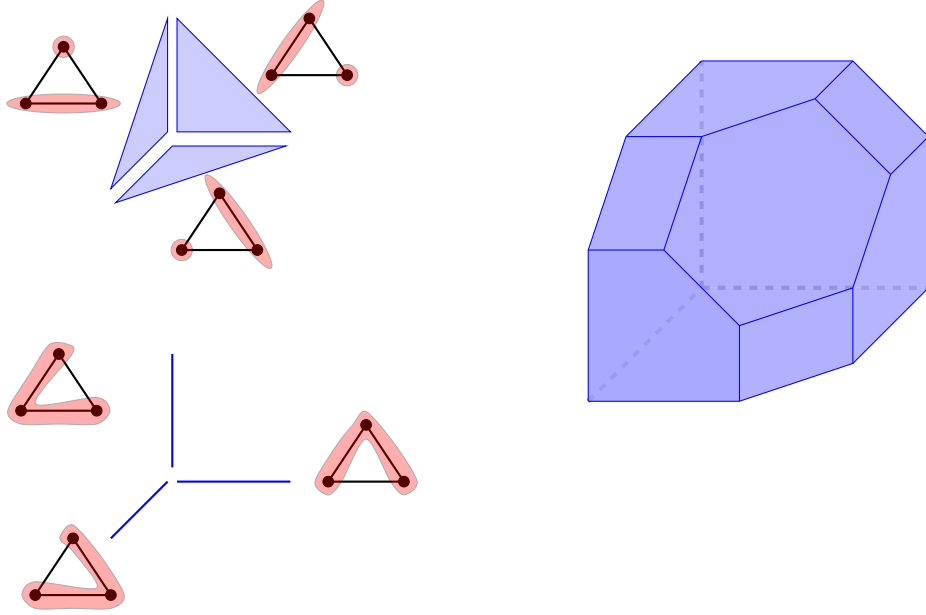


Figure 3.7: Newton polytope associated to the edge weight integration only for a three-site one-loop graph. *On the left:* The simplices building blocks and their tubings. *On the right:* The Newton polytope is a nestohedron which can be realised by truncating the top-dimensional simplex (a tetrahedron) via the tubings associated to the underlying graph.

parameter is negative – it is related to metric warp factor of the type  $a(\eta) \sim \eta^\gamma$ , with  $\gamma > 0$ ). For the sake of simplicity, let us consider graphs with no tree substructure, in such a way that the number of loop edges is the number of total edges. At one-loop, the poles of the canonical function of the relevant polytope can depend on either one or two  $y$ -variables (since the rule for the linear polynomial,  $q_g$ , tells us that it has the  $y$ 's that the tube cuts in the graph). Consequently, the Newton polytope associated to a one-loop graph is given by a weighted Minkowski sum of triangles and segments, irrespectively of the dimension. This implies that just the two-site one-loop graph involves the top-dimensional simplex. Nevertheless, as for the tree graphs, it is possible to realise this nestohedron starting with the top-dimensional simplex, and truncating based on tubings on the underlying subgraphs – see Figure 3.7. The facets are then identified by the co-vectors

$$\mathcal{W}'^{(j)} = \begin{pmatrix} 0 \\ -\mathbf{e}_j \end{pmatrix}, \quad \mathcal{W}^{(j_1 \dots j_{n_e^{(g)}})} = \begin{pmatrix} \lambda^{(j_1 \dots j_{n_e^{(g)}})} \\ \mathbf{e}_{j_1 \dots j_{n_e^{(g)}}} \end{pmatrix},$$

where  $n_e^{(g)} = 1, \dots, n_e$ , with  $\lambda^{(j_1 \dots j_{n_e^{(g)}})}$  being given by the number of tubings associated to a given facet, as in the tree case.

The loop integration can also be considered as the Mellin transform of an integrand (3.57), and hence the Newton polytope get shifted by the vector  $(1, \beta) - \beta := (\beta_e)_{e \in \mathcal{E}}$  – made out by the Mellin parameters, which reflects into the co-vectors identifying the facets

by the shift

$$\begin{aligned}\lambda'^{(j)} &\longrightarrow \tilde{\lambda}'^{(j)} = -\beta_{e_j} \\ \lambda^{(j_1 \dots j_{n_e(\mathfrak{g})})} &\longrightarrow \tilde{\lambda}^{(j_1 \dots j_{n_e(\mathfrak{g})})} = \lambda^{(j_1 \dots j_{n_e(\mathfrak{g})})} + \sum_{e \in \mathcal{E}_{\mathfrak{g}}^{\text{ext}}} \beta_e,\end{aligned}$$

where, as usual,  $\mathcal{E}_{\mathfrak{g}}^{\text{ext}}$  is the set of edges departing from the subgraph  $\mathfrak{g}$  – if  $\beta_e = \beta$ ,  $\forall e \in \mathcal{E}$ , then the shift becomes simply  $\lambda^{(j_1 \dots j_{n_e(\mathfrak{g})})} \longrightarrow \tilde{\lambda}^{(j_1 \dots j_{n_e(\mathfrak{g})})} = \lambda^{(j_1 \dots j_{n_e(\mathfrak{g})})} + n_e(\mathfrak{g})\beta$ . For the sake of simplicity, let us focus on one-loop graphs.

The infra-red behaviour of the integrals associated to them, according to the nestohedron analysis, is encoded into the sector identified by  $\{\mathcal{W}'^{(j)}, j = 1, \dots, n_e\}$ . Note that the change of variables dictated by this sector map the  $y$ 's into themselves. Hence, the integral in this sector is the very same original integral but with the domain of integration which is bounded by an arbitrary cut-off according to the contour of integration  $\Gamma$ . As we argued earlier, the non-negativity condition imposed by the contour of integration, make the integral divergent just when one of the edge variables approaches zero. In order to determine the degree of divergence along the directions  $\{\mathcal{W}'^{(j)}, j = 1, \dots, n_e\}$  it is necessary to understand how the measure contributes. As for the time being we are restricting ourselves to one-loop and to graphs with no tree substructure, the graphs are all polygons – thus they have the same number of sites and edges. It is convenient to label the edge connecting the site  $s_j$  to the site  $s_{j+1}$  with  $y_{j,j+1}$ . Firstly, as we argued earlier, the non-negative condition selects which divergent direction can be taken simultaneously. This implies that even in a given sector identified by a set of compatible co-vectors of the Newton polytope, the singularity that would be reached along two (or more) directions cannot be accessed. It is therefore convenient to separate them by considering any given sector where this phenomenon occurs as a union of sectors, each of which contains just the directions which are allowed by the non-negative condition from the integration contour. For example, let us consider the sectors which contains the singularity at  $y_{12} \longrightarrow 0$ . The further split highlighted above can be obtained via the change of variables

$$y_{12} = P_{23} \frac{\omega}{1 + \omega}, \quad y_{j,j+1} = P_{2\dots j} + 2\omega_{j,j+1} \frac{\omega}{1 + \omega}$$

Under this change of variable, the edge-weight integration measure acquires the form<sup>13</sup>

$$\mu_d(y^2, P^2) = \left[ \frac{\omega}{(1 + \omega)^2} \right]^{d-n_e-1} \tilde{\mu}_d(\omega, \omega_{ij})$$

In this case, the singularity for  $y_{12} \longrightarrow 0$  is separated from the others that are pushed to infinity:

$$\mathcal{I}_{\Delta}^{(1)} = \int_0^{+\infty} \frac{d\omega}{\omega} \omega^{\beta+d-3} \int_{\Gamma'} \prod_{e \in \mathcal{E}} d\omega_e \left[ P_{2\dots j_e} + P_{23}\omega_e \frac{\omega}{1 + \omega} \right]^{\beta_e-1} \tilde{\mu}_d(\omega, \omega_e) \Omega(\omega, \omega_e; \mathcal{X}),$$

---

<sup>13</sup>This is straightforward to see considering that the Cayley-Menger determinant which characterises it



where factors of  $(1 + \omega)$  have been absorbed into  $\tilde{\mu}_d(\omega, \omega_e)$ . Having the directions which are not compatible with  $y_{12} \rightarrow 0$  be pushed to infinity, the sector  $\Delta$  can be further decomposed in two sectors, one containing the divergence at  $y_{12} \rightarrow 0$  only:

$$\mathcal{I}_{\Delta}^{(1)} = \int_0^1 \frac{d\omega}{\omega} \omega^{\beta+d-3} \int_{\Gamma'} \prod_{e \in \mathcal{E}} d\omega_e \left[ P_{2\dots j_e} + P_{23}\omega_e \frac{\omega}{1+\omega} \right]^{\beta_e-1} \tilde{\mu}_d(\omega, \omega_e) \Omega(\omega, \omega_e; \mathcal{X})$$

In this form, the extraction of the leading and subleading divergences proceeds as discussed in the previous sections.

The second subsector contains divergences that occur when other  $y$ 's approach zero. However, polygons are symmetric objects, so the results for these divergences can be obtained from the one for  $y_{12}$  via a simple relabelling.

For the ultraviolet divergences, the domain of integration forces all of the  $y$ 's to approach infinity in the same way, which means that only the direction  $\mathcal{W}^{(1 \dots n_e)}$  becomes divergent. Similarly, one can focus on the sectors which are bounded by the co-vector  $\mathcal{W}^{(1 \dots n_e)}$ , and separate the related singularities from the others via the following change of variables

$$y_{12} = \omega_{12}, \quad y_{j,j+1} = \omega_{12} + P_{j,j+1}\omega_{j,j+1}$$

For higher loops, a similar strategy applies: it is possible to construct the Newton polytope in a similar fashion, and then restrict the divergent directions allowed by the non-negative condition from the contour of integration. In order to impose such a condition, it is convenient to proceed in a loop by loop fashion – which is also a way in which both measure and contour of integration are constructed. This also allows working recursively, applying the lower-loop treatment to the higher loop graphs.

Let us now consider both  $x$  and  $y$  integration at the same time. This allows understanding the interplay between divergences coming from the loop modes ( $y$ -integration), and the ones coming from the expansion of the universe ( $x$ -integration).

In this case, it is possible to determine the possible divergent directions in an unconstrained fashion from the analysis of the full Newton polytope, and, as in the previous

---

can be written as:

$$\begin{aligned} \text{CM}(y_{i,i+1}^2, P_{2\dots j+1}^2) &= \omega^2 \text{CM}(P_{2\dots j+1}^2) + \frac{1}{4} \sum_{i=1}^{n-1} \left\{ \left[ (-1)^i (\omega^2 + P_{i,i+1}^2 - (P_{i,i+1} - \omega \omega_{i,i+1})^2) \right] \times \right. \\ &\quad \left. \times \sum_{j=1}^{n-1} (-1)^{j+1} (\omega^2 + P_{j,j+1} - (P_{j,j+1} + \omega \omega_{j,j+1})^2) G_{\sigma_j} \right\} \\ &= \omega^2 \text{CM}(P_{2\dots j+1}^2) + \frac{\omega^2}{4} \sum_{i,j=1}^{n-1} (-1)^{i+j+1} \{ (\omega(1 - \omega_{i,i+1}^2) - 2 a_{i,i+1} P_{i,i+1}) \times \\ &\quad \times (\omega(1 - \omega_{j,j+1}^2) - 2 \omega_{j,j+1} P_{j,j+1}) \text{CM}_{\sigma_j} \} \end{aligned}$$

where  $\text{CM}_{\sigma_j}$  is the determinant of a minor of the total Cayley-Menger matrix, which contains only entries depending on  $P_e$ .

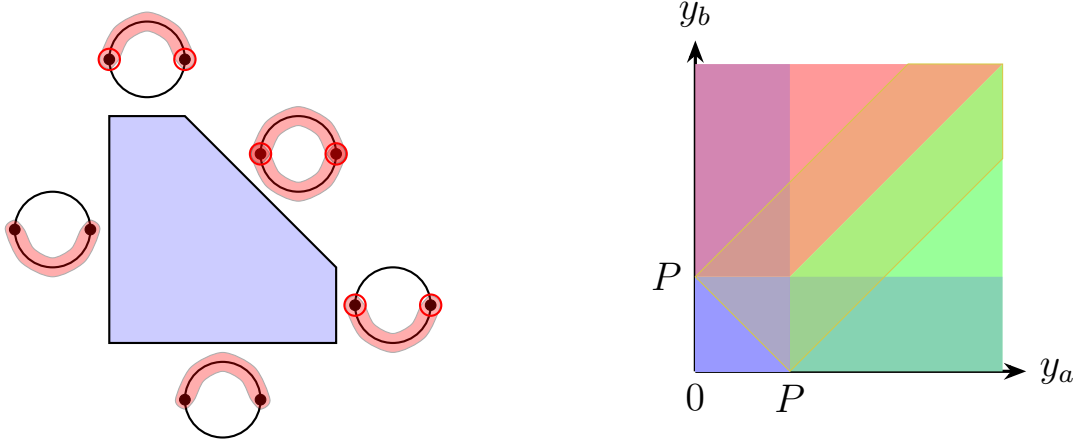


Figure 3.8: *On the left:* The Newton polytope associated to the edge weight integration for the two-site one-loop graph is a nestohedron whose facets are identified by certain tubings. They correspond to directions in which the integral might diverge. The number of tubings instead correspond to how these directions are approached. A subset of these directions are selected by the integration contour. *On the right:* The knowledge of compatible facets of the Newton polytope allows to decompose  $\mathbb{R}_+^2$  in sectors, which can be restricted onto the domain of integration via the non-negativity condition which defines it.

discussion, constrain them with the non-negative conditions from the edge-weight integration contour.

In this case, the Newton polytope remains a nestohedron situated in  $\mathbb{P}^{n_s+n_e}$ . Although the top-dimensional simplex does not match any of the linear polynomials found in the denominators, it can still be represented as a sequential truncation derived from the underlying graph of the top-dimensional simplex. The top-dimensional simplex, which lacks any associated tubing, undergoes sequential truncation through simplices in  $\mathbb{P}^{n_s^{(\mathfrak{g})}+n_e^{\text{ext}}}$ , where  $n_s^{(\mathfrak{g})}$  denotes the number of sites within the subgraph  $\mathfrak{g} \subseteq \mathcal{G}$ , and  $n_e^{\text{ext}}$  represents the number of edges emanating from it. All facets correspond to tubings in a manner consistent with the descriptions provided in the preceding sections. Since the top-dimensional simplex does not correspond to any denominator, it is devoid of associated tubing and thus does not influence the asymptotic behaviour, serving solely for the construction itself. The subsequent analysis follows from the discussion regarding  $y$  integration.

### 3.3.3 Example: The two-site one-loop graph

It is instructive to illustrate the procedure discussed above in some concrete, simple, but yet non-trivial and illustrative example, the bubble integral. This integral can be explicitly written as:

$$\mathcal{I}_{\mathcal{G}}^{(1)} = \prod_{s \in \mathcal{V}} \left[ \frac{dx_s}{x_s} x^\alpha \right] \int_{\Gamma} \prod_{e \in \mathcal{E}} \left[ \frac{dy_e}{y_e} y_e^\beta \right] \frac{[-\text{CM}(y^2, P^2)]^{\frac{d-3}{2}}}{P^{d-2}} \Omega(x, y; \mathcal{X}) \quad (3.58)$$

where  $\Omega(x, y; \mathcal{X})$  is the canonical function of the (generalised/weighted) cosmological polytopes associated to this graph, and the contour of integration is:

$$\Gamma := \left\{ x \in \mathbb{R}_+^2, y \in \mathbb{R}_+^2 \mid -\text{CM}(y^2, P^2) \geq 0 \right\}.$$

Note that for  $d = 3$  the measure of integration simplifies, with the only novelty with respect to the previous case given by the contour of integration  $\Gamma$ . As discussed previously, the contour of integration selects a subset of possible divergent directions that would come from the analysis of the integrand alone. In particular, the edge weights can get to zero just once at a time – as  $y_a \rightarrow 0$  then  $y_b \rightarrow P$ , and vice versa, when  $y_b \rightarrow 0$ ,  $y_a \rightarrow P$  –, while they have to approach infinity simultaneously.

Let us look at the asymptotic structure by first considering the Newton polytope associated to the integrand  $\Omega(x, y; \mathcal{X})$ . In order to give a general account, let us consider the following form

$$\Omega(x, y; \mathcal{X}) = \frac{\mathbf{n}_\delta(x, y; \mathcal{X})}{[q_{\mathcal{G}}(x, y; \mathcal{X})]^{\tau_{\mathcal{G}}} [q_{\mathfrak{g}_a}(x, y; \mathcal{X})]^{\tau_{\mathfrak{g}_a}} [q_{\mathfrak{g}_b}(x, y; \mathcal{X})]^{\tau_{\mathfrak{g}_b}} [q_{\mathfrak{g}_1}(x, y; \mathcal{X})]^{\tau_{\mathfrak{g}_1}} [q_{\mathfrak{g}_2}(x, y; \mathcal{X})]^{\tau_{\mathfrak{g}_2}}}$$

where

$$\begin{aligned} q_{\mathcal{G}} &:= x_1 + x_2 + \mathcal{X}_{\mathcal{G}}, & q_{\mathfrak{g}_a} &:= x_1 + x_2 + 2y_a + \mathcal{X}_{\mathcal{G}}, & q_{\mathfrak{g}_b} &:= x_1 + x_2 + 2y_b + \mathcal{X}_{\mathcal{G}} \\ q_{\mathfrak{g}_1} &:= x_1 + y_a + y_b + \mathcal{X}_{\mathfrak{g}_1}, & q_{\mathfrak{g}_2} &:= x_2 + y_a + y_b + \mathcal{X}_{\mathfrak{g}_2} \end{aligned}$$

Let us begin with consider solely the loop integration – as mentioned earlier this is sensible for those cases in which the integration over the site weight is absent. The Newton polytope then lives in  $\mathbb{P}^2$  and it is a nestohedron built via sequential truncation of a triangle via two segments corresponding to two of its sides – combinatorially it is the same polytope obtained in the two-site tree graph:

$$\mathcal{W}^{(1)} = \begin{pmatrix} -\beta_{\mathcal{R}} \\ -1 \\ 0 \end{pmatrix}, \quad \mathcal{W}'^{(2)} = \begin{pmatrix} -\beta_{\mathcal{R}} \\ 0 \\ -1 \end{pmatrix}, \quad \mathcal{W}^{(1)} = \begin{pmatrix} \lambda^{(1)} \\ 1 \\ 0 \end{pmatrix}, \quad \mathcal{W}^{(2)} = \begin{pmatrix} \lambda^{(2)} \\ 0 \\ 1 \end{pmatrix}, \quad \mathcal{W}^{(12)} = \begin{pmatrix} \lambda^{(12)} \\ 1 \\ 1 \end{pmatrix},$$

where  $\lambda^{(1)} := \beta - \tau_{\mathfrak{g}_a} - \tau_{\mathfrak{g}_1} - \tau_{\mathfrak{g}_2}$ ,  $\lambda^{(2)} := \beta - \tau_{\mathfrak{g}_b} - \tau_{\mathfrak{g}_1} - \tau_{\mathfrak{g}_2}$  and  $\lambda^{(12)} := 2\beta - \tau_{\mathfrak{g}_a} - \tau_{\mathfrak{g}_b} - \tau_{\mathfrak{g}_1} - \tau_{\mathfrak{g}_2}$ .

The restriction onto the contour of integration allows three out of these five directions:  $\mathcal{W}^{(1)}$ ,  $\mathcal{W}'^{(2)}$  and  $\mathcal{W}^{(12)}$ . So the sectors contributing to the infra-red divergences are  $\Delta_{2'1'}$ ,  $\Delta_{1'2}$  and  $\Delta_{12'}$ , which are respectively identified by  $(\mathcal{W}^{(2')}, \mathcal{W}^{(1')})$ ,  $(\mathcal{W}^{(1)}, \mathcal{W}'^{(2)})$  and  $(\mathcal{W}^{(1)}, \mathcal{W}^{(2)})$ ; while the sectors  $\Delta_{2,12}$  and  $\Delta_{12,1}$  – respectively bounded by  $(\mathcal{W}^{(2)}, \mathcal{W}^{(12)})$  and  $(\mathcal{W}^{(12)}, \mathcal{W}^{(1)})$  – codify the ultraviolet divergences. In the sector  $\Delta_{2'1'}$ , the integral acquires

the form<sup>14</sup>

$$\mathcal{I}_{\Delta_{2'1'}} = \int_0^P \frac{d\zeta'_1}{\zeta'_1} (\zeta'_1)^\beta \int_{P-\zeta'_1}^P \frac{d\zeta'_2}{\zeta'_2} (\zeta'_2)^\beta \frac{[\text{CM}(\zeta'^2, P^2)]^{\frac{d-3}{2}}}{P^{d-2}} \Omega(x, \zeta'; \mathcal{X}) \quad (3.59)$$

where  $\Omega(x, \zeta'; \mathcal{X})$  can be thought to be expresses via one of its triangulation with physical poles only.

This sector contains two singularities which cannot be taken simultaneously. It is useful to make the contour of integration independent of any integration variable

$$\mathcal{I}_{\Delta_{2'1'}} = \int_0^{+\infty} \frac{d\omega_1}{\omega_1} \frac{\omega_1^{\beta+d-1}}{(1+\omega_1)^{2(\beta+(d-3))+1}} \int_{-1}^0 d\omega_2 (1+\omega_1(1+\omega_2))^{\beta-1} \tilde{\mu}(\omega_1, \omega_2) \Omega(\omega_1, \omega_2, \mathcal{X}) \quad (3.60)$$

where  $\tilde{\mu}(\omega_1, \omega_2) := [(1-\omega_2)(1+\omega_2)(2+(1+\omega_2)\omega_1)(2+(3+\omega_2)\omega_1)]^{(d-3)/2}$  – it is achieved via  $\zeta'_1 = P\omega_1(1+\omega_1)^{-1}$ ,  $\zeta'_2 = P(1+\omega_2\omega_1(1+\omega_1)^{-1})$ . In this form the two divergences, originally approached as  $y_a \rightarrow 0$  and  $y_b \rightarrow 0$  separately, are clearly separated: the former is reached as  $\omega_1 \rightarrow 0$  while the latter as  $\omega_1 \rightarrow +\infty$ .

The integral (3.60) can be further decomposed into two subsectors  $\Delta_{2'1'} := \Delta_{2'} \cup \Delta_{1'}$ , each of which containing just one of the two divergences. For example,

$$\mathcal{I}_{\Delta_{2'}} = \int_0^1 \frac{d\omega_1}{\omega_1} \frac{\omega_1^{\beta+d-3}}{(1+\omega_1)^{2(\beta+(d-3))+1}} \int_{-1}^0 d\omega_2 (1+\omega_1(1+\omega_2))^{\beta-1} \tilde{\mu}(\omega_1, \omega_2) \Omega(\omega_1, \omega_2, \mathcal{X})$$

and the divergent terms can be extracted expanding around  $\omega_1 \rightarrow 0$

$$\mathcal{I}_{\Delta_{2'}} = \frac{\mathfrak{a}}{\beta+d-3} \Omega(0, \mathcal{X}) + \dots$$

– at leading order, the canonical function becomes independent on  $\omega_2$ , and  $\mathfrak{a}$  represents the integral over  $\omega_2$  which is just a number. As we observed at tree-level, also at loops the coefficient of the leading divergence can be obtained by restricting the canonical function onto a special hyperplane.

The other divergence along the other infrared divergence can be deduced from this one, as the original integral is completely symmetric under the exchange of the two edge weights.

Finally, let us comment on the analysis of both the site- and edge-weight integration simultaneously. In this case, the Newton polytope lives in  $\mathbb{P}^4$ . Constructing, as usual, the nestohedron as a truncation based on the underlying graph, and considering a generic

<sup>14</sup>A peculiarity of this case is that it is the only one in which the Cayley-Menger determinant factorises in a product of linear polynomials

$$-\text{CM}(y^2, P^2) = (y_a + y_b + P)(y_a - y_b + P)(y_a + y_b - P)(-y_a + y_b + P)$$

with the zeroes reached at the boundary of the domain of integration. Consequently, it is possible to have an explicit form for the contour of integration, with  $y_a \in \mathbb{R}_+$  and  $y_b \in [|y_a - P|, y_a + P]$  or, which is the same  $\Delta_{\text{IR}} \cup \Delta_{\text{UV}} \equiv \{y_a \in [0, P], y_b \in [P - y_a, y_a + P]\} \cup \{y_a \in [P, +\infty[, y_b \in [y_a - P, y_a + P]]\}$

point in a system of local coordinates in  $\mathcal{P}^4$  of the form  $(t_1, t_a, t_b, t_2)$  labelling the powers of  $(x_1, y_a, y_b, x_2)$  respectively, its facets are given by

$$\mathcal{W}'^{(j)} = \begin{pmatrix} \lambda'^{(j)} \\ -\mathbf{e}_j \end{pmatrix}, \quad \mathcal{W}^{(j)} = \begin{pmatrix} \lambda^{(j)} \\ \mathbf{e}_j \end{pmatrix}, \quad \mathcal{W}^{(23)} = \begin{pmatrix} \lambda^{(23)} \\ \mathbf{e}_{23} \end{pmatrix}, \quad \mathcal{W}^{(1\dots 4)} = \begin{pmatrix} \lambda^{(1\dots 4)} \\ \mathbf{e}_{1\dots 4} \end{pmatrix}$$

where

$$\begin{aligned} \lambda'^{(1)} &= -\alpha_R = \lambda'^{(4)}, & \lambda'^{(2)} &= -\beta_R = \lambda'^{(3)}, \\ \lambda^{(1)} &= \alpha_R - \tau_{\mathcal{G}} - \tau_{\mathfrak{g}_a} - \tau_{\mathfrak{g}_b} - \tau_{\mathfrak{g}_1}, & \lambda^{(2)} &= \beta_R - \tau_{\mathfrak{g}_a} - \tau_{\mathfrak{g}_1} - \tau_{\mathfrak{g}_2}, \\ \lambda^{(3)} &= \beta_R - \tau_{\mathfrak{g}_b} - \tau_{\mathfrak{g}_1} - \tau_{\mathfrak{g}_2}, & \lambda^{(4)} &= \alpha_R - \tau_{\mathcal{G}} - \tau_{\mathfrak{g}_a} - \tau_{\mathfrak{g}_b} - \tau_{\mathfrak{g}_2}, \\ \lambda^{(23)} &= 2\beta_R - \tau_{\mathfrak{g}_a} - \tau_{\mathfrak{g}_b} - \tau_{\mathfrak{g}_1} - \tau_{\mathfrak{g}_2}, & \lambda^{(1\dots 4)} &= 2(\alpha_R + \beta_R) - \tau_{\mathcal{G}} - \tau_{\mathfrak{g}_a} - \tau_{\mathfrak{g}_b} - \tau_{\mathfrak{g}_1} - \tau_{\mathfrak{g}_2}. \end{aligned}$$

Some comments are now in order. First, note that the collection of co-vectors  $\{\mathcal{W}'^{(j)}, \mathcal{W}^{(j)}, \mathcal{W}^{(23)}\}$  constitute the five possible divergent directions emerging from the analysis of the sole edge weight integration. The non-negativity condition imposed by the contour of integration, prevents the integral to become divergent along more than one direction  $\{\mathcal{W}'^{(j)}, j = 2, 3\}$  and  $\{\mathcal{W}^{(j)}, j = 2, 3\}$ . Hence, those sectors involving more than one of these directions can be further split, as we saw earlier. Secondly, the infra-red behaviour is encoded into the  $\{\mathcal{W}'^{(j)}, j = 2, 3\}$  for internal low energy modes, while  $\{\mathcal{W}^{(j)}, j = 4, 1\}$  codify the ones due to the expansion of the universe. Finally,  $\lambda^{(1\dots 4)}$  encodes the effect of internal high energy modes as the universe expands.

Finally, let us consider a sector  $\Delta_{41}$  containing both  $\mathcal{W}^{(1)}$  and  $\mathcal{W}^{(4)}$  and take either of the two to be divergent, . *i.e.*  $\lambda^{(1)} \geq 0$  or  $\lambda^{(4)} \geq 0$ . Then, following what discussed above for the site-weight integration, and taking  $\lambda^{(j)} \rightarrow 0$  the integral factorises into an integral over the remaining site-weight integration and an integral over the edge weight only

$$\mathcal{I}_{\Delta_{41}} = \frac{1}{-\lambda^{(j)}} \int_0^{+\infty} \prod_{s \in \mathcal{V}} [dx_s] \frac{1}{\text{Vol}\{\text{GL}(1)\}} \Omega(x, y = 0; \mathcal{X} = 0) \times \mathcal{I}_{\Delta_{41}}^{(\varepsilon)}$$

where  $\mathcal{I}_{\Delta_{41}}^{(\varepsilon)}$  can be cast in the terms of the usual loop momentum as

$$\mathcal{I}_{\Delta_{41}}^{(\varepsilon)} := \int d^d l \frac{1}{l^\beta (\vec{l} + \vec{P})^\beta}.$$

Interestingly enough, the contribution from the site-weight integration is related to the restriction of the relevant cosmological polytopes along a special hyperplane  $\bigcap_{e \in \mathcal{E}} \widetilde{\mathcal{W}}^{(\mathfrak{g}_e)}$ , while the edge weight integration can be recast in a flat-space loop integral associated to the same graph.

### 3.4 $\lambda\phi^4$ examples at loop level

Typically, when discussing infrared divergences in de Sitter, the most worked example is a minimally coupled massless scalar field with a quartic self-interacting coupling. Here

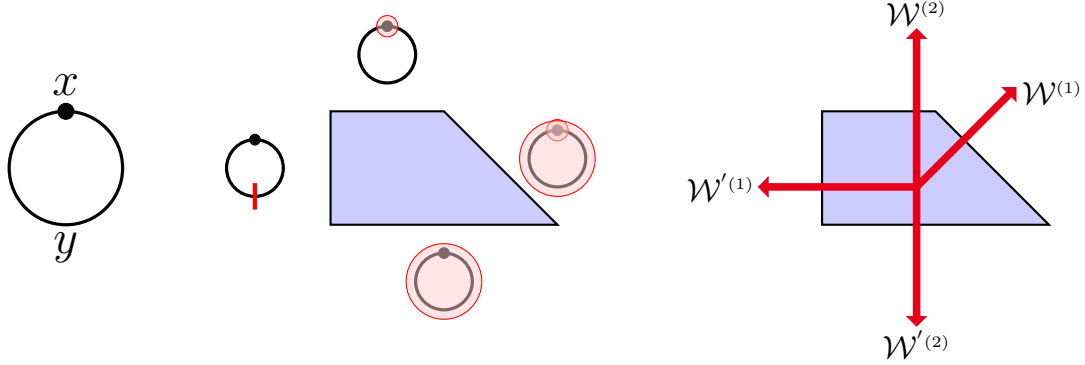


Figure 3.9: *On the left:* The one-site one loop graph. *Center:* the realisation of the Newton polytope for the integral (3.61) associated to the one-site one-loop graph in terms of tubings. *On the right:* Possible divergent directions for the integral (3.61).

we discuss contributions to the two-point function, at one- and two-loops. We start with the first loop level contribution, which comes from the tadpole diagram. It's integral representation is:

$$\mathcal{I}_{\mathcal{G}}^{(1)} = \int_0^\infty \frac{dx}{x} x^\alpha \int_0^\infty \frac{dy}{y} y^\beta \frac{\partial^2}{\partial x^2} \frac{1}{(x + X_{\mathcal{G}})(x + X_{\mathcal{G}} + 2y)}, \quad (3.61)$$

where the parameters  $\alpha$  and  $\beta$  are analytically continued to regularise the integral, which has the form of a usual Mellin transform of a rational function. The Newton polytope is the weighted Minkowski sum of a triangle and a segment in  $\mathbb{P}^2$  and can be realised as sequential truncation of the triangle – see Figure 3.9. Therefore, it has four possible divergent directions, given by the co-vectors associated to the tubings:

$$\mathcal{W}'^{(1)} = \begin{pmatrix} -\alpha_{\mathcal{R}} \\ -1 \\ 0 \end{pmatrix}, \quad \mathcal{W}'^{(2)} = \begin{pmatrix} -\beta_{\mathcal{R}} \\ 0 \\ -1 \end{pmatrix}, \quad \mathcal{W}^{(2)} = \begin{pmatrix} \beta_{\mathcal{R}} - 3 \times 1 \\ 0 \\ 1 \end{pmatrix}, \quad \mathcal{W}^{(12)} = \begin{pmatrix} \alpha_{\mathcal{R}} + \beta_{\mathcal{R}} - 3 \times 2 \\ 1 \\ 1 \end{pmatrix}, \quad (3.62)$$

where in the first entries of  $\mathcal{W}^{(1)}$  and  $\mathcal{W}^{(2)}$  has been emphasised the contribution of the weight  $\tau_{\mathcal{R}}$  and the number of tubings  $n^{(\mathfrak{g})}$  as  $\tau \times n^{(\mathfrak{g})}$ . Note also that for the time being, the numerator of (3.61) has not been taking into account. It is a second order polynomial with 6 monomials. So, we could split the integral into a sum of integrals according to the monomial expansion of the numerator: for each term, the Newton polytope is the same as in Figure 3.9 but shifted by the powers of the relevant monomial. Then, the integral is convergent in the overlap among these Newton polytopes. Then, the co-vectors have the same form as (3.62), but with

$$(\alpha_{\mathcal{R}}, \beta_{\mathcal{R}}) \longrightarrow (\alpha_{\mathcal{R}}, \beta_{\mathcal{R}}) + (\rho_x, \rho_y),$$

where:

$$(\rho_x, \rho_y) = \{(0, 0), (1, 0), (2, 0), (0, 1), (1, 1), (1, 2)\}.$$

Alternatively, we could decompose the integrand according to a triangulation of the generalised cosmological polytope with physical poles only,

$$\mathcal{I}_{\mathcal{G}}^{(1)} = \int_0^{+\infty} \frac{dx}{x} x^\alpha \int_0^{+\infty} \frac{dy}{y} y^\beta \left[ \frac{2}{(x+X_{\mathcal{G}})^3(x+X_{\mathcal{G}}+2y)} + \frac{2}{(x+X_{\mathcal{G}})^2(x+X_{\mathcal{G}}+2y)^2} + \frac{2}{(x+X_{\mathcal{G}})(x+X_{\mathcal{G}}+2y)^3} \right].$$

Each term shows the same Newton polytope arising, but with different weights, while the Mellin parameters are unchanged.

Therefore, the integration domain is divided into four sectors  $\Delta_{2',1'}$ ,  $\Delta_{1',2}$ ,  $\Delta_{2,12}$  and  $\Delta_{12,2'}$ , which are respectively bounded by  $(\mathcal{W}'^{(2)}, \mathcal{W}'^{(1)})$ ,  $(\mathcal{W}'^{(1)}, \mathcal{W}^{(2)})$ ,  $(\mathcal{W}^{(2)}, \mathcal{W}^{(12)})$ , and  $(\mathcal{W}^{(12)}, \mathcal{W}'^{(2)})$ .

The leading infra-red divergence is captured by the sector  $\Delta_{12,2'}$ , with the two directions  $(\mathcal{W}^{(12)}, \mathcal{W}^{(2)})$  becoming simultaneously divergent for  $\lambda^{(12)} := \alpha_{\mathbf{R}} + \beta_{\mathbf{R}} - (\tau_{\mathbf{g}} + \tau_{\mathcal{G}}) - \rho_x - \rho_y \geq 0$  and  $\lambda'^{(2)} := -\beta_{\mathbf{R}-\rho_y} \geq 0$ , and developing a double pole when these conditions are satisfied simultaneously. More precisely, this sector captures the simultaneous divergence from the infinite volume (*i.e.*  $x \rightarrow +\infty$ ) and from the low energy mode in the loop (*i.e.*  $y \rightarrow 0$ ).

Subleading divergences are taken into account by supplementing this sector with  $\Delta_{1',2}$  and  $\Delta_{12,2'}$ , where the two directions  $(\mathcal{W}'^{(2)}, \mathcal{W}'^{(1)})$  diverge individually.

Let us explicitly consider an integral in the sector  $\Delta_{2',1'}$

$$\mathcal{I}_{\Delta_{12,2'}} = 2^{1-\beta} [X_{\mathcal{G}}]^{\alpha-4} \int_0^1 \frac{d\zeta_{12}}{\zeta_{12}} (\zeta_{12})^{-\lambda^{(12)}} \int_0^1 \frac{d\zeta'_2}{\zeta'_2} (\zeta'_2)^{-\lambda'^{(2)}} \frac{1}{(1+\zeta_{12})^{\tau_{\mathcal{G}}} (1+\zeta_{12}+\zeta'_2)^{\tau_{\mathbf{g}}}} \quad (3.63)$$

where  $x$  and  $y$  have been rescaled by  $X_{\mathcal{G}}$  and  $X_{\mathcal{G}}/2$  respectively, and  $(x, y) = (\zeta_{12}^{-1}, \zeta'_2 \zeta_{12}^{-1})$ . If  $(\lambda^{(12)}, \lambda'^{(2)}) \rightarrow (0, 0)$ , the divergence is logarithmic and can be readily extracted to be

$$\begin{aligned} \mathcal{I}_{\Delta_{12,2'}} &= 2^{1-\beta_{\star}} [X_{\mathcal{G}}]^{\alpha_{\star}-4} \int_0^1 \frac{d\zeta_{12}}{\zeta_{12}} (\zeta_{12})^{-\lambda^{(12)}} \int_0^1 \frac{d\zeta'_2}{\zeta'_2} (\zeta'_2)^{-\lambda'^{(2)}} + \dots \\ &= 2^{1-\beta_{\star}} [X_{\mathcal{G}}]^{\alpha_{\star}-4} \frac{1}{(-\lambda^{(12)})(\lambda'^{(2)})} + \dots \end{aligned} \quad (3.64)$$

where  $(\alpha_{\star}, \beta_{\star})$  are the values of the Mellin parameters computed at  $(\lambda^{(12)}, \lambda'^{(2)}) = (0, 0)$ .

For power-law divergences as well as to extract the subleading contribution from this sector, as we discussed earlier, it is convenient to express the integrand via a Mellin-Barnes representation, allowing to perform the integration and mapping  $\mathcal{I}_{\Delta_{12,2'}}$  into a double sum

$$\mathcal{I}_{\Delta_{12,2'}} = \frac{1}{\Gamma(\tau_{\mathbf{g}})} \sum_{k \geq 0} \frac{(-1)^k}{\Gamma(k+1)} \sum_{m \geq 0} \frac{(-1)^m}{\Gamma(m+1)} \frac{\Gamma(\tau_{\mathbf{g}}+m)}{\Gamma(\tau_{\mathcal{G}}+\tau_{\mathbf{g}}+m)} \frac{\Gamma(\tau_{\mathcal{G}}+\tau_{\mathbf{g}}+m+k)}{(k-\lambda^{(12)})(m-\lambda'^{(2)})} \quad (3.65)$$

One can readily see that the integral develops poles when  $(\lambda^{(12)}, \lambda'^{(2)})$  are non-negative and makes it straightforward to extract the information for the specific values of interest, obtaining both the information about double and simple poles.

The leading ultraviolet divergence is along  $\mathcal{W}^{(2)}$  and therefore is captured by the two sectors  $\Delta_{2,12}$  and  $\Delta_{1',2'}$ , and can be extracted in a similar fashion.

From equation (3.63), we see the generality of this procedure. At no point we have introduced any information about the specific theory we have. In the subsequent equations there is the underlying assumption that the theory must have logarithmic divergences in (3.64), or power law divergences (3.65), but that is it. We can use the above results to compute the leading terms for a theory with quartic couplings ( $\varphi^4$ ), in de Sitter, and massless scalars. We will apply this to the correlator, in particular to the disconnected component, for which the total energy singularity is replaced by a factor of  $1/y$ , thus  $(\tau_{\mathcal{G}}, \tau_{\mathfrak{g}}) = (0, 4)$ , and  $(\alpha_*, \beta_*) = (4, 0)$ , in this case the numerator is still one, so  $(\rho_x, \rho_y) = (0, 0)$ . This means that we are in the case where  $(\lambda^{(12)}, \lambda'^{(2)}) = (0, 0)$ , and the result (3.64) applies directly. From this we learn that we have two logarithmic divergences. One of the divergences coming from the  $x$ -integration, which in the related literature is referred to as secular divergence. The other logarithmic divergence comes from the massless state running in the loop, and this is a standard infrared divergence. The coefficient of the leading divergence is also proportional to  $p^{-3}$ , where  $p$  is the external momentum. All of this agrees with the literature on the subject, check [147]. In the above discussion, we considered only the disconnected component contributing to the correlator. For this process, there are only two contributions to the correlator, the disconnected part and the wavefunction. To compute the contribution from the wavefunction, we have the total energy singularity but one less factor of  $y$  in the denominator. Then,  $(\lambda^{(12)}, \lambda'^{(2)}) = (-1, -1)$  which means we have no divergences anymore. This is a verification of the fact that the disconnected components contributing to the correlator are the most divergent, and thus contribute with the leading divergences. This has been noted in the literature, and in particular one can check [156] for a detailed discussion on this. We hope that this simple example has motivated the generality of our method, we can use it to compute leading and sub-leading divergences, for the different terms in the correlator, as well as for different theories and cosmologies. It becomes particularly simple to compare different theories, as the Newton polytope is the same for a given process, and we just need to change the parameters on which the  $\lambda$ -function depends on.

### The two-site two-loop graph

Let us now look at the contribution for two-loop level, given by the two-site two-loop graph – see Figure 3.10. As for the one-loop case discussed above, we consider the following general form for the integral associated to this graph

$$\mathcal{I}_{\mathcal{G}}^{(2)} = \int_{\mathbb{R}_+^2} \prod_{s \in \mathcal{V}} \left[ \frac{dx_s}{x_s} x_s^{\alpha_s} \right] \int_{\Gamma^{(2)}} \prod_{e \in \mathcal{E}} \frac{dy_e}{y_e} y_e^{\beta_e - 1} \Omega_{\mathcal{G}}(x, y; \mathcal{X})$$

where

$$\Omega_{\mathcal{G}}(x, y; \mathcal{X}) = \frac{\mathbf{n}_{\delta}(x, y; \mathcal{X})}{[q_{\mathcal{G}}]^{\tau_{\mathcal{G}}} \left[ \prod_{e=a,b,c} [q_{\mathfrak{g}_e}]^{\tau_{\mathfrak{g}_e}} \right] \left[ \prod_{(e_1, e_2)} [q_{\mathfrak{g}_{(e_1, e_2)}}]^{\tau_{\mathfrak{g}_{(e_1, e_2)}}} \right] \left[ \prod_{j=1,2} [q_{\mathfrak{g}_j}]^{\tau_{\mathfrak{g}_j}} \right]}$$



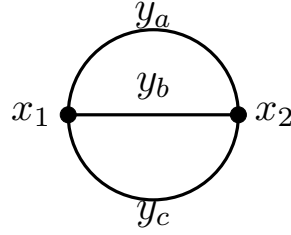


Figure 3.10: Two-site two-loop graph. The associated Newton polytope is lives in  $\mathbb{P}^5$  and characterised by 16 facets. They signal the possible divergent direction, which are further limited by the non-negativity condition from the integration contour.

where  $\mathfrak{g}_{a/b/c}$  is the subgraph with the edge labelled by  $a/b/c$  departing from it,  $\mathfrak{g}_{(e_1, e_2)}$  is the subgraph with the pair  $(e_1, e_2)$  of edges departing from it (where  $(e_1, e_2) = \{(a, b), (b, c), (c, a)\}$ ), and as usual  $\mathfrak{g}_j$  is the subgraph made out of the site  $s_j$  only. The linear polynomials  $\{q_{\mathfrak{g}}, \mathfrak{g} \subseteq \mathcal{G}\}$  are then explicitly given by

$$q_{\mathfrak{g}} := \sum_{s \in \mathfrak{V}_{\mathfrak{g}}} x_s + \sum_{e \in \mathcal{E}_{\mathfrak{g}}^{\text{ext}}} y_e + \mathcal{X}_{\mathfrak{g}}$$

First, note that were we to consider the site integration only, the associated nestohedron would be the very same as for the other two-site graphs examined, with the  $\mathcal{W}$ 's differing only by their  $\lambda$ -component: the possible divergences are the same, what differs is the way that such divergences are approached.

The edge weight integration is more interesting. It can be recast in the form of an iterated integral with two-site one-loop graphs. Thus, we can easily use the lesson from the analysis in the previous example: for each loop integration, the non-negative condition imposed by the contour of integration restrict the number of possible divergent directions. Hence, we can perform a full Newton polytope analysis, decompose the integral according to these sectors, and each sector involving directions that cannot become simultaneously divergent because of the contour non-negativity condition, can be split in subsectors each of which contain only the directions which can become divergent simultaneously.

The Newton polytope for the full integral lives in  $\mathbb{P}^5$  with a generic point given by,  $(\rho_1, \rho_a, \rho_b, \rho_c, \rho_2)$  which are respectively the powers of  $(y_1, y_a, y_b, y_c, x_2)$ . Its facets are given by

$$\begin{aligned} \mathcal{W}'^{(j)} &= \begin{pmatrix} \lambda'^{(j)} \\ -\mathbf{e}_j \end{pmatrix}, & \mathcal{W}^{(j)} &= \begin{pmatrix} \lambda^{(j)} \\ \mathbf{e}_j \end{pmatrix}, & \mathcal{W}^{(j_1, j_2)} &= \begin{pmatrix} \lambda^{(j_1, j_2)} \\ \mathbf{e}_{j_1, j_2} \end{pmatrix}, \\ \mathcal{W}^{(234)} &= \begin{pmatrix} \lambda^{(234)} \\ \mathbf{e}_{234} \end{pmatrix}, & \mathcal{W}^{(1 \dots 5)} &= \begin{pmatrix} \lambda^{(1 \dots 5)} \\ \mathbf{e}_{1 \dots 5} \end{pmatrix} \end{aligned}$$

where  $(j_1, j_2) = \{((2, 3), (3, 4), (4, 2))\}$ . While in the one-loop case the integration contour was forbidding to take simultaneously two divergences both identified by one of the  $\mathcal{W}$ 's co-vectors, in this case some of them are allowed, *e.g.*  $\mathcal{W}'^{(2)}$  and  $\mathcal{W}'^{(4)}$  – they belong to different loop subgraphs.

The above example would give us the contribution to the correlator coming from the wavefunction coefficient corresponding to two-point, two-loop sunrise diagram. Which would be very sub-leading. Let us now think what is the contribution for the leading divergence in the two-loop two-point correlator. One feature that is made more apparent from the wavefunction and from this formalism, is that the disconnected component of the correlator gives the leading divergence. This is the case, because every time we delete an edge we increase the power of the singularity  $1/y$  of the corresponding edge, thus making the integral more singular. Simultaneously, we decrease the number of singularities in the denominator given that there are less sub-diagrams when once we delete an edge. Here, the disconnected component is the product of two contact four point wavefunction coefficients. Therefore, from the previous calculation, where a single contact four-point wavefunction came from the disconnected component, and gave us a simple pole in  $\alpha$ , this time we will obtain a double pole,  $1/(\alpha - \alpha_*)^2$ . An interesting feature of the leading divergence, is that the  $x$ -variable (site) integration and the  $y$ -variable (loop) integration factorized. We have just discussed the site integration, now we turn to the loop integration. The fact that it factorized, means that the factor from the loop integration, is just the two-loop integrals over  $1/(y_a y_b y_c)^{3-\beta}$ . The measure of each loop integral will contribute with  $y^{d-1}$ , thus, when in  $d = 3$  we will have precisely two logarithmic divergences coming from each loop integral, and we will obtain a double pole in  $\beta$ . This precisely agrees with [147, 156].

From this discussion we learn that the leading divergences, coming from the fully disconnected part of the correlator, given that they are just products of contact wavefunction coefficients and momentum integrals, can be just as easily computed in our formalism. At the same time, we believe that our techniques allow for a much more tractable computation the sub-leading terms, in particular when we still have a factorization of the momentum integral, and other tree-level integrals which are not contact terms, which in general, using other methods, can be very hard to compute.

## 3.5 Infrared Finite Computables

The above discussion establishes a general and systematic method to compute divergences in cosmological integrals. In this section, we discuss a systematic approach that eliminates these divergences, and constructs infrared finite quantities.

### 3.5.1 Tree-level subtractions

As in general the canonical function of a polytope is a rational function with a non-trivial numerator, it is convenient to consider one of its triangulations with no spurious boundaries and study the asymptotic behaviour of the integral of each simplex following what it has been discussed in the previous section.

Each simplex in the canonical form triangulation is isomorphic to the others and can be transformed into one another through a local coordinate transformation [86]. This characteristic is mirrored in the structure of the corresponding nestohedra, which can

likewise be mapped into one another. This implies that the nestohedra associated to the simplices can also be mapped into each other and, consequently, they show the same divergent directions, with their co-vectors  $\{\mathcal{W}^{(\mathfrak{g})}, \mathfrak{g} \subseteq \mathcal{G}\}$  that differ just for the projective component, *i.e.* for the degree of divergence along the same directions, which is fixed by the number of tubings associated to the relevant facets. As a consequence, the polytope identified by the overlap of the nestohedra is identified by the covectors

$$\mathcal{W}'^{(j_1)} = \begin{pmatrix} \lambda'^{(j_1)} \\ -\mathfrak{e}_{j_1} \end{pmatrix}, \quad \mathcal{W}^{(j_1 \dots j_{n_s(\mathfrak{g})})} = \begin{pmatrix} \min\{\lambda^{(j_1 \dots j_{n_s(\mathfrak{g})})}\} \\ \mathfrak{e}_{j_1 \dots j_{n_s(\mathfrak{g})}} \end{pmatrix} \quad (3.66)$$

with the  $\min\{\lambda^{(j_1 \dots j_{n_s(\mathfrak{g})})}\}$  being the minimum taken among all the nestohedra for the covectors with the same  $\mathfrak{e}_{j_1 \dots j_{n_s(\mathfrak{g})}}$ .

Let us separately focus on each integral emerging from the canonical form triangulation of the cosmological polytope, by taking the one returning the OFPT representation. Despite this choice not being necessary, it allows for a more straightforward formulation of the subtraction rules as diagrammatic operations<sup>15</sup>.

Let us also treat separately logarithmic and power-law divergences, as in the discussion of the infrared asymptotics.

**Logarithmic divergences** – As we saw in the previous section, the infrared logarithmic divergences are encoded in all the sectors containing the covector  $\mathcal{W}^{(1 \dots n_s)}$  which can be written all together as

$$\begin{aligned} \mathcal{I}_{\mathcal{G}_o}^{(0)} \Big|_{\text{div}} [\alpha, \mathcal{G}_c] &= \frac{1}{-\lambda^{(1 \dots n_s)}} \int_{\mathbb{R}_+^{n_s}} \prod_{s \in \mathcal{V}} \left[ \frac{dx}{x} x^{\alpha - \tau_{\mathfrak{g}_s}} \right] \frac{1}{\text{Vol}\{GL(1)\}} \frac{1}{[q_{\mathcal{G}}(x, \mathcal{X}_{\mathcal{G}} = 0)]^{\tau_{\mathcal{G}}}} \prod_{\mathfrak{g} \in \mathcal{G}_c \setminus \{\mathfrak{g}_s\}} [q_{\mathfrak{g}}(x, \mathcal{X}_{\mathfrak{g}} = 0)]^{\tau_{\mathfrak{g}}} \\ &= \int_{\mathbb{R}_+^{n_s}} \prod_{s \in \mathcal{V}} \left[ \frac{dx}{x} x^{\alpha - \tau_{\mathfrak{g}_s}} \right] \frac{1}{[q_{\mathcal{G}}(x, \mathcal{X}_{\mathcal{G}} = 0)]^{\tau_{\mathcal{G}}}} \prod_{\mathfrak{g} \in \mathcal{G}_c \setminus \{\mathfrak{g}_s\}} [q_{\mathfrak{g}}(x, \mathcal{X}_{\mathfrak{g}} = 0)]^{\tau_{\mathfrak{g}}} \end{aligned} \quad (3.67)$$

where we have restored the full integration by rewriting the pole  $1/(-\lambda^{(1 \dots n_s)})$  an integral form.

The sum over  $\{\mathcal{G}_c\}$  has then the very same divergent structure of the integrals associated to the graphs obtained by all possible forms of collapsing two adjacent sites, assigning to the newly generated sites a weight given by the sum of the weight of the sites that have been collapsed, shifting the Mellin parameter associated to such site-weight integration by the related  $-\tau_{\mathfrak{g}}$ , and summing over all possibilities with a sign given by  $-1$  to the power

<sup>15</sup>Indeed, as the asymptotic analysis does not depend on the specific triangulation chosen, the same holds for the procedure that leads to the finite quantity. Also, using tubings and markings as in [195], it is possible to assign graphical rules also for the subtractions starting from other triangulations. However, as the main point of this work is to provide a proof of concept, we leave this to future work.





Let us consider our integrals just over the loop momenta, with the  $\{x_s, s \in \mathcal{V}\}$  parametrising the actual external kinematics – this occurs, for example, for the conformally coupled scalars with conformal interactions. One can construct the associated nestohedron and consider the covectors compatible with the integration contour  $\Gamma$ . Then, the previous statement about the asymptotic structure translates in the statement that: in the ultraviolet the covector  $\mathcal{W}^{(1 \dots n e)}$  is the only divergent direction, and the sectors defined through it are the only one contributing to such a divergence; in the infrared instead the directions  $\{\mathcal{W}'^{(j)}\}$  corresponding to the same loop ought to be taken separately.

Let us now consider just the integration over the site weights. This is relevant for example in the case the loop integration is finite both in the infrared and in the ultraviolet – an example in the cosmological context is given by the one-loop box graph contribution to the wavefunction in  $d = 3$ . Then the construction of the thick graphs can follow the tree-level discussion. However, a comment is in order. Both graphs contributing to the wavefunction and the ones contributing to the in-in correlators show a total energy singularity and, when it is approached upon analytic continuation outside the physical sheet, its coefficient for both quantities is the high energy limit of the flat-space scattering amplitude. When with the subtractions we define an infrared finite quantity, ideally it would be desirable that its flat-space limit returns a flat-space infrared finite quantity. It has been long known that, in the case of the flat-space one-loop box integral, subtracting it by the triangles obtained by collapsing two vertices and replacing the suppressed propagator by the Mandelstam invariant associated to that channel, returns an infrared finite quantity – see [222] and references there in. Even in flat-space, how to consistently construct such infrared finite quantities is not generally known at all order perturbation theory. Here, rather than plainly mimicking the procedure outlined at tree-level, as a proof of concept, we address the question about which infrared-finite cosmological computable returns an infrared-finite flat-space quantity, in the case of the one-loop graph contribution to the wavefunction.

The one-loop box integral we are interested in is given in the OFPT representation by

$$\begin{aligned}
 & \begin{array}{c} x_2 \ y_{23} \ x_3 \\ \bullet \quad \quad \bullet \\ | \quad \quad | \\ \bullet \quad \quad \bullet \\ x_1 \ y_{41} \ x_4 \end{array} = \int_0^{+\infty} \left[ \frac{dx}{x} x^\alpha \right] \int_{\Gamma_4} [dy \ y] \mu_d(y, \mathcal{X}) \times \\
 & \times \frac{1}{q_G \prod_{s \in \mathcal{V}} q_{\mathfrak{g}_s}} \left\{ \frac{1}{q_{\mathfrak{g}_{[2,1]}}} \left[ \frac{1}{q_{\mathfrak{g}_{[2,4]}}} \left( \frac{1}{q_{\mathfrak{g}_{23}}} + \frac{1}{q_{\mathfrak{g}_{34}}} \right) + \frac{1}{q_{\mathfrak{g}_{23} q_{\mathfrak{g}_{41}}}} + \right. \right. \\
 & \left. \left. + \frac{1}{q_{\mathfrak{g}_{[3,1]}}} \left( \frac{1}{q_{\mathfrak{g}_{34}}} + \frac{1}{q_{\mathfrak{g}_{41}}} \right) \right] + \text{cycl. perms} \right\} \tag{3.72}
 \end{aligned}$$

where  $q_{[j,k]} := x_j + \dots + x_k + y_{j-1,j} + y_{k,k+1} + \mathcal{X}_{[j,k]}$  and  $\mathcal{X}_{[j,k]} := X_j + \dots + X_k$ , and  $\Gamma_4$  is the integration contour obtained from the positivity conditions on the volume of a simplex in  $\mathbb{P}^4$  and of all its faces – see [165]. The leading divergent direction in the site weight

integration is identified by  $\mathcal{W}^{(1\dots 4)} := (4\alpha - 8, \mathbf{e}_{1\dots 4})^T$  for each of the simplices and hence it possesses a logarithmic singularity for  $\alpha = 2$ . Were we to follow the analysis from sector decomposition, as for the tree-level case discussed earlier, then the associated thick graph would be defined by subtracting all the possible way of collapsing two adjacent sites, where the collapsing operation as defined for the tree case

$$\begin{aligned}
& \begin{array}{c} x_2 \ y_{23} \ x_3 \\ \bullet \quad \bullet \quad \bullet \\ y_{12} \text{---} \square \text{---} y_{34} \\ \bullet \quad \bullet \quad \bullet \\ x_1 \ y_{41} \ x_4 \end{array} = \begin{array}{c} x_2 \ y_{23} \ x_3 \\ \bullet \quad \bullet \quad \bullet \\ y_{12} \text{---} \square \text{---} y_{34} \\ \bullet \quad \bullet \quad \bullet \\ x_1 \ y_{41} \ x_4 \end{array} - x_1 + \begin{array}{c} x_3 \\ \bullet \\ y_{23} \text{---} \triangle \text{---} y_{34} \\ \bullet \quad \bullet \\ y_{41} \text{---} x_4 \end{array} \\
& - \begin{array}{c} x_2 + x_3 \\ \bullet \quad \bullet \\ y_{12} \text{---} \triangle \text{---} y_{34} \\ \bullet \quad \bullet \\ x_1 \ y_{41} \ x_4 \end{array} - \begin{array}{c} x_2 \ y_{23} \\ \bullet \quad \bullet \\ y_{12} \text{---} \triangle \text{---} y_{34} \\ \bullet \quad \bullet \\ x_1 \ y_{41} \ x_4 \end{array} + x_4 - \begin{array}{c} x_2 \ y_{23} \ x_3 \\ \bullet \quad \bullet \quad \bullet \\ y_{12} \text{---} \triangle \text{---} y_{34} \\ \bullet \quad \bullet \\ x_4 + x_1 \end{array} \\
& + x_1 + x_2 \text{---} \bigcirc \text{---} x_3 + x_4 + \begin{array}{c} x_2 + x_3 \\ \bullet \quad \bullet \\ \bigcirc \\ \bullet \quad \bullet \\ x_1 + x_4 \end{array}
\end{aligned} \tag{3.73}$$

Some comments are now in order. First, note that each triangle diagram depends just on three edge weights, rather than the original four, but the integration is still over the four edge weights: the integration along this missing edge weight can be performed returning the integration measure and the integration contour of a triangle graph – see [165]. Secondly, this thick graph stays ultraviolet finite both in the site and edge weight integrations. Furthermore, as anticipated, were we to take the flat-space limit, we *would not* obtain the known flat-space infrared safe combination among box and triangle diagrams: the collapsing operation implies a shift by one of the Mellin parameter in the integration measure for the weights associated to the two sites that have been collapsed (maintaining the correct dimensionality). So this procedure returns a computable that is infrared finite at a generic point in the physical kinematic region but develops infrared divergences due to soft and collinear limits in the edge weights in the flat-space limit.

Alternatively, we can take into account the behaviour of the integral *outside* the physical

region and design a subtraction which is still finite in the flat-space limit:

$$\begin{aligned}
& \begin{array}{c} x_2 \ y_{23} \ x_3 \\ \bullet \quad \bullet \quad \bullet \\ | \quad | \quad | \\ \bullet \quad \bullet \quad \bullet \\ x_1 \ y_{41} \ x_4 \end{array} = \begin{array}{c} x_2 \ y_{23} \ x_3 \\ \bullet \quad \bullet \quad \bullet \\ | \quad | \quad | \\ \bullet \quad \bullet \quad \bullet \\ x_1 \ y_{41} \ x_4 \end{array} - \frac{1}{s_{23}s_{41}} \left( \begin{array}{c} x_3 \\ \bullet \\ y_{23} \quad \bullet \\ \diagup \quad \diagdown \\ y_{41} \quad \bullet \\ \bullet \\ x_4 \end{array} - \begin{array}{c} x_2 \\ \bullet \\ y_{23} \quad \bullet \\ \diagdown \quad \diagup \\ y_{41} \quad \bullet \\ \bullet \\ x_1 \end{array} + x_4 \right) - \\
& - \frac{1}{s_{12}s_{34}} \left( \begin{array}{c} x_2 + x_3 \\ \bullet \\ y_{12} \quad \bullet \\ \diagup \quad \diagdown \\ x_1 \ y_{41} \ x_4 \end{array} - \begin{array}{c} x_2 \ y_{23} \ x_3 \\ \bullet \quad \bullet \quad \bullet \\ \diagdown \quad \diagup \\ x_4 + x_1 \end{array} \right) - \left( \frac{1}{s_{41}} + \frac{1}{s_{12}} \right) \begin{array}{c} x_2 \ y_{23} \ x_3 \\ \bullet \quad \bullet \quad \bullet \\ | \quad | \quad | \\ \bullet \quad \bullet \quad \bullet \\ x_1 \ y_{41} \ x_4 \end{array} - \text{perm.} \\
& + \frac{1}{s_{23}s_{41}} \begin{array}{c} x_2 \ y_{23} \ x_3 \\ \bullet \quad \bullet \quad \bullet \\ | \quad | \quad | \\ \bullet \quad \bullet \quad \bullet \\ x_1 \ y_{41} \ x_4 \end{array} + \text{perm.} - \frac{1}{s_{23}s_{34}s_{41}} \left( \begin{array}{c} x_3 \\ \bullet \\ y_{23} \quad \bullet \\ \diagup \quad \diagdown \\ y_{41} \quad \bullet \\ \bullet \\ x_4 \end{array} + \begin{array}{c} x_2 \\ \bullet \\ y_{23} \quad \bullet \\ \diagdown \quad \diagup \\ y_{41} \quad \bullet \\ \bullet \\ x_1 \end{array} \right) + \text{perm} \\
& + \frac{1}{s_{12}s_{23}s_{34}s_{41}} x_1 + x_2 \bullet \bullet x_3 + x_4 + \text{perm}
\end{aligned} \tag{3.74}$$

where  $s_{ij} := x_i + x_j + X_i + X_j + P_{ij}$ ,  $P_{ij} := |\vec{p}_i + \vec{p}_j|$ , the red dashed circle indicate that the singularity associated to the subgraph it identifies has been removed, and the permutations indicated with *perm.* are for the term appearing immediately before. Note that the introduction of the bubble introduces a spurious singularity in the ultraviolet. It can be removed via the introduction of further terms. It is straightforward to check that, in the flat-space limit, just the first five terms in the right-hand-side contribute, returning the flat-space infrared finite combination of Feynman graphs.

Let us close this section with a comment on (3.74). It represents a proof of concept that a quantity which is both infrared finite in an expanding universe stays infrared finite in its flat-space limit. Comparing with (3.73), if on one side it has the nice feature just mentioned that (3.73) does not have, on the other side it is utterly more complicated, and it would be desirable to have a simpler object with an infrared-finite flat-space limit. If such a computable exists, a similar analysis to the one discussed in this paper but for unphysical kinematics, *i.e.* allowing for some energies to be negative, would be a systematic approach to define it. However, it would require some extra care because, for unphysical kinematics, the polynomial appearing in the integrand are no longer all sums of positive quantities and at least some loci given by the vanishing of the polynomials in the denominators, intersect the integration contour. We leave this to future work.

### 3.5.3 Examples

**The two-site tree graph** – Let us consider the two-site tree graph integral:

$$I_2^{(2)} = \int_{\mathbb{R}_+^2} \left[ \frac{dx}{x} x^\alpha \right] \frac{1}{(x_1 + x_2 + \mathcal{X}_g)(x_1 + \mathcal{X}_{g_1})(x_2 + \mathcal{X}_{g_2})} \tag{3.75}$$



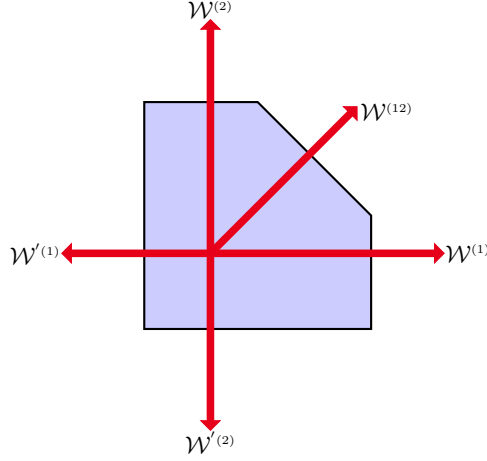


Figure 3.11: Nestohedron associated to the two-site tree graph. It shows divergences along the normal vectors  $\{\mathcal{W}^{(12)}, \mathcal{W}^{(j)}, \mathcal{W}'^{(j)}, j = 1, 2\}$  that identify its facets. The potential IR divergences are captured by the sectors containing  $\mathcal{W}^{(12)}, \mathcal{W}^{(1)}, \mathcal{W}^{(2)}$ .

It can diverge along the following directions [165] – see Figure 3.11:

$$\mathcal{W}^{(12)} = \begin{pmatrix} 2\alpha - 3 \\ \mathbf{e}_{12} \end{pmatrix}, \mathcal{W}^{(j)} = \begin{pmatrix} \alpha - 2 \\ \mathbf{e}_j \end{pmatrix}, \mathcal{W}'^{(j)} = \begin{pmatrix} -\alpha \\ -\mathbf{e}_j \end{pmatrix} \quad (3.76)$$

with  $j = 1, 2$ . The integral is well-defined for values of  $\alpha$  that identify a point inside the nestohedron, which implies that all the  $\lambda$ 's ought to be strictly negative, *i.e.* for  $\alpha \in ]0, 3/2[$ . It shows a logarithmic divergence in the IR for  $\lambda^{(12)} := 2\alpha - 3 = 0$ , which is captured by the two sectors  $\Delta_{2,12}$  and  $\Delta_{12,1}$ , respectively delimited by the pairs  $(\mathcal{W}^{(2)}, \mathcal{W}^{(12)})$  and  $(\mathcal{W}^{(12)}, \mathcal{W}^{(1)})$ .

Then, an IR-finite quantity can be defined by subtracting the graph obtained by collapsing the two sites onto each other, assigning to the newly generated site the weight given by the sum of the weights of the two sites that have been collapsed

$$\begin{array}{c} \bullet \\ \text{---} \end{array} \begin{array}{c} \bullet \\ \text{---} \end{array} = \begin{array}{c} \bullet \\ \text{---} \end{array} \begin{array}{c} \bullet \\ \text{---} \end{array} - \begin{array}{c} \blacksquare \\ \text{---} \end{array} \begin{array}{c} \bullet \\ \text{---} \end{array} \begin{array}{c} \bullet \\ \text{---} \end{array} \quad x_1 + x_2 \quad (3.77)$$

The collapsing operation implies a shift by one of the Mellin parameters in the integration measure, such that

$$\begin{array}{c} \blacksquare \\ \text{---} \end{array} \begin{array}{c} \bullet \\ \text{---} \end{array} \begin{array}{c} \bullet \\ \text{---} \end{array} = \int_{\mathbb{R}_+^2} \left[ \frac{dx}{x} x^{\alpha-1} \right] \frac{1}{x_1 + x_2 + \mathcal{X}_{\mathcal{G}}} \quad (3.78)$$

Note that this rule provides a subtraction scheme at integrand level. Then, the double line two-site tree graph corresponds to the integral

$$\begin{array}{c} \bullet \\ \text{---} \end{array} \begin{array}{c} \bullet \\ \text{---} \end{array} = - \int_{\mathbb{R}_+^2} \left[ \frac{dx}{x} x^{\alpha-1} \right] \frac{\mathcal{X}_{\mathfrak{g}_2} x_1 + \mathcal{X}_{\mathfrak{g}_1} x_2 + \mathcal{X}_{\mathfrak{g}_1} \mathcal{X}_{\mathfrak{g}_2}}{(x_1 + x_2 + \mathcal{X}_{\mathcal{G}})(x_1 + \mathcal{X}_{\mathfrak{g}_1})(x_2 + \mathcal{X}_{\mathfrak{g}_2})} \quad (3.79)$$

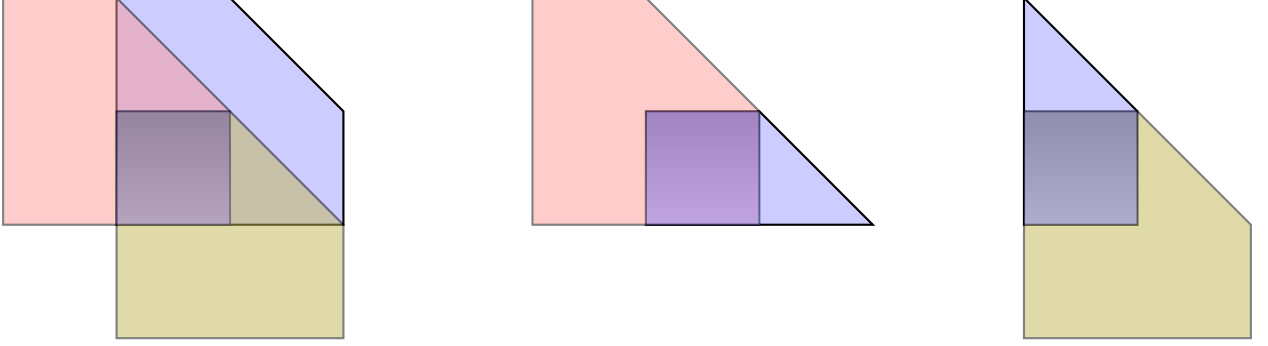


Figure 3.12: Convergence polytope associated to the two-site tree thick graph. It is given the overlap of the Newton polytopes of the integrals in which it can be decomposed as a sum, with in this case is a square – it is indicated by the shaded blue region. *Left:* The integral is decomposed according to the monomials in the numerator. *Center:* The numerator is decomposed as  $\mathcal{X}_{g_2}x_1 + \mathcal{X}_{g_1}(x_2 + \mathcal{X}_{g_2})$ . *Right:* The numerator is decomposed as  $\mathcal{X}_{g_1}x_2 + \mathcal{X}_{g_2}(x_1 + \mathcal{X}_{g_1})$ .

As a check, we can study the asymptotic behaviour of (3.79). As discussed in [165, 205], we can partial fraction the integrand, study separately the integrals in the resulting sum, and finally obtain the region of convergence by overlapping the Newton polytopes associated to them – see Figure 3.12.

Irrespectively of the partial fraction chosen, the convergence region is given by a square with vertices  $\{(1, 1 - \alpha, 1 - \alpha), (1, 1 - \alpha, 2 - \alpha), (1, 2 - \alpha, 2 - \alpha), (1, 2 - \alpha, 1 - \alpha)\}$ , whose facets are identified by the co-vectors

$$\mathcal{W}_c^{(j)} = \begin{pmatrix} \alpha - 2 \\ \mathbf{e}_j \end{pmatrix}, \quad \mathcal{W}_c'^{(j)} = \begin{pmatrix} 1 - \alpha \\ -\mathbf{e}_j \end{pmatrix}, \quad (3.80)$$

where  $j = 1, 2$ . The double-line two-site tree graph thus converges for  $\alpha \in ]1, 2[$ . The point for  $\alpha = 3/2$ , which in the original two-site graph generated a logarithmic divergence, now lies inside the Newton polytope of the double-line two-site graph. Note that for  $\alpha = 3/2$ , (3.79) stays UV finite.

Finally, note that for  $\alpha \geq 2$  the double-line two-site tree graph diverges in the infrared: this corresponds to a power-law divergence in the original two-site tree graph, to which the leading divergence has been subtracted. This is manifest in the Newton polytope picture (Fig. 3.12): it is a square with the same divergent directions as the pentagon associated to the original graph, except for  $\mathbf{e}_{12}$ .

Let us now consider the case of a power-law divergence. For definiteness let us consider the case  $\alpha = 2$ , *i.e.*  $\lambda^{(12)} = 1$  and  $\lambda^{(j)} = 0$ . The infrared divergences are now encoded into four sectors, namely  $\{\Delta_{2,12}, \Delta_{12,1}, \Delta_{1',2}, \Delta_{1,2'}\}$  – *i.e.* those respectively identified by the pairs of covectors  $\{(\mathcal{W}^{(2)}, \mathcal{W}^{(12)}), (\mathcal{W}^{(12)}, \mathcal{W}^{(1)}), (\mathcal{W}^{(1')}, \mathcal{W}^{(2)}), (\mathcal{W}^{(1)}, \mathcal{W}^{(2)})\}$ . In the sector

$\Delta_{2,12}$ , the integral acquires the form

$$\begin{aligned} \mathcal{I}_{\Delta_{2,12}} &= \int_0^1 \frac{d\zeta_{12}}{\zeta_{12}} \zeta_{12}^{-\lambda^{(12)}} \int_0^1 \frac{d\zeta_2}{\zeta_2} \zeta_2^{-\lambda^{(2)}} \times \\ &\times \frac{1}{(1 + \zeta_2 + \mathcal{X}_G \zeta_2 \zeta_{12})(1 + \mathcal{X}_{g_1} \zeta_{12})(1 + \mathcal{X}_{g_2} \zeta_2 \zeta_{12})} \end{aligned} \quad (3.81)$$

where  $x_1 = \zeta_{12}^{-1}$  and  $x_2 = \zeta_2^{-1} \zeta_{12}^{-1}$ . As discussed in [165], the divergent terms can be isolated via a Mellin-Barnes representation for the integrand, yielding

$$\begin{aligned} \mathcal{I}_{\Delta_{2,12}} &= \int_0^1 \frac{d\zeta_{12}}{\zeta_{12}} \zeta_{12}^{-\lambda^{(12)}} \int_0^1 \frac{d\zeta_2}{\zeta_2} \frac{\zeta_2^{-\lambda^{(2)}}}{1 + \zeta_2} - \\ &- \mathcal{X}_{g_1} \int_0^1 \frac{d\zeta_{12}}{\zeta_{12}} \zeta_{12}^{-\lambda^{(12)}+1} \int_0^1 \frac{d\zeta_2}{\zeta_2} \frac{\zeta_2^{-\lambda^{(2)}}}{1 + \zeta_2} - \\ &- \mathcal{X}_{g_2} \int_0^1 \frac{d\zeta_{12}}{\zeta_{12}} \zeta_{12}^{-\lambda^{(12)}+1} \int_0^1 \frac{d\zeta_2}{\zeta_2} \frac{\zeta_2^{-\lambda^{(2)}+1}}{1 + \zeta_2} - \\ &- \mathcal{X}_G \int_0^1 \frac{d\zeta_{12}}{\zeta_{12}} \zeta_{12}^{-\lambda^{(12)}+1} \int_0^1 \frac{d\zeta_2}{\zeta_2} \frac{\zeta_2^{-\lambda^{(2)}+1}}{(1 + \zeta_2)^2} + \dots \end{aligned} \quad (3.82)$$

Repeating this analysis for all the sectors, gathering all the terms together, and restoring the original variables, it is easy to see that this divergent structure is captured by

$$\begin{aligned} \mathcal{I}_2^{(0)}|_{\text{ct}} &= \int_0^\infty \prod_{j=1}^2 \left[ \frac{dx_j}{x_j} x_j^{\alpha-1} \right] \left( 1 + \mathcal{X}_G \frac{\partial}{\partial \mathcal{X}_G} - \frac{\mathcal{X}_{g_1}}{x_1} - \frac{\mathcal{X}_{g_2}}{x_2} \right) \frac{1}{x_1 + x_2 + \mathcal{X}_G} \\ &+ \int_0^{+\infty} \prod_{j=1}^2 \left[ \frac{dx_j}{x_j} x_j^{\alpha-2} \right] \frac{x_1 \mathcal{X}_{g_2}^2 + x_2 \mathcal{X}_{g_1}^2}{(x_1 + \mathcal{X}_{g_1})(x_2 + \mathcal{X}_{g_2})} \end{aligned} \quad (3.83)$$

and the infrared finite thick graph can be defined as

$$\bullet \text{---} \bullet = \bullet \text{---} \bullet - \square - \bullet \text{---} \text{---} \bullet \quad (3.84)$$

$x_1 \quad x_2 \quad x_1 \quad x_2 \quad x_1 + x_2 \quad x_1 \quad x_2$

where now the collapsing operation includes the operator in the first term in (3.83), while the second term in (3.83) can be represented via a cut operation<sup>17</sup>. As stressed in the main text, while these rules are general – the thick graph can be defined in terms of collapsing and cuts –, the explicit form relies on the degree of divergence (as well as on whether (some of) the  $\lambda$ 's are integer or not).

**Three-site tree graph** – In this case, the integrand has a non-trivial numerator. Considering its OFPT representation, the convergence of its Mellin transform is given by the

<sup>17</sup>The formula (3.83) is presented in a somewhat compact way – expanding it according to the monomials in the numerator, it becomes manifest that this contribution is factorised.

overlap between the two nestohedra associated to each of the OFPT terms – see Figure 3.4. Following the procedure outlined above, for logarithmic divergencies, one can obtain a finite term by subtracting from the original graph the sum of the graphs obtained by collapsing all the pairs of sites connected by an edge, assigning to the newly generated site the sum of the weights of the sites that have been collapsed and shifting the Mellin parameter by  $-1$  in the site weight integration related to the sites that have been collapsed:

$$\begin{array}{c} \bullet \text{---} \bullet \text{---} \bullet \\ x_1 \quad x_2 \quad x_3 \end{array} = \begin{array}{c} \bullet \text{---} \bullet \text{---} \bullet \\ x_1 \quad x_2 \quad x_3 \end{array} - \begin{array}{c} \bullet \text{---} \blacksquare \\ x_1 \quad x_2 + x_3 \end{array} - \begin{array}{c} \blacksquare \text{---} \bullet \\ x_1 + x_2 \quad x_3 \end{array} \quad (3.85)$$

where

$$\begin{array}{c} \bullet \text{---} \blacksquare \\ x_1 \quad x_2 + x_3 \end{array} = \int_{\mathbb{R}_+} \frac{dx_1}{x_1} x_1^\alpha \int_{\mathbb{R}_+^2} \left[ \frac{dx}{x} x^{\alpha-1} \right] \times \\ \times \frac{1}{(x_1 + x_2 + x_3 + \mathcal{X}_{\mathcal{G}})(x_1 + \mathcal{X}_{\mathfrak{g}_1})(x_2 + x_3 + \mathcal{X}_{\mathfrak{g}_{23}})} \quad (3.86)$$

and similarly for the third term in the right-hand-side of (3.85).

**Four-site tree graph** – As one last example of the subtraction scheme at tree level, we can consider a bigger chain where we need to add back a term which has two pairs of contracted vertices, see the diagrammatic expression (3.87). Naturally, the explicit expressions become too large to write down here, however a simple counting exercise shows that the number of terms matches. From the normal four-chain graph we have five terms in OFPT representation, then we have to subtract six three chains, and we know that each of them has two terms in OFTP representation, then we must add one back which comes from the contracting two pairs at the same time and we get a simple two chain, which is only one term. So in the end we have that  $5 - 6 + 1 = 0$ . This provides a quick check that the algorithm works. What is happening is that the second and fourth terms in the expression (3.87) are counting the same term twice, which corresponds to the tubing, in the russian doll picture, where we have to disjoint tubes one enclosing the  $x_1$  and  $x_2$  sites, and another one enclosing the  $x_3$  and  $x_4$  sites. Naturally, this is added back by contracting the two pairs of sites at once.

$$\begin{array}{c} \bullet \text{---} \bullet \text{---} \bullet \text{---} \bullet \\ x_1 \quad x_2 \quad x_3 \quad x_4 \end{array} = \begin{array}{c} \bullet \text{---} \bullet \text{---} \bullet \text{---} \bullet \\ x_1 \quad x_2 \quad x_3 \quad x_4 \end{array} - \begin{array}{c} \blacksquare \text{---} \bullet \text{---} \bullet \\ x_1 + x_2 \quad x_3 \quad x_4 \end{array} - \begin{array}{c} \bullet \text{---} \blacksquare \text{---} \bullet \\ x_1 \quad x_2 + x_3 \quad x_4 \end{array} \\ - \begin{array}{c} \bullet \text{---} \bullet \text{---} \blacksquare \\ x_1 \quad x_2 \quad x_3 + x_4 \end{array} + \begin{array}{c} \blacksquare \text{---} \blacksquare \\ x_1 + x_2 \quad x_3 + x_4 \end{array} \quad (3.87)$$

## 3.6 Discussion

In this chapter we introduced a novel formalism to compute infrared divergences for a large class of scalar field theories in FLRW backgrounds. This formalism makes use of tropical

geometry ideas in order to compute any cosmological integral as a Laurent series in the appropriate analytic regulator. Using this knowledge we formulated a class of infrared finite computables, by constructing a subtraction scheme which takes advantage of the OFPT representation of the wavefunction. The whole chapter is highly technical but establishes a formalism for computing divergences that differs significantly from what has been done so far in the literature. Firstly, it is based on the computation of cosmological correlators through the wavefunction, instead of in-in formalism. The wavefunction turns the computation of leading divergences into a far simpler problem, given that the leading divergence will be given by the product of multiple contact wavefunction coefficients, times a flat-space-like Feynman integral, as we shown in the  $\lambda\phi^4$  examples. Secondly, there is a reason why the resummation of sub-leading divergences has very little discussion in the literature, it simply a very technically difficult problem. Our formalism, turns the computation of the sub-leading divergences of the correlator into a more tractable problem. It is in fact simply a straightforward, albeit cumbersome, computation. But unlike leading computations, where we can easily keep track of them because of their simple structure in terms of contact diagrams, sub-leading divergences produce in general complicated expressions which will depend on wavefunction coefficients other than contact diagrams, or the very sub-leading may have non-trivial contributions from other regions, other than the region where the loop integration and the vertex integration decouple. Nevertheless, the first sub-leading contributions are given by disconnected contributions for the correlator where the only tree-level coefficients contribute, and the loop integration factorizes. Here, our Newton polytope analysis can become quite useful still as the leading divergence for each of these terms will have the simple form given by (3.53). What we did not address in this chapter is the re-summation mechanism which one can use to compute the non-perturbative effects. From all the literature on the subject, we have learned, in different ways, that stochastic inflation reproduces the leading logarithms from perturbation theory. This is usually done by introducing a cut-off regulator, to obtain a theory for the long wavelength spectrum of the theory, and then match with the computations from stochastic inflation. The fact that our approach to computing these divergences uses an analytic regulator, and a different parameterization of the wavefunction/correlator, makes it less obvious how to match with the computations of stochastic inflation. Therefore, one issue that we leave to solve in the future is how to formulate a renormalization scheme for the long wavelength modes that allows us to connect with the results of stochastic inflation, and hopefully this will provide a framework to re-sum the sub-leading contributions, or at least provide a criteria that the divergence coefficients have to obey such that re-summation is allowed, and the theory is well behaved.



# Chapter 4

## Towards integrating cosmological integrals

The computation of cosmological correlators has mainly two motivations. One is phenomenological, for example the leading contribution to the coupling of the inflaton to fermions appears at one loop [223–226]. The second one follows from the previous section, where we have already discussed the importance of loop contributions in order to understand the stability of perturbation theory, and ultimately the consistency of the underlying theory. Therefore, below we will study the integrated wavefunction using the method of differential equations. We integrate the one-loop two-site wavefunction coefficient for general FLRW cosmologies, and study the integrated wavefunction coefficient for the one-loop three-site graph, we prove that its function space goes beyond Goncharov polylogarithms and also includes elliptic iterated integrals. Finally, we discuss the simplicity of the correlator with respect to the wavefunction and prove that the elliptic integrals cancel in the correlator, and its function space can only be built out of Goncharov polylogarithms.

### 4.1 Differential Equations for Twisted Period Integrals

In this section we discuss the differential equations method, which has been used to great success in the computation of Feynman integrals [227, 228], and more recently for the integration of tree level cosmological correlators [229, 230]. The purpose of this discussion is to in the later sections employ this method in the computation of loop cosmological integrals. Firstly, we outline the method:

- Define the family of integrals;
- Find the integration by parts identities, relating different integrals in the family;
- Solve the system of linear equations, to find a basis of *master integrals*;

- Derive the linear differential equations for the *master integrals*;
- Choose a basis of master integrals where the differential equations are in canonical form;
- Find the boundary values;
- Solve the differential equations;

We will go over each of these steps in the following text. For a generic family of integrals of the form:

$$\mathcal{I}_{a_0, \dots, a_n}[\epsilon, \mathbf{c}, \mathcal{X}] = \int_{\Gamma} d^k \mathbf{x} \kappa^{b_0 + \epsilon c_0} \frac{1}{D_1^{b_1 + \epsilon c_1} \dots D_n^{b_n + \epsilon c_n}}, \quad (4.1)$$

where  $D_i$  are linear polynomials, and  $\kappa$  is a general polynomial, which depend on  $\mathbf{x} = \{x_1, \dots, x_k\}$  integration variables, and the kinematic invariants  $\mathcal{X}$ . The labels  $a_i = b_i + \epsilon c_i$ . The regulators  $\epsilon$ , and  $\mathbf{c} = \{c_0, \dots, c_n\}$  are such the  $\mathcal{I}_{a_0, \dots, a_n}[\epsilon, \mathbf{c}, \mathcal{X}]$  converges in the domain of integration. And the integration region,  $\Gamma$ , is such that the integrand when evaluated on the boundaries vanishes. Finally, the parameters  $a_i$  are integers. We also are considering that  $n \geq k$ .

One can consider even more generic families of integrals, however for the purposes of studying cosmological integrals we find that, (4.1), is sufficiently general for both tree and loop integrals that appear in cosmological correlators.

#### 4.1.1 Integral Identities and basis of *Master Integrals*

Firstly, we discuss partial fraction identities. Remember that the fact that the number of variables of integration is equal or less than the number of linear denominators,  $D_i$ , means that we can always write any linear function of the variables of integration as a linear combination of  $k$  denominators,  $D_i$ 's, plus some function of the kinematics. This includes the  $n - k$  denominators. More concretely we can write:

$$D_j = \sum_i t_i D_i + f(\mathcal{X}), \quad (4.2)$$

where the sum on the right is over a subset of  $k$  denominators, and  $D_j$  on the left is part of the subset of denominators excluded from the  $k$   $D_i$ 's we choose as a basis. The coefficients  $t_i$  are numbers. And the function  $f(\mathcal{X})$  is whatever is needed to make the equality correct, provided it depends solely on the external kinematics. Using (4.2), we can easily translate it into an equality between different integrals of the type (4.1). It turns into:

$$\mathcal{I}_{a_j-1} = \sum_i t_i \mathcal{I}_{a_i-1} + f(\mathcal{X}) \mathcal{I}, \quad (4.3)$$

where in the labels we just write the parameters which are shifted,  $\mathcal{I}_{a_0, \dots, a_j-1, \dots, a_n} \equiv \mathcal{I}_{a_j-1}$ . We call the identities of the type (4.3), partial fraction identities.



Now we discuss how to obtain other linear identities which relate integrals labeled by different integers  $a_i$ . If we consider the assumption that the integrand vanishes at the boundaries of  $\Gamma$ , then in general, we can say that the action of a total derivative simply vanishes:

$$\sum_i \int_{\Gamma} d^k \mathbf{x} \partial_{x_i} \left\{ \kappa^{a_0 + \epsilon c_0} \frac{N_i}{D_1^{b_1 + \epsilon c_1} \dots D_n^{b_n + \epsilon c_n}} \right\} = 0. \quad (4.4)$$

Here, we are considering a general numerator,  $N_i$ , for purposes which will later be more clear. Of course, one can always write the numerator as a polynomial function of the denominators, and then expand it to shift the parameters,  $a_i$ , and relating the initial integral to a sum of integrals of the type (4.1). Then, if we act with the derivative we obtain:

$$\sum_i \int_{\Gamma} d^k \mathbf{x} \left\{ \frac{b_0 + \epsilon c_0}{\kappa} (\partial_{x_i} \kappa) N_i + (\partial_{x_i} N_i) + N_i \sum_{\sigma_k} \frac{(-b_{\sigma_k} + \epsilon c_{\sigma_k}) D'_{\sigma_k}}{D_{\sigma_k}} \right\} \frac{\kappa^{b_0 + \epsilon c_0}}{\prod_{j=1}^n D_j^{b_j + \epsilon c_j}} = 0. \quad (4.5)$$

Now, we could choose a constant numerator, for example  $N_i = 1$ , and it is clear that (4.5) generates an identity (similar to (4.3)) which relates different integrals in the family (4.1)). However, we can also go a step further and pick a numerator such that:

$$\sum_i (\partial_{x_i} \kappa) N_i = h_0 \kappa. \quad (4.6)$$

This leads to simpler identities which relate only integrals with the same value of  $a_0$ . To find a polynomial  $N_i$  such that (4.6) is true, we can simply make an *ansatz* for  $N_i$  and  $h_0$ , and then fix their form by demanding (4.6) (this is in fact very simple and fast to implement). Or, we can make use of the more formal ideas related to Groebner bases, and find the the Groebner basis for the polynomial ideal:

$$\langle \partial_{x_i} \kappa, \dots, \partial_{y_k} \kappa, \kappa \rangle. \quad (4.7)$$

This will give us a basis to construct polynomials  $N_i$  for which (4.6) is true. And thus the first term in (4.5) becomes simpler [231, 232].

Now that we know how to find linear equations which relate different elements of the family (4.1), we can find the basis of *master integrals*. If we think of every integral in the family defined above to be a point in a vector space, then we expect that this vector space has a basis. It turns out, that the existence of integration by parts identities generally means that this basis is finite. By solving the linear equations derived from IBPs (using Gaussian elimination), we can write any integral in the family as a linear combination of a finite basis of elements in the family, these are usually referred to as *master integrals*. In practice, one can find a basis by generating a large number of identities for a large set of integrals of the family, and then use the Laporta algorithm to reduce every element of this set to the basis. In principle, if the set is sufficiently large then the basis should be the correct one. To prove what is the correct number of master integrals of the family, then one needs to use the formalism of twisted cohomology which we will not go in depth here, and just refer the reader to the literature on intersection theory and twisted cohomology.

### 4.1.2 Differential Equations for *Master Integrals*

Finding the differential equations for the basis of *master integrals* is straightforward. Similarly to the above discussion, if we act with a derivative with respect to the external kinematics on the integral  $\mathcal{I}_{a_0, \dots, a_n}[\epsilon, \mathbf{c}, \mathcal{X}]$ , then we will obtain a linear combination of integrals of the same family. From the previous discussion, we can write any integral of this family in terms of a basis of master integrals, thus we can write the derivative of a master integral in terms of a linear combination of other master integrals. More concretely, let us consider a vector of  $n$  master integrals,

$$\vec{f}(\mathcal{X}, \epsilon, \mathbf{c}) = \{\mathcal{I}_1, \dots, \mathcal{I}_n\}, \quad (4.8)$$

then the above statement is simply that we can write the derivative with respect to an external kinematic parameter,  $\mathcal{X}_i$ , of a master integral as a linear combination of all the master integrals, that translates into the form:

$$\partial_{\mathcal{X}_i} \vec{f} = A_{\mathcal{X}_i} \vec{f}, \quad (4.9)$$

where  $A$  is a  $n \times n$  matrix whose entries depend on the regulators, and external kinematics. However, there are infinitely many bases of master integrals, and depending on which one, naturally, the matrix  $A$  will have a different form. When the kernel of all the elements in the basis is logarithmic, a particular useful basis is one that leads to a *canonical form* for the differential equations, where  $A$  has the dependence in the regulator  $\epsilon$  factorised, and we can write:

$$\partial_{\mathcal{X}_i} \vec{f} = \epsilon A_{\mathcal{X}_i}(\mathcal{X}, \mathbf{c}) \vec{f}, \quad (4.10)$$

where here,  $\vec{f}$  is a different choice of basis which leads to the canonical form for the differential equations. Furthermore, we can combine the different differential equations (one per kinematic invariant) to write:

$$d\vec{f} = \epsilon(d\tilde{A})\vec{f}, \quad (4.11)$$

where the operator  $d = \sum_i d\mathcal{X}_i \partial_{\mathcal{X}_i}$ , and  $\partial_{\mathcal{X}_i} \tilde{A} = A_{\mathcal{X}_i}$ . Then, the solution of these differential equations can be formally written as a path ordered exponential,

$$f(\mathcal{X}, \epsilon, \mathbf{c}) = \mathbb{P} \exp \left\{ \epsilon \int_{\mathcal{C}} d\tilde{A}(\mathcal{X}, \mathbf{c}) \right\} f(\mathcal{X}_0, \epsilon, \mathbf{c}). \quad (4.12)$$

Here the vector  $f(\mathcal{X}_0, \epsilon, \mathbf{c})$  defines the boundary conditions, at the point  $\mathcal{X}_0$  in kinematic space. The  $\epsilon$  factorization allows writing the above exponential as an expansion in  $\epsilon$ , and each term in the series is an iterated integrals over a logarithmic kernel [233], which means the answer can be expressed in terms of multi-polylogarithms. In particular,

$$f(\mathcal{X}, \epsilon, \mathbf{c}) = \left( \mathbb{I} + \epsilon \int_{\mathcal{C}} d\tilde{A} + \epsilon^2 \int_{\mathcal{C}} d\tilde{A} \int_{\mathcal{C}} d\tilde{A} + \dots \right) f(\mathcal{X}_0, \epsilon, \mathbf{c}). \quad (4.13)$$

In general, the difficult task is to find a basis of master integrals which leads to a canonical form for the differential equations. And then find the boundary conditions which allow

integrating over the contour  $\mathcal{C}$  to the physical kinematical space  $\mathcal{X}$ . In the following sections we will go through some examples of the application of this algorithm, for loop level integrals. At the end, we will look at an example of an integral where the basis integrals do not always have logarithmic kernels, but some of them have elliptic kernels. In order to identify the function space of the solutions of differential equations it is useful to introduce the *Picard-Fuchs* operator.

In general, differential equations have a block-triangular structure, whose homogeneous sector univocally determines the space of functions appearing in its solution. In particular, each homogeneous block of dimension  $k \times k$  can be equivalently rewritten as a single  $k^{\text{th}}$ -order differential equation for a single master integral  $\mathcal{I}_i$ , as:

$$\mathcal{L}_k \mathcal{I}_i = 0, \quad \mathcal{L}_k = \frac{\partial^k}{\partial \mathcal{X}^k} + \sum_{j=0}^{k-1} c_j(\mathcal{X}) \frac{\partial^j}{\partial \mathcal{X}^j}, \quad (4.14)$$

with  $c_j(\mathcal{X})$  rational functions in the kinematic variable  $\mathcal{X}$ . In the multivariate case, given  $\{\mathcal{X}_i\}_{i=1}^m$  kinematic variables, this can be achieved by first making the change of variables  $\mathcal{X}_i \rightarrow a_i \lambda$ , setting  $a_k = 1$ , and then constructing the higher order operator with respect to  $\lambda$ . This operator is known as Picard-Fuchs operator [234], and by studying its factorization property it is possible to determine the geometries of the appearing integrals [234, 235]: if it factorizes in differential operators of order 1, only polylogarithms [236, 237] appear, for  $r > 1$  instead we can have the appearance of Calabi-Yau  $(r-1)$ -folds [238–240].

## 4.2 Differential equations for one loop cosmological integrals

In this section, we apply the method of differential equations to evaluate loop cosmological integrals. The evaluation of loop cosmological correlators is still very underdeveloped when comparing with the evaluation of loop Feynman integrals. Here, we believe we make a step forward in this direction. We compute the one loop two-site wavefunction coefficient for general power-law FLRW cosmologies. Furthermore, we compute the differential equations for the one-loop three-site integral, and show that this family of integrals contains elliptic polylogarithms in its function space.

## 4.3 Integrals over the one-loop measure

Before diving into specific one-loop integrals, we will discuss the integral family associated just to the integration measure, in the case where no denominators are present, namely considering integrals of the type:

$$\mathcal{I}_{\{1\}}^{(n_s, 1; 0)} := \int_{\Gamma} \prod_{e \in \mathcal{E}(1)} [dy_e] \mu_d(y; \mathcal{X}) = \kappa_0 \int_{\Gamma} \kappa^\gamma(y), \quad (4.15)$$

where  $\mu_d$  was given in the previous chapter. One can relate the integration measure of one-loop  $n$ -sites cosmological integrals, with that obtained from the Baikov polynomial [241, 242] of one-loop  $n$ -points Feynman integrals with different masses on external legs and with massless propagators, in Euclidean space, by considering  $\{y_e^2, e \in \mathcal{E}^{(1)}\}$ . This property is relevant, because the number of master integrals for these Feynman integral families admits a recursive formula, given by:

$$\nu_n^{(\text{FI})} = \sum_{k=2}^n \frac{n!}{k! (n-k)!} = 2^n - (n+1), \quad (4.16)$$

where exactly 1 master integral per sector appears. Integration by parts identities will shift powers of denominators by integer units, relating integrals on different sub-sectors. Rewriting equation (4.15) in Baikov variables, one obtains a family of one-loop  $n$ -points Feynman integrals with variables raised to half-integer powers:

$$\mathcal{I}_{\{1\}}^{(n_s, 1; 0)} = \frac{\kappa_0}{2^n} \int \frac{\prod_{e \in \mathcal{E}^{(1)}} dy_e^2}{\prod_{e \in \mathcal{E}^{(1)}} [y_e^2]^{1/2}} [\kappa(y^2)]^\epsilon, \quad (4.17)$$

which in momentum space correspond to:

$$\mathcal{I}_{\{1\}}^{(n_s, 1; 0)} = \frac{1}{2^n} \int_{\mathbb{R}^n} d\vec{l} \frac{1}{|\vec{l}| |\vec{l} + \vec{P}_1| \cdots \left| \vec{l} + \sum_{j=1}^{n_s-1} \vec{P}_j \right|}. \quad (4.18)$$

In general, such integral belongs to the integral family:

$$\mathcal{I}_{\{\tau_{\mathfrak{g}}\}}^{(n_s, 1; 0)} := \int \frac{\prod_{e \in \mathcal{E}^{(1)}} dy_e^2}{\prod_{e \in \mathcal{E}^{(1)}} (y_e^2)^{\tau_e}} [\kappa(y^2)]^\epsilon \quad (4.19)$$

$$= \int_{\mathbb{R}^{n_s}} d\vec{l} \frac{1}{[(\vec{l})^2]^{\tau_{12}} \cdots [(\vec{l} + \vec{P}_1 + \cdots + \vec{P}_{n_s-1})^2]^{\tau_{n_s, 1}}} \quad (4.20)$$

with  $\tau_e \in \mathbb{Z} + 1/2$ ,  $e \in \mathcal{E}^{(1)}$ . Integrals of the type of equation (4.17) cannot be related to subsectors where some denominators do not appear, and for each master Feynman integral appearing with  $k$  external legs, we have a sector with  $\nu_k^{(\text{FI})}$  master cosmological integrals. The total number of master integral of the zero sector is:

$$\nu_{n_s}^{(\text{CI})} = \sum_{k=2}^{n_s} \frac{n_s!}{k! (n_s - k)!} \nu_k^{(\text{FI})}, \quad (4.21)$$

where the various subsectors are appearing in the with differential equations blocks of dimension  $\nu_k^{(\text{FI})}$ . Summing the series, we obtain:

$$\nu_{n_s}^{(\text{CI})} = 3^{n_s} - 2^{n_s-1} (2 + n_s). \quad (4.22)$$

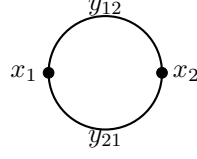


Figure 4.1: One-loop two-site diagram. The corresponding integrand has 5 denominators, each corresponding to a connected subgraph of the above graph. Two subgraphs enclose each of the two sites, then two subgraphs enclose both sites and cut one edge twice and finally there is the full graph which corresponds to the total energy pole.

### 4.3.1 One-loop Two-site graph

In this section, we discuss how to apply the method of differential equations in the simplest case of the one-loop two-site integral, for the flat-space wavefunction, and allows us to get insights on the integrated function, – see Figure 4.1.

Let us consider the following representation for this integral:

$$\mathcal{I}_{(2,1)} = \int_{\mathbb{R}_+^2} \prod_{s \in \mathcal{V}} \left[ \frac{dx_s}{x_s} x_s^\alpha \right] \mathcal{I}_{\{1\}}^{(2,1)}, \quad (4.23)$$

$$\mathcal{I}_{\{1\}}^{(2,1)} = \kappa_0 \int_{\Gamma} \prod_{e \in \mathcal{E}^{(1)}} [dy_e y_e] \frac{\kappa^\chi}{q_{\mathcal{G}} q_{\mathfrak{g}_1} q_{\mathfrak{g}_2}} \left( \frac{1}{q_{\mathcal{G}_{12}}} + \frac{1}{q_{\mathcal{G}_{21}}} \right) \quad (4.24)$$

where  $\mathcal{E}^{(1)} := \{e_{12}, e_{21}\}$  is the set of the two edges connecting the sites  $s_1$  and  $s_2$ , and:

$$\kappa = \left[ (y_{12} + P)^2 - y_{21}^2 \right] \left[ y_{21}^2 - (y_{12} - P)^2 \right], \quad (4.25)$$

and  $\kappa_0 = P^{-1}$ . While  $\mathfrak{g}_j$  identifies the subgraph containing just the site  $s_j$  (whose weight is  $x_j + X_j$ ) and  $\mathcal{G}_{ij} := \mathcal{G} \setminus \{e_{ij}\}$  is the subgraph obtained from  $\mathcal{G}$  by deleting the edge between the sites  $s_i$  and  $s_j$  – in this simple case where there are only two sites, the two edges are indicated by reversing the order of the labels of the sites they connect. The linear polynomials associated to these subgraphs can be explicitly written as,

$$\begin{aligned} q_{\mathcal{G}} &= \tilde{x}_1 + \tilde{x}_2, \\ q_{\mathfrak{g}_1} &= \tilde{x}_1 + y_{12} + y_{21}, \\ q_{\mathfrak{g}_2} &= \tilde{x}_2 + y_{12} + y_{21}, \\ q_{\mathcal{G}_{12}} &= \tilde{x}_1 + \tilde{x}_2 + 2y_{12}, \\ q_{\mathcal{G}_{21}} &= \tilde{x}_1 + \tilde{x}_2 + 2y_{21}. \end{aligned} \quad (4.26)$$

where for simplicity we denoted  $\tilde{x}_i = x_i + X_i$ .

**Loop edge weight integration** – Upon exploiting the invariance of the integrand under the  $y_{12} \leftrightarrow y_{21}$  exchange, and the partial fraction relations emerging from the identity:

$$q_{\mathfrak{g}_1} - q_{\mathfrak{g}_2} = \tilde{x}_1 - \tilde{x}_2, \quad (4.27)$$

the integral  $\mathcal{I}_{\{1\}}^{(2,1)}$ , appearing in (4.24), can be recast as a combination of twisted period integrals (4.1), corresponding to two sets of two denominators, namely  $\{q_{\mathfrak{g}_1}, q_{\mathcal{G}_{12}}\}$  and  $\{q_{\mathfrak{g}_2}, q_{\mathcal{G}_{21}}\}$ . The latter set can be mapped onto the former, by exchanging  $\tilde{x}_1 \leftrightarrow \tilde{x}_2$ . Therefore, the computational complexity of the problem reduces remarkably to the evaluation of just one type of period integrals, defined as:

$$\mathcal{I}_{\tau_{\mathfrak{g}_1} \tau_{\mathcal{G}_{12}}}^{(2,1)} := \int_{\Gamma} \kappa^{\chi} \varphi_{\tau_{\mathfrak{g}_1} \tau_{\mathcal{G}_{12}}} , \quad \varphi_{\tau_{\mathfrak{g}_1} \tau_{\mathcal{G}_{12}}} := \frac{dy_{12} dy_{21}}{q_{\mathfrak{g}_1}^{\tau_{\mathfrak{g}_1}} q_{\mathcal{G}_{12}}^{\tau_{\mathcal{G}_{12}}}} . \quad (4.28)$$

By writing down the integration by parts identities, as explained in the beginning of this chapter and more concretely in equation (4.5), and then solving for a basis, we can identify that the number of master integrals to be 6. And the basis can be chosen as:  $\mathcal{I} = \{\mathcal{I}_{00}, \mathcal{I}_{10}, \mathcal{I}_{01}, \mathcal{I}_{02}, \mathcal{I}_{-11}, \mathcal{I}_{11}\}$ .

As described in section 4.3, the sector without denominators contains  $\nu_2^{(\text{CI})} = 1$  master integrals, which has been chosen as  $\mathcal{I}_{00}$ , and in momentum space it can be rewritten as a massless one-loop two point function with massive external momenta, belonging to the integral family  $\mathcal{I}_{\tau_{\mathfrak{g}_1} \tau_{\mathfrak{g}_2}}$ , with denominators raised to with half-integer exponents, in Euclidean space:

$$\mathcal{I}_{\tau_{\mathfrak{g}_1} \tau_{\mathfrak{g}_2}} := \int \frac{d\vec{\ell}}{[(\vec{\ell})^2]^{\tau_{\mathfrak{g}_1}} [(\vec{\ell} + \vec{P})^2]^{\tau_{\mathfrak{g}_2}}} , \quad \tau_{\mathfrak{g}_j} \in \mathbb{Z} + \frac{1}{2} . \quad (4.29)$$

With a change of basis  $\mathcal{J} = \mathcal{R} \cdot \mathcal{I}$ , through the rotation matrix  $\mathcal{R}$ ,

$$\mathcal{R} = \begin{pmatrix} \frac{(2\epsilon+1)^2}{P^2} & 0 & 0 & 0 & 0 & 0 \\ 0 & \frac{\epsilon(2\epsilon+1)}{P} & 0 & 0 & 0 & 0 \\ 0 & 0 & \frac{\epsilon(4\epsilon+1)}{P} & \frac{\epsilon(\tilde{x}_1 + \tilde{x}_2)}{P} & 0 & 0 \\ 0 & 0 & 0 & -\epsilon & 0 & 0 \\ -\frac{\epsilon(2\epsilon+1)}{2P(\tilde{x}_1 + \tilde{x}_2)} & 0 & -\frac{\epsilon(2\epsilon+1)(\tilde{x}_1 - \tilde{x}_2)}{2P(\tilde{x}_1 + \tilde{x}_2)} & 0 & \frac{\epsilon(2\epsilon+1)}{P(\tilde{x}_1 + \tilde{x}_2)} & 0 \\ 0 & 0 & 0 & 0 & 0 & \epsilon^2 \end{pmatrix} \quad (4.30)$$

it is possible to find a family of master integrals:

$$\begin{aligned} \mathcal{J}_1 &= \frac{(1+2\epsilon)^2}{P^2} \mathcal{I}_{00} , \\ \mathcal{J}_2 &= \frac{\epsilon(1+2\epsilon)}{P} \mathcal{I}_{10} , \\ \mathcal{J}_3 &= \frac{1}{P} \left( \epsilon(1+4\epsilon) \mathcal{I}_{01} + \epsilon(\tilde{x}_1 + \tilde{x}_2) \mathcal{I}_{02} \right) , \\ \mathcal{J}_4 &= -\epsilon \mathcal{I}_{02} , \\ \mathcal{J}_5 &= \frac{\epsilon(1+2\epsilon)}{2P(\tilde{x}_1 + \tilde{x}_2)} \left( \mathcal{I}_{-11} - \mathcal{I}_{00} + (\tilde{x}_2 - \tilde{x}_1) \mathcal{I}_{01} \right) , \\ \mathcal{J}_6 &= \epsilon^2 \mathcal{I}_{11} , \end{aligned} \quad (4.31)$$

obeying a canonical system of differential equations [118, 243, 244], as defined in (4.10), where the total differential matrix,

$$\begin{aligned} d\mathbb{A} &= \hat{\mathbb{A}}_{\tilde{x}_1} d\tilde{x}_1 + \hat{\mathbb{A}}_{\tilde{x}_2} d\tilde{x}_2 + \hat{\mathbb{A}}_P dP \\ &= \sum_{i=1}^8 \mathbb{M}_i d\log(w_i) , \end{aligned} \quad (4.32)$$

is in  $d\log$  form:  $\mathbb{M}_i$  are the constant matrices:

$$\begin{aligned} \mathbb{M}_1 &= \begin{pmatrix} 4 & 0 & 0 & 0 & 0 & 0 \\ 0 & 2 & 0 & 0 & 0 & 0 \\ 0 & 0 & 2 & 0 & 0 & 0 \\ 0 & 0 & 0 & 0 & 0 & 0 \\ 0 & 0 & 0 & 0 & 2 & 0 \\ 0 & 0 & 0 & 0 & 0 & 0 \end{pmatrix}, \quad \mathbb{M}_2 = \begin{pmatrix} 0 & 0 & 0 & 0 & 0 & 0 \\ 0 & 0 & 0 & 0 & 0 & 0 \\ 0 & 0 & 0 & 0 & 0 & 0 \\ -\frac{1}{2} & 0 & 0 & 2 & 0 & 0 \\ 0 & 0 & 0 & 0 & 2 & 0 \\ 0 & 0 & 0 & 0 & 0 & 0 \end{pmatrix}, \\ \mathbb{M}_3 &= \begin{pmatrix} 0 & 0 & 0 & 0 & 0 & 0 \\ \frac{1}{2} & 1 & 0 & 0 & 0 & 0 \\ 0 & 0 & 0 & 0 & 0 & 0 \\ 0 & 0 & 0 & 0 & 0 & 0 \\ 0 & 0 & 0 & 0 & 0 & 0 \\ 0 & 0 & \frac{1}{4} & \frac{1}{2} & \frac{1}{2} & 1 \end{pmatrix}, \quad \mathbb{M}_4 = \begin{pmatrix} 0 & 0 & 0 & 0 & 0 & 0 \\ 0 & 0 & 0 & 0 & 0 & 0 \\ 0 & 0 & 0 & 0 & 0 & 0 \\ 0 & 0 & 0 & 0 & 0 & 0 \\ 0 & 0 & 0 & 0 & 0 & 0 \\ 0 & \frac{1}{2} & -\frac{1}{4} & -\frac{1}{2} & \frac{1}{2} & 1 \end{pmatrix}, \\ \mathbb{M}_5 &= \begin{pmatrix} 0 & 0 & 0 & 0 & 0 & 0 \\ 0 & 0 & 0 & 0 & 0 & 0 \\ \frac{1}{2} & 0 & 1 & 2 & 0 & 0 \\ \frac{1}{4} & 0 & \frac{1}{2} & 1 & 0 & 0 \\ 0 & 0 & 0 & 0 & 0 & 0 \\ 0 & 0 & 0 & 0 & 0 & 0 \end{pmatrix}, \quad \mathbb{M}_6 = \begin{pmatrix} 0 & 0 & 0 & 0 & 0 & 0 \\ -\frac{1}{2} & 1 & 0 & 0 & 0 & 0 \\ 0 & 0 & 0 & 0 & 0 & 0 \\ 0 & 0 & 0 & 0 & 0 & 0 \\ 0 & 0 & 0 & 0 & 0 & 0 \\ 0 & 0 & -\frac{1}{4} & \frac{1}{2} & -\frac{1}{2} & 1 \end{pmatrix}, \\ \mathbb{M}_7 &= \begin{pmatrix} 0 & 0 & 0 & 0 & 0 & 0 \\ 0 & 0 & 0 & 0 & 0 & 0 \\ 0 & 0 & 0 & 0 & 0 & 0 \\ 0 & 0 & 0 & 0 & 0 & 0 \\ 0 & 0 & 0 & 0 & 0 & 0 \\ 0 & -\frac{1}{2} & \frac{1}{4} & -\frac{1}{2} & -\frac{1}{2} & 1 \end{pmatrix}, \quad \mathbb{M}_8 = \begin{pmatrix} 0 & 0 & 0 & 0 & 0 & 0 \\ 0 & 0 & 0 & 0 & 0 & 0 \\ -\frac{1}{2} & 0 & 1 & -2 & 0 & 0 \\ \frac{1}{4} & 0 & -\frac{1}{2} & 1 & 0 & 0 \\ 0 & 0 & 0 & 0 & 0 & 0 \\ 0 & 0 & 0 & 0 & 0 & 0 \end{pmatrix}, \end{aligned} \quad (4.33)$$

whereas the letters  $w_i \in \{P, \tilde{x}_1 + \tilde{x}_2, \tilde{x}_1 + P, \tilde{x}_2 + P, \tilde{x}_1 + \tilde{x}_2 + 2P, \tilde{x}_1 - P, \tilde{x}_2 - P, \tilde{x}_1 + \tilde{x}_2 - 2P\}$  (the last three entries correspond to spurious singularities) form a rational alphabet. The system of differential equations admits a solution in terms of iterated integrals, as shown in (4.12), which in this case give rise to generalized polylogarithms [236, 237, 245, 246]. The analytic expression for our master integrals up to order  $\mathcal{O}(\epsilon^2)$  is obtained after fixing boundary conditions as follows:

- $\mathcal{J}_1, \mathcal{J}_5$  can be obtained by direct integration, since in momentum space they appear as massless two-points functions  $\mathcal{G}_{a_1, a_2}$  with half-integer exponents in Euclidean space, of the type of equation (4.29) whose solution is known [247].
- $\mathcal{J}_2, \mathcal{J}_4, \mathcal{J}_6$  can be fixed order by order in  $\epsilon$  imposing regularity conditions in the spurious poles, at the point  $(\tilde{x}_1, \tilde{x}_2, P) = (1, 1, 1)$ .
- $\mathcal{J}_4$  can be fixed by matching with the direct integration at  $(\tilde{x}_1, \tilde{x}_2, P) = (0, 0, 1)$ , which at this point becomes of the form of integral of equation (4.29).

Using the results of the master integrals and inputting them in the result obtained for the flat-space wavefunction coefficient as a linear combination of the basis,  $\mathcal{I}_{\{1\}}^{(2,1)}$  reads as,

$$\begin{aligned}
\mathcal{I}_{\{1\}}^{(2,1)} &= -\frac{1}{\epsilon(\tilde{x}_1 + \tilde{x}_2)} + \frac{(-2\log(P) - \gamma_E + 2 - \log(4\pi))}{\tilde{x}_1 + \tilde{x}_2} \\
&+ \frac{2}{\tilde{x}_1^2 - \tilde{x}_2^2} \left[ \tilde{x}_2 \log\left(\frac{P + \tilde{x}_1}{P}\right) - \tilde{x}_1 \log\left(\frac{P + \tilde{x}_2}{P}\right) \right] \\
&- \frac{1}{P} \left[ \frac{\pi^2}{6} + \text{Li}_2\left(\frac{P - \tilde{x}_2}{P + \tilde{x}_1}\right) + \text{Li}_2\left(\frac{P - \tilde{x}_1}{P + \tilde{x}_2}\right) \right] \\
&+ \frac{1}{2} \log^2\left(\frac{P + \tilde{x}_1}{P + \tilde{x}_2}\right) \Big]. \tag{4.34}
\end{aligned}$$

This result agrees with what is known in the literature.

**Site weight integration** – The integration over the  $x$ -variables of equation (4.23) can be performed directly in terms of known Mellin transforms [248], and via the Method of Brackets [249, 250]. Such method is based on Ramanujan’s master theorem which states that given a complex valued function  $g(x)$ , which can be Taylor expanded around  $x \rightarrow 0$  as:

$$g(x) = \sum_{k=0}^{\infty} \frac{G(k)}{k!} (-x)^k, \tag{4.35}$$

then its Mellin transform is given by

$$\int_0^{\infty} x^{s-1} g(x) dx = \Gamma(s) G(-s). \tag{4.36}$$

The final result, which is symmetric under the exchange of  $X_1 \leftrightarrow X_2$ , can be expressed as a linear combination of *Hypergeometric* functions  ${}_2F_1$  and  ${}_3F_2$  and logarithms, and reads as:



$$\begin{aligned}
\mathcal{I}_{(2,1)} = & \frac{2^{-3-2\alpha} \pi^{3/2} (X_1 + X_2)^{1+2\alpha} \csc(\pi\alpha)^2 \Gamma\left(-\frac{1}{2} - \alpha\right)}{\Gamma[-\alpha]} \left(2 - \frac{1}{\epsilon} - \log(4\pi e^{\gamma_E} P^2)\right) \\
& + \frac{\pi^{3/2} \csc^2(\pi\alpha)}{8(\alpha+1)^2 P} \left[ -4\sqrt{\pi} \left( (P+X_1)^{\alpha+1} - 2(X_1-P)^{\alpha+1} \right) (P+X_2)^{\alpha+1} \right. \\
& - \frac{4^{-\alpha} \Gamma\left(-\alpha - \frac{1}{2}\right) (X_1+X_2)^{2\alpha+2}}{\Gamma(-\alpha)} {}_2F_1\left(1, -2(\alpha+1); -\alpha; \frac{P+X_1}{X_1+X_2}\right) \Big] \\
& + \frac{\pi^2 \csc(\pi\alpha) \csc(2\pi\alpha) (P+X_1)^\alpha}{4\alpha+2} \left[ -2(P+X_1) \left( (P-X_2)^\alpha + (-1)^\alpha (P+X_2)^\alpha \right) \right. \\
& + (-1)^\alpha (X_1-X_2) (P+X_1)^\alpha {}_2F_1\left(1-\alpha, -2\alpha; 1-2\alpha; \frac{X_1-X_2}{P+X_1}\right) \\
& + (X_1+X_2) (P+X_1)^\alpha {}_2F_1\left(1-\alpha, -2\alpha; 1-2\alpha; \frac{X_1+X_2}{P+X_1}\right) \Big] \\
& - \frac{\pi^{5/2} 4^{-\alpha-1} \csc(\pi\alpha) \csc(2\pi\alpha)}{\Gamma(-\alpha) \Gamma\left(\alpha + \frac{3}{2}\right) (P+X_1)} \left[ (-1)^\alpha (X_1-X_2)^{2\alpha+2} {}_3F_2\left(1, 1, \alpha+2; 2, 2\alpha+3; \frac{X_1-X_2}{P+X_1}\right) \right. \\
& + (X_1+X_2)^{2\alpha+2} {}_3F_2\left(1, 1, \alpha+2; 2, 2\alpha+3; \frac{X_1+X_2}{P+X_1}\right) \Big] \\
& + \frac{\pi^{5/2} 2^{-2\alpha-1} \csc(\pi\alpha) \csc(2\pi\alpha)}{\Gamma(-\alpha) \Gamma\left(\alpha + \frac{3}{2}\right)} \left( (-1)^\alpha (X_1-X_2)^{2\alpha+1} + (X_1+X_2)^{2\alpha+1} \right) \log\left(\frac{P+X_1}{P}\right) \\
& + (X_1 \leftrightarrow X_2).
\end{aligned}$$

### 4.3.2 One-loop three-site graph

Let us move on to the next-to-simplest one-loop case, constituted by the one-loop three-site integral – See Fig. 4.2. As we will show, it has some distinctive features which were absent in the previous case. The easiest to spot is the fact that now the volumes in the loop integral measure are higher degree polynomials that no longer factorize in a product of linear polynomials. Actually, such a factorization occurs for the one-loop two-site case only.

In what follows, we restrict ourselves to the case in which there is just one external state at each site, so that  $|\vec{P}_i| \rightarrow X_i$ . Reducing the number of scales from six to three simplifies the problem while still capturing all the essential complexities.

The representation for the integrand coming from one of the signed triangulations of the underlying cosmological polytope, which corresponds to the choice  $\mathcal{G}_\circ = \{\mathcal{G}, \mathfrak{g}_1, \mathfrak{g}_2, \mathfrak{g}_3\}$ , is given in terms of the sum of six simplices. Interestingly, it is enough to focus on the study of the differential equations for one of them, as the others can be derived through permutations of integration variables and external kinematics. Explicitly, such representation for

the integrand yields the following form for the integral  $\mathcal{I}_{\{1\}}^{(3,1)}$ :

$$\begin{aligned} \mathcal{I}_{\{1\}}^{(3,1)} = \kappa_0 \int_{\Gamma} \prod_{e \in \mathcal{E}^{(1)}} [dy_e y_e] & \frac{\kappa^\chi}{q_{\mathcal{G}} \prod_{j=1}^3 q_{\mathfrak{g}_j}} \left[ \frac{1}{q_{\mathcal{G}_{12}}} \left( \frac{1}{q_{\mathfrak{g}_{23}}} + \frac{1}{q_{\mathfrak{g}_{31}}} \right) + \right. \\ & \left. + \frac{1}{q_{\mathcal{G}_{23}}} \left( \frac{1}{q_{\mathfrak{g}_{31}}} + \frac{1}{q_{\mathfrak{g}_{12}}} \right) + \frac{1}{q_{\mathcal{G}_{31}}} \left( \frac{1}{q_{\mathfrak{g}_{12}}} + \frac{1}{q_{\mathfrak{g}_{23}}} \right) \right] \end{aligned} \quad (4.37)$$

where  $\kappa$  is:

$$\kappa = \begin{vmatrix} 0 & 1 & 1 & 1 & 1 \\ 1 & 0 & y_{12}^2 & y_{23}^2 & y_{31}^2 \\ 1 & y_{12}^2 & 0 & P_2^2 & P_1^2 \\ 1 & y_{23}^2 & P_2^2 & 0 & P_3^2 \\ 1 & y_{31}^2 & P_1^2 & P_3^2 & 0 \end{vmatrix}, \quad (4.38)$$

$\kappa_{\circ}$  is:

$$\kappa_{\circ} = \begin{vmatrix} 0 & 1 & 1 & 1 & 1 \\ 1 & 0 & P_2^2 & P_1^2 & \\ 1 & P_2^2 & 0 & P_3^2 & \\ 1 & P_1^2 & P_3^2 & 0 & \end{vmatrix}, \quad (4.39)$$

and  $\chi = \frac{d-4}{2}$ . Furthermore, for regularization purposes, we can consider  $d = 3 + 2\epsilon$ . The set of edges  $\mathcal{E}^{(1)}$  is given by  $\mathcal{E}^{(1)} := \{e_{12}, e_{23}, e_{31}\}$ . Finally, it is useful to write here the explicit expression for the linear polynomials  $\{q_{\mathfrak{g}}, \mathfrak{g} \subseteq \mathcal{G}\}$ , whose associated subgraphs follow the same conventions introduced in the previous section with  $\mathfrak{g}_{s_1 \dots s_{\tilde{n}_s}}$  being the connected subgraph containing the sites  $s_1, \dots, s_{\tilde{n}_s}$ , while  $\mathcal{G}_{ij} := \mathcal{G} \setminus \{e_{ij}\}$  is the subgraph obtained from  $\mathcal{G}$  by deleting the edge  $e_{ij}$  connecting the sites  $s_i$  and  $s_j$ :

$$\begin{aligned} q_{\mathcal{G}} &= \sum_{i=1}^3 X_i, \\ q_{\mathfrak{g}_j} &= y_{j-1,j} + X_j + y_{j,j+1}, \\ q_{\mathcal{G}_{j,j+1}} &= \sum_{s=1}^3 X_s + y_{j,j+1}, \end{aligned} \quad (4.40)$$

with  $j = 1, 2, 3$ .

Partial fraction identities allows focusing only on subsets of three denominators: the evaluation can then be split into two types of contributions, separating the calculation of the sectors with denominators  $\{q_{\mathfrak{g}_j}, j = 1, 2, 3\} \cup \{q_{\mathfrak{g}_{23}}\}$ , and of ones containing  $q_{\mathcal{G}_{12}}$  and the pairs  $\{(q_{\mathfrak{g}_j}, q_{\mathfrak{g}_{j+1}}), (q_{\mathfrak{g}_j}, q_{\mathfrak{g}_{24}}); j = 1, 2, 3\}$ .

**Polylogarithmic sector** – Let us begin with the sector identified by  $\{q_{\mathfrak{g}_j}, j = 1, 2, 3\} \cup$

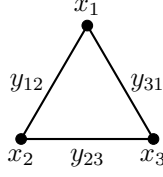


Figure 4.2: One loop three-site diagram. The corresponding integrand has 10 denominators, each corresponding to a connected subgraph of the above graph. Three subgraphs which enclose a single site, three which enclose two sites at a time, three which enclose all three sites but cut each edge twice and finally the full graph which corresponds to the total energy singularity.

$\{q_{\mathfrak{g}23}\}$ . The associated integrals can be written as

$$\begin{aligned} \mathcal{I}_{\tau_{\mathfrak{g}1} \tau_{\mathfrak{g}2} \tau_{\mathfrak{g}3} \tau_{\mathfrak{g}23}} &= \int_{\Gamma} \mu_d \varphi_{\tau_{\mathfrak{g}1} \tau_{\mathfrak{g}2} \tau_{\mathfrak{g}3} \tau_{\mathfrak{g}23}} , \\ \varphi_{\tau_{\mathfrak{g}1} \tau_{\mathfrak{g}2} \tau_{\mathfrak{g}3} \tau_{\mathfrak{g}23}} &= \frac{\prod_{e \in \mathcal{E}^{(1)}} dy_e}{q_{\mathfrak{g}1}^{\tau_{\mathfrak{g}1}} q_{\mathfrak{g}2}^{\tau_{\mathfrak{g}2}} q_{\mathfrak{g}3}^{\tau_{\mathfrak{g}3}} q_{\mathfrak{g}23}^{\tau_{\mathfrak{g}23}}} . \end{aligned} \quad (4.41)$$

As described earlier, writing down the integration by parts identities (4.5) and solving for a basis, we find that the integral family has 15 master integrals, whose master forms can be chosen as:

$$\begin{aligned} e_1 &= \varphi_{0000} , & e_2 &= y_{12}^2 \varphi_{0000} , & e_3 &= y_{23}^2 \varphi_{0000} , \\ e_4 &= y_{31}^2 \varphi_{0000} , & e_5 &= y_{12} \varphi_{0000} , & e_6 &= y_{23} \varphi_{0000} , \\ e_7 &= y_{31} \varphi_{0000} , & e_8 &= \varphi_{1000} , & e_9 &= \varphi_{0100} , \\ e_{10} &= \varphi_{0010} , & e_{11} &= y_{23} \varphi_{0001} , & e_{12} &= y_{31} \varphi_{0001} , \\ e_{13} &= y_{12} \varphi_{0001} , & e_{14} &= \varphi_{0002} , & e_{15} &= \varphi_{1110} . \end{aligned} \quad (4.42)$$

As described in section 4.3, the sub-sector without denominators contains  $\nu_3^{(\text{CI})} = 7$  master integrals, and its differential equations are shown in figure 4.3. Heuristically, this large number can be motivated by rewriting the measure of the integral in momentum space, which belongs to the integral family:

$$\mathcal{I}_{\tau_1 \tau_2 \tau_3}^{(3, 1; 0)} = \int_{\mathbb{R}^3} d\vec{l} \frac{1}{[(\vec{l})^2]^{\tau_1} [(\vec{l} + \vec{P}_1)^2]^{\tau_2} [(\vec{l} + \vec{P}_1 + \vec{P}_2)^2]^{\tau_3}} , \quad (4.43)$$

where  $\tau_i \in \mathbb{Z} + 1/2$ . The integral in equation (4.43) is the one-loop three-point function with massive external momenta of mass  $P_i$  and with massless denominator raised to half-integer powers, in Euclidean spacetime. Integration by parts in  $y_e$  will mix integrals with denominators raised to half-integer powers with those raised to integer ones, a property that does not hold for momentum space integration by parts identities, and which effectively increases the number of master integrals.

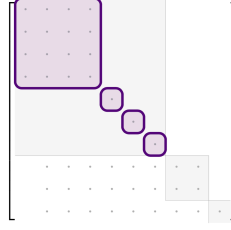


Figure 4.3: Zero sector of the one-loop three-site-graph. The first four integrals form a  $4 \times 4$  homogeneous diagonal block, corresponding to the one-loop three point function with denominator raised to half-integer powers, and each of the subsequent three integrals form a  $1 \times 1$  diagonal block, and can be identified with one-loop two-point functions with denominators raised to half integer powers.

It is possible to find a  $\epsilon$ -factorized form for the differential equation matrices obeyed by these integrals [243, 251–254]. Also in this case, the total differential can be written in  $d\log$  form, indicating that the space of functions consists of generalized polylogarithms, and the alphabet for this sector, together with the equivalent sectors in the remaining three similar integrals (obtained by replacing  $q_{\mathfrak{g}23}$  with  $q_{j,j+1}$ ,  $j \neq 2$ ), reads:

$$W = \{X_1, X_2, X_3, X_1 + X_2, X_2 + X_3, X_1 + X_3, -X_3 + X_1 - X_2, X_3 + X_1 - X_2, -X_3 + X_1 + X_2, X_3 + X_1 + X_2\}. \quad (4.44)$$

In the generic case of multiple external legs, in which  $x_i \neq P_i$ , the basis of this sector increases to 34. The function space consists only of generalized polylogarithms, but algebraic letters appear in the alphabet.

**Elliptic sector** – Let us now turn our attention to the sectors containing the denominator  $q_{\mathcal{G}_{12}}$ :

$$\begin{aligned} \mathcal{I}_{\tau_{\mathfrak{g}}\tau_{\mathfrak{g}'}\tau_{\mathcal{G}_{12}}} &= \int_{\Gamma} \mu_d \varphi_{\tau_{\mathfrak{g}}\tau_{\mathfrak{g}'}\tau_{\mathcal{G}_{12}}}, \\ \varphi_{\tau_{\mathfrak{g}}\tau_{\mathfrak{g}'}\tau_{\mathcal{G}_{12}}} &= \frac{\prod_{e \in \mathcal{E}^{(1)}} dy_e}{q_{\mathfrak{g}}^{\tau_{\mathfrak{g}}} q_{\mathfrak{g}'}^{\tau_{\mathfrak{g}'}} q_{\mathcal{G}_{12}}^{\tau_{\mathcal{G}_{12}}}}, \end{aligned} \quad (4.45)$$

where  $(\mathfrak{g}, \mathfrak{g}')$  takes values in the set of pairs  $\{(\mathfrak{g}_j, \mathfrak{g}_{j+1}), (\mathfrak{g}_j, \mathfrak{g}_{23})\}$ .

The sub-sector containing only the denominator  $q_{\mathcal{G}_{12}}$ , has 9 master integrals, that can be chosen as follows:

$$\begin{aligned} e_1 &= y_{23}y_{31}\varphi_{001}, & e_2 &= y_{23}\varphi_{001}, & e_3 &= y_{23}\varphi_{002}, \\ e_4 &= y_{31}\varphi_{001}, & e_5 &= y_{31}\varphi_{002}, & e_6 &= \varphi_{002}, \\ e_7 &= \varphi_{001}, & e_8 &= y_{23}^2\varphi_{001}, & e_9 &= y_{31}^2\varphi_{001}, \end{aligned} \quad (4.46)$$

and whose shape of the differential equation is shown in Fig.4.4. Constructing the Picard-

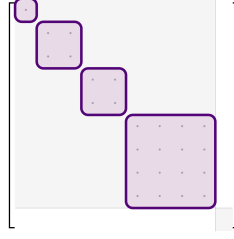


Figure 4.4: Homogeneous sector of the one-loop three-site graph with denominator  $q_a$ . There are a total of 9 master integrals, which decouple in blocks of dimensions  $1 \times 1, 2 \times 2, 2 \times 2, 4 \times 4$ . In the last block, the elliptic family appears.

Fuchs operators for each homogeneous block of the differential equation in  $d = 3$ , where we used the change of variables:  $X_1 \rightarrow a_1 \lambda$ ,  $X_2 \rightarrow \lambda$ ,  $X_3 \rightarrow 1$ , we found a differential operator of third order  $\mathcal{L}_3$ , corresponding to the sector formed by the last 3 master integrals of equation (4.46), which factorizes [255] in one operator of first order and one of second order, as  $\mathcal{L}_3 = \mathcal{L}_1 \mathcal{L}_2$ . The operator  $\mathcal{L}_2$  reads:

$$\begin{aligned} \mathcal{L}_2 = & \frac{d^2}{d\lambda^2} + \frac{5(a^2 - 1)^2 \lambda^4 - 6(a^2 + 1) \lambda^2 + 1}{(a^2 - 1)^2 \lambda^5 - 2(a^2 + 1) \lambda^3 + \lambda} \frac{d}{d\lambda} \\ & + \frac{3(a^2 - 1)^2 \lambda^2 - 2(a^2 + 1)}{(a^2 - 1)^2 \lambda^4 - 2(a^2 + 1) \lambda^2 + 1} , \end{aligned} \quad (4.47)$$

and its solution is an elliptic function:

$$\psi_{1,2}(K^2) , \quad K^2 = \frac{(a - 1)^2 \lambda^2 - 1}{(a + 1)^2 \lambda^2 - 1} . \quad (4.48)$$

Remarkably, the space of functions gets richer already at one-loop level with respect to the Feynman integral case. As a consistency check of our result, we expect the elliptic function to disappear in the flat spacetime limit, in which  $q_{\mathcal{G}} \rightarrow 0$ . With the change of variables:  $q_{\mathcal{G}} = \sum_{i=1}^3 X_i$ ,  $q_m = X_1 - X_2$ , the flat spacetime singularity becomes manifest, and with the additional change,  $q_{\mathcal{G}} = \lambda_{\mathcal{G}} a_{\mathcal{G}}$  and  $q_m = \lambda$ , one can again find the reparametrization of equation (4.47) in the variables  $(a_s, \lambda)$ . Sending  $q_{\mathcal{G}} \rightarrow 0$ , the second order Picard-Fuchs operator factorizes in two linear differential operators:

$$\mathcal{L}_1 = \frac{d}{d\lambda} + \frac{2\lambda^4 + 5\lambda^2 - 1}{(\lambda - 1)\lambda(\lambda + 1)(\lambda^2 + 1)} , \quad (4.49)$$

$$\mathcal{L}_1 = \frac{d}{d\lambda} + \frac{\lambda}{(\lambda - 1)(\lambda + 1)} . \quad (4.50)$$

Consistently with the known answer of the one-loop three-site integral computation in flat space, as a non-trivial check, it is nice to verify that indeed, in the flat space limit, the elliptic subsector simplifies into polylogarithms. In the study of this sector, algebraic

letters appear of the form  $(P + \sqrt{Q})/(P - \sqrt{Q})$ , with

$$\begin{aligned} Q = & 3X_1^4 + 4X_1^3(X_2 + X_3) - 2X_1^2(7X_2^2 + 2X_2X_3 + 3X_3^2) \\ & + 4X_1(X_2 - 3X_3)(X_2 + X_3)^2 \\ & + (3X_2 - 5X_3)(X_2 + X_3)^3. \end{aligned} \quad (4.51)$$

## 4.4 Correlator versus Wavefunction

So far the two examples we discussed are integrals contributing to the wavefunction. It is interesting to understand what happens when we consider the correlator. Because as we apply the Born rule, it will lead to the cancellation of some singularities in the integrand. Let us first consider the bubble diagram. The correlator for the bubble can be explicitly written as:

$$\begin{aligned} \langle \phi_{k_1} \phi_{k_2} \rangle^{1\text{-loop}} = & 2\psi_2^{(1)}(k_1, k_2) + \frac{2\psi_4^{(0)}(k_1, y_{12}, y_{12}, k_2)}{2y_{12}} + \frac{2\psi_4^{(0)}(k_1, y_{21}, y_{21}, k_2)}{2y_{21}} + \\ & \frac{2\psi_3^{(0)}(k_1, y_{12}, y_{21}) 2\psi_3^{(0)}(k_2, y_{12}, y_{21})}{2y_{21}2y_{12}} \\ = & \frac{x_1 + x_2 + y_{12} + y_{21} + k_1 + k_2}{y_{12}y_{21}(x_1 + x_2 + k_1 + k_2)(x_1 + y_{12} + y_{21} + k_1)(x_2 + y_{12} + y_{21} + k_2)}. \end{aligned} \quad (4.52)$$

Where remarkably, the singularities  $(x_1 + x_2 + 2y_{12})$ , and the equivalent one for the other edge, cancel out in the sum, and we have two other singularities instead  $y_{12}$ , and  $y_{21}$ . This means we cannot simply obtain the correlator from the wavefunction, but we need to consider a larger integral family, which accounts for the two new singularities. But it has more interesting implications for the triangle integral, where the corresponding singularities also cancel in the correlator, that is, the singularities  $(x_1 + x_2 + x_3 + 2y_{12})$ ,  $(x_1 + x_2 + x_3 + 2y_{23})$  and  $(x_1 + x_2 + x_3 + 2y_{31})$  cancel, and we have new singularities,  $y_{12}$ ,  $y_{23}$  and  $y_{31}$ . We will not write the full expression for the triangle as it is too cumbersome. This is remarkable, as we find that the elliptic sector contributing to the wavefunction comes precisely from these singularities. Therefore, it is possible that the correlator is simpler than the wavefunction, although the introduction of new singularities may lead to a new elliptic sector. We leave the study of the correlator for future work.

## 4.5 Discussion

In this section we employed the method of differential equations in order to compute loop wavefunction coefficients. This method has shown to be quite effective at compute any integral with a rational integrand, thus encompassing many useful classes of integrals in physics, the most relevant one being Feynman integrals. For cosmological correlators,

differential equations have been used to compute tree-level cosmological correlators, and here we extend their application for loop level. We were able to compute the full two-point one-loop wavefunction coefficient for conformally coupled states. When computing the flat-space wavefunction coefficient for one-loop three point we found that the differential equations contain elliptic sectors. This constitutes a significant hurdle in finding a canonical form for the differential equations, as most of the strategies and methods rely on the integrand being a logarithmic kernel, instead of elliptic. As we argued in the previous section, the singularities producing the elliptic sector in the differential equations cancel out in the correlator, and new singularities appear. It remains to be studied whether the new singularities also give rise to an elliptic sector, and thus whether the correlator is actually a simpler function than the wavefunction. However, computing the wavefunction can still be a valuable endeavor given that using the Born rule one can compute any given observable, and not just  $n$ -point correlation functions. Thus the wavefunction gives a larger insight into the nature of loop cosmological observables. Given this discussion, the significant difficulties that we found for the next to simplest one-loop example, as well as the fact that loop contributions will be very hard to measure in the near future, due to the fact that we expect them to be very suppressed with respect to tree level, why should we compute loop cosmological correlators? The argument is simple, even though tree-level is what we can expect to measure in the near future, the whole theory we are working on relies on the expectation that perturbation theory, under certain assumptions, works. Now, if we were to find that there is some fundamental flaw in loop computations that whole expectation would crumble. Such an example comes from the previous chapter, where we studied the infrared divergences of these integrals. Therefore, here we are simply trying to compute the simplest one-loop examples with the goal of studying their analytic structure and how it differs from flat space and the tree-level coefficients. From this work, there are two natural directions to follow, one is to finish the triangle computation, but studying the recent developments in integrating elliptic kernels. The other direction, is to study the correlators directly and understand if the ellipticity is still there, and even if it is, whether they are simpler than the wavefunction or not, as claimed in [113].





# Chapter 5

## Combinatorial Structure of the Wavefunction

In this chapter, we discuss a novel combinatorial description for the wavefunction. In particular, we describe a geometric object, called Cosmohedron, which encodes the integrand of the full wavefunction, both a tree and loop level. This new geometric description departs from the current geometric understanding of the wavefunction, which is encoded in cosmological polytopes [31], in several ways. Firstly, the cosmohedron gives the description of the full wavefunction, as opposed to a graph-by-graph description. The cosmohedron also introduces in itself a graph geometry, in terms of graph associahedra (which we describe in section 5.1.1), that we will connect with the cosmological polytope in section ???. Then, the cosmohedron relies on an entirely new parameterization of the wavefunction in terms of sub-polygons of the momentum polygon. And finally, we hope that this new combinatorial description of the wavefunction can help us connect the  $\text{Tr}\phi^3$  scalar wavefunction to other theories, such as those with pions and non-supersymmetric Yang-Mills. In the first sections below, we will describe graph associahedra and their connection with cosmological polytopes. Then, we will build on this to construct the cosmohedron, both combinatorially as well as its embedding. We will then describe how to extract the wavefunction from the geometry. Afterwards, we will describe how this picture generalizes for loops. And finally, we will briefly describe the combinatorial picture for the correlator.

### 5.1 Combinatorial Wavefunction

#### 5.1.1 Graph Associahedra

The cosmohedron, which is a geometry encoding the full wavefunction also implies a geometry for individual graphs, different from cosmological polytopes [31], which were introduced in the second section. We call the single-graph geometry, graph associahedra, and we start by describing this. As we have explained in section 2, from the *old fashioned perturbation theory* representation of the integrand, the rational function can be decomposed into several

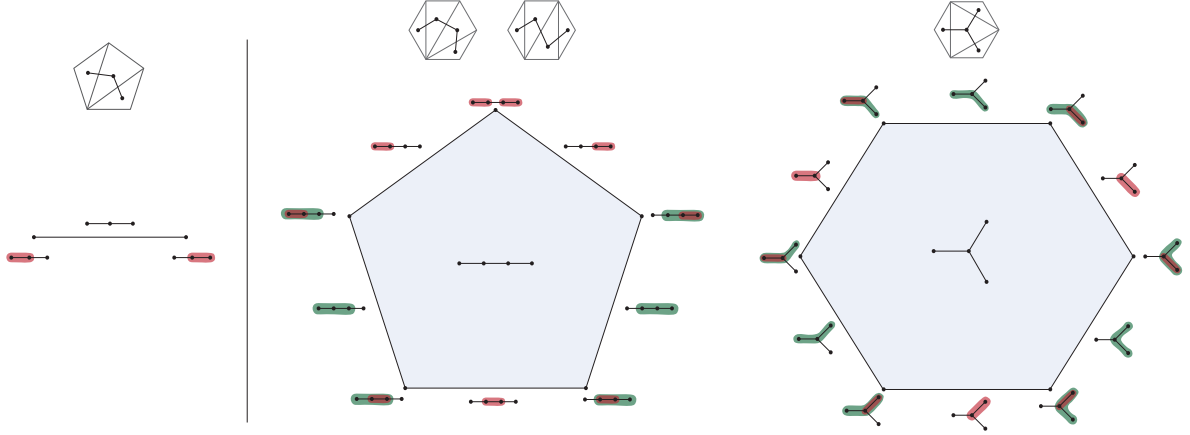


Figure 5.1: 5(left) and 6(right) point graph associahedron. When drawing the graph we omit the external legs to make manifest that for the purpose of the combinatorics of tubings what matters is the topology of the graph with just the internal edges.

terms with numerator one and singularities corresponding to tubes which are not partially overlapping between themselves. The graph as a polytope where each facet corresponds to a tube, and a face of general dimension correspond to partial tubings  $\tau$ , where by increasing the co-dimension of the face the tubing will have a higher number of non-overlapping tubes corresponding to it, such that its formal definition is:

$$\tau' \text{ is a face of } \tau \text{ if } \tau \subset \tau', \quad (5.1)$$

examples of graph associahedra a five, six and seven points can be found in figure 5.1 Its facets have a well defined factorization structure, consider any single tube  $T$  of a graph  $G$ , then we have

$$\text{Facet}_T(\mathcal{A}_G) = \mathcal{A}_T \times \mathcal{A}_{G/T}, \quad (5.2)$$

where  $G/T$  is the graph obtained by shrinking all of  $T$  to a single point.

### Examples

At 5-points, let us fix the triangulation to be that containing chords  $\{(1, 3), (1, 4)\}$  (all the remaining triangulations are simply given by cyclic rotations of this one). In this case, we can factor out from all the russian dolls a factor of  $1/(E_t \mathcal{P}_{1,2,3} \mathcal{P}_{1,3,4} \mathcal{P}_{1,4,5})$ , and after doing this we get that the contribution to  $\Psi^{(5)}$  coming from this graph is simply:

$$\Psi_{\{(1,3),(1,4)\}}^{(5)} = \frac{1}{E_t \mathcal{P}_{1,2,3} \mathcal{P}_{1,3,4} \mathcal{P}_{1,4,5}} \left( \frac{1}{\mathcal{P}_{1,2,3,4}} + \frac{1}{\mathcal{P}_{1,3,4,5}} \right),$$

which means we only have two terms. Therefore, we can associate each term with the boundary of a one-dimensional line-segment (see figure 5.1, left). Each vertex of the line

segment is then associated with a tube which encloses either the left and middle sites, or the right and middle sites.

At 6-points, there are now different types of triangulation to consider. Let us start with the simplest analog of what we had at 5-points, *i.e.* the triangulation containing chords  $\{(1, 3), (1, 4), (1, 5)\}$ . In this case, we have 5 different terms which we can write as:

$$\Psi_{\{(1,3),(1,4),(1,5)\}}^{(6)} = \frac{1}{E_t \mathcal{P}_{1,2,3} \mathcal{P}_{1,3,4} \mathcal{P}_{1,4,5} \mathcal{P}_{1,5,6}} \left( \frac{1}{\mathcal{P}_{1,2,3,4} \mathcal{P}_{1,2,3,4,5}} + \frac{1}{\mathcal{P}_{1,2,3,4} \mathcal{P}_{1,4,5,6}} \right. \\ \left. + \frac{1}{\mathcal{P}_{1,4,5,6} \mathcal{P}_{1,3,4,5,6}} + \frac{1}{\mathcal{P}_{1,3,4,5} \mathcal{P}_{1,3,4,5,6}} + \frac{1}{\mathcal{P}_{1,3,4,5} \mathcal{P}_{1,2,3,4,5}} \right) \quad (5.3)$$

so we see there are five different subpolygons entering inside the brackets –  $\mathcal{P}_{1,2,3,4}$ ,  $\mathcal{P}_{1,3,4,5}$ ,  $\mathcal{P}_{1,4,5,6}$  squares and  $\mathcal{P}_{1,2,3,4,5}$ ,  $\mathcal{P}_{1,3,4,5,6}$  pentagons – each of which can be associated to an edge of a pentagon, such that each of the five vertices where two edges meet gives one of the terms inside brackets in (5.3) (see figure 5.1, center).

So we have that the graph associahedron for  $\Psi_{\{(1,3),(1,4),(1,5)\}}^{(6)}$  is a pentagon. Obviously, the same is true for all the six triangulations that are cyclic rotations of  $\{(1, 3), (1, 4), (1, 5)\}$ . In addition, it is easy to check that the same is true for the 6 triangulations obtained by cyclic rotations of triangulations  $\{(1, 3), (3, 5), (1, 5)\}$  and  $\{(1, 3), (1, 4), (4, 6)\}$ , *i.e.* that for all these triangulations once we factor out  $E_t$  and the perimeters of the triangles in the triangulation, the rest of the wavefunction has precisely 5 terms that can be associated to vertices of a pentagon in exactly the same way we did for the case of  $\Psi_{\{(1,3),(1,4),(1,5)\}}^{(6)}$ . This is ultimately because the associated dual graph for these triangulations where we omit the external legs is also a chain (see figure 5.1, middle).

However, if instead we consider triangulation  $\{(1, 3), (3, 5), (1, 5)\}$  (or  $\{(2, 4), (4, 6), (2, 6)\}$ ) we have that after we factor out the common part, we are still left with six terms:

$$\Psi_{\{(1,3),(3,5),(1,5)\}}^{(6)} = \frac{1}{E_t \mathcal{P}_{1,2,3} \mathcal{P}_{3,4,5} \mathcal{P}_{1,5,6} \mathcal{P}_{1,3,5}} \left( \frac{1}{\mathcal{P}_{1,2,3,5} \mathcal{P}_{1,2,3,4,5}} + \frac{1}{\mathcal{P}_{1,2,3,4,5} \mathcal{P}_{1,3,4,5}} + \frac{1}{\mathcal{P}_{1,3,4,5,6} \mathcal{P}_{1,3,4,5}} \right. \\ \left. + \frac{1}{\mathcal{P}_{1,3,4,5,6} \mathcal{P}_{1,3,5,6}} + \frac{1}{\mathcal{P}_{1,3,5,6} \mathcal{P}_{1,2,3,5,6}} + \frac{1}{\mathcal{P}_{1,2,3,5,6} \mathcal{P}_{1,2,3,5}} \right), \quad (5.4)$$

therefore, for this type of triangulation the graph associahedron is given by a hexagon, where each edge is associated with one of the six subpolygons appearing inside brackets and each vertex associated to one of the terms in (5.4) (see figure 5.1, right). Indeed, in this case, the dual graph (after removing the external legs) has a star topology which is different from that of the chain that we found for the remaining triangulations of the hexagon.

At 7-points, there are a total of 42 triangulations. These amount to 6 different cyclic classes of triangulations. From these 6 cyclic classes (represented by one of its triangulations),

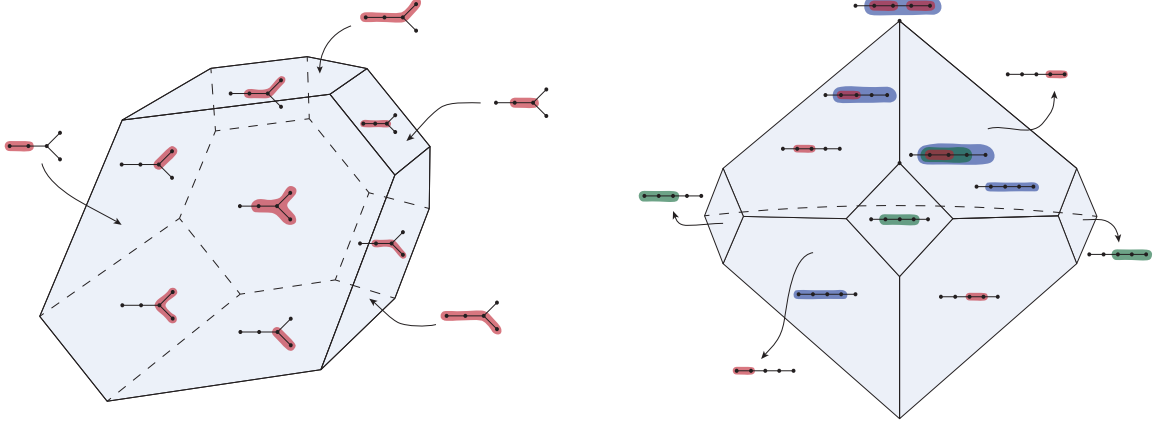


Figure 5.2: (Left) 7-point graph associahedra for triangulations from the cyclic classes  $\{(1, 3), (1, 4), (4, 6), (1, 6)\}$ ,  $\{(1, 3), (3, 5), (1, 5), (1, 6)\}$ . (Right) 7-point graph associahedra for triangulations from the cyclic classes  $\{(1, 3), (1, 4), (1, 5), (1, 6)\}$ ,  $\{(1, 3), (1, 4), (1, 5), (5, 7)\}$ ,  $\{(1, 3), (1, 4), (4, 7), (5, 7)\}$ ,  $\{(1, 3), (3, 7), (3, 6), (4, 6)\}$ .

there are four,

$$\begin{aligned} &\{(1, 3), (1, 4), (1, 5), (1, 6)\}, \{(1, 3), (1, 4), (1, 5), (5, 7)\}, \\ &\{(1, 3), (1, 4), (4, 7), (5, 7)\}, \{(1, 3), (3, 7), (3, 6), (4, 6)\}, \end{aligned}$$

which produce the graph topology corresponding to a chain with four nodes, for which the graph associahedron we can see in the right of figure 5.2. If we pick  $\Psi_{\{(1,3),(1,4),(1,5),(1,6)\}}^{(7)}$ , the wavefunction coefficient for this graph will have 14 terms. Two of these terms are represented in figure 5.2 (two highlighted vertices), after factorizing  $E_t$  and the perimeters of the triangles, they are:

$$\frac{1}{\mathcal{P}_{134567} \mathcal{P}_{1345} \mathcal{P}_{1567}}, \frac{1}{\mathcal{P}_{134567} \mathcal{P}_{13456} \mathcal{P}_{1345}},$$

where the first term corresponds to the tubing at the top of the figure, and the second term corresponds to the tubing in the middle. The triangulations coming from cyclic rotations produce the same graph associahedron, as well as all the other triangulations in the remaining 3 cyclic classes. Since now the facets of the associahedron are two-dimensional, it is easier to illustrate the factorization properties of the facets. For example, the facets associated to the pentagon subpolygons (the green tubes in figure 5.2) are squares, since they are the product of a segment—the graph associahedron of three-site chain—with another segment, seeing that when we shrink the green tubes to a node, we obtain three site chains. All the other facets in figure 5.2 (right) are pentagons. Considering they always result from the factorization of the five-site chain into a four-site chain, whose graph associahedron is a pentagon, and a two-site chain whose graph associahedron is a point.

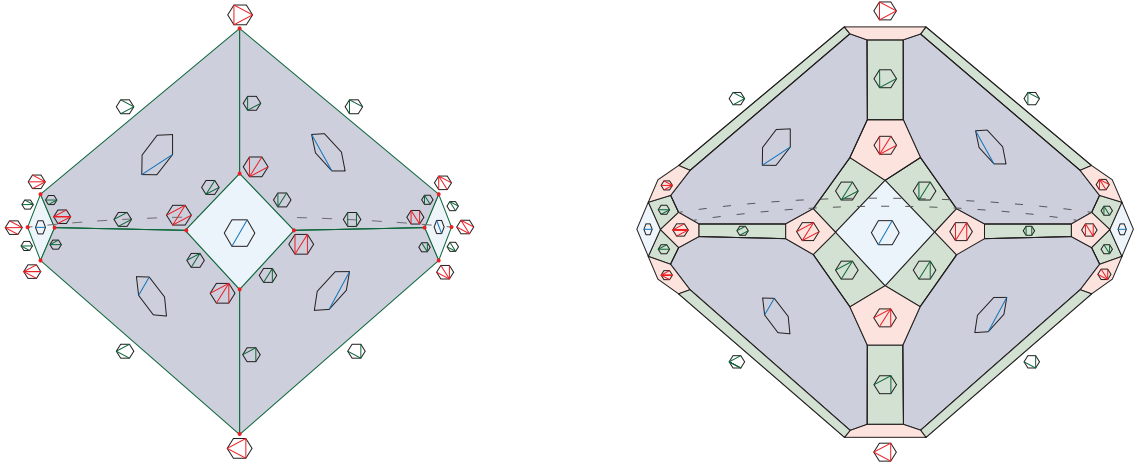


Figure 5.3: associahedron (left) and cosmohedron (right) at 6-points

The other two cyclic classes,

$$\{(1, 3), (1, 4), (4, 6), (1, 6)\}, \{(1, 3), (3, 5), (1, 5), (1, 6)\},$$

produce the graph topology we see at the left in figure 5.2. The graph associahedron in this case has 18 vertices, which match the number of terms in the wavefunction coefficient associated with these type of triangulations.

### 5.1.2 The Cosmohedron

Now, we want to understand the combinatorics of the full wavefunction. We know from amplitudes that the ABHY Associahedron [93] encodes the combinatorics of the full scattering amplitude for a theory of colored cubic scalars. The associahedron is originally the object that captures the combinatorics of triangulations of polygons. But, from section 2 we know that these triangulations are dual to Feynman graphs. In the associahedron, each face corresponds to a partial triangulation of the polygon. For example, the facets are labeled by partial triangulations with a single internal cord, and a co-dimension  $n$  face is labeled by a triangulation with  $n$  internal cords. Then, the faces of a given facet are refinements of the partial triangulation corresponding to the facet, and this refinement keeps going as we increase the co-dimension of the faces. Ultimately, the vertices are full triangulations and the sum of them corresponds to the full scattering amplitude. A more detailed description of the ABHY associahedron can be found in appendix A.

Now, from the graph associahedron we know that a single graph of the  $n$ -point wavefunction has a corresponding  $n - 4$  geometry. Whilst from the associahedron the single graphs correspond to the vertices of the polytope. This suggests how to construct the cosmohedron from the associahedron. We should take each vertex in the associahedron and “blow-up” into a facet. This inevitably forces that every other face of the associahedron is similarly “blown-up” into a facet.

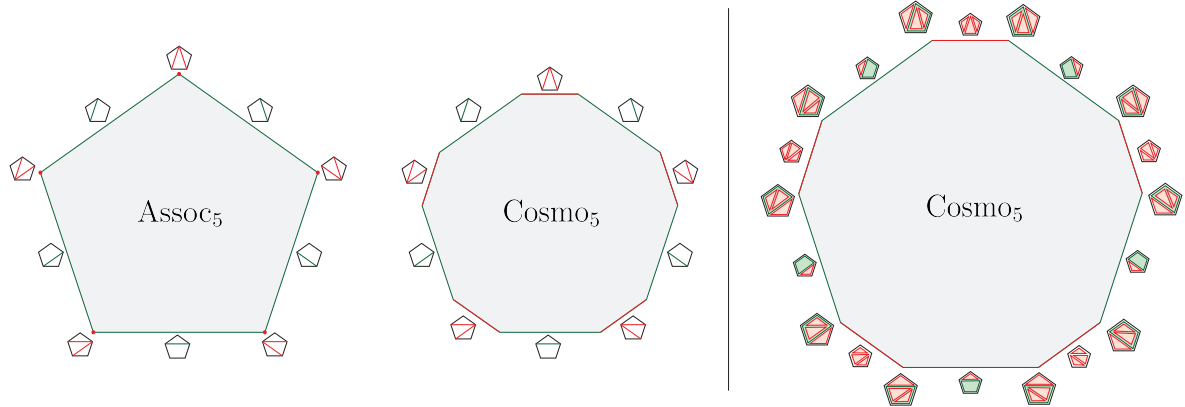


Figure 5.4: (Left) associahedron (pentagon) and cosmohedron (decagon) at 5-points. (Right) 5-point cosmohedron with respective labelling of facets in terms of relevant sub-polygons.

For  $n = 5$  the associahedron is a pentagon and we just “blow up” each vertex of the  $n = 5$  pentagon, into the graph associahedron, which is a segment. Naturally, we get a decagon, whose vertices are now labeled by russian dolls for the  $n = 5$  wavefunction, as shown in figure 5.4.

For the cosmohedron, edges represent both partial and full triangulations. Each of these triangulations includes a set of sub-polygons. The Russian doll configurations at a given vertex consist of the sub-polygons present in the union of those on the edges meeting at that vertex. The scenario for  $n = 6$  presents additional complexity. As noted earlier, 12 of the 14 triangulations have graphs that form four-site chains, with their graph associahedra being pentagons. The two triangulations  $\{(1, 3), (3, 5), (1, 5)\}$  and  $\{(2, 4), (4, 6), (2, 6)\}$  have hexagons as their graph associahedra. To “blow up” these vertices into pentagons and hexagons, the introduction of new faces is needed. It is not trivial that this procedure necessarily works for this three dimensional case, but remarkably it works. This transformation from the six-point associahedron to the cosmohedron is shown in Figure 5.3. We proceed to establish the combinatorial framework for the cosmohedron applicable to any  $n$ . In the associahedron, faces were linked to sets of non-intersecting chords, adhering to the structure defined by (A.4). A similar approach is taken for the cosmohedron. Rather than sets of non-intersecting chords  $C$ , our focus shifts to sets of non-overlapping sub-polygons  $P$ . Typically, two sub-polygons are considered non-overlapping if their chords do not intersect; they may either be nested or entirely separate. Additionally, a “Russian doll” condition is applied to the set  $P$ : for any sub-polygons  $X$  and  $Y$  in  $P$  where  $Y$  is contained within  $X$ ,  $X$  must be entirely encompassed by other sub-polygons within it.

Having defined our subsets  $P$ , the defining property of the cosmohedron is exactly as it was for the associahedron. The cosmohedron has faces for all  $P$ , such that

$$P' \text{ is a face of } P \text{ if } P \subset P'. \quad (5.5)$$

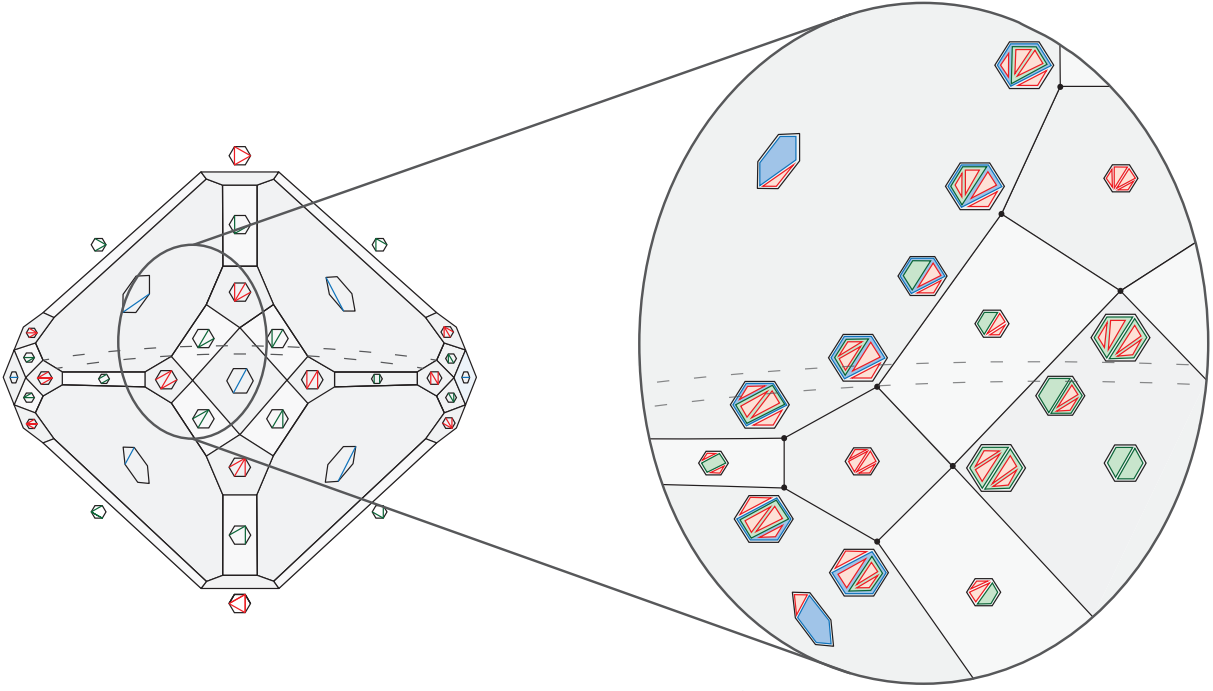


Figure 5.5:  $\text{Cosmo}_6$  with labelling of different codimension facets in terms of relevant subpolygons

The interior of the cosmohedron can be thought as associated with  $P = (1, 2, \dots, n)$  the full polygon. The co-dimension-1 facets of the cosmohedron are associated with  $P'$  that correspond to the sub-polygons in any partial triangulation of the  $n$ -gon. This combinatorial rule for the labelling of the faces is illustrated in figure 5.5 for  $n = 6$  example.

A remarkable feature of the associahedron is how the factorization structure of scattering amplitudes is fully encoded in the structure of its facets. For example, a facet corresponds to a partial triangulation of a single internal cord, thus this cord splits the momentum polygon into two subpolygons. The corresponding facet of the associahedron will reflect that and it is exactly the product of the lower point associahedra corresponding to the division of the momentum polygon given by the cord. This precisely reflects the fact that the scattering amplitude, when approaching a singularity exactly factorizes into the lower point scattering amplitudes. For the cosmohedron there is a similar picture. Each facet is associated with a set of non-intersecting chords  $C$ , which provide a partial triangulation of the  $n$ -gon. From this set  $C$ , we derive a collection of sub-polygons denoted as  $\{P_C\}$ . Additionally, we obtain a dual graph  $G_C$ . This graph is constructed by placing a vertex at the center of each sub-polygon and connecting these vertices when their corresponding sub-polygons share an edge. Then, we have

$$\text{Facet}_C[\text{Cosmo}_n] = \prod_{P_i \in P_C} \text{Cosmo}_{P_i} \times \mathcal{A}_{G_C}. \quad (5.6)$$

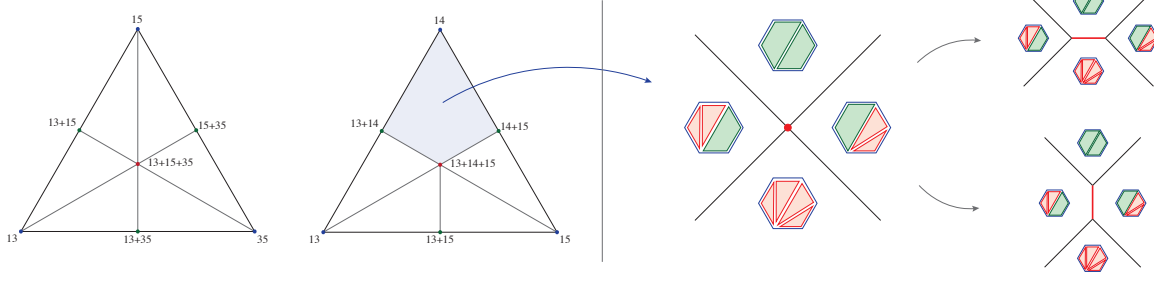


Figure 5.6: (Left) "Cosmologizing" the  $n = 6$  associahedron fan to obtain the  $\text{Cosmo}_6$  fan. In light blue, we highlight the cone corresponding to the non-simple vertex. (Right) Labelling of the four-facets meeting at the non-simple vertex, as well as the two possible "blow up"s into simple vertices. In both cases, we create a new edge (marked in red) that is already labelled by a full russian doll.

Given that our 6-point cosmohedron is three-dimensional, it serves as a useful example for illustrating facet factorization. In Figure 5.3, the red facets represent full triangulations. Consequently, these facets will precisely match the graph associahedron of the corresponding graph, as all sub-polygons are triangles. The green facets correspond to partial triangulations involving two chords. In this case, the sub-polygons consist of a square and two triangles. This configuration allows for the insertion of three nodes within each of the sub-polygons, forming a three-site chain as the only possible graph. Thus, the facets will consistently be squares, given that the cosmohedron associated with the 4-point wavefunction is a line interval, similar to the graph associahedron of the three-site chain.

Finally, we consider the blue facets, which relate to a partial triangulation with a single chord. There are two categories of blue facets: one where the chord divides the hexagon into a pentagon and a triangle, and another where the chord splits the hexagon into two squares. For both categories, the dual graph is a two-site chain, whose graph associahedron is a point. In the first category (darker blue), we observe the factorization of the 5-point cosmohedron and the 3-point (which is a point), resulting in decagonal facets corresponding to the 5-point cosmohedron. The second category (lighter blue) results from the factorization into two 4-point cosmohedra, which are segments, leading to square facets.

## 5.2 Embedding

The fan of the cosmohedron can be obtained starting from the fan of the associahedron. The  $g$ -vectors associated with the curves  $(i, j)$  of the associahedron, split the  $(n-3)$ -dimensional  $g$ -vector space into cones, each representing a triangulation. The cosmohedron's fan is obtained from the associahedral fan by sub-dividing each cone, where the new rays are obtained by summing all subsets of rays in a cone of the associahedron.



Consider the example of the cone of the 6-point associahedron bounded by the curves  $\{(1, 3), (1, 5), (3, 5)\}$ . Since we are only concerned with the direction of the rays, we can projectively represent this cone as a two-dimensional triangle with vertices at  $(g_{1,3}, g_{3,5}, g_{1,5})$ , as shown in Figure 5.6 (left, blue vertices only). To refine this cone, we start by adding rays that correspond to all possible subset sums of the rays  $\{(1, 3), (3, 5), (1, 5)\}$  that bound the parent cone. This includes the original rays  $g_{1,3}, g_{3,5}, g_{1,5}$ , along with  $g_{1,3} + g_{3,5}, g_{3,5} + g_{1,5}, g_{1,3} + g_{1,5}$  (in green), and  $g_{1,3} + g_{3,5} + g_{1,5}$  (in red). These additions introduce midpoints and the barycenter of the two-dimensional triangle, which corresponds to the original cone. We then construct new cones by connecting the vertices and midpoints of the triangle to the barycenter, as illustrated in Figure 5.6. This process generates numerous new cones, each corresponding to the Russian doll vertices of the cosmohedron. Notably, the central ray  $(g_{1,3}, g_{3,5}, g_{1,5})$  is bounded by six cones. The corresponding facet of the cosmohedron is a hexagon, which is the appropriate graph associahedron for the graph associated with this triangulation. The scenario becomes more complex when considering a different triangulation of the associahedron, such as one bounded by  $\{(1, 3), (1, 4), (1, 5)\}$ , where the graph associahedron is a pentagon rather than a hexagon. We start again with the parent rays and include all subset sums associated with them, providing us with the vertices  $(g_{1,3}, g_{1,4}, g_{1,5})$ , midpoints  $(g_{1,3} + g_{1,4}, g_{1,3} + g_{1,5}, g_{1,4} + g_{1,5})$ , and the barycenter  $g_{1,3} + g_{1,4} + g_{1,5}$  (see Figure 5.6, middle). To form the cones, we connect all these points to the barycenter, except for the edge connecting  $g_{1,4}$  to  $g_{1,3} + g_{1,4} + g_{1,5}$ , as highlighted in Figure 5.6. This results in a cone bounded by four rays  $(g_{1,3} + g_{1,4}, g_{1,4}, g_{1,4} + g_{1,5}, g_{1,3} + g_{1,4} + g_{1,5})$ , meaning the corresponding vertex of the cosmohedron belongs to four facets (as illustrated on the right of Figure 5.6). This reflects the fact that the cosmohedron is not a simple polytope. Additionally, there are five cones touching the central ray, so the facet of the cosmohedron associated with the triangulation  $\{(1, 3), (1, 4), (1, 5)\}$  is a pentagon, which correctly corresponds to the graph associahedron of the associated diagram.

The combinatorics for the full fans of the six-point associahedron and cosmohedron are illustrated in Figure 5.7. The fan is three-dimensional, and the figure shows all the cones of the fan, except for the cone in the back. For the associahedron (left of Figure 5.7), we observe the familiar nine rays corresponding to the facets and 14 cones corresponding to the vertices of the associahedron. The five cones meeting at a ray corresponding to the pentagonal faces are shaded in dark blue, and the four cones meeting at a ray corresponding to the square faces of the associahedron are shaded in light blue. For the pentagon, the fifth cone is located on the back triangle and is not shaded to avoid clutter.

For the cosmohedron (right of Figure 5.7), we add the midpoints on all edges and barycenters, connecting them with edges as shown. We have highlighted the collection of cones that form the decagon (dark blue), hexagon (dark pink), pentagon (light pink), and square (light blue and green) facets of the cosmohedron. Only eight of the ten cones of the decagon are visible in the picture; the remaining two are on the back triangle of the fan and are not shaded to avoid clutter.

In summary, we can obtain the cosmohedron fan by starting with the associahedron fan as follows: look at a cone of the associahedron fan, which is defined by a collection of  $g$ -vectors  $g_C$ , each associated to a chord  $C$  entering the triangulation  $T$  dual to the cone, take

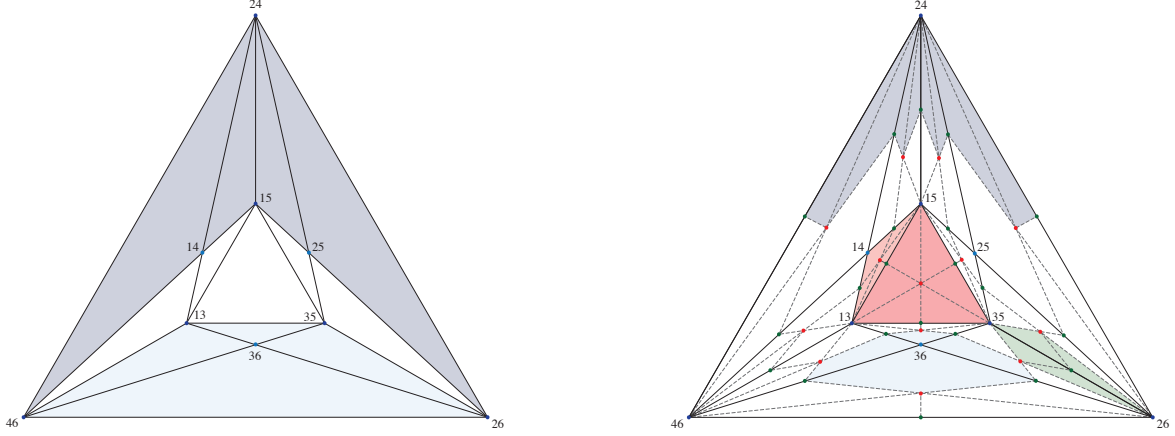


Figure 5.7: (Left) Fan of the 6-point associahedron. (Right) Fan of the 6-point cosmohe-dron that can be obtained by “cosmologizing” the associahedron one.

all possible subsets  $\mathcal{S} = (C_1, C_2, \dots, C_k)$  with all  $C_i \in T$ , of any length  $k = 1, 2, \dots, n-3$ , and to each such subset add a ray:

$$g_{\mathcal{S}} = \sum_{C \in \mathcal{S}} g_C. \quad (5.7)$$

This defines all the rays of the cosmohe-dron fan, and therefore the facets of the cosmohe-dron. Collections of these rays give us cones that specify the vertices of the cosmohe-dron. But these cones are not always simplices – cosmohe-dra are not simple polytopes.

In the context of  $\text{Cosmo}_n$ , each facet corresponds to a partial triangulation defined by a set of non-intersecting chords  $C$ . For each such set  $C$ , we establish an inequality:

$$\sum_{c \in C} X_c \geq \epsilon_C, \quad (5.8)$$

where  $\epsilon_C \ll c_{i,j}$  for any pair  $(i, j)$ . Here,  $c_{i,j}$  denotes the non-planar Mandelstam variables that dictate the positioning of various facets in the associahedron’s embedding, as detailed in Appendix A. This constraint ensures that the new inequalities only trim the faces of the associahedron.

The parameters  $\epsilon_C$  must satisfy specific relations and hierarchies to correctly embed the cosmohe-dron. These relate  $\epsilon$  values for sets  $C$  and  $C'$  to those of their union  $(C \cup C')$  and intersection  $(C \cap C')$ . Specifically, we require the following inequalities:

$$\epsilon_C + \epsilon_{C'} < \epsilon_{C \cup C'} + \epsilon_{C \cap C'}, \quad (5.9)$$

when  $C \cap C'$  is either empty or entirely to the left or right of  $C$  and  $C'$ . Otherwise, we enforce equalities:

$$\epsilon_C + \epsilon_{C'} = \epsilon_{C \cup C'} + \epsilon_{C \cap C'}. \quad (5.10)$$

The equalities in (5.10) imply the existence of non-simple vertices. Since the facets containing a given vertex involve at most  $(n - 3)$  variables  $X_{i,j}$  in their respective facet inequalities (5.8), any non-simple vertex arises when more than  $(n - 3)$  facet inequalities are saturated. This imposes an equality of the type in equation (5.10).

We can simplify conditions (5.10) and (5.9) further. The equalities are satisfied if we express  $\epsilon_C$  as a sum over variables  $\delta_P$  associated with each sub-polygon of the partial triangulation given by  $C$ . That is, we define:

$$\epsilon_C = \sum_{P \text{ of } C} \delta_P. \quad (5.11)$$

In turn, the inequalities for  $\epsilon_C$  are ensured by similar inequalities for  $\delta_P$ :

$$\delta_P + \delta_{P'} < \delta_{P \cap P'} + \delta_{P \cup P'}. \quad (5.12)$$

Additionally, we must ensure that the  $\delta$  for the full polygon,  $\delta_{(12\dots n)}$ , is set to zero. It is straightforward to parameterize  $\delta_P$ 's that satisfy these constraints. For example, any convex function of the number of edges ( $\#P$ ) of  $P$  that vanishes when  $\#P = n$  will satisfy these inequalities. A simple choice is:

$$\delta_P = \delta(n - \#P)^2. \quad (5.13)$$

Here,  $\delta$  is a uniform small factor that can be made as small as necessary to ensure that  $\delta_P$ , and hence  $\epsilon_C$ , are all much smaller than the  $c_{i,j}$  defining the underlying associahedron.

This framework defines the embedding of the cosmohedron, inherently including an embedding for the graph associahedra introduced in Section 5.1.1 to encode the combinatorics of Russian dolls graph by graph. To explicitly determine the embedding, we simply need to consider a facet corresponding to the full triangulation that is dual to the graph of interest.

**Embedding for the graph associahedron** The graph associahedra are particular facets of cosmohedra, corresponding to complete triangulations  $T$  of the  $n$ -gon. For a given  $T$ , we can associate a dual graph  $G$  in the usual way. This facet of the cosmohedron is associated with the inequality  $\sum X_I \geq \sum \delta_{T_i}$ , where  $X_I$  are all the chords in the triangulation and  $\delta_{T_i}$  are associated with each triangle of the triangulation (as given in (5.8) and (5.11)). By going on this facet, we are saturating this to the equality

$$\sum_I X_I = \sum_i \delta_{T_i}. \quad (5.14)$$

In terms of the dual graph  $G$ , we can think of  $\delta_{T_i}$  as associated with a small circle surrounding the  $i$ -th vertex of  $G$ .

Obviously, the other facets of the cosmohedron that meet the one associated with  $T$  must correspond to partial triangulations that are coarsenings of  $T$ . These will become facets of the graph associahedron for  $T$ , so the inequalities cutting out the graph associahedron are all of the form  $\sum_J X_J \geq \sum \delta_p$ , with  $J$  depending on the partial triangulation

we're considering. We can denote these inequalities easily in the language of the tubes. The partial triangulation gives a collection of non-overlapping sub-polygons  $p$ , which can be denoted on  $G$  by a collection of non-overlapping tubes we will also label by  $p$ .

Then,  $\sum_J X_J$  is the sum over all the edges of  $G$  that are cut by the tubes. Clearly, the smallest tubes, which encircle a single vertex, corresponding to triangle sub-polygons, are special. We can label our partial triangulation by specifying a collection of larger (not triangle) tubes,  $P$ , and having done this, understanding that the vertices not encircled by tubes, are encircled with small ones. The inequalities are then

$$\sum_{e \text{ not in } P} X_e \geq \sum \delta_P + \sum \delta_t, \quad (5.15)$$

where the sum is over the edges  $e$  that are not contained in the interior of any big tube in  $P$ , and  $t$  are the tubes encircling the single vertices not encircled by the set of big tubes  $P$ .

But it is now trivial to see that the inequalities associated with more than one of these larger tube are all redundant, following from those for single tubes. Consider the simple example of the triangulation  $\{(1, 3), (1, 4), (1, 5)\}$  for  $n = 6$ . We are working on the support of

$$X_{1,3} + X_{1,4} + X_{1,5} = \delta_{1,2,3} + \delta_{1,3,4} + \delta_{1,4,5}. \quad (5.16)$$

The partial triangulations  $\{(1, 3), (1, 4)\}$  is associated with a single tube – corresponding to square  $(1, 4, 5, 6)$ –, as is that for  $(14, 15)$ , and the inequalities are

$$X_{1,3} + X_{1,4} \geq \delta_{1,2,3} + \delta_{1,3,4} + \delta_{1,4,5,6}, \quad X_{1,4} + X_{1,5} \geq \delta_{1,2,3,4} + \delta_{1,4,5} + \delta_{1,5,6}. \quad (5.17)$$

But adding these inequalities and using (5.16) we have that

$$\begin{aligned} X_{1,3} + X_{1,4} + X_{1,4} + X_{1,5} &\geq \delta_{1,2,3} + \delta_{1,3,4} + \delta_{1,4,5,6} + \delta_{1,2,3,4} + \delta_{1,4,5} + \delta_{1,5,6} \\ \Rightarrow X_{1,4} &\geq \delta_{1,2,3,4} + \delta_{1,4,5,6}, \end{aligned} \quad (5.18)$$

which is the two-tube inequality associated with the partial triangulation  $\{(1, 4)\}$ . This obviously extends to any number of tubes: on the support of  $\sum_J X_J = \sum_i \delta_{T_i}$ , the sum of the inequalities for single tubes implies the inequality for multi-tubes, and so these are redundant.

We can naturally define the variables for the graph without referring to the underlying triangulation. Thus, we associate variables  $X_e$  with the edges of  $G$ , and constants  $\delta_P$  with single tubes  $P$ . The graph associahedron is then cut out by the inequalities:

$$\sum_{e \text{ not in } P} X_e \geq \delta_P + \sum_{v \text{ not in } P} \delta_v, \quad (5.19)$$

where  $\delta_v$  is associated to the small encircling of vertex  $v$ . The  $\delta_P$  satisfy our ubiquitous inequalities

$$\delta_P + \delta_{P'} < \delta_{P \cup P'} + \delta_{P \cap P'} \quad (5.20)$$

where, as for the full cosmohedron,  $\delta_{\text{all}} = 0$ .

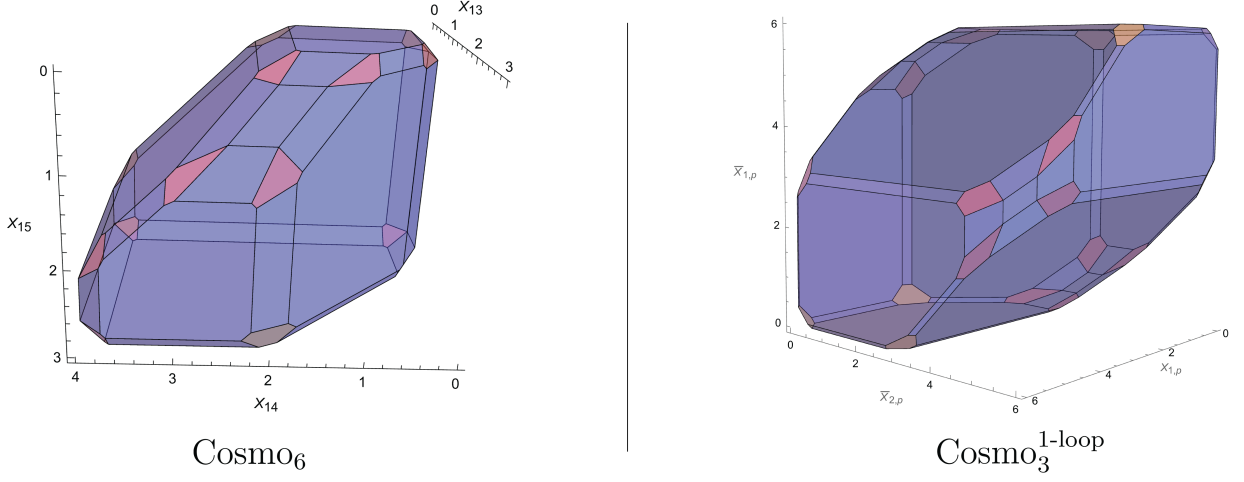


Figure 5.8: Realizations of cosmohedra. (Left) Embedding of  $\text{Cosmo}_6$  with pentagonal facets highlighted in pink and hexagonal ones highlighted in yellow. (Right) Embedding of the  $\text{Cosmo}_3^{1\text{-loop}}$ . The purple facets correspond to partial triangulations, and the pink and yellow facets correspond to full triangulations.

It is amusing that the graph associahedron for linear chains are simply associahedra; in this case, all the myriad properties of  $\text{Tr}(\phi^3)$  amplitudes following from the connection with the associahedron are inherited by the wavefunction for these single graphs. Indeed, the Minkowski sum decomposition and corresponding stringy integrals exist for all graph associahedra, so cousins of full *stringy*  $\text{Tr}(\phi^3)$  amplitudes exist, associated with single graphs for the wavefunction! This gives an interesting entry-point into possible stringy formulations for cosmological wavefunctions we leave to future work.

We will now illustrate the set of equalities and inequalities for the case of  $\text{Cosmo}_6$ .

**6-point Cosmohedron** –For the 6-point cosmohedron, we have 44 different  $\epsilon_C$ , and we can form 105 sets  $\{\epsilon_C, \epsilon_{C'}, \epsilon_{C \cup C'}, \epsilon_{C \cap C'}\}$ . From these, 12 will be equalities<sup>1</sup>, for example:

$$\epsilon_{\{(1,3),(1,4)\}} + \epsilon_{\{(1,4),(1,5)\}} = \epsilon_{\{(1,4)\}} + \epsilon_{\{(1,3),(1,4),(1,5)\}}. \quad (5.21)$$

Note that in this case we have  $C = \{(1,3), (1,4)\}$ ,  $C' = \{(1,4), (1,5)\}$ , and  $C \cap C' = \{(1,4)\}$ . So we have that  $(1,4)$  divides the hexagon into two smaller squares and  $C$  fills one of the squares (the one to the left of  $C \cap C'$ ) while  $C'$  fills the other (the one to the right of  $C \cap C'$ ). Therefore, we have that  $C$  is to the left of  $C \cap C'$  and  $C'$  is to the right of  $C \cap C'$ , and therefore we must have an equality.

<sup>1</sup>There is one for each triangulation whose graph associahedron is a pentagon, as in all such cases we have a non-simple vertex.

This equality follows from saturating the four facet inequalities:

$$\begin{aligned} X_{(1,4)} &\geq \epsilon_{\{(1,4)\}}, & X_{(1,3)} + X_{(1,4)} + X_{(1,5)} &\geq \epsilon_{\{(1,3),(1,4),(1,5)\}}, \\ X_{(1,3)} + X_{(1,4)} &\geq \epsilon_{\{(1,3),(1,4)\}}, & X_{(1,4)} + X_{(1,5)} &\geq \epsilon_{\{(1,4),(1,5)\}}, \end{aligned} \quad (5.22)$$

thus ensuring the existence of the vertex touched by the four facets (which is precisely the one highlighted in figure 5.6). From figure 5.3, it is clear there are 12 such vertices in total, which in the embedding come from the 12 equalities. The remaining 93 sets will form inequalities, for example:

$$\begin{aligned} \epsilon_{\{(1,3)\}} + \epsilon_{\{(1,4)\}} &< \epsilon_{\{(1,3),(1,4)\}}, \\ \epsilon_{\{(1,3),(1,4)\}} + \epsilon_{\{(1,3),(1,5)\}} &< \epsilon_{\{(1,3)\}} + \epsilon_{\{(1,3),(1,4),(1,5)\}}. \end{aligned} \quad (5.23)$$

In the first case, we have that  $C \cap C' = \emptyset$ , and therefore we have an inequality. In the second case, we have that both  $C$  and  $C'$  are to the right of  $C \cup C'$  and so we also have an inequality.

Finding  $\epsilon_C$  which satisfy all 105 relations will ensure that the facet inequalities (5.8) define the cosmohedron for the 6-point wavefunction. Finding such a solution is simpler if we impose the map (5.11). For example,

$$\begin{aligned} \epsilon_{\{(1,3),(1,4)\}} &= \delta_{(1,2,3)} + \delta_{(1,3,4)} + \delta_{(1,4,5,6)}, & \epsilon_{\{(1,4),(1,5)\}} &= \delta_{(1,2,3,4)} + \delta_{(1,4,5)} + \delta_{(1,5,6)}, \\ \epsilon_{\{(1,4)\}} &= \delta_{(1,2,3,4)} + \delta_{(1,4,5,6)}, & \epsilon_{\{(1,3),(1,4),(1,5)\}} &= \delta_{(1,2,3)} + \delta_{(1,3,4)} + \delta_{(1,4,5)} + \delta_{(1,5,6)}, \end{aligned} \quad (5.24)$$

which immediately satisfies (5.21), as all  $\delta_P$  in the first line match the ones in the second line. This mapping will take (5.23) to,

$$\begin{aligned} \delta_{(1,3,4,5,6)} + \delta_{(1,2,3,4)} &< \delta_{(1,3,4)} + \delta_{(1,2,3,4,5,6)}, \\ \delta_{(1,4,5,6)} + \delta_{(1,4,5,6)} &< \delta_{(1,3,4,5,6)} + \delta_{(1,4,5)}, \end{aligned}$$

which are precisely of the form (5.12). This mapping imposed on all 105 relations will satisfy all 12 equalities and will make several of the 93 inequalities linearly dependent on each other. Thus, we will have only 57 inequalities of the form (5.12), which will be satisfied if we parametrize the  $\delta_P$  with the convex function (5.13),

$$\delta_P = \delta(6 - \#P)^2.$$

Therefore, imposing the mapping (5.11) in the facet inequalities (5.8), with the parametrization (5.13), defines the 6-point cosmohedron. A picture of the embedded object is presented on the right of figure 5.8.

**Higher-point cosmohedra** Beyond 6-points, the cosmohedron will be 4-dimensional, or higher. Nevertheless, the construction of these polytopes follows exactly the same procedure, and below we list the different  $\mathcal{F}$ -vectors (*i.e.* the numbers of the different codimension faces) of the cosmohedra up to 9-points:

	codim-1	codim-2	codim-3	codim-4	codim-5	codim-6
4-points	2	—	—	—	—	—
5-points	10	10	—	—	—	—
6-points	44	114	72	—	—	—
7-points	196	952	1400	644	—	—
8-points	902	7116	18040	18528	6704	—
9-points	4278	50550	194616	332664	262728	78408

Table 5.1: The  $\mathcal{F}$ -vector of Cosmohedra up to 9-points.

	codim-1	codim-2	codim-3	codim-4	codim-5	codim-6
4-points	2	—	—	—	—	—
5-points	5	5	—	—	—	—
6-points	9	21	14	—	—	—
7-points	14	56	84	42	—	—
8-points	20	120	300	330	132	—
9-points	27	225	825	1485	1287	429

Table 5.2: The  $\mathcal{F}$ -vector of Associahedra up to 9-points.

where codim stands for the codimension of the faces.

As a comparison, we can list the  $\mathcal{F}$ -vector for the associahedron of the respective amplitudes:

As a quick check, one can add all the entries of the  $\mathcal{F}$ -vector for one of the  $n$ -points associahedron above, and confirm that will match the number of codimension-1 faces (*i.e.* facets) in the corresponding cosmohedron. We know this is the case because the cosmohedron is obtained by “shaving” each face of the associahedron, and the facets of the cosmohedron are associated to partial/full triangulations (which is precisely the information encoded by the different codim faces of the associahedron).

**Relation to cosmological polytopes** Now that we understand the embedding for single graphs, the graph associahedron, it is important to establish the connection with what has been previously been known for single graph geometries, the cosmological polytope. For the graph associahedra, we work with independent variables  $p$  associated to every tube. But to compare with the standard wavefunction and with cosmological polytopes, we work with the energy variables,  $x$  and  $y$ . Where the  $x_v$  variables stand for the sum of the energies entering each vertex, and  $y_e$  for the energy of each internal edge of  $G$ . Of course, the  $x, y$  variables determine the  $p$  associated with every tube, via

$$\mathcal{P}_p = \sum_{v \text{ in } p} x_v + \sum_{e \text{ entering } p} y_e, \quad (5.25)$$

the sum over the energies of the vertices contained inside  $p$  together with the external edges entering  $p$  – the familiar energy pole associated with the tube  $p$ . Note that this enforces certain equalities between the  $\mathcal{P}_p$ 's:

$$\mathcal{P}_p + \mathcal{P}_{p'} = \mathcal{P}_{p \cup p'} + \mathcal{P}_{p \cap p'}. \quad (5.26)$$

In fact, it is easy to see that we can work backwards – imposing these natural equalities on the perimeters  $\mathcal{P}_p$  implies that they can be expressed in terms of  $x_v, y_e$  variables associated with the graph.

Let us now discuss the cosmological polytope for a graph with  $V$  vertices and  $E$  edges. It is usually described as a projective polytope in  $E + V - 1$  dimensions; of course this is equivalently thought of as a cone over this polytope in  $E + V$  dimensions. This cone is cut out by the simple inequalities, for every tube  $p$

$$\mathcal{P}_p \geq 0, \quad \text{or} \quad \sum_{v \text{ in } p} x_v + \sum_{e \text{ entering } p} y_e \geq 0. \quad (5.27)$$

Now, in the story of the graph associahedron, we are factoring out the total-energy singularity, as well as those associated with the small tubes encircling each vertex. Thus, it is natural to expect that the relationship with the graph associahedron and the cosmological polytope is revealed when we slice the cosmological polytope on the plane

$$\sum_v x_v = E_t, \quad x_v + \sum_{e \text{ connected to } v} y_e = t_v, \quad (5.28)$$

where we hold  $E_t, t_v > 0$  as constants.

Indeed, as we now see, this slice of the cosmological polytope is very closely related to the graph associahedron. For instance, for the simplest cases of the 2-dimensional graph associahedra, corresponding to the 4-site chain and star graphs (shown in figure 5.1, right), this slice of the cosmological polytope gives us precisely the familiar pentagon and hexagon. But more generally, it is obvious that this sliced cosmological polytope cannot be precisely the same as the graph associahedron – the graph associahedron knows about the general perimeters, not about the specialization associated with working with  $x$ 's and  $y$ 's.

To actually match the two objects, we have to realise that the sliced cosmological polytope is obtained by a *degeneration* of the graph associahedron, when the  $\delta_P$  occurring in the inequalities cutting out the graph associahedron saturate most of the inequalities they satisfy. Indeed, we have that

$$\begin{cases} \delta_P + \delta_{P'} < \delta_{P \cup P'} + \delta_{P \cap P'}, & \text{if } P \cap P' \text{ is a single vertex or } P \cup P' \text{ is everything,} \\ \delta_P + \delta_{P'} = \delta_{P \cup P'} + \delta_{P \cap P'}, & \text{otherwise.} \end{cases} \quad (5.29)$$

Imposing these equalities has the effect of shrinking some of the faces of the graph associahedra – the graph associahedra are all simple polytopes, but the sliced cosmological polytopes are not. For instance, for the case of the 5 site chain where the graph associahedron is the usual three-dimensional associahedron (see figure 5.2, right), while the sliced



cosmological polytope still has 9 faces, but only has 12 vertices and 19 edges instead of the usual 14 vertices and 21 edges; two of the edges of the usual associahedron are then contracted to a point in the sliced cosmological polytope.

It is straightforward to establish the connection between the sliced cosmological polytope and this degeneration of the graph associahedron. We simply take the graph, and solve for the  $x_v$  variables by setting all the perimeters associated with the small tubes encircling the vertices to  $t_v$ . We are left only with  $y_e$  variables. These satisfy a single equality (from the  $E_t$  equation in (5.28)), and the rest of the inequalities coming from (5.27). Then the inequality for any large tube  $P$  becomes

$$\sum_{e \text{ not in } P} (2y_e) \geq \sum_{v \text{ not in } P} t_v - E_t. \quad (5.30)$$

If we identify  $2y_e \equiv X_e$ , these are just the inequalities for cutting out the graph associahedron (5.19), but with a special choice for the RHS of the inequality. Comparing with the RHS of the  $P$  inequality for the graph associahedron  $\delta_P + \sum_{v \text{ not in } P} \delta_v$  we have that

$$\delta_P = \sum_{v \text{ not in } P} (t_v - \delta_v) - E_t. \quad (5.31)$$

Further matching  $\sum_e 2y_e = \sum_v t_v - E_t$  (from (5.28)) with  $\sum_e X_e = \sum_v \delta_v$  (from the facet defined by the graph associahedron in the cosmohedron (5.14)) lets us identify

$$\sum_v (t_v - \delta_v) = E_t. \quad (5.32)$$

It is then very easy to see that the choice for  $\delta_P$  in (5.31) satisfies the inequalities and equalities given for the degenerated graph associahedron we defined above (5.29).

## 5.3 Computing the Wavefunction from the Cosmohedron

In this section we discuss how the cosmohedron can help us compute the cosmological wavefunction. Firstly, we discuss how the combinatorial structure of the cosmohedron makes evident a recursive formulation for the wavefunction, shown in (2.45). As well as the russian doll picture. Then we will discuss how can we obtain the wavefunction from the canonical form of the polytope.

### 5.3.1 The geometry of recursive factorization

In section 2.5, we explained how there are two equivalent representations of the wavefunction – one as a sum over diagrams and their respective russian dolls (2.46), the other via the recursive representation in terms of cuts given in (2.45).

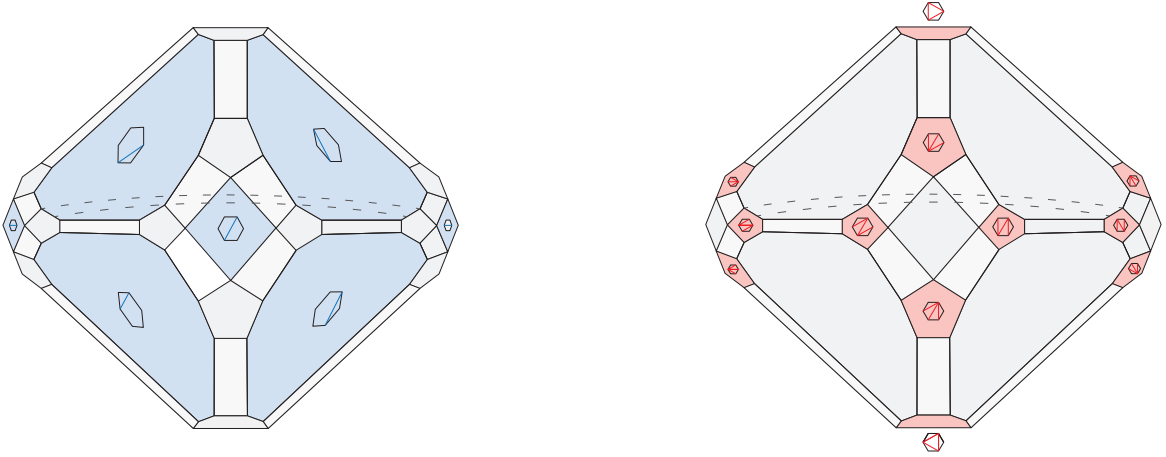


Figure 5.9: (Left) Set of facets corresponding to partial triangulations with a single chord that by themselves contain *all* vertices of the cosmohedron. (Right) Set of facets corresponding to full triangulations that also touch *all* vertices.

We would now like to point out how the geometry of the cosmohedron makes both representations of the wavefunction completely obvious. Let's do this by looking at the three-dimensional cosmohedron (see figure 5.9). Recall that every term in the russian doll expansion of the wavefunction is associated with a vertex of the cosmohedron.

Now, the point is that there are a number of natural ways of attaching any vertex of the cosmohedron uniquely to some facet of the cosmohedron. We can consider the “maximal” facets of the cosmohedron that correspond to complete triangulations  $T$ , and associate a vertex corresponding to a given russian doll with its corresponding triangulation. In this way, the collection of all vertices can be organized into first collecting all the facets associated with triangulations  $T$ , and then looking at the vertices of each facet, as given in (2.46). This is obviously the first representation or what we called the russian doll picture. But there is another interesting way of associating vertices with facets: every vertex can also be naturally attached to one of the “minimal” facets of the cosmohedron corresponding to a single chord. The corresponding facet is just the product of cosmohedra for the left and right factors on the cut. Hence, we can run through all the vertices by summing over all these facets, and then take the vertices on them. This way of collecting the vertices gives us the recursive computation of the wavefunction in terms of the sum over cuts, as in (2.45). The russian doll and cut-recursive picture of the polytope are shown in figure 5.9. Of course, we can uniquely associate vertices to facets in other ways interpolating between the two extremes we have discussed, corresponding to different ways of running the recursive sum over cuts, but deciding to represent some of the lower wavefunction factors directly as a sum over russian dolls.

### 5.3.2 Wavefunction from Geometry

As we have highlighted earlier, and seen in the  $n = 6$  example, cosmohedra are *not* simple polytopes. This is to be contrasted with the associahedron which indeed is a simple polytope (as we can see from its fan construction as well as in figure 5.3 for the  $n = 6$  case).

As we will explain now, this feature turns out to be extremely crucial to have an object that reproduces the combinatorial feature of russian dolls (as described in (5.5)), and therefore that encodes the information of the wavefunction.

Let's say instead we “blow-up” all the non-simple vertices to obtain a simple polytope. For simplicity let's look at the case of  $n = 6$ , which is the first case this happens, and look at the non-simple vertex associated with cone  $\{g_{1,4}, g_{1,3} + g_{1,4}, g_{1,4} + g_{1,5}, g_{1,3} + g_{1,4} + g_{1,5}\}$  highlighted in figure 5.6. In these vertices, the four faces meet –  $\{(1, 4)\}$ ,  $\{(1, 3), (1, 4)\}$ ,  $\{(1, 4), (1, 5)\}$  and  $\{(1, 3), (1, 4), (1, 5)\}$  – and the union of their respective subpolygons forms the russian doll containing triangles  $\{(1, 2, 3), (1, 3, 4), (1, 4, 5), (1, 5, 6)\}$  and the two squares  $\{(1, 2, 3, 4), (1, 4, 5, 6)\}$ . Now there are two ways in which we can blow up this vertex, one way is by adding an edge connecting rays  $g_{1,4}$  and  $g_{1,3} + g_{1,4} + g_{1,5}$  – the object we obtain in this case corresponds to the full barycentric subdivision of the associahedron, which we will later on denote by *Permuto-cosmohedron*; another way is by adding an edge connecting rays  $g_{1,3} + g_{1,4}$  and  $g_{1,4} + g_{1,5}$ . At the level of the polytope, the first type of blow up would lead to the object on the top right of figure 5.6 while the second one leads to the one on the bottom right of figure 5.6.

However, note that in both cases, the object we obtain after the “blow-up” does *not* encode the combinatorics of russian dolls correctly. This is because if we look at the new edge (represented in red in figure 5.6), it is labelled by the union of the subpolygons of the facets that meet along it, which in both cases means that it is already labelled by the full russian doll associated with the original non-simple vertex.

This is an important difference between the cosmohedron and the associahedron. We will now proceed to discuss the realization of the geometry that precisely reproduces the combinatorics of the cosmohedron. As we will see, this embedding starts from the kinematic embedding of the associahedron as in [93] and adds some extra inequalities that precisely shave off this polytope exactly in the way that produces the correct polytope with non-simple vertices.

In the previous section, we described the set of inequalities that carve out the cosmohedron, together with the set of constraints on  $\epsilon_C$  required to produce the correct polytope. As we saw, in addition to the inequalities (5.9), we also had equalities, which ultimately imply that the polytope we have is not *simple*. We now want to explain a systematic way to blow up the polytope into another polytope which is simple – the permuto-cosmohedron<sup>2</sup> – which will be the object from which we can ultimately extract the wavefunction (as we explain in the next section).

Let's go back to the fan definition of the polytope. As explained previously, we can go

---

<sup>2</sup>This object already appeared earlier when we explained the “blow-up” of the non-simple vertex for the  $n = 6$  case.

from the associahedron fan to the cosmohedron fan by adding rays corresponding to all possible subsets of chords entering on a given triangulation – corresponding therefore to all possible partial triangulations. However, not all rays are connected to each other, which is why the cosmohedron is not simple.

We have already explored in detail the non-simple vertex at 6-points where facets  $\{(1, 4)\}$ ,  $\{(1, 3), (1, 4)\}$ ,  $\{(1, 4), (1, 5)\}$ ,  $\{(1, 3), (1, 4), (1, 5)\}$  meet in section 5.2. In particular, we explained how the two different “blow-up” led to objects that did not consistently describe the combinatorics of russian dolls.

However, let’s now go back to the blow up in which we produce an edge between facets  $\{(1, 4)\}$  and  $\{(1, 3), (1, 4), (1, 5)\}$  – this corresponds to the full *barycentric subdivision* of the associahedron fan into a permutohedron fan, leading to what we called the *permuto-cosmohedron*. For this new object, we can think of each vertex as labeling the ways in which we can get a full triangulation by listing chords in a particular order. In particular, for two vertices produced in the blow up, these correspond to cases in which we start with  $(1, 4)$  and then we have two possible ways to continue to the full triangulation:

$$\begin{aligned} \{(1, 4)\} &\rightarrow \{(1, 4), (1, 3)\} \rightarrow \{(1, 4), (1, 3), (1, 5)\}, \\ \{(1, 4)\} &\rightarrow \{(1, 4), (1, 5)\} \rightarrow \{(1, 4), (1, 3), (1, 5)\}, \end{aligned} \tag{5.33}$$

each of which corresponds to one of the vertices we obtain after *simplifying* the non-simple vertex of the original cosmohedron.

The permuto-cosmohedron is then a simple polytope whose vertices label all the possible orderings of building full triangulations out of partial triangulations. For general  $n$ , the fan definition of the permuto-cosmohedron is simply given by the full barycentric subdivision of the respective  $\text{Assoc}_n$  fan. This object has manifestly more vertices than the cosmohedron and therefore is not precisely tailored to the wavefunction. Nonetheless, as we will see momentarily, this permutuhedral blow-up will provide us a natural way of extracting the full wavefunction from the geometry.

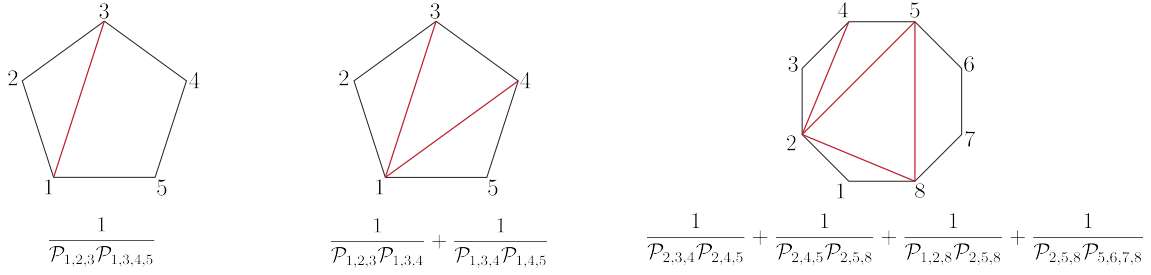
Before proceeding to the extraction of the wavefunction let’s discuss the embedding of the permuto-cosmohedron. For the cosmohedron we saw that for each facet associated with a given collection of chords,  $C$ , we have an inequality of the form of (5.8), where the  $\epsilon_C$ ’s satisfy both equalities (5.10) and inequalities (5.9). To produce the full permuto-cosmohedron all we need to do is turn the *equalities* (5.10) into inequalities, with the same sign, *i.e.* we have that for *any* collection of chords  $C$  and  $C'$ :

$$\epsilon_C + \epsilon_{C'} < \epsilon_{C \cup C'} + \epsilon_{C \cap C'}, \tag{5.34}$$

this then turns all the non-simple vertices into simple ones and gives us precisely the blow-up corresponding to the permuto-cosmohedron.

Let’s now discuss how to extract the wavefunction from the geometry. We will start by defining the canonical form of the graph associahedron for a single graph, and then proceed to the generalization that gives us the full wavefunction from the cosmohedron.

The connection between the wavefunction and geometry for single graphs is by now the familiar one. For a single diagram/ $n$ –pt triangulation, with  $(n - 3)$  chords, we have

Figure 5.10: Examples of  $1/X_C$  for different faces of  $n = 5$  and  $n = 8$  cosmohedron.

a  $(n - 4)$ -dimensional graph associahedron. The graph associahedron is simple, hence one computation of the canonical form of the graph associahedron is given by summing over all vertices – corresponding to complete tubings/russian dolls – and multiplying by  $1/\mathcal{P}$ 's for all the tubes corresponding to the facets meeting at the vertex. This gives us a term with  $(n - 4)$  poles. Of course, *every* tubing associated with the diagram has the  $E_{\text{total}}$  tube surrounding the entire graph, as well as the small circles encircling every vertex – corresponding to the triangles entering the triangulation dual to the graph. Hence, we have

$$\Psi_G = \frac{1}{\mathcal{P}_{\text{tot}}} \times \prod_{v \in G} \frac{1}{\mathcal{P}_v} \times \Omega(\mathcal{A}_G), \quad (5.35)$$

where  $\mathcal{P}_{\text{tot}}$  is the perimeter of the full  $n$ -gon corresponding to  $E_t$ , and  $\mathcal{P}_v$  the perimeter of each triangle entering the underlying triangulation.

The extraction of the wavefunction for the sum over all diagrams is much more interesting. Let's consider the simple polytope we get by blowing-up the cosmohedron as described in the previous section – the permuto-cosmohedron. Each facet of this polytope is associated a partial triangulation given by a collection of non-overlapping chords  $C$ . Let  $n_C$  be the number of non-triangle subpolygons entering in the partial triangulation defined by  $C$ , then we define

$$\frac{1}{X_C} \equiv \frac{1}{n_C} \sum_{P, P' \text{ meeting on edge}} \frac{1}{\mathcal{P}_P \mathcal{P}_{P'}}, \quad (5.36)$$

where we consider the products of the perimeters of the subpolygons entering in  $C$  that share an edge, and sum over them (see figure 5.10). So this means that to each facet, instead of associating a single singularity (like we do to extract the amplitude from the associahedron), we associate *pairs of singularities*. It is clear that we could not associate a single singularity to each facet simply because the dimensionality of the  $\text{Cosmo}_n$  does not match the number of singularities on  $\Psi_n$ . This new feature reflects that even the way we extract the wavefunction from the canonical form of cosmohedra requires a generalization from what is done in the amplitudes case.

We now look at the canonical form for the permutohedron, associating  $X_C$  (5.36)). Since the permuto-cosmohedron is simple, the canonical form is the sum over all vertices

weighted by the product of all  $\frac{1}{X_C}$ 's for the facets that meet on the vertex. While this manifestly has only simple poles in terms of  $\frac{1}{X_C}$ , it will clearly have terms with simple poles as well as double and higher poles when written in terms of the  $\frac{1}{\mathcal{P}_P}$ . But the claim is that the wavefunction is given by the part of the canonical form with only simple poles:

$$\Psi = \frac{1}{E_t} \times \Omega(X_C)|_{\text{single poles in } \mathcal{P}_P}. \quad (5.37)$$

**5-point example** – At five points the cosmohedron is simple, therefore it coincides with the permuto-cosmohedron. Then, we can directly compute the poles of each facet,  $X_C$ , according to (5.36). Let's consider the facet labelled by the cords  $\{(1,3), (1,4)\}$ , the singularity pairs we associate to it are (see figure 5.10):

$$\frac{1}{X_{\{(1,3), (1,4)\}}} = \frac{1}{\mathcal{P}_{123} \mathcal{P}_{134}} + \frac{1}{\mathcal{P}_{134} \mathcal{P}_{145}}.$$

Similarly, we can compute the singularity pairs of the facets that meet facet  $\{(1,3), (1,4)\}$  – those are  $\{(1,3)\}$ , and  $\{(1,4)\}$  – for which we have:

$$\frac{1}{X_{\{(1,3)\}}} = \frac{1}{\mathcal{P}_{123} \mathcal{P}_{1345}}, \quad \frac{1}{X_{\{(1,4)\}}} = \frac{1}{\mathcal{P}_{1234} \mathcal{P}_{145}}.$$

We can now compute the contributions of each of these two vertices to the wavefunction:

$$\begin{aligned} \frac{1}{X_{\{(1,3), (1,4)\}} X_{\{(1,3)\}}} &= \frac{1}{\mathcal{P}_{123}^2 \mathcal{P}_{134} \mathcal{P}_{1345}} + \frac{1}{\mathcal{P}_{123} \mathcal{P}_{134} \mathcal{P}_{145} \mathcal{P}_{1345}}, \\ \frac{1}{X_{\{(1,3), (1,4)\}} X_{\{(1,4)\}}} &= \frac{1}{\mathcal{P}_{123} \mathcal{P}_{134} \mathcal{P}_{145} \mathcal{P}_{1234}} + \frac{1}{\mathcal{P}_{134} \mathcal{P}_{145}^2 \mathcal{P}_{1234}}. \end{aligned}$$

According to (5.37), in the first line above, we send the first term to zero, and in the second line we send the second term to zero. So we are left with precisely the russian dolls contributing to each vertex (see figure 5.4). When we sum these two terms, they add up to the wavefunction of the graph corresponding to the triangulation  $\{(1,3), (1,4)\}$ . By computing the contributions from the remaining vertices of the decagon, we obtain the full wavefunction at 5-points.

**6-point example** – Let us now see how the prescription in (5.37) gives us the correct contribution in the blown up vertices at 6-points. Let us use our running example of the vertices in (5.33) as an example (see top right of figure 5.6). For the first line in (5.33), which corresponds to one vertex of the permuto-cosmohedron, the pairs of singularities are:

$$\begin{aligned} \frac{1}{X_{\{(1,4)\}} X_{\{(1,3), (1,4)\}} X_{\{(1,3), (1,4), (1,5)\}}} &= \left( \frac{1}{2\mathcal{P}_{1234} \mathcal{P}_{1456}} \right) \left( \frac{1}{\mathcal{P}_{123} \mathcal{P}_{134}} + \frac{1}{\mathcal{P}_{134} \mathcal{P}_{1456}} \right) \times \\ &\times \left( \frac{1}{\mathcal{P}_{123} \mathcal{P}_{134}} + \frac{1}{\mathcal{P}_{134} \mathcal{P}_{145}} + \frac{1}{\mathcal{P}_{145} \mathcal{P}_{156}} \right), \end{aligned}$$

where the  $\frac{1}{2}$  in the first factor comes from the fact that the facet  $\{(1,4)\}$  has two non-triangle subpolygons, two squares, thus  $n_C = 2$  in (5.36). As for the second line in (5.33), the other vertex coming from the blow up, the contribution will be:

$$\frac{1}{X_{\{(1,4)\}} X_{\{(1,4),(1,5)\}} X_{\{(1,3),(1,4),(1,5)\}}} = \left( \frac{1}{2\mathcal{P}_{1234}\mathcal{P}_{1456}} \right) \left( \frac{1}{\mathcal{P}_{1234}\mathcal{P}_{145}} + \frac{1}{\mathcal{P}_{145}\mathcal{P}_{156}} \right) \times \\ \times \left( \frac{1}{\mathcal{P}_{123}\mathcal{P}_{134}} + \frac{1}{\mathcal{P}_{134}\mathcal{P}_{145}} + \frac{1}{\mathcal{P}_{145}\mathcal{P}_{156}} \right).$$

After sending all double poles (or higher) to zero, one can check that the added contribution of the two vertices above is:

$$2 \left( \frac{1}{2\mathcal{P}_{123}\mathcal{P}_{134}\mathcal{P}_{145}\mathcal{P}_{156}\mathcal{P}_{1234}\mathcal{P}_{1456}} \right),$$

which is precisely the russian doll term associated with the original non-simple vertex in the cosmohedron (see figure 5.6). The remaining non-simple vertices follow the same blow up into two vertices, and all other vertices are simple. Following the same prescription as in the examples above, one can compute the 6-point wavefunction from the permuto-cosmohedron.

## 5.4 Loop Cosmohedron

The generalization of the ABHY associahedron to one-loop  $\text{Tr}[\phi^3]$  integrands was shown in [101–103, 256], and the all-loop extension is given by surfacehedra [102]. It is then very natural to expect the construction of the loop cosmohedron to also be extended. The facet inequalities are essentially the same as for tree-level, with the difference that instead of chords in a polygon, we have curves on the punctured disk. Using the generalized kinematics proposed in [102], we consider all curves that are not homotopic to each other, and assign a different variable to each of these, such that a curve from  $i$  to  $j$  going through the left of the puncture,  $X_{i,j}$ , is assigned a different variable than the one going through the right,  $X_{j,i}$ . In addition, at loop-level (and in particular at one-loop), we also have the tadpole variables  $X_{i,i}$ , and loop variables ending on the puncture  $p$ ,  $X_{i,p}$ , and  $\tilde{X}_{i,p}$  (The doubling of the variables ending on the puncture,  $X_{i,p}$  and  $\tilde{X}_{i,p}$ , is important to obtain a closed polytope at one-loop as explained in [102]).

So just like at tree-level the rays of the cosmohedron fan/its facets are labeled by collections of curves,  $\mathcal{C}$ , which correspond to subsurface tilings of the punctured disk. Then, we associate to these facets the  $\epsilon$  inequalities and equalities we saw at tree-level. The map (5.11) once more guarantees that all equalities are automatically satisfied, and similarly for inequalities as long as  $\delta_{P_n} = 0$  (where  $P_n$  now stands for the punctured disk with  $n$ -points in the boundary).

From the examples presented, we can also observe how the factorization (5.6) holds at loop-level. Let us consider figure 5.11 (right), the red and yellow facets correspond to graph associahedra directly, since they are full triangulations. Then the green facets

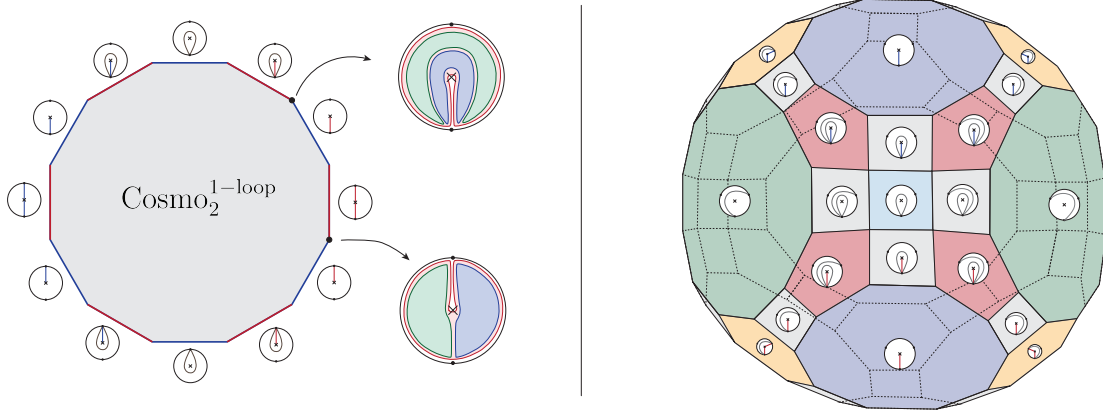


Figure 5.11: (Left) cosmohedron 2-point 1-loop, edges are labelled by partial triangulations with a single curve (where we have two types of curves ending in the puncture, marked in red and blue), and vertices correspond to full triangulations. We can read off the russian doll at each vertex by taking the union of the subsurfaces entering on each edge. (Right) cosmohedron 3-point 1-loop. Highlighted in blue and green we have facets labeled by a single curve (squares, decagons and dodecagons); in gray facets labeled by two curves (squares); and in red and yellow faces labelled by full triangulations (pentagons and hexagons) – corresponding to the graph-associahedra for the loop graphs.

are dodecagons since they correspond to the product of a 3-point tree level cosmohedron, which is a point, a two-point loop level cosmohedron, which is a dodecagon, and a graph associahedron corresponding to the two-site chain, which is a point. The dark blue facets are decagons, since they correspond to the product of a 5-point tree level cosmohedron (a decagon), and the graph associahedron of a tadpole (a point). Then, the light blue facets are squares, since they correspond to the product of a 4-point tree-level cosmohedron, which is an interval, a one-point one-loop cosmohedron, which is also an interval, and the graph associahedron of the two-site chain (which is a point).

Now, the most obvious picture for generalizing the cosmohedron to all loops therefore proceeds by generalizing the picture of “cosmologizing” the Feynman fan. This proceeds precisely in the same way as for the tree-level cosmohedron. We subdivide every cone in  $g$ -vector space into smaller cones, by considering all possible sums of the  $g$ -vectors in a given cone. This yields the fan for the loop cosmohedron, which allows us to write the facet inequalities:

$$\sum_{\text{chords } c \text{ in } C} X_c \geq \epsilon_C,$$

where  $C$  is a given partial triangulation of the punctured disk. For the loop case, the propagator variable  $X_{i,j}$  differs from  $X_{j,i}$ , since the chord can go around the loop in two different ways<sup>3</sup>. We will also have propagators attached to tadpoles,  $X_{i,i}$ . As well as the

<sup>3</sup>Even though when we assign momentum to these curves in the standard way, *i.e.* by homology, they



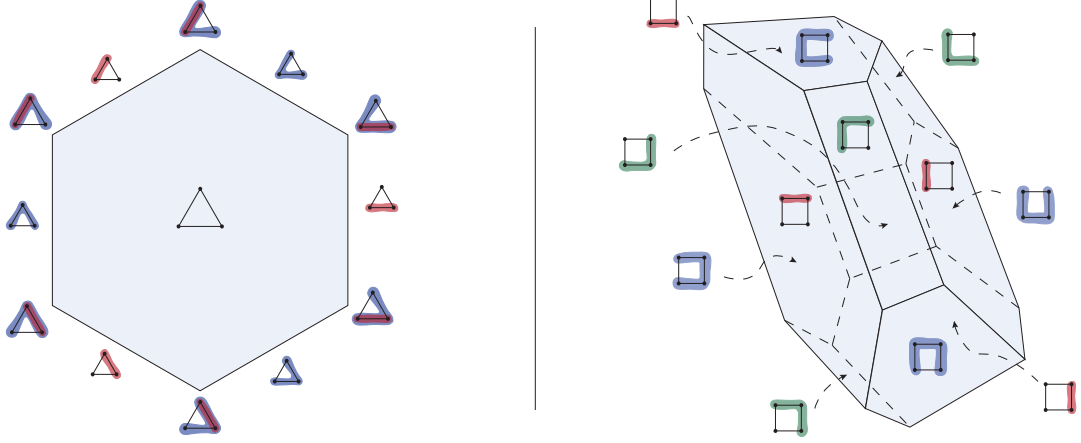


Figure 5.12: (Left) Graph associahedron for the triangle graph. (Right) Graph associahedron for the box graph.

propagators in the loop,  $X_{i,p}$  and  $\tilde{X}_{i,p}$  (where  $p$  is labelling the puncture).

The constants in the facet inequalities,  $\epsilon_C$ , obey the same equalities and inequalities as in tree level, (5.10) and (5.9), respectively. Also at loop level, the equalities are automatically satisfied if we map each  $\epsilon_C$  to the sum of the sub-surfaces in the correspondent partial triangulation,

$$\epsilon_C = \sum_{P \text{ of } C} \delta_P,$$

And the inequalities in the  $\epsilon$  are all automatically satisfied if we satisfy the inequalities:

$$\delta_P + \delta_{P'} < \delta_{P \cup P'} + \sum_{\tilde{P} \in \{P \cap P'\}} \delta_{\tilde{P}}, \quad (5.38)$$

where the sum over  $\delta_{\tilde{P}}$  is reflecting the fact that at loop level the intersection of two sub-surfaces can be given by two or more disjoint surfaces.

**Graph associahedra at loop-level** At loop level, the graph associahedron is obtained exactly the same way as for tree-level. For each triangulation, we associate a node to each subsurface, and connect the nodes between subsurfaces that share an edge, building the dual graph,  $G_T$ . Then the graph associahedron,  $\mathcal{A}_G$ , is the polytope whose facets correspond to the different tubes of the graph (not including the tubes that enclose single vertices nor the tube that encloses the full graph), and the vertices correspond to complete tubings. The factorization property, defined by eq.(5.2), holds at loop level. Let's now give some simple examples at one-loop.

---

both have the same momentum.

**Three-point triangle diagram** The graph associahedron of the triangle diagram is a hexagon (see figure 5.12, left), precisely matching the six russian dolls one can find in the graph. The triangle graph is dual to the triangulation of the punctured disk containing curves  $\{(p, 1), (p, 2), (p, 3)\}$ . The facets in figure 5.12 (left) either correspond to blue tubes or to red tubes, both are segments.

The red tube corresponds to the product of the graph associahedron of the two site chain, which is a point, with the graph associahedron of the bubble (obtained by shrinking the red tube to a node), which is a segment.

The blue tube corresponds to the product of the graph associahedron of the three-site chain, which is a segment, with the graph associahedron of the tadpole (obtained by shrinking the blue tubes to a node), which is a point.

All the terms will correspond to the product of a blue tube with a red tube, which is clear by the facet intersections in figure 5.12 (left), and respective labeling (which are the nesting of the red tube in the blue tube). One such term, after factoring out the total energy and the triangles, is:

$$\frac{1}{\mathcal{P}_{(1,2),(2,3),(3,1),(p,1)} \mathcal{P}_{(1,2),(2,3),(p,1),(p,3)}},$$

the remaining 5 terms are just variations of this one, as one can see by the labels of figure 5.12 (left).

**Four-point box diagram** The graph associahedron for the four-point box diagram has 20 vertices, 32 edges and 14 facets, as can be seen in the right of figure 5.12. This corresponds to the triangulation  $\{(p, 1), (p, 2), (p, 3), (p, 4)\}$  of the punctured disk. The graph associahedron will have three types of facets, the tubes with two sites (red tubes in figure 5.12) will be hexagons, the tubes with three sites (green tubes in figure 5.12) will be squares, the tubes with four sites (blue tubes in figure 5.12) will be pentagons.

The red tubes will correspond to the product graph associahedron of the two-site chain (subgraph inside the red tube), which is a point, with the graph associahedron of the triangle diagram (obtained after shrinking any red tube in the box), which we can see from the left of figure 5.12, that is a hexagon.

The green tubes will correspond to the product of the graph associahedron of the three-site chain, which is an interval, with the graph associahedron of the bubble (obtained by shrinking any green tube in the box diagram in the right of figure 5.12), which is also a segment. The product is a square.

Finally, the blue tubes will correspond to the product of the graph associahedron of the four-site chain, which is a pentagon (as can be verified in the left of figure 5.1), with the graph associahedron of the tadpole, which is a point.

In total, the polytope has 20 vertices, precisely matching the number of russian dolls in the graph. There will be 16 terms which correspond to a tubing which has a blue, a green and a red tube. One such term, after factoring out the total energy and the triangles, is:

$$\frac{1}{\mathcal{P}_{(1,2),(2,3),(3,4),(4,1),(p,1)} \mathcal{P}_{(1,2),(2,3),(3,4),(p,1),(p,4)} \mathcal{P}_{(1,2),(2,3),(p,1),(p,3)}},$$

and one can consider 16 similar tubings. In the polytope of figure 5.12, one can identify these terms by finding the vertices that are intersections of facets labeled by a blue tube, a green tube and a red tube. The other 4 terms correspond to the product of a blue tube with two red tubes, one such example is:

$$\frac{1}{\mathcal{P}_{(1,2),(2,3),(3,4),(4,1),(p,1)} \mathcal{P}_{(1,2),(2,3),(p,1),(p,3)} \mathcal{P}_{(3,4),(4,1),(p,1),(p,1)}}.$$

Again one can count four vertices in figure 5.12 which are the intersection of two facets labeled by a red tube and one facet labeled by a blue tube.

**One-loop cosmohedra realization** As described earlier, the embedding of the loop cosmohedra is done exactly in the same way as in the tree-level case. We now proceed to give some explicit examples.

**Two-points** The one-loop two-points associahedron is a hexagon, thus the corresponding cosmohedron will be a dodecagon. The Feynman fan is given by the g-vectors:

$$g_{1,1}, g_{2,2}, g_{p,1}, g_{p,2}, g_{\tilde{p},1}, g_{\tilde{p},2},$$

and we “cosmologize” it by adding the following linear combinations of g-vectors:

$$g_{1,1} + g_{p,1}, g_{2,2} + g_{p,2}, g_{p,1} + g_{p,2},$$

as well as the other three rays with  $g_{p,i} \rightarrow g_{\tilde{p},i}$ . Now that we have the form of our facet inequalities, we only need to parametrize the  $\epsilon$  constants which will “shave off” the underlying loop associahedron polytope. The  $\epsilon$  will have to satisfy 6 inequalities in order to yield the correct polytope and since in this case the polytope is two-dimensional, and thus simple, there are no equalities to be imposed on the  $\epsilon$ -space,

$$\epsilon_{\{(1,1)\}} + \epsilon_{\{(p,1)\}} < \epsilon_{\{(1,1),(p,1)\}}, \quad \epsilon_{\{(p,1)\}} + \epsilon_{\{(p,2)\}} < \epsilon_{\{(p,1),(p,2)\}},$$

and the remaining four are obtained by the mappings  $p \rightarrow \tilde{p}$  and/or  $1 \rightarrow 2$ . These inequalities transform into intersections and unions of sub-surfaces when using the mapping (5.11):

$$\begin{aligned} \delta_{\{(1,1)\}} + \delta_{\{(1,2),(2,1),(p,1)\}} &< \delta_{\{(1,1),(p,1)\}}, \\ \delta_{\{(1,2),(2,1),(p,1)\}} + \delta_{\{(1,2),(2,1),(p,2)\}} &< \delta_{\{(1,2),(p,1),(p,2)\}} + \delta_{\{(2,1),(p,1),(p,2)\}}, \end{aligned}$$

respectively. Here, the  $\delta_P$  are labelled by the cords that bound the sub-surface. The second inequality is an example of the case where the intersection of the surfaces on the left-hand side is given by multiple disjoint sub-surfaces.

**Three-points** At three-points the cosmohedron is three-dimensional, it has 108 vertices, 168 edges and 62 facets. This means we will have 62  $\epsilon_C$ , which will form 138 inequalities, and 12 equalities. One such equality is:

$$\epsilon_{\{(1,1),(1,3)\}} + \epsilon_{\{(1,1),(p,1)\}} = \epsilon_{\{(1,1)\}} + \epsilon_{\{(1,1),(1,3),(p,1)\}},$$

and the other 11 equalities are variations of this one. On the other hand, two examples of inequalities are:

$$\begin{aligned} \epsilon_{\{(1,1)\}} + \epsilon_{\{(1,3)\}} &< \epsilon_{\{(1,1),(1,3)\}}, \\ \epsilon_{\{(p,1),(p,2)\}} + \epsilon_{\{(p,1),(p,3)\}} &< \epsilon_{\{(p,1),(p,2),(p,3)\}} + \epsilon_{\{(p,1)\}}, \end{aligned}$$

which have the corresponding form in terms of overlaps of sub-surfaces:

$$\begin{aligned} \delta_{\{(1,1),(1,2),(2,3),(3,1)\}} + \delta_{\{(1,3),(3,1)\}} &< \delta_{\{(1,1),(1,3),(3,1)\}}, \\ \delta_{\{(1,2),(2,3),(p,1),(p,3)\}} + \delta_{\{(2,3),(3,1),(p,1),(p,2)\}} &< \delta_{\{(2,3),(p,2),(p,3)\}} + \delta_{\{(1,2),(2,3),(3,1),(p,1)\}}, \end{aligned}$$

where the union in the first line is the total energy sub-surface, which we set to zero. This example also provides a good illustration of the factorization of the facets at one-loop. The facets labelled by the cords  $\{(2, 1)\}$ ,  $\{(3, 2)\}$  or  $\{(1, 3)\}$  will be dodecagons, since they constitute the factorization into the one-loop two-points cosmohedron, the tree level three-point cosmohedron and the two-site chain graph associahedron, which are a dodecagon, and two points, respectively. Thus, the cosmohedron will have three dodecagon facets. Then, the facets labelled by the cords  $\{(p, 1)\}$ ,  $\{(p, 2)\}$  or  $\{(p, 3)\}$ , (as well as the facets with  $p \rightarrow \tilde{p}$ ) will be decagons, since here the facet factorizes into one sub-surface with five boundaries and no puncture, thus it will be the cosmohedron of the five point wavefunction, which is a decagon, and the graph associahedron of the one site graph, which is a point. The cosmohedron will have 6 decagon facets. Finally, the facets labelled by the cords  $\{(1, 1)\}$ ,  $\{(2, 2)\}$  or  $\{(3, 3)\}$  will be squares. Since they represent the factorization of the facet into a square and the one-loop one-point sub-surface, and the graph associated to it is the two-site chain. Thus, the facet is the product of two segments and a point, which is a square. Following this factorisation properties, one can find the remaining facets of the cosmohedron.

**Extracting the loop wavefunction from geometry** Extracting the wavefunction from the cosmohedron at loop level is very similar to tree level. One starts by constructing the permuto-cosmohedron, which follows from turning the equalities into inequalities, and then constructing the canonical form for the polytope and extracting the part with only simple poles.

Firstly, we will discuss how to build the permuto-cosmohedron at loop level. We have seen in the beginning of this section that the structure of the equalities and inequalities is exactly the same. And each equality corresponds to a non-simple vertex in the cosmohedron. Then, to “simplify” these vertices one turns the equalities into inequalities in the same way as we did at tree level:

$$\epsilon_C + \epsilon_{C'} = \epsilon_{C \cup C'} + \epsilon_{C \cap C'} \rightarrow \epsilon_C + \epsilon_{C'} < \epsilon_{C \cup C'} + \epsilon_{C \cap C'}.$$

Finding a parametrization of the  $\epsilon$  satisfying all inequalities, will ensure we obtain the permuto-cosmohedron at loop level.

To extract the full wavefunction, the pairs of singularities we associate to each facet have to be slightly reformulated, relative to the tree level case. If we consider a given facet and the corresponding partial triangulation, labeled by the set of cords  $C$ , and  $n_C$  being the number of sub-surfaces with more than three bounding edges in the partial triangulation, then we still define,

$$\frac{1}{X_C} \equiv \frac{1}{n_C} \left( \sum_{P, P' \text{ meeting on edge}} \frac{1}{\mathcal{P}_P \mathcal{P}_{P'}} \right). \quad (5.39)$$

However, when in the set  $C$  there is only one chord connecting the inner puncture to the disk boundary,  $(p, i)$ , then the partial triangulation will have a sub-surface with two edges which go around this chord – say  $\{(i, p), (p, i)\}$  – like we see for the subsurfaces in red and blue in the (left) top russian doll depicted in figure 5.11. In these cases we have to associate a triangle sub-surface to the chord,  $(p, i)$ , which we will define to be  $\mathcal{P}_P \equiv \mathcal{T}_{(p, i)}$ . And this sub-surface borders only with the sub-surface which goes around the cord  $(p, i)$ . The wavefunction is defined from the permuto-cosmohedron in the same way as at tree-level, except in the end, after selecting the single poles in the canonical form, we set all  $\mathcal{T}_{(p, i)} \rightarrow 1$ . Therefore, we can write,

$$\Psi = \left( \frac{1}{E_t} \times \Omega(X_C)|_{\text{single poles in } \mathcal{P}_P} \right) \Big|_{\mathcal{T}_{(p, i)} \rightarrow 1}. \quad (5.40)$$

**One-loop two-point wavefunction** The cosmohedron for the one-loop two-point wavefunction is simple, therefore is equivalent to the permutahedral “blow-up”. The cosmohedron is a dodecagon, and here we will discuss explicitly how to compute the contributions from three vertices, since the remaining ones are some variation of these. First, let us consider the vertex which results from the intersection of the facets  $\{(p, 1)\}$  and  $\{(p, 1), (p, 2)\}$ . Then according to the above discussion we can write:

$$\frac{1}{X_{\{(p, 1)\}}} = \frac{1}{\mathcal{P}_{(1, 2), (2, 1), (p, 1)} \mathcal{T}_{(p, 1)}}, \quad \frac{1}{X_{\{(p, 1), (p, 2)\}}} = \frac{1}{\mathcal{P}_{(1, 2), (p, 1), (p, 2)} \mathcal{P}_{(2, 1), (p, 1), (p, 2)}}.$$

Therefore, the contribution from this vertex is:

$$\frac{1}{E_t \mathcal{P}_{(1, 2), (2, 1), (p, 1)} \mathcal{P}_{(1, 2), (p, 1), (p, 2)} \mathcal{P}_{(2, 1), (p, 1), (p, 2)}},$$

where we have set the value of  $\mathcal{T}_{(p, 1)}$  to one at the end. Then, we can compute the contribution of the vertex which is the intersection of the facet  $\{(p, 1)\}$  and  $\{(1, 1), (p, 1)\}$ ,

$$\frac{1}{X_{\{(p, 1)\}}} = \frac{1}{\mathcal{P}_{(1, 2), (2, 1), (p, 1)} \mathcal{T}_{(p, 1)}}, \quad \frac{1}{X_{\{(1, 1), (p, 1)\}}} = \frac{1}{\mathcal{P}_{(1, 1), (1, 2), (2, 1)} \mathcal{P}_{(1, 1), (p, 1)}} + \frac{1}{\mathcal{P}_{(1, 1), (p, 1)} \mathcal{T}_{(p, 1)}},$$

which in the end will lead to the contribution,

$$\frac{1}{E_t \mathcal{P}_{(1, 2), (2, 1), (p, 1)} \mathcal{P}_{(1, 2), (2, 1), (1, 1)} \mathcal{P}_{(1, 1), (p, 1)}},$$

keep in mind that we dropped the terms with  $\mathcal{T}_{(p,1)}^2$ , just like for any other sub-surface, and only in the end we set  $\mathcal{T}_{(p,1)} \rightarrow 1$ . And finally, we can compute the contribution from the vertex at the intersection of the facets  $\{(1,1)\}$  and  $\{(1,1), (p,1)\}$ ,

$$\frac{1}{X_{\{(1,1)\}}} = \frac{1}{\mathcal{P}_{(1,1),(1,2),(2,1)}\mathcal{P}_{(1,1)}}, \quad \frac{1}{X_{\{(1,1),(p,1)\}}} = \frac{1}{\mathcal{P}_{(1,1),(1,2),(2,1)}\mathcal{P}_{(1,1),(p,1)}} + \frac{1}{\mathcal{P}_{(1,1),(p,1)}\mathcal{T}_{(p,1)}},$$

and its contribution to the wavefunction is:

$$\frac{1}{E_t \mathcal{P}_{(1,1),(1,2),(2,1)}\mathcal{P}_{(1,1)}\mathcal{P}_{(1,1),(p,1)}}.$$

**One-loop three-point wavefunction** Now we will proceed with the three-point one-loop example. Here we will compute one contribution from a non-simple vertex and one of the terms in the triangle diagram, since these are the vertices that best illustrate the differences with the tree-level computations. Let us start with the non-simple vertex, where the facets  $\{(1,1)\}$ ,  $\{(1,1), (1,3)\}$ ,  $\{(1,1), (p,1)\}$ , and  $\{(1,1), (1,3), (p,1)\}$  meet. The permutahedral “blow-up” splits it into two vertices, one of which, is the intersection of the facets  $\{(1,1)\}$ ,  $\{(1,1), (1,3)\}$ , and  $\{(1,1), (1,3), (p,1)\}$ , and another  $\{(1,1)\}$ ,  $\{(1,1), (p,1)\}$ , and  $\{(1,1), (1,3), (p,1)\}$ . For the first vertex, we can write,

$$\frac{1}{X_{\{(1,1)\}}} = \frac{1}{\mathcal{P}_{(1,1),(1,2),(2,3),(3,1)}\mathcal{P}_{(1,1)}}, \quad \frac{1}{X_{\{(1,1),(1,3)\}}} = \frac{1}{\mathcal{P}_{(1,2),(1,3),(2,3)}\mathcal{P}_{(1,1),(1,3),(3,1)}} + \frac{1}{\mathcal{P}_{(1,1)}\mathcal{P}_{(1,1),(1,3),(3,1)}},$$

$$\frac{1}{X_{\{(1,1),(1,3),(p,1)\}}} = \frac{1}{\mathcal{P}_{(1,2),(2,3),(1,3)}\mathcal{P}_{(1,1),(1,3),(3,1)}} + \frac{1}{\mathcal{P}_{(1,1),(p,1)}\mathcal{P}_{(1,1),(1,3),(3,1)}} + \frac{1}{\mathcal{P}_{(1,1),(p,1)}\mathcal{T}_{(p,1)}},$$

for the second vertex the partial triangulation with two cords will differ, it is,

$$\frac{1}{X_{\{(1,1),(p,1)\}}} = \frac{1}{\mathcal{P}_{(1,1),(1,2),(2,3),(3,1)}\mathcal{P}_{(1,1),(p,1)}} + \frac{1}{\mathcal{P}_{(1,1),(p,1)}\mathcal{T}_{(p,1)}}.$$

Naturally, both vertices will give the same contribution, which is,

$$\frac{1}{2E_t \mathcal{P}_{(1,1),(1,2),(2,3),(3,1)}\mathcal{P}_{(1,1)}\mathcal{P}_{(1,1),(p,1)}\mathcal{P}_{(1,2),(2,3),(1,3)}\mathcal{P}_{(1,1),(1,3),(3,1)}}.$$

Since they are two, the one-half will cancel. Finally, we will look at the vertex at the intersection of the facets,  $\{(p,1)\}$ ,  $\{(p,1), (p,2)\}$ , and  $\{(p,1), (p,2), (p,3)\}$ . This is one of the 6 vertices in the facet of the cosmohedron which corresponds to the triangle diagram. For this vertex, we can write,

$$\frac{1}{X_{\{(p,1)\}}} = \frac{1}{\mathcal{P}_{(1,2),(2,3),(3,1),(p,1)}\mathcal{T}_{(p,1)}}, \quad \frac{1}{X_{\{(p,1),(p,2)\}}} = \frac{1}{\mathcal{P}_{(1,2),(p,1),(p,2)}\mathcal{P}_{(2,3),(3,1),(p,1),(p,2)}},$$

$$\frac{1}{X_{\{(p,1),(p,2),(p,3)\}}} = \frac{1}{\mathcal{P}_{(1,2),(p,1),(p,2)}\mathcal{P}_{(2,3),(p,2),(p,3)}} + \frac{1}{\mathcal{P}_{(2,3),(p,2),(p,3)}\mathcal{P}_{(3,1),(p,1),(p,3)}} + \frac{1}{\mathcal{P}_{(1,2),(p,1),(p,2)}\mathcal{P}_{(3,1),(p,1),(p,3)}}.$$

This leads to the contribution, for this vertex,

$$\frac{1}{E_t \mathcal{P}_{(1,2),(p,1),(p,2)} \mathcal{P}_{(2,3),(p,2),(p,3)} \mathcal{P}_{(3,1),(p,1),(p,3)} \mathcal{P}_{(2,3),(3,1),(p,1),(p,2)} \mathcal{P}_{(1,2),(2,3),(3,1),(p,1)}},$$

which we can check to be one of the tubings of the triangle diagram.

## 5.5 Cosmological correlahedra

In this section, we will describe a combinatorial object that encodes all the contributions to the correlator in  $\text{Tr}(\phi^3)$  theory. As we will see, they naturally combine into a “sandwich” of associahedra and cosmohedra in a single higher-dimensional polytope.

In section 2 we described how to compute correlators from the wavefunction, and we further discussed it in the examples of section 3.3. But now we need to discuss how to embed the picture of deleting edges in diagrams we had for correlators, into the momentum polygon picture. It is quite simple, the fully connected terms have their representation fully in terms of the Russian doll picture, as we saw for the cosmohedron. The disconnected terms, we consider a mixture of cords and sub-polygons. For example, if we were to consider a graph with one edge deleted, then at the level of the momentum polygon we associate an internal cord to the deleted edge, and the Russian doll picture for each of the two sub-polygons arising from the division of the full momentum polygon by the cord. Therefore, we can write:

$$\text{Corr}_n = \Phi_n + \sum_{\mathcal{C} \neq \emptyset} \prod_{(i,j) \in \mathcal{C}} \frac{1}{k_{i,j}} \times \prod_{\mathcal{P} \text{ compatible } \mathcal{C}} \Psi_{\mathcal{P}}, \quad (5.41)$$

where the first term corresponds to the fully connected part which does not depend on cords, and just gives us the full wavefunction. The combinatorics of the full correlator is then clearly a hybrid between those of amplitudes (non-crossing chords) and the wavefunction (non-overlapping sub-polygons).

Now, it is natural to expect any geometry for the full correlator to live in one higher dimension than the associahedron/cosmohedron. The reason is that while all the terms in the wavefunction have an  $E_t$  singularity, which is not explicitly included as a facet in the cosmohedron, this is not the case for the full correlator – some terms have  $E_t$  singularities (those coming from  $\Psi_n$  in (5.41)) and others don’t (the remaining terms in (5.41)). Thus, it stands to reason to think about an object in one higher dimension, roughly corresponding to  $E_t$ , with a “bottom” facet associated with  $E_t$ , which looks like the cosmohedron. If this object is to include the combinatorics of non-overlapping chords, then we know that these objects alone, with no reference to sub-polygons at all, are captured by the associahedron. So it is reasonable to expect that the “cosmological correlahedron” we are looking for should be a sort of sandwich in an extra dimension, with the cosmohedron at the “bottom”, and an associahedron maximally far away, at the “top” of the new direction.

This can also be nicely motivated by trying to guess what the fan of this higher-dimensional object might look like. Let us consider the simplest possible case of  $n = 4$ .

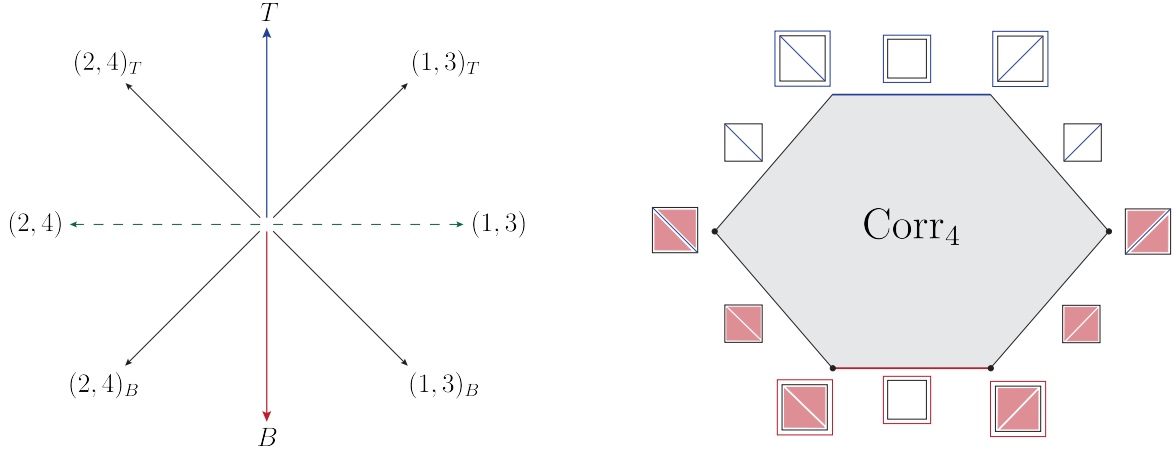


Figure 5.13: (Left) Fan of the cosmological correlahedron for  $n = 4$ . In dashed, we represent the underlying associahedron fan. (Right) 4-points cosmological correlahedron.

The fan for the associahedron has the two usual rays for g-vectors  $(1, 3)$ ,  $(2, 4)$ , pointing in opposite directions in one dimension. But we will introduce two new rays, “ $B$ ” and “ $T$ ” (for “bottom” and “top”) pointing in opposite directions in a second direction. We know we want to have facets of the correlator polytope corresponding to two different kinds of single chords: one where the single chord is associated with subpolygons (like we saw earlier for the wavefunction), and another where it is associated simply with the  $|\vec{k}|$  in the correlator. We will thus record images of the rays  $(1, 3)$ ,  $(2, 4)$  on the bottom and top, by defining

$$\begin{aligned} (1, 3)_B &= (1, 3) + B, & (2, 4)_B &= (2, 4) + B, \\ (1, 3)_T &= (1, 3) + T, & (2, 4)_T &= (2, 4) + T. \end{aligned} \quad (5.42)$$

This gives us the six rays  $T$ ,  $(1, 3)_T$ ,  $(1, 3)_B$ ,  $B$ ,  $(2, 4)_B$ ,  $(2, 4)_T$ , which is naturally associated with the hexagon shown in figure 5.13. We see that this hexagon has an interval at the top and one at the bottom, naturally associated with the  $n = 4$  associahedron and cosmohedron respectively. Note that the top facet only has vertices of the associahedron, and does not by itself correspond to any terms in the correlator. But the remaining four vertices (highlighted in black in figure 5.13) are naturally associated with all the terms in the correlator.

Let’s move on to the next example at  $n = 5$ , where we will see almost all the relevant structure for general  $n$ . We again start from the rays of the associahedron, which we can label with the chords  $(1, 3)$ ,  $(1, 4)$ ,  $(2, 4)$ ,  $(2, 5)$ ,  $(2, 6)$ , now living in two dimensions, and add  $B, T$  pointing in opposite directions in an extra third direction. We then produce the rays  $(i, j)_B = (i, j) + B$  and  $(i, j)_T = (i, j) + T$  as before. But on the bottom, we continue to produce the rest of the rays for the cosmohedron as we have described before, by producing the sums of the bottom rays. To produce the cones, we begin by connecting all the bottom rays to  $B$  and all the top rays to  $T$ . Next, we connect all the bottom rays amongst each



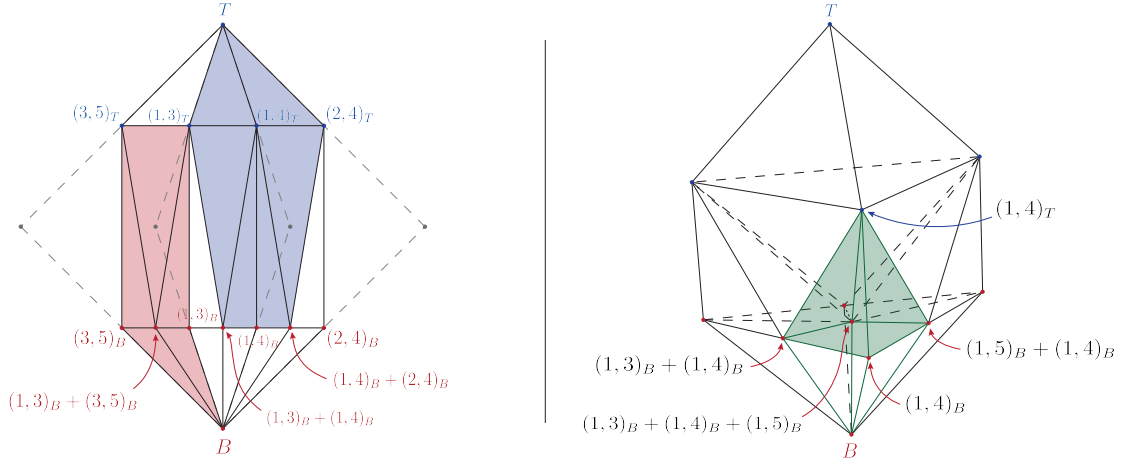


Figure 5.14: (Left) Projection of the  $n = 5$  cosmological correlahedron fan. In dashed we represent the underlying associahedron fan with rays  $(3, 5)$ ,  $(1, 3)$ ,  $(1, 4)$  and  $(2, 4)$  marked in gray, with the added dimension corresponding to  $E_t$ . Shaded in red we highlight the pentagonal facet which is touching the base  $\text{Cosmo}_5$ , and in blue the hexagonal facet which is touching the top  $\text{Assoc}_5$ . (Right) 3-dimensional projection of the  $\text{Corr}_6$  fan, coming from the underlying 3-dimensional associahedron cone containing rays  $(1, 3)$ ,  $(1, 4)$ ,  $(1, 5)$ . In green, we highlight a square pyramid corresponding to a non-simple vertex of  $\text{Corr}_6$ .

other as for the cosmohehedron, while all the top rays are connected to each other as they are for the associahedron. Finally, the top and bottom are connected by a very simple rule: an  $(i, j)_T$  is connected to every bottom ray that contains  $(i, j)$ . The fan for the  $n = 5$  is three-dimensional but as usual we can draw a projective picture of it two-dimensionally, and this is drawn in figure 5.14 (left); a combinatorial representation of the wavefunction is shown in the top of figure 5.16 (at the end of the note). Again, we see that the “top” facet is the associahedron, and the “bottom” facet is a cosmohehedron. All the faces in between are labelled by mixtures of the “top” chords – which we can think of as the  $|\vec{k}|$  chords in the wavefunction, and “bottom” chords – which give us nested subpolygons. Apart from the vertices on the top associahedron facet (marked in blue), the rest of the vertices precisely correspond to all the terms in the correlator (marked in black).

The cosmological correlahedron has a natural combinatorial definition for all  $n$ . Faces are labelled by  $\{C, P\}$ , where  $C$  is a collection of non-overlapping chords as for associahedra, and  $P$  is a collection of non-overlapping subpolygons satisfying the russian doll rule as for cosmohehedra, except that we now include the “full perimeter” as subpolygons, and we have two full perimeters labelled by  $T, B$ . There are two special faces, the “top” facet where  $\{C = \text{empty}, P = P_{\text{full, top}}\}$  and the “bottom” facet where  $\{C = \text{empty}, P = P_{\text{full, bottom}}\}$ . No subpolygons, nor  $P_{\text{full, bottom}}$  are allowed to occur in the list with  $P_{\text{full, top}}$ . Then, the cosmological correlahedron generalizes the notion of compatibility for associahedra and

cosmohedra in the obvious way:

$$\{C', P'\} \text{ is a face of } \{C, P\} \text{ if } C \subset C' \text{ and } P \subset P'. \quad (5.43)$$

At  $n = 6$  the fan is four-dimensional, but we can draw a relevant piece of it three-dimensionally, as done in figure 5.14 (right). The rays are produced and connected to form cones in exactly the way we described above: starting with the rays of the associahedron  $(i, j)$ , producing  $(i, j)_B = (i, j) + B$  and  $(i, j)_T = (i, j) + T$ , producing the rest of the rays of the cosmohedron from the bottom rays, and connecting all the bottom rays as for cosmohedra, the top rays are connected as for associahedra, and every top  $(i, j)_T$  ray to every bottom rays that contains  $(i, j)$ . Again remarkably, the cones are non-overlapping, and apart from the purely top ones giving all the triangulations of the  $n$ -gon, the rest of the cones are associated with every term in the correlator.

As for cosmohedra, starting with  $n = 6$  we encounter the phenomenon of non-simple vertices for the cosmological correlahedron. In the figure, the five rays  $(1, 4)_T$  together with  $(1, 4)_B, (1, 3)_B + (1, 4)_B, (1, 5)_B + (1, 4)_B, (1, 3)_B + (1, 4)_B + (1, 5)_B$  form a square-pyramid, associated with a single term in the correlator.

The picture for the fan of the cosmological correlahedron can clearly be extended to loops, and an example of a three-dimensional polytope for the 1-loop bubble is shown in the bottom of figure 5.16 (at the end of the note).

It is also natural to cut out the cosmological correlahedron by inequalities, extending those of associahedra and cosmohedra in the obvious way, involving “shaving parameters”  $\epsilon_{T,B}$  for both the top and bottom rays. We have checked that the polytopes produced in this way have exactly the correct combinatorics for  $n = 6$ , and that they have the correct number of vertices to account for the correlator up to  $n = 8$ . In figure 5.15 we show the embedding of the  $n = 5$  cosmological correlahedron as well as the embedding of the facet  $(1, 4)_T$  of the  $n = 6$  one. For general  $n$ , we expect an interesting relation between  $\epsilon_{T,B}$  to produce the correct combinatorics. We leave an exploration of this question, as well as the systematics of extracting the correlator from the geometry, to future work.

## 5.6 Discussion

In this chapter we introduced a novel combinatorial definition of the wavefunction, the cosmohedron. It comes with its own graph geometry, the graph associahedra, which correspond to facets of the cosmohedron. We also construct the embedding of the cosmohedron, which naturally arises from the ABHY associahedron.

This construction has many interesting things to point out. Firstly, the obvious one is that it is highly non-trivial that the wavefunction can be fully accounted for through this construction, both at tree and loop level. This obviously was made possible by thinking about the wavefunction in terms of independent perimeter variables from the momentum polygon. However, the cosmohedron is clearly not the end of the story. In constructions like the ABHY associahedron, or cosmological polytopes, the respective integrand can be fully extracted from a traditional canonical form. For the cosmohedron we need to attribute

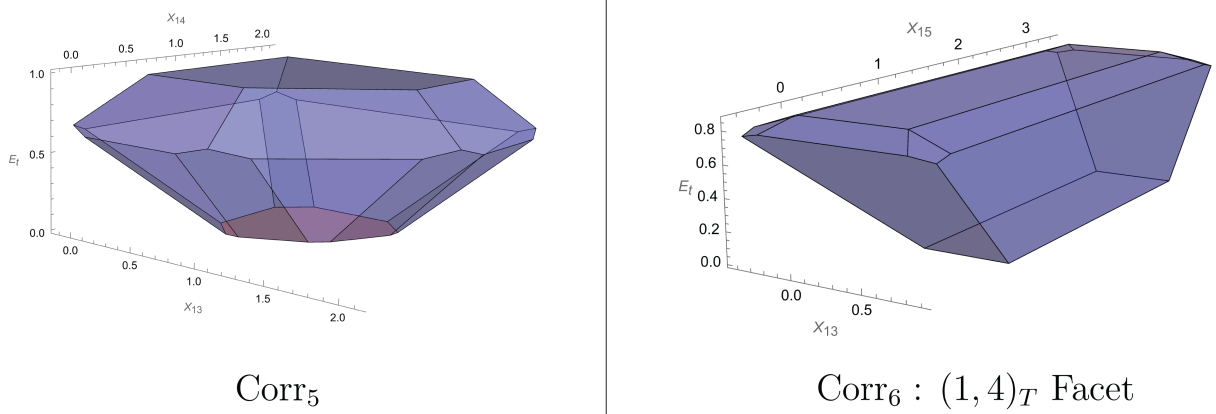







Figure 5.15: (Left) Embedding of the  $\text{Corr}_5$ . (Right) Embedding of the  $(1,4)_T$  facet of  $\text{Corr}_6$ .

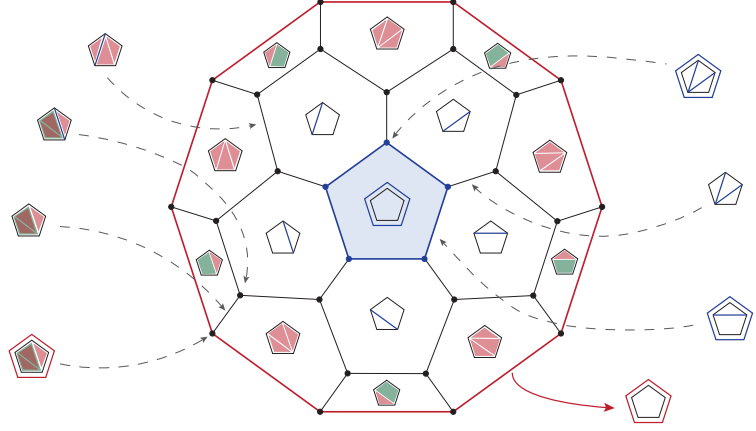
to each facet a pair of singularities, unlike the typical facet relation for the associahedron, and furthermore, in the cosmohedron we need to truncate the canonical form obtained. This begs the question about whether there is a bigger object from which the standard canonical form procedure gives us the correct wavefunction, or whether the canonical form we have has actually a deeper physical meaning in the truncated part. An interesting question to be asked, which can lead to progress in this problem, is whether there is a way to embed the cosmohedron which is not as dependent on the Associahedron construction. In practice, when we construct the cosmohedron, firstly we construct the associahedron inequalities, which by themselves already depend on the non-planar constants  $c_{ij}$ . Then, we “blow-up” the faces, or in other words, we trim the faces by new faces (given by the “blow-up” of the fan), where the trimming is controlled by small  $\epsilon$  parameters, which obey very simple inequalities between themselves, and very importantly have to be smaller than the  $c_{ij}$  constants. The interesting question is: is there a way to make  $\epsilon_C$  and  $c_{ij}$  on the same footing? This could force us to re-think the embedding of the cosmohedron in a way that makes the canonical form a more standard object like in other cases we have seen in amplitudes, and cosmology.

Nevertheless, the graph associahedra, which we can associate to each diagram, is a simple polytope and has a standard canonical form giving the correct wavefunction for the graph. Therefore these objects make the obvious first candidate to try and find a Minkowski sum of simplices decomposition of the graph associahedra, which would allow us to construct a “stringy” integrand, as was done for the associahedron [105].



$\text{Corr}_5$ :




Top Front Facet:   $\text{Assoc}_5$   
 Bottom/Back Facet:   $\text{Cosmo}_5$

  $(1,3)_T$ : Hexagon  
  $(1,3)_B + (3,5)_B$ : Pentagon  
  $(1,3)_B$ : Square



$\text{Corr}_2^{1\text{-loop}}$ :

Top Front Facet:   $\text{Assoc}_2^{1\text{-loop}}$   
 Bottom/Back Facet:   $\text{Cosmo}_2^{1\text{-loop}}$

  $(1,p)_T$ : Hexagon  
  $(1,p)_B + (2,p)_B$ : Pentagon  
  $(1,p)_B$ : Square

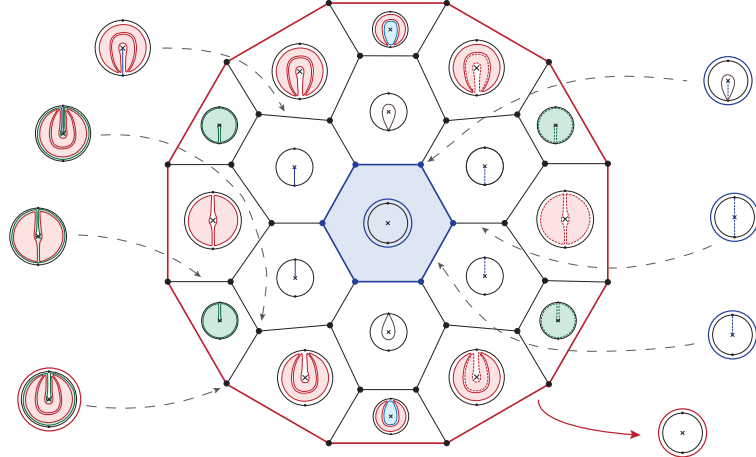


Figure 5.16: The top figure shows the combinatorial structure of the three-dimensional  $n = 5$  cosmological correlahedron, looked at from above. We see the top pentagon facet as the  $n = 5$  associahedron, and the bottom decagon as the  $n = 5$  cosmohedron. A number of other facets, edges and vertices are labelled by collections  $(C, P)$  of non-overlapping chords and subpolygons. There are 30 vertices. The top 5 vertices (marked in blue) all correspond to triangulations of the associahedron, the rest of the vertices are all the terms in the correlator. The bottom figure shows exactly the same for the  $n = 2$ , 1-loop correlator. As for the amplitude polytopes, there are two kinds of “loop” variable, touching the puncture. The top facet is the hexagon familiar from the amplitude. The bottom is the dodecagon for the cosmohedron. The vertices not on the top facet all correspond to the terms in the correlator.

# Chapter 6

## Conclusion

In the previous chapters, we discussed the different aspects of the cosmological wavefunction, its analytical structure, its integration and a novel combinatorial formulation. In this section, we review and discuss the main outcomes of all of this work. We also point out future interesting research directions which can follow from here.

**Main Results** In chapter 3, we develop a parameterisation of the integrals which contribute to cosmological observables, which we call cosmological integrals, be it cosmological correlators, or simply the wavefunction. This parameterisation works for any topology, that is with any number of loops, which before was not understood. The importance of it comes from the fact that its generality allows putting on equal footing an integral contributing to any observable, graph topology, and various different models of inflation. This is of course a very important feature to have if one wants to understand the general features of quantum field theory in quasi-de Sitter spacetimes, which is the underlying assumption of inflation.

In the subsequent sub-sections we make use of methods that preserve this generality. In fact, after defining this parameterisation we develop a new formalism which computes the divergences of any cosmological integral. This formalism makes use of ideas such as the Newton polytope associated to the integrand, and then employing the method of sector decomposition to compute the integral as a series in the regulator. We were able to find a connection between the diagram associated to the integral and the different sectors in the integration regions, as well as their degree of divergence. This allows simply from the graph to immediately obtain the integrals over a cube region corresponding to each sector tiling the full integration region. Then, extracting the divergences is a straightforward subtraction scheme. For the leading logarithmic divergences we are able to find a general form for the coefficient. Our formalism has several very nice features. For starters, it is completely general, in the sense that we only need to input the specific parameters of the theory, (*i.e.* which observable, which background, which lagrangian, and how many external states) very late in the computation. It also makes straightforward the identification of the different regions contributing to the divergences, whether it is secular growth or a loop divergence, or a mix of both. This indeed agrees with the literature. Finally, it makes

very obvious that the contributions to the leading divergences come from the disconnected part of the wavefunction, which is a product of tree-level wavefunctions. This also had been proven recently in the literature. Using this formalism we were able to develop a systematic subtraction scheme that subtracts the leading secular divergences, and at one loop we were able to also construct a finite computable. This allows constructing infrared finite computables at tree level (and less divergent computables at loop level). It remains to be seen what are (if there are) the natural cosmological observables which produce these infrared finite quantities, we leave that for future work.

In chapter 4, we turn to the integration of cosmological integrals. To do this we employ the method of differential equations, which in recent years has been used massively in the computation of Feynman integrals. In general, cosmological integrals hold the structure of twisted period integrals. As such, we were able to derive integration by parts identities for the integral families of the one-loop two-site wavefunction coefficient, and the one-loop three-site wavefunction coefficient. We were able to obtain an analytic form for the one-loop two-site in general FLRW power law cosmologies. Additionally, we were able to show that the integral family of one-loop three site wavefunction contains elliptic polylogarithms, which was unknown from the previous literature on computing cosmological observables.

In chapter 5, we introduce the cosmohedron, a geometrical object which encodes the combinatorics of wavefunction. The cosmohedron is obtained by associating a facet to each partial triangulation of the momentum polygon. Then, the inequalities associated to these facets are controlled by a constant,  $\epsilon_C$ , which itself must satisfy inequalities and equalities related to different  $\epsilon_C$ . As we have seen, this allows constructing the embedding for the cosmohedron, where each vertex corresponds directly to a Russian doll term contributing to the wavefunction. Besides the cosmohedron, we also constructed a graph polytope, the graph associahedra, which corresponds to certain facets of the cosmohedron, those corresponding to full triangulations, and thus graphs. We also provide a way to extract the wavefunction from the cosmohedron, by first providing a prescription to “blow-up” the non-simple vertices, and then assigning pairs of singularities to each facet and keeping only the simple poles in the canonical form. Furthermore, we extrapolate all of this to loop level  $\text{Tr}[\phi^3]$ . We also construct the generalization of the cosmohedron for the correlator. Finally, we connect the graph associahedron picture for single diagrams and show how it connects with cosmological polytopes. We show that the graph associahedron is a particular slice of the cosmological polytope.

**Future directions** Regarding the work on infrared divergences there are couple of natural directions to take. For the first direction, it would be interesting to take our formalism and show how the leading divergences reproduce Starobinski’s stochastic inflation. Furthermore, despite having been argued that the sub-leading divergences follow a similar stochastic dynamics, it is not entirely clear how this is realized. Ideally, the probability distribution function given by the norm squared of the wavefunction should follow exact renormalisation group equations. And finally, it would be interesting to understand what kind of behaviour these divergences must satisfy in order to re-sum.

Another possible direction follows from the study of infrared finite computables. We simply showed that it is possible to formulate infrared finite quantities, however it would be interesting to see if there is a novel computable that precisely matches our proposal. For example in flat-space, where it has been known for long time that a certain combination at one loop between the box diagram and the triangle ones is infrared finite [222], there exist an observable, the Wilson loops with a Lagrangian insertion [257–259], whose perturbative expansion [260] returns precisely this combination and has a geometrical interpretation [261]. The existence of the thick graph rules open the question about a more generally defined computable whose originates such rules. We have left its possible independent, first principle, definition to future work.

Regarding the use of differential equations to compute cosmological correlators, first and foremost it would be interesting to conclude our analysis of the triangle graph. Even though elliptic integrals appear in the differential equations, it is not entirely clear they will appear in the integrated answer for the wavefunction. Furthermore, it would be interesting to extend this approach to the full site plus loop integration, and not simply the loop integral. And finally, it is trivial to extend the method to compute correlators, it would be interesting to see if there are any simplifications when comparing to the wavefunction.

Finally, in the cosmohedron it would be interesting to explore how this novel way of extracting the wavefunction has a larger physical meaning, or whether there is some other object which leads to the cosmohedron where an “honest” canonical form computes the wavefunction. We explained how to get the cosmological wavefunction under a single integral for the cosmohedron, however it would be interesting to extend our analysis to higher order polynomial interactions, and other types of massive states, not simply conformally coupled. Additionally, we only provided a general rule to embed the correlator polytope. It would be interesting to complete our analysis and understand the type of inequalities between the constants that appear in this embedding, and the equivalent picture of the graph associahedron, but for the correlator given by a single graph. Finally, we know from flat-space scattering amplitudes that there is a worldsheet formulation for  $\text{Tr}[\phi^3]$  amplitudes. The close connection between the associahedron and the cosmohedron leads us to think whether such a picture exists for the wavefunction.





# Appendix A

## The ABHY Associahedron

The associahedron,  $\text{Assoc}_n$ , is a polytope that encodes the combinatorics of triangulations of  $n$ -gons. Concretely,  $\text{Assoc}_n$  is an  $(n - 3)$ -dimensional simple polytope whose faces are associated to partial/full triangulations of the  $n$ -gon, or what is the same, collections of non-overlapping chords of the  $n$ -gon. The codimension-1 faces are associated to partial triangulations with a single chord, codimension 2 faces with those with two chords, and so on until we reach the vertices, which are labelled by  $(n - 3)$  non-overlapping chords specifying a full triangulation.

If we denote a collection of non-overlapping chords by  $\mathcal{C}$ , then the associahedron is the polytope whose face structure reflects the combinatorics of compatible chords, which can be stated as the fundamental property that:

$$\mathcal{C}' \text{ is a face of } \mathcal{C} \text{ if } \mathcal{C} \subset \mathcal{C}'.$$

One simple way of constructing the associahedron combinatorially is via *mutations*. This is if we start on a given vertex of the associahedron, corresponding to a full triangulation of the  $n$ -gon, we can generate the vertices that are connected to it by performing mutations: given the collection of chords in a triangulation, each chord is then a diagonal of a square defined by the boundary edges and the remaining chords on the triangulation. A mutation flips one of the chords to the other diagonal of the square in which it is contained. Since a triangulation contains  $n - 3$  chords, starting at a given vertex we can mutate in  $n - 3$  different ways, which means that at any vertex of our polytope  $(n - 3)$  edges meet, which tells us the polytope is *simple*. Following this procedure, we can generate the full polytope, and we further conclude that any two vertices are connected via an edge if and only if their triangulations are related by a mutation.

For example, suppose we do this exercise for  $n = 4$ . In that case, there are only two triangulations and the geometry is one-dimensional – the  $\text{Assoc}_4$  is a line interval with two vertices, one at each boundary of the interval, labeling the two possible triangulations. In this case it is trivial, but indeed we see a mutation relates the two triangulations.

At  $n = 5$ , we should find a two-dimensional geometry, which ends up being a pentagon as depicted in the left of figure 5.1. We see that each edge is associated with partial trian-

gulations with a single chord, and the vertices are labeling all the possible 5 triangulations of the pentagon.

Similarly, for  $n = 6$ , the  $\text{Assoc}_6$  is a three-dimensional polytope, with 9 codimension one facets – one associated to each chord of the hexagon – 21 codimension-2 facets – associated to collections of two non-overlapping chords – and finally 14 vertices, each labeling one triangulation of the hexagon (see figure 5.3, left).

One remarkable property of the associahedron is the factorization structure associated with its boundaries – the boundaries of associahedra are given by products of lower-point associahedra. This feature stands as the geometric avatar of factorization of tree-level scalar amplitudes into products of lower-point amplitudes. For example, if we look at the 5-point associahedron (figure 5.4, left) then we see that each boundary – the edges – are naturally associated with a partial triangle with a single chord which divides the pentagon into a square and a triangle. Indeed, the boundary is then given by the product of the lower-point associahedron associated to the smaller polygons appearing in the partial triangulation. In this case, the 3-point associahedron is a point and the 4-point is the line segment described above, so we get simply a line interval. Similarly, at 6-points, we see that the polytope has 6 pentagonal facets and 3 square facets. The first six, correspond to partial triangulations including a single chord  $(i, i + 2)$  which divides the hexagon into a pentagon and a triangle, therefore we expect to get  $\text{Assoc}_5 \times \text{Assoc}_3$ , which is indeed what we have since these facets are pentagons. As for the square facets, these correspond to partial triangulations with a single chord of the type  $(i, i + 3)$  which divides the hexagon into two squares, and therefore we get that these facets are  $\text{Assoc}_4 \times \text{Assoc}_4$ , which is precisely a square.

We stress that is not at all obvious a priori that the combinatorics of partial triangulations can be captured by a polytope. It's existence, and it's factorization properties on facets are most naturally understood from a particular realization in terms of a simple set of inequalities we will review in a moment.

Now that we have understood how the combinatorial information associated to cubic tree graphs is organized in this polytope, and in particular how its boundary structure encodes the basic factorization features of amplitudes, let's see how we can connect these physical observables to this geometry.

In a theory of colored scalars interacting via cubic interactions –  $\text{Tr}(\phi^3)$  theory – we can write the amplitudes perturbatively over sums of cubic diagrams. Namely at leading order, once we fix an ordering for the external particles, say *e.g.* the standard ordering  $(1, 2, \dots, n - 1, n)$ , we get contributions from all the possible tree-level planar Feynman diagrams – which are precisely dual to triangulations of the  $n$ -gon. In particular, if we associate to each edge of the  $n$ -gon a momentum of the particle in the scattering process,  $p_1^\mu, p_2^\mu, \dots, p_n^\mu$ , then given a triangulation we have that the  $\text{length}^2$  of the chords entering in the triangulation precisely give us the momentum square flowing through the propagators in the dual cubic graph. Let's denote the  $(\text{length})^2$  of a chord going from vertex  $i$  to vertex  $j$  by  $X_{i,j}$  then we have:

$$X_{i,j} = (p_i + p_{i+1} + \dots + p_{j-1})^2, \quad (\text{A.1})$$

where we have  $X_{i,j} = X_{j,i}$  and  $X_{i,i+1} = 0$  since we are considering our particles to be massless and therefore we have  $p_i^2 = 0$ . Therefore, we can write  $\text{Tr}(\phi^3)$  amplitudes at tree-level as a sum over all possible cubic Feynman diagrams – all possible triangulations of the  $n$ -gon – where for each diagram we have a factor of one over the product of the  $X_{i,j}$  corresponding to the chords entering in the triangulation:

$$\mathcal{A}_n(X_{i,j}) = \sum_{\text{triang. } \mathcal{T}} \prod_{X_{i,j} \in \mathcal{T}} \frac{1}{X_{i,j}}. \quad (\text{A.2})$$

This way of writing the amplitude makes manifest that it is a function exclusively of the  $X_{i,j}$ 's which are usually called the planar variables – as they correspond to the invariants associated to momentum flowing through propagators of planar tree diagrams. Note, however, that the planar variables are *not* all the possible Lorentz invariants dot product of momentum one can consider, for example we also have the dot products  $p_i \cdot p_j$  with  $i$  and  $j$  non-adjacent. In particular, at  $n$ -points we have  $n$  chosen 2 dot products of momenta, but due to momentum conservation only  $n(n-3)/2$  of these are actually independent. Quite nicely  $n(n-3)/2$ , is precisely the number of  $X_{i,j}$  we have for an  $n$ -gon, and therefore we have that the planar variables form a *basis of kinematic space*, where momentum conservation is automatically implemented by the fact that they lived in a *closed* momentum polygon.

This means that the non-planar variables – corresponding to dot products of non-adjacent particles — can be written in terms of the planar ones. Let us call the non-planar invariants by  $c_{i,j} = -2p_i \cdot p_j$  with  $i, j$  not adjacent. Then we have:

$$c_{i,j} = X_{i,j} + X_{i+1,j+1} - X_{i,j+1} - X_{i+1,j}. \quad (\text{A.3})$$

Now that we have defined the kinematic space the amplitude lives in as well as given a precise definition of the amplitude in this space (A.2), we can proceed to understand how to connect this object to the geometry of the associahedron. The first step is to embed the associahedron in kinematic space - where the amplitude is defined - this is we want to define a set of inequalities in  $X_{i,j}$  space that carve out this polytope. This embedding was introduced in [93] and we will summarize it here. As explained above, each facet of this geometry is associated with a partial triangulation with a single chord, and therefore is naturally associated with a given  $X_{i,j}$ . Therefore, to each facet we associate the inequality:

$$X_{i,j} \geq 0. \quad (\text{A.4})$$

So we have that all  $X$ 's are positive inside the polytope and vanish in the respective facets. However, as explained earlier the  $\text{Assoc}_n$  is an  $n-3$ -dimensional object, and the current inequalities naively define a cone in an  $n(n-3)/2$  dimensional space. So in order to bring it to the correct dimension we intersect this cone with the “ABHY” plane defined as follows: Pick a triangulation say  $\{X_{1,3}, X_{1,4}, \dots, X_{1,n-1}\}$  and consider the kinematic basis containing the  $X$ 's in the triangulation as well as the collection of non-planar variables  $\mathcal{C} = \{c_{1,3}, c_{1,4}, \dots, c_{1,n-1}, c_{2,4}, c_{2,5}, \dots, c_{2,n-1}, \dots, c_{3,5}, \dots, c_{n-3,n-1}\}$  which contains exactly

$n(n-3)/2 - (n-3)$   $c$ 's. Then since this forms a basis we can write all  $X$ 's in terms of the  $X$ 's in the chosen triangulation and the  $c_{i,j}$ 's in this collection. If we fix the non-planar variables in  $\mathcal{C}$  to be *positive* then (A.4) defines an  $n-3$  dimensional geometry in the space spanned by  $X_{1,3}, X_{1,4}, \dots, X_{1,n-1}$  which is precisely the associahedron.

Given this embedding, the amplitude is given by the canonical form of this polytope. There are various motivations for the ABHY inequalities, from a "causal diamond" picture [101] in kinematic space to recording the data of curves on surfaces [102]. It is striking that none of these refer to summing over all diagrams. The connection with the usual Feynman diagrams arises from a particular way of computing the canonical form of the associahedron. Indeed for any simple polytope, there is a natural triangulation, taking the inverse product of the facet inequalities meeting at each vertex and summing over all vertices, corresponding to an especially obvious triangulation of the *dual* polytope. Since each vertex of the associahedron corresponds to a complete triangulation, this expression for the canonical form of a simple polytope turns into the Feynman diagram expansion.

# Bibliography

- [1] **Planck** Collaboration, N. Aghanim *et al.*, “Planck 2018 results. VI. Cosmological parameters,” *Astron. Astrophys.* **641** (2020) A6, [arXiv:1807.06209](#) [[astro-ph.CO](#)]. [Erratum: *Astron. Astrophys.* 652, C4 (2021)].
- [2] E. Hubble, “A relation between distance and radial velocity among extra-galactic nebulae,” *Proc. Nat. Acad. Sci.* **15** (1929) 168–173.
- [3] A. A. Penzias and R. W. Wilson, “A Measurement of excess antenna temperature at 4080-Mc/s,” *Astrophys. J.* **142** (1965) 419–421.
- [4] A. H. Guth, “The Inflationary Universe: A Possible Solution to the Horizon and Flatness Problems,” *Phys. Rev. D* **23** (1981) 347–356.
- [5] A. D. Linde, “A New Inflationary Universe Scenario: A Possible Solution of the Horizon, Flatness, Homogeneity, Isotropy and Primordial Monopole Problems,” *Phys. Lett. B* **108** (1982) 389–393.
- [6] A. Albrecht and P. J. Steinhardt, “Cosmology for Grand Unified Theories with Radiatively Induced Symmetry Breaking,” *Phys. Rev. Lett.* **48** (1982) 1220–1223.
- [7] A. A. Starobinsky, “Dynamics of Phase Transition in the New Inflationary Universe Scenario and Generation of Perturbations,” *Phys. Lett.* **117B** (1982) 175–178.
- [8] **WMAP** Collaboration, D. N. Spergel *et al.*, “First year Wilkinson Microwave Anisotropy Probe (WMAP) observations: Determination of cosmological parameters,” *Astrophys. J. Suppl.* **148** (2003) 175–194, [arXiv:astro-ph/0302209](#).
- [9] **WMAP** Collaboration, C. L. Bennett *et al.*, “First year Wilkinson Microwave Anisotropy Probe (WMAP) observations: Preliminary maps and basic results,” *Astrophys. J. Suppl.* **148** (2003) 1–27, [arXiv:astro-ph/0302207](#).
- [10] **WMAP** Collaboration, D. N. Spergel *et al.*, “Wilkinson Microwave Anisotropy Probe (WMAP) three year results: implications for cosmology,” *Astrophys. J. Suppl.* **170** (2007) 377, [arXiv:astro-ph/0603449](#).

- [11] **Planck** Collaboration, P. A. R. Ade *et al.*, “Planck 2013 results. XVI. Cosmological parameters,” *Astron. Astrophys.* **571** (2014) A16, [arXiv:1303.5076 \[astro-ph.CO\]](#).
- [12] **Planck** Collaboration, Y. Akrami *et al.*, “Planck 2018 results. X. Constraints on inflation,” *Astron. Astrophys.* **641** (2020) A10, [arXiv:1807.06211 \[astro-ph.CO\]](#).
- [13] D. Baumann, “Inflation,” in *Theoretical Advanced Study Institute in Elementary Particle Physics: Physics of the Large and the Small*, pp. 523–686. 2011. [arXiv:0907.5424 \[hep-th\]](#).
- [14] D. Baumann and L. McAllister, *Inflation and String Theory*. Cambridge Monographs on Mathematical Physics. Cambridge University Press, 5, 2015. [arXiv:1404.2601 \[hep-th\]](#).
- [15] D. Baumann, *Cosmology*. Cambridge University Press, 7, 2022.
- [16] S. Weinberg, *Cosmology*. 2008.
- [17] S. Dodelson and F. Schmidt, *Modern Cosmology*. Academic Press, 2020.
- [18] D. H. Lyth and A. Riotto, “Particle physics models of inflation and the cosmological density perturbation,” *Phys. Rept.* **314** (1999) 1–146, [arXiv:hep-ph/9807278](#).
- [19] L. Senatore, “Lectures on inflation,” in *Theoretical Advanced Study Institute in Elementary Particle Physics: New Frontiers in Fields and Strings*, pp. 447–543. 2017. [arXiv:1609.00716 \[hep-th\]](#).
- [20] T. S. Bunch and P. C. W. Davies, “Quantum Field Theory in de Sitter Space: Renormalization by Point Splitting,” *Proc. Roy. Soc. Lond. A* **360** (1978) 117–134.
- [21] B. Allen, “Vacuum States in de Sitter Space,” *Phys. Rev. D* **32** (1985) 3136.
- [22] J. M. Maldacena, “Non-Gaussian features of primordial fluctuations in single field inflationary models,” *JHEP* **05** (2003) 013, [arXiv:astro-ph/0210603 \[astro-ph\]](#).
- [23] S. Weinberg, “Quantum contributions to cosmological correlations,” *Phys. Rev. D* **72** (2005) 043514, [arXiv:hep-th/0506236](#).
- [24] S. Weinberg, “Quantum contributions to cosmological correlations. II. Can these corrections become large?,” *Phys. Rev. D* **74** (2006) 023508, [arXiv:hep-th/0605244](#).
- [25] C. Cheung, P. Creminelli, A. L. Fitzpatrick, J. Kaplan, and L. Senatore, “The Effective Field Theory of Inflation,” *JHEP* **03** (2008) 014, [arXiv:0709.0293 \[hep-th\]](#).

- [26] S. Weinberg, “Effective Field Theory for Inflation,” *Phys. Rev. D* **77** (2008) 123541, [arXiv:0804.4291 \[hep-th\]](#).
- [27] X. Chen, “Primordial Non-Gaussianities from Inflation Models,” *Adv. Astron.* **2010** (2010) 638979, [arXiv:1002.1416 \[astro-ph.CO\]](#).
- [28] Y. Wang, “Inflation, Cosmic Perturbations and Non-Gaussianities,” *Commun. Theor. Phys.* **62** (2014) 109–166, [arXiv:1303.1523 \[hep-th\]](#).
- [29] J. S. Schwinger, “Brownian motion of a quantum oscillator,” *J. Math. Phys.* **2** (1961) 407–432.
- [30] L. V. Keldysh, “Diagram technique for nonequilibrium processes,” *Zh. Eksp. Teor. Fiz.* **47** (1964) 1515–1527.
- [31] N. Arkani-Hamed, P. Benincasa, and A. Postnikov, “Cosmological Polytopes and the Wavefunction of the Universe,” [arXiv:1709.02813 \[hep-th\]](#).
- [32] Y. Wang, G.-B. Zhao, C.-H. Chuang, M. Pellejero-Ibanez, C. Zhao, F.-S. Kitaura, and S. Rodriguez-Torres, “The clustering of galaxies in the completed SDSS-III Baryon Oscillation Spectroscopic Survey: a tomographic analysis of structure growth and expansion rate from anisotropic galaxy clustering,” *Mon. Not. Roy. Astron. Soc.* **481** (2018) no. 3, 3160–3166, [arXiv:1709.05173 \[astro-ph.CO\]](#).
- [33] N. Arkani-Hamed and J. Maldacena, “Cosmological Collider Physics,” [arXiv:1503.08043 \[hep-th\]](#).
- [34] **POLARBEAR** Collaboration, P. A. R. Ade *et al.*, “A Measurement of the Cosmic Microwave Background B-Mode Polarization Power Spectrum at Sub-Degree Scales with POLARBEAR,” *Astrophys. J.* **794** (2014) no. 2, 171, [arXiv:1403.2369 \[astro-ph.CO\]](#). [Erratum: *Astrophys. J.* 848, 73 (2017)].
- [35] S. J. Parke and T. R. Taylor, “An Amplitude for  $n$  Gluon Scattering,” *Phys. Rev. Lett.* **56** (1986) 2459.
- [36] F. A. Berends and W. T. Giele, “Recursive Calculations for Processes with  $n$  Gluons,” *Nucl. Phys. B* **306** (1988) 759–808.
- [37] M. L. Mangano, S. J. Parke, and Z. Xu, “Duality and Multi - Gluon Scattering,” *Nucl. Phys. B* **298** (1988) 653–672.
- [38] F. A. Berends, W. T. Giele, and H. Kuijf, “On relations between multi - gluon and multigraviton scattering,” *Phys. Lett. B* **211** (1988) 91–94.
- [39] F. A. Berends, W. T. Giele, and H. Kuijf, “Exact and Approximate Expressions for Multi - Gluon Scattering,” *Nucl. Phys. B* **333** (1990) 120–159.

- [40] D. A. Kosower, “Light Cone Recurrence Relations for QCD Amplitudes,” *Nucl. Phys. B* **335** (1990) 23–44.
- [41] M. L. Mangano and S. J. Parke, “Multiparton amplitudes in gauge theories,” *Phys. Rept.* **200** (1991) 301–367, [arXiv:hep-th/0509223](#).
- [42] Z. Bern, L. J. Dixon, D. C. Dunbar, and D. A. Kosower, “One loop n point gauge theory amplitudes, unitarity and collinear limits,” *Nucl. Phys. B* **425** (1994) 217–260, [arXiv:hep-ph/9403226](#).
- [43] Z. Bern, L. J. Dixon, D. C. Dunbar, and D. A. Kosower, “Fusing gauge theory tree amplitudes into loop amplitudes,” *Nucl. Phys. B* **435** (1995) 59–101, [arXiv:hep-ph/9409265](#).
- [44] Z. Bern and A. G. Morgan, “Massive loop amplitudes from unitarity,” *Nucl. Phys. B* **467** (1996) 479–509, [arXiv:hep-ph/9511336](#).
- [45] Z. Bern, L. J. Dixon, and D. A. Kosower, “Progress in one loop QCD computations,” *Ann. Rev. Nucl. Part. Sci.* **46** (1996) 109–148, [arXiv:hep-ph/9602280](#).
- [46] Z. Bern, L. J. Dixon, and D. A. Kosower, “Unitarity based techniques for one loop calculations in QCD,” *Nucl. Phys. B Proc. Suppl.* **51** (1996) 243–249, [arXiv:hep-ph/9606378](#).
- [47] Z. Bern, L. J. Dixon, D. C. Dunbar, and D. A. Kosower, “One loop selfdual and N=4 superYang-Mills,” *Phys. Lett. B* **394** (1997) 105–115, [arXiv:hep-th/9611127](#).
- [48] F. Cachazo, P. Svrcek, and E. Witten, “MHV vertices and tree amplitudes in gauge theory,” *JHEP* **09** (2004) 006, [arXiv:hep-th/0403047](#).
- [49] R. Britto, F. Cachazo, and B. Feng, “New recursion relations for tree amplitudes of gluons,” *Nucl. Phys. B* **715** (2005) 499–522, [arXiv:hep-th/0412308](#).
- [50] R. Britto, F. Cachazo, B. Feng, and E. Witten, “Direct proof of tree-level recursion relation in Yang-Mills theory,” *Phys. Rev. Lett.* **94** (2005) 181602, [arXiv:hep-th/0501052](#) [[hep-th](#)].
- [51] J. Bedford, A. Brandhuber, B. J. Spence, and G. Travaglini, “A Recursion relation for gravity amplitudes,” *Nucl. Phys. B* **721** (2005) 98–110, [arXiv:hep-th/0502146](#).
- [52] P. Benincasa, C. Boucher-Veronneau, and F. Cachazo, “Taming Tree Amplitudes In General Relativity,” *JHEP* **11** (2007) 057, [arXiv:hep-th/0702032](#).
- [53] C. Cheung, “On-Shell Recursion Relations for Generic Theories,” *JHEP* **03** (2010) 098, [arXiv:0808.0504](#) [[hep-th](#)].



- [54] N. Arkani-Hamed, F. Cachazo, and J. Kaplan, “What is the Simplest Quantum Field Theory?,” *JHEP* **09** (2010) 016, [arXiv:0808.1446 \[hep-th\]](#).
- [55] L. F. Alday, B. Eden, G. P. Korchemsky, J. Maldacena, and E. Sokatchev, “From correlation functions to Wilson loops,” *JHEP* **09** (2011) 123, [arXiv:1007.3243 \[hep-th\]](#).
- [56] L. J. Mason and D. Skinner, “The Complete Planar S-matrix of N=4 SYM as a Wilson Loop in Twistor Space,” *JHEP* **12** (2010) 018, [arXiv:1009.2225 \[hep-th\]](#).
- [57] S. Caron-Huot, “Notes on the scattering amplitude / Wilson loop duality,” *JHEP* **07** (2011) 058, [arXiv:1010.1167 \[hep-th\]](#).
- [58] J. M. Drummond, J. Henn, V. A. Smirnov, and E. Sokatchev, “Magic identities for conformal four-point integrals,” *JHEP* **01** (2007) 064, [arXiv:hep-th/0607160](#).
- [59] J. M. Drummond, J. M. Henn, and J. Plefka, “Yangian symmetry of scattering amplitudes in N=4 super Yang-Mills theory,” *JHEP* **05** (2009) 046, [arXiv:0902.2987 \[hep-th\]](#).
- [60] N. Arkani-Hamed, J. L. Bourjaily, F. Cachazo, S. Caron-Huot, and J. Trnka, “The All-Loop Integrand For Scattering Amplitudes in Planar N=4 SYM,” *JHEP* **01** (2011) 041, [arXiv:1008.2958 \[hep-th\]](#).
- [61] N. Arkani-Hamed, F. Cachazo, C. Cheung, and J. Kaplan, “A Duality For The S Matrix,” *JHEP* **03** (2010) 020, [arXiv:0907.5418 \[hep-th\]](#).
- [62] N. Arkani-Hamed, J. Bourjaily, F. Cachazo, and J. Trnka, “Local Spacetime Physics from the Grassmannian,” *JHEP* **01** (2011) 108, [arXiv:0912.3249 \[hep-th\]](#).
- [63] N. Arkani-Hamed, F. Cachazo, and C. Cheung, “The Grassmannian Origin Of Dual Superconformal Invariance,” *JHEP* **03** (2010) 036, [arXiv:0909.0483 \[hep-th\]](#).
- [64] C. Sleight and M. Taronna, “Bootstrapping Inflationary Correlators in Mellin Space,” *JHEP* **02** (2020) 098, [arXiv:1907.01143 \[hep-th\]](#).
- [65] C. Sleight and M. Taronna, “From dS to AdS and back,” *JHEP* **12** (2021) 074, [arXiv:2109.02725 \[hep-th\]](#).
- [66] C. Sleight and M. Taronna, “From AdS to dS exchanges: Spectral representation, Mellin amplitudes, and crossing,” *Phys. Rev. D* **104** (2021) no. 8, L081902, [arXiv:2007.09993 \[hep-th\]](#).
- [67] M. Hogervorst, J. a. Penedones, and K. S. Vaziri, “Towards the non-perturbative cosmological bootstrap,” [arXiv:2107.13871 \[hep-th\]](#).

- [68] L. Di Pietro, V. Gorbenko, and S. Komatsu, “Analyticity and unitarity for cosmological correlators,” *JHEP* **03** (2022) 023, [arXiv:2108.01695 \[hep-th\]](#).
- [69] A. Ghosh, N. Kundu, S. Raju, and S. P. Trivedi, “Conformal Invariance and the Four Point Scalar Correlator in Slow-Roll Inflation,” *JHEP* **07** (2014) 011, [arXiv:1401.1426 \[hep-th\]](#).
- [70] S. Albayrak and S. Kharel, “Towards the higher point holographic momentum space amplitudes,” *JHEP* **02** (2019) 040, [arXiv:1810.12459 \[hep-th\]](#).
- [71] S. Albayrak and S. Kharel, “Towards the higher point holographic momentum space amplitudes. Part II. Gravitons,” *JHEP* **12** (2019) 135, [arXiv:1908.01835 \[hep-th\]](#).
- [72] S. Albayrak, C. Chowdhury, and S. Kharel, “New relation for Witten diagrams,” *JHEP* **10** (2019) 274, [arXiv:1904.10043 \[hep-th\]](#).
- [73] S. Albayrak, C. Chowdhury, and S. Kharel, “Study of momentum space scalar amplitudes in AdS spacetime,” *Phys. Rev. D* **101** (2020) no. 12, 124043, [arXiv:2001.06777 \[hep-th\]](#).
- [74] S. Albayrak and S. Kharel, “Spinning loop amplitudes in anti-de Sitter space,” *Phys. Rev. D* **103** (2021) no. 2, 026004, [arXiv:2006.12540 \[hep-th\]](#).
- [75] S. Jazayeri, E. Pajer, and D. Stefanyszyn, “From locality and unitarity to cosmological correlators,” *JHEP* **10** (2021) 065, [arXiv:2103.08649 \[hep-th\]](#).
- [76] H. Goodhew, S. Jazayeri, and E. Pajer, “The Cosmological Optical Theorem,” *JCAP* **04** (2021) 021, [arXiv:2009.02898 \[hep-th\]](#).
- [77] S. Melville and G. L. Pimentel, “de Sitter S matrix for the masses,” *Phys. Rev. D* **110** (2024) no. 10, 103530, [arXiv:2309.07092 \[hep-th\]](#).
- [78] S. Melville and G. L. Pimentel, “A de Sitter S-matrix from amputated cosmological correlators,” *JHEP* **08** (2024) 211, [arXiv:2404.05712 \[hep-th\]](#).
- [79] P. Benincasa, A. J. McLeod, and C. Vergu, “Steinmann Relations and the Wavefunction of the Universe,” *Phys. Rev. D* **102** (2020) 125004, [arXiv:2009.03047 \[hep-th\]](#).
- [80] P. Benincasa, “Amplitudes meet Cosmology: A (Scalar) Primer,” [arXiv:2203.15330 \[hep-th\]](#).
- [81] M. Carrillo González and S. Céspedes, “Causality Bounds on the Primordial Power Spectrum,” [arXiv:2502.19477 \[hep-th\]](#).
- [82] J. M. Maldacena and G. L. Pimentel, “On graviton non-Gaussianities during inflation,” *JHEP* **09** (2011) 045, [arXiv:1104.2846 \[hep-th\]](#).

- [83] N. Arkani-Hamed, P. Benincasa, and A. Postnikov, “Cosmological Polytopes and the Wavefunction of the Universe,” [arXiv:1709.02813 \[hep-th\]](#).
- [84] P. Benincasa, “Amplitudes meet Cosmology: A (Scalar) Primer,” [arXiv:2203.15330 \[hep-th\]](#).
- [85] N. Arkani-Hamed and P. Benincasa, “On the Emergence of Lorentz Invariance and Unitarity from the Scattering Facet of Cosmological Polytopes,” [arXiv:1811.01125 \[hep-th\]](#).
- [86] P. Benincasa, “From the flat-space S-matrix to the Wavefunction of the Universe,” [arXiv:1811.02515 \[hep-th\]](#).
- [87] N. Arkani-Hamed, D. Baumann, H. Lee, and G. L. Pimentel, “The Cosmological Bootstrap: Inflationary Correlators from Symmetries and Singularities,” [arXiv:1811.00024 \[hep-th\]](#).
- [88] D. Baumann, D. Green, A. Joyce, E. Pajer, G. L. Pimentel, C. Sleight, and M. Taronna, “Snowmass White Paper: The Cosmological Bootstrap,” in *2022 Snowmass Summer Study*, 3, 2022. [arXiv:2203.08121 \[hep-th\]](#).
- [89] D. Baumann, C. Duaso Pueyo, A. Joyce, H. Lee, and G. L. Pimentel, “The cosmological bootstrap: weight-shifting operators and scalar seeds,” *JHEP* **12** (2020) 204, [arXiv:1910.14051 \[hep-th\]](#).
- [90] D. Baumann, C. Duaso Pueyo, A. Joyce, H. Lee, and G. L. Pimentel, “The Cosmological Bootstrap: Spinning Correlators from Symmetries and Factorization,” [arXiv:2005.04234 \[hep-th\]](#).
- [91] P. Benincasa and G. Dian, “The Geometry of Cosmological Correlators,” [arXiv:2401.05207 \[hep-th\]](#).
- [92] N. Arkani-Hamed and J. Trnka, “The Amplituhedron,” *JHEP* **10** (2014) 030, [arXiv:1312.2007 \[hep-th\]](#).
- [93] N. Arkani-Hamed, Y. Bai, S. He, and G. Yan, “Scattering Forms and the Positive Geometry of Kinematics, Color and the Worldsheet,” *JHEP* **05** (2018) 096, [arXiv:1711.09102 \[hep-th\]](#).
- [94] H. Frost, “Biadjoint scalar tree amplitudes and intersecting dual associahedra,” *JHEP* **06** (2018) 153, [arXiv:1802.03384 \[hep-th\]](#).
- [95] P. Banerjee, A. Laddha, and P. Raman, “Stokes polytopes: the positive geometry for  $\phi^4$  interactions,” *JHEP* **08** (2019) 067, [arXiv:1811.05904 \[hep-th\]](#).
- [96] G. Salvatori and S. Stanojevic, “Scattering Amplitudes and Simple Canonical Forms for Simple Polytopes,” *JHEP* **03** (2021) 067, [arXiv:1912.06125 \[hep-th\]](#).

- [97] P. Raman, “The positive geometry for  $\phi^p$  interactions,” [arXiv:1906.02985](#) [[hep-th](#)].
- [98] P. B. Aneesh, M. Jagadale, and N. Kalyanapuram, “Accordiohedra as positive geometries for generic scalar field theories,” *Phys. Rev. D* **100** (2019) no. 10, 106013, [arXiv:1906.12148](#) [[hep-th](#)].
- [99] L. Ferro and T. Lukowski, “Amplituhedra, and beyond,” *J. Phys. A* **54** (2021) no. 3, 033001, [arXiv:2007.04342](#) [[hep-th](#)].
- [100] E. Herrmann and J. Trnka, “The SAGEX Review on Scattering Amplitudes, Chapter 7: Positive Geometry of Scattering Amplitudes,” [arXiv:2203.13018](#) [[hep-th](#)].
- [101] N. Arkani-Hamed, S. He, G. Salvatori, and H. Thomas, “Causal diamonds, cluster polytopes and scattering amplitudes,” *JHEP* **11** (2022) 049, [arXiv:1912.12948](#) [[hep-th](#)].
- [102] N. Arkani-Hamed, H. Frost, G. Salvatori, P.-G. Plamondon, and H. Thomas, “All Loop Scattering As A Counting Problem,” [arXiv:2309.15913](#) [[hep-th](#)].
- [103] N. Arkani-Hamed, H. Frost, G. Salvatori, P.-G. Plamondon, and H. Thomas, “All Loop Scattering For All Multiplicity,” [arXiv:2311.09284](#) [[hep-th](#)].
- [104] N. Arkani-Hamed, T.-C. Huang, and Y.-T. Huang, “The EFT-Hedron,” *JHEP* **05** (2021) 259, [arXiv:2012.15849](#) [[hep-th](#)].
- [105] N. Arkani-Hamed, S. He, and T. Lam, “Stringy canonical forms,” *JHEP* **02** (2021) 069, [arXiv:1912.08707](#) [[hep-th](#)].
- [106] S. He, Z. Li, P. Raman, and C. Zhang, “Stringy canonical forms and binary geometries from associahedra, cyclohedra and generalized permutohedra,” *JHEP* **10** (2020) 054, [arXiv:2005.07395](#) [[hep-th](#)].
- [107] N. Arkani-Hamed, Q. Cao, J. Dong, C. Figueiredo, and S. He, “Surface Kinematics and ”The” Yang-Mills Integrand,” [arXiv:2408.11891](#) [[hep-th](#)].
- [108] N. Arkani-Hamed and C. Figueiredo, “Circles and Triangles, the NLSM and  $\text{Tr}(\Phi^3)$ ,” [arXiv:2403.04826](#) [[hep-th](#)].
- [109] N. Arkani-Hamed, Q. Cao, J. Dong, C. Figueiredo, and S. He, “Scalar-Scaffolded Gluons and the Combinatorial Origins of Yang-Mills Theory,” [arXiv:2401.00041](#) [[hep-th](#)].
- [110] N. Arkani-Hamed, Q. Cao, J. Dong, C. Figueiredo, and S. He, “Hidden zeros for particle/string amplitudes and the unity of colored scalars, pions and gluons,” [arXiv:2312.16282](#) [[hep-th](#)].

- [111] N. Arkani-Hamed, Q. Cao, J. Dong, C. Figueiredo, and S. He, “NLSM  $\subset$   $\text{Tr}(\phi^3)$ ,” [arXiv:2401.05483](#) [hep-th].
- [112] N. Arkani-Hamed, D. Baumann, A. Hillman, A. Joyce, H. Lee, and G. L. Pimentel, “Differential Equations for Cosmological Correlators,” [arXiv:2312.05303](#) [hep-th].
- [113] C. Chowdhury, A. Lipstein, J. Mei, I. Sachs, and P. Vanhove, “The Subtle Simplicity of Cosmological Correlators,” [arXiv:2312.13803](#) [hep-th].
- [114] T. Heckelbacher, I. Sachs, E. Skvortsov, and P. Vanhove, “Analytical evaluation of cosmological correlation functions,” *JHEP* **08** (2022) 139, [arXiv:2204.07217](#) [hep-th].
- [115] C. Chowdhury, A. Lipstein, J. Marshall, J. Mei, and I. Sachs, “Cosmological Dressing Rules,” [arXiv:2503.10598](#) [hep-th].
- [116] P. Benincasa, G. Brunello, M. K. Mandal, P. Mastrolia, and F. Vazão, “On one-loop corrections to the Bunch-Davies wavefunction of the universe,” [arXiv:2408.16386](#) [hep-th].
- [117] C. Chowdhury and K. Singh, “Analytic results for loop-level momentum space Witten diagrams,” *JHEP* **12** (2023) 109, [arXiv:2305.18529](#) [hep-th].
- [118] J. M. Henn, “Multiloop integrals in dimensional regularization made simple,” *Phys. Rev. Lett.* **110** (2013) 251601, [arXiv:1304.1806](#) [hep-th].
- [119] L. H. Ford, “Quantum Instability of De Sitter Space-time,” *Phys. Rev. D* **31** (1985) 710.
- [120] I. Antoniadis, J. Iliopoulos, and T. N. Tomaras, “Quantum Instability of De Sitter Space,” *Phys. Rev. Lett.* **56** (1986) 1319.
- [121] N. C. Tsamis and R. P. Woodard, “Strong infrared effects in quantum gravity,” *Annals Phys.* **238** (1995) 1–82.
- [122] N. C. Tsamis and R. P. Woodard, “The Quantum gravitational back reaction on inflation,” *Annals Phys.* **253** (1997) 1–54, [arXiv:hep-ph/9602316](#).
- [123] N. C. Tsamis and R. P. Woodard, “Matter contributions to the expansion rate of the universe,” *Phys. Lett. B* **426** (1998) 21–28, [arXiv:hep-ph/9710466](#).
- [124] A. M. Polyakov, “De Sitter space and eternity,” *Nucl. Phys. B* **797** (2008) 199–217, [arXiv:0709.2899](#) [hep-th].
- [125] L. Senatore and M. Zaldarriaga, “On Loops in Inflation,” *JHEP* **12** (2010) 008, [arXiv:0912.2734](#) [hep-th].

- [126] A. M. Polyakov, “Decay of Vacuum Energy,” *Nucl. Phys. B* **834** (2010) 316–329, [arXiv:0912.5503 \[hep-th\]](#).
- [127] S. B. Giddings and M. S. Sloth, “Semiclassical relations and IR effects in de Sitter and slow-roll space-times,” *JCAP* **01** (2011) 023, [arXiv:1005.1056 \[hep-th\]](#).
- [128] S. B. Giddings and M. S. Sloth, “Cosmological diagrammatic rules,” *JCAP* **07** (2010) 015, [arXiv:1005.3287 \[hep-th\]](#).
- [129] C. P. Burgess, R. Holman, L. Leblond, and S. Shandera, “Breakdown of Semiclassical Methods in de Sitter Space,” *JCAP* **10** (2010) 017, [arXiv:1005.3551 \[hep-th\]](#).
- [130] D. Marolf and I. A. Morrison, “The IR stability of de Sitter QFT: results at all orders,” *Phys. Rev. D* **84** (2011) 044040, [arXiv:1010.5327 \[gr-qc\]](#).
- [131] D. Marolf and I. A. Morrison, “The IR stability of de Sitter: Loop corrections to scalar propagators,” *Phys. Rev. D* **82** (2010) 105032, [arXiv:1006.0035 \[gr-qc\]](#).
- [132] A. Rajaraman, “On the proper treatment of massless fields in Euclidean de Sitter space,” *Phys. Rev. D* **82** (2010) 123522, [arXiv:1008.1271 \[hep-th\]](#).
- [133] D. Krotov and A. M. Polyakov, “Infrared Sensitivity of Unstable Vacua,” *Nucl. Phys. B* **849** (2011) 410–432, [arXiv:1012.2107 \[hep-th\]](#).
- [134] S. B. Giddings and M. S. Sloth, “Cosmological observables, IR growth of fluctuations, and scale-dependent anisotropies,” *Phys. Rev. D* **84** (2011) 063528, [arXiv:1104.0002 \[hep-th\]](#).
- [135] D. Marolf and I. A. Morrison, “The IR stability of de Sitter QFT: Physical initial conditions,” *Gen. Rel. Grav.* **43** (2011) 3497–3530, [arXiv:1104.4343 \[gr-qc\]](#).
- [136] S. B. Giddings and M. S. Sloth, “Fluctuating geometries, q-observables, and infrared growth in inflationary spacetimes,” *Phys. Rev. D* **86** (2012) 083538, [arXiv:1109.1000 \[hep-th\]](#).
- [137] L. Senatore and M. Zaldarriaga, “On Loops in Inflation II: IR Effects in Single Clock Inflation,” *JHEP* **01** (2013) 109, [arXiv:1203.6354 \[hep-th\]](#).
- [138] G. L. Pimentel, L. Senatore, and M. Zaldarriaga, “On Loops in Inflation III: Time Independence of zeta in Single Clock Inflation,” *JHEP* **07** (2012) 166, [arXiv:1203.6651 \[hep-th\]](#).
- [139] A. M. Polyakov, “Infrared instability of the de Sitter space,” [arXiv:1209.4135 \[hep-th\]](#).

- [140] L. Senatore and M. Zaldarriaga, “A Note on the Consistency Condition of Primordial Fluctuations,” *JCAP* **1208** (2012) 001, [arXiv:1203.6884 \[astro-ph.CO\]](#).
- [141] M. Beneke and P. Moch, “On “dynamical mass” generation in Euclidean de Sitter space,” *Phys. Rev. D* **87** (2013) 064018, [arXiv:1212.3058 \[hep-th\]](#).
- [142] E. T. Akhmedov, “Lecture notes on interacting quantum fields in de Sitter space,” *Int. J. Mod. Phys. D* **23** (2014) 1430001, [arXiv:1309.2557 \[hep-th\]](#).
- [143] D. Anninos, “De Sitter Musings,” *Int. J. Mod. Phys. A* **27** (2012) 1230013, [arXiv:1205.3855 \[hep-th\]](#).
- [144] E. T. Akhmedov, U. Moschella, K. E. Pavlenko, and F. K. Popov, “Infrared dynamics of massive scalars from the complementary series in de Sitter space,” *Phys. Rev. D* **96** (2017) no. 2, 025002, [arXiv:1701.07226 \[hep-th\]](#).
- [145] B.-L. Hu, “Infrared Behavior of Quantum Fields in Inflationary Cosmology – Issues and Approaches: an overview,” [arXiv:1812.11851 \[gr-qc\]](#).
- [146] E. T. Akhmedov, U. Moschella, and F. K. Popov, “Characters of different secular effects in various patches of de Sitter space,” *Phys. Rev. D* **99** (2019) no. 8, 086009, [arXiv:1901.07293 \[hep-th\]](#).
- [147] V. Gorbenko and L. Senatore, “ $\lambda\phi^4$  in dS,” [arXiv:1911.00022 \[hep-th\]](#).
- [148] M. Mirbabayi, “Infrared dynamics of a light scalar field in de Sitter,” *JCAP* **12** (2020) 006, [arXiv:1911.00564 \[hep-th\]](#).
- [149] M. Baumgart and R. Sundrum, “De Sitter Diagrammar and the Resummation of Time,” *JHEP* **07** (2020) 119, [arXiv:1912.09502 \[hep-th\]](#).
- [150] T. Cohen and D. Green, “Soft de Sitter Effective Theory,” *JHEP* **12** (2020) 041, [arXiv:2007.03693 \[hep-th\]](#).
- [151] D. Green and R. A. Porto, “Signals of a Quantum Universe,” *Phys. Rev. Lett.* **124** (2020) no. 25, 251302, [arXiv:2001.09149 \[hep-th\]](#).
- [152] M. Baumgart and R. Sundrum, “Manifestly Causal In-In Perturbation Theory about the Interacting Vacuum,” *JHEP* **03** (2021) 080, [arXiv:2010.10785 \[hep-th\]](#).
- [153] M. Mirbabayi, “Markovian dynamics in de Sitter,” *JCAP* **09** (2021) 038, [arXiv:2010.06604 \[hep-th\]](#).
- [154] T. Cohen, D. Green, A. Premkumar, and A. Ridgway, “Stochastic Inflation at NNLO,” *JHEP* **09** (2021) 159, [arXiv:2106.09728 \[hep-th\]](#).

- [155] A. Premkumar, “Regulating loops in de Sitter spacetime,” *Phys. Rev. D* **109** (2024) no. 4, 045003, [arXiv:2110.12504 \[hep-th\]](#).
- [156] S. Céspedes, A.-C. Davis, and D.-G. Wang, “On the IR Divergences in de Sitter Space: loops, resummation and the semi-classical wavefunction,” [arXiv:2311.17990 \[hep-th\]](#).
- [157] A. Bzowski, P. McFadden, and K. Skenderis, “Renormalisation of IR divergences and holography in de Sitter,” [arXiv:2312.17316 \[hep-th\]](#).
- [158] D. Boyanovsky and H. J. de Vega, “Particle decay in inflationary cosmology,” *Phys. Rev. D* **70** (2004) 063508, [arXiv:astro-ph/0406287](#).
- [159] D. Boyanovsky, H. J. de Vega, and N. G. Sanchez, “Particle decay during inflation: Self-decay of inflaton quantum fluctuations during slow roll,” *Phys. Rev. D* **71** (2005) 023509, [arXiv:astro-ph/0409406](#).
- [160] D. Boyanovsky, H. J. de Vega, and N. G. Sanchez, “Quantum corrections to slow roll inflation and new scaling of superhorizon fluctuations,” *Nucl. Phys. B* **747** (2006) 25–54, [arXiv:astro-ph/0503669](#).
- [161] D. Boyanovsky, H. J. de Vega, and N. G. Sanchez, “Quantum corrections to the inflaton potential and the power spectra from superhorizon modes and trace anomalies,” *Phys. Rev. D* **72** (2005) 103006, [arXiv:astro-ph/0507596](#).
- [162] D. I. Podolsky, “Dynamical renormalization group methods in theory of eternal inflation,” *Grav. Cosmol.* **15** (2009) 69–74, [arXiv:0809.2453 \[gr-qc\]](#).
- [163] C. P. Burgess, L. Leblond, R. Holman, and S. Shandera, “Super-Hubble de Sitter Fluctuations and the Dynamical RG,” *JCAP* **03** (2010) 033, [arXiv:0912.1608 \[hep-th\]](#).
- [164] C. P. Burgess, R. Holman, and G. Tasinato, “Open EFTs, IR effects & late-time resummations: systematic corrections in stochastic inflation,” *JHEP* **01** (2016) 153, [arXiv:1512.00169 \[gr-qc\]](#).
- [165] P. Benincasa and F. Vazão, “The Asymptotic Structure of Cosmological Integrals,” [arXiv:2402.06558 \[hep-th\]](#).
- [166] A. Achúcarro, V. Atal, C. Germani, and G. A. Palma, “Cumulative effects in inflation with ultra-light entropy modes,” *JCAP* **02** (2017) 013, [arXiv:1607.08609 \[astro-ph.CO\]](#).
- [167] D.-G. Wang, G. L. Pimentel, and A. Achúcarro, “Bootstrapping multi-field inflation: non-Gaussianities from light scalars revisited,” *JCAP* **05** (2023) 043, [arXiv:2212.14035 \[astro-ph.CO\]](#).



- [168] A. Achucarro, S. Cespedes, A.-C. Davis, and G. A. Palma, “The hand-made tail: non-perturbative tails from multifield inflation,” *JHEP* **05** (2022) 052, [arXiv:2112.14712 \[hep-th\]](#).
- [169] G. Panagopoulos and E. Silverstein, “Primordial Black Holes from non-Gaussian tails,” [arXiv:1906.02827 \[hep-th\]](#).
- [170] P. Creminelli, S. Dubovsky, A. Nicolis, L. Senatore, and M. Zaldarriaga, “The Phase Transition to Slow-roll Eternal Inflation,” *JHEP* **09** (2008) 036, [arXiv:0802.1067 \[hep-th\]](#).
- [171] N. Arkani-Hamed, S. Dubovsky, A. Nicolis, E. Trincherini, and G. Villadoro, “A Measure of de Sitter entropy and eternal inflation,” *JHEP* **05** (2007) 055, [arXiv:0704.1814 \[hep-th\]](#).
- [172] S. Dubovsky, L. Senatore, and G. Villadoro, “The Volume of the Universe after Inflation and de Sitter Entropy,” *JHEP* **04** (2009) 118, [arXiv:0812.2246 \[hep-th\]](#).
- [173] M. Lewandowski and A. Perko, “Leading slow roll corrections to the volume of the universe and the entropy bound,” *JHEP* **12** (2014) 060, [arXiv:1309.6705 \[hep-th\]](#).
- [174] D. H. Lyth and Y. Rodriguez, “The Inflationary prediction for primordial non-Gaussianity,” *Phys. Rev. Lett.* **95** (2005) 121302, [arXiv:astro-ph/0504045](#).
- [175] M. Sasaki and E. D. Stewart, “A General analytic formula for the spectral index of the density perturbations produced during inflation,” *Prog. Theor. Phys.* **95** (1996) 71–78, [arXiv:astro-ph/9507001](#).
- [176] D. Wands, “Local non-Gaussianity from inflation,” *Class. Quant. Grav.* **27** (2010) 124002, [arXiv:1004.0818 \[astro-ph.CO\]](#).
- [177] A. A. Starobinsky, “Multicomponent de Sitter (Inflationary) Stages and the Generation of Perturbations,” *JETP Lett.* **42** (1985) 152–155.
- [178] T. Tanaka, T. Suyama, and S. Yokoyama, “Use of delta N formalism - Difficulties in generating large local-type non-Gaussianity during inflation -,” *Class. Quant. Grav.* **27** (2010) 124003, [arXiv:1003.5057 \[astro-ph.CO\]](#).
- [179] D. Seery, “One-loop corrections to the curvature perturbation from inflation,” *JCAP* **02** (2008) 006, [arXiv:0707.3378 \[astro-ph\]](#).
- [180] M. van der Meulen and J. Smit, “Classical approximation to quantum cosmological correlations,” *JCAP* **11** (2007) 023, [arXiv:0707.0842 \[hep-th\]](#).

- [181] A. A. Starobinsky, “Stochastic De Sitter (Inflationary) Stage in the Early Universe,” *Lect. Notes Phys.* **246** (1986) 107–126.
- [182] A. A. Starobinsky and J. Yokoyama, “Equilibrium state of a selfinteracting scalar field in the De Sitter background,” *Phys. Rev. D* **50** (1994) 6357–6368, [arXiv:astro-ph/9407016](#).
- [183] P. Benincasa and F. Vazão, “Cosmological Infrared Subtractions & Infrared-Safe Computables,” [arXiv:2405.19979](#) [[hep-th](#)].
- [184] M. Beneke, P. Hager, and A. F. Sanfilippo, “Cosmological Correlators in massless  $\phi^4$ -theory and the Method of Regions,” [arXiv:2312.06766](#) [[hep-th](#)].
- [185] G. F. Sterman and M. E. Tejeda-Yeomans, “Multiloop amplitudes and resummation,” *Phys. Lett. B* **552** (2003) 48–56, [arXiv:hep-ph/0210130](#).
- [186] P. Benincasa, M. Giroux, H. S. Hannesdottir, S. Mizera, C. Pasiecznik, and F. Vazão, “Records from the S-Matrix Marathon: Observables in Expanding Universes,” 9, 2024. [arXiv:2409.14947](#) [[hep-th](#)].
- [187] P. Benincasa, G. Brunello, M. K. Mandal, P. Mastrolia, and F. Vazão, “On one-loop corrections to the Bunch-Davies wavefunction of the universe,” [arXiv:2408.16386](#) [[hep-th](#)].
- [188] N. Arkani-Hamed, C. Figueiredo, and F. Vazão, “Cosmohedra,” [arXiv:2412.19881](#) [[hep-th](#)].
- [189] P. Benincasa, “Cosmological Polytopes and the Wavefunction of the Universe for Light States,” [arXiv:1909.02517](#) [[hep-th](#)].
- [190] N. Bittermann and A. Joyce, “Soft limits of the wavefunction in exceptional scalar theories,” *JHEP* **03** (2023) 092, [arXiv:2203.05576](#) [[hep-th](#)].
- [191] D. Anninos, T. Anous, D. Z. Freedman, and G. Konstantinidis, “Late-time Structure of the Bunch-Davies De Sitter Wavefunction,” *JCAP* **1511** (2015) no. 11, 048, [arXiv:1406.5490](#) [[hep-th](#)].
- [192] A. Hillman and E. Pajer, “A Differential Representation of Cosmological Wavefunctions,” [arXiv:2112.01619](#) [[hep-th](#)].
- [193] P. Benincasa and W. J. T. Bobadilla, “Physical representations for scattering amplitudes and the wavefunction of the universe,” *SciPost Phys.* **12** (2022) no. 6, 192, [arXiv:2112.09028](#) [[hep-th](#)].
- [194] P. Benincasa and G. Dian, “The Geometry of Cosmological Correlators,” [arXiv:2401.05207](#) [[hep-th](#)].

- [195] P. Benincasa and W. J. T. Bobadilla, “Physical representations for scattering amplitudes and the wavefunction of the universe,” *SciPost Phys.* **12** (2022) no. 6, 192, [arXiv:2112.09028 \[hep-th\]](#).
- [196] M. Juhnke-Kubitzke, L. Solus, and L. Venturello, “Triangulations of cosmological polytopes,” [arXiv:2303.05876 \[math.CO\]](#).
- [197] P. Benincasa and M. Parisi, “Positive geometries and differential forms with non-logarithmic singularities. Part I,” *JHEP* **08** (2020) no. 08, 023, [arXiv:2005.03612 \[hep-th\]](#).
- [198] G. Dian, P. Heslop, and A. Stewart, “Internal boundaries of the loop amplituhedron,” *SciPost Phys.* **15** (2023) no. 3, 098, [arXiv:2207.12464 \[hep-th\]](#).
- [199] N. Arkani-Hamed, D. Baumann, A. Hillman, A. Joyce, H. Lee, and G. L. Pimentel, “Differential Equations for Cosmological Correlators,” [arXiv:2312.05303 \[hep-th\]](#).
- [200] N. Arkani-Hamed, C. Figueiredo, H. Frost, and G. Salvatori, “Tropical Amplitudes For Colored Lagrangians,” [arXiv:2402.06719 \[hep-th\]](#).
- [201] E. R. Speer, “Analytic renormalization,” *Journal of Mathematical Physics* **9** (1968) no. 9, 1404–1410, <https://doi.org/10.1063/1.1664729>.  
<https://doi.org/10.1063/1.1664729>.
- [202] S. Albayrak, P. Benincasa, and C. D. Pueyo, “Perturbative Unitarity and the Wavefunction of the Universe,” [arXiv:2305.19686 \[hep-th\]](#).
- [203] L. M. Blumenthal, *Theory and Applications of Distance Geometry*. Chealsea, New York, 1970.
- [204] C. D’Andrea and M. Sombra, “The Cayley-Menger determinant is irreducible for  $n \geq 3$ ,” [arXiv:math/0406359 \[math.AC\]](#).
- [205] L. Nilsson and M. Passare, “Mellin transforms of multivariate rational functions,” *Journal of Geometric Analysis* **23** (2010) , [arXiv:1010.5060 \[math.CV\]](#).
- [206] C. Berkesch, J. Forsgard, and M. Passare, “Euler-Mellin integrals and A-hypergeometric functions,” [arXiv:1103.6273 \[math.CV\]](#).
- [207] T. Binoth and G. Heinrich, “An automatized algorithm to compute infrared divergent multiloop integrals,” *Nucl. Phys. B* **585** (2000) 741–759, [arXiv:hep-ph/0004013](#).
- [208] T. Binoth and G. Heinrich, “Numerical evaluation of multiloop integrals by sector decomposition,” *Nucl. Phys. B* **680** (2004) 375–388, [arXiv:hep-ph/0305234](#).

- [209] C. Bogner and S. Weinzierl, “Resolution of singularities for multi-loop integrals,” *Comput. Phys. Commun.* **178** (2008) 596–610, [arXiv:0709.4092 \[hep-ph\]](#).
- [210] G. Heinrich, “Sector Decomposition,” *Int. J. Mod. Phys. A* **23** (2008) 1457–1486, [arXiv:0803.4177 \[hep-ph\]](#).
- [211] T. Kaneko and T. Ueda, “A Geometric method of sector decomposition,” *Comput. Phys. Commun.* **181** (2010) 1352–1361, [arXiv:0908.2897 \[hep-ph\]](#).
- [212] T. Kaneko and T. Ueda, “Sector Decomposition Via Computational Geometry,” *PoS ACAT2010* (2010) 082, [arXiv:1004.5490 \[hep-ph\]](#).
- [213] N. Arkani-Hamed, A. Hillman, and S. Mizera, “Feynman polytopes and the tropical geometry of UV and IR divergences,” *Phys. Rev. D* **105** (2022) no. 12, 125013, [arXiv:2202.12296 \[hep-th\]](#).
- [214] E. Panzer, “Hepp’s bound for Feynman graphs and matroids,” *Ann. Inst. H. Poincaré D Comb. Phys. Interact.* **10** (2022) no. 1, 31–119, [arXiv:1908.09820 \[math-ph\]](#).
- [215] J. Drummond, J. Foster, O. Gürdoğan, and C. Kalousios, “Algebraic singularities of scattering amplitudes from tropical geometry,” *JHEP* **04** (2021) 002, [arXiv:1912.08217 \[hep-th\]](#).
- [216] J. Drummond, J. Foster, O. Gürdoğan, and C. Kalousios, “Tropical fans, scattering equations and amplitudes,” *JHEP* **11** (2021) 071, [arXiv:2002.04624 \[hep-th\]](#).
- [217] M. Borinsky, H. J. Munch, and F. Tellander, “Tropical Feynman integration in the Minkowski regime,” *Comput. Phys. Commun.* **292** (2023) 108874, [arXiv:2302.08955 \[hep-ph\]](#).
- [218] A. Postnikov, “Permutohedra, associahedra, and beyond,” [arXiv:math/0507163 \[math.CO\]](#).
- [219] Postnikov, Alexander and Reiner, Victor and Williams, Lauren, “Faces of Generalized Permutohedra,” [arXiv:math/0609184 \[math.CO\]](#).
- [220] M. Carr and S. L. Devadoss, “Coxeter complexes and graph-associahedra,” [arXiv:math/0407229 \[math.QA\]](#).
- [221] S. L. Devadoss, “A Realization of Graph-Associahedra,” [arXiv:math/0612530 \[math.CO\]](#).
- [222] C. Anastasiou and G. Sterman, “Removing infrared divergences from two-loop integrals,” *JHEP* **07** (2019) 056, [arXiv:1812.03753 \[hep-ph\]](#).

- [223] D. Green, M. Lewandowski, L. Senatore, E. Silverstein, and M. Zaldarriaga, “Anomalous Dimensions and Non-Gaussianity,” *JHEP* **10** (2013) 171, [arXiv:1301.2630 \[hep-th\]](#).
- [224] X. Chen, Y. Wang, and Z.-Z. Xianyu, “Standard Model Mass Spectrum in Inflationary Universe,” *JHEP* **04** (2017) 058, [arXiv:1612.08122 \[hep-th\]](#).
- [225] X. Chen, Y. Wang, and Z.-Z. Xianyu, “Standard Model Background of the Cosmological Collider,” *Phys. Rev. Lett.* **118** (2017) no. 26, 261302, [arXiv:1610.06597 \[hep-th\]](#).
- [226] M. McAneny, A. K. Ridgway, M. P. Solon, and M. B. Wise, “Stochastic bias from loops of massive particles during inflation,” *Phys. Lett. B* **785** (2018) 332–337, [arXiv:1712.07657 \[astro-ph.CO\]](#).
- [227] J. M. Henn, “Multiloop integrals in dimensional regularization made simple,” *Phys. Rev. Lett.* **110** (2013) 251601, [arXiv:1304.1806 \[hep-th\]](#).
- [228] J. Henn, A. Matijašić, J. Miczajka, T. Peraro, Y. Xu, and Y. Zhang, “Complete function space for planar two-loop six-particle scattering amplitudes,” [arXiv:2501.01847 \[hep-ph\]](#).
- [229] N. Arkani-Hamed, D. Baumann, A. Hillman, A. Joyce, H. Lee, and G. L. Pimentel, “Differential Equations for Cosmological Correlators,” [arXiv:2312.05303 \[hep-th\]](#).
- [230] N. Arkani-Hamed, D. Baumann, A. Hillman, A. Joyce, H. Lee, and G. L. Pimentel, “Kinematic Flow and the Emergence of Time,” [arXiv:2312.05300 \[hep-th\]](#).
- [231] J. Bosma, K. J. Larsen, and Y. Zhang, “Differential equations for loop integrals in Baikov representation,” *Phys. Rev. D* **97** (2018) no. 10, 105014, [arXiv:1712.03760 \[hep-th\]](#).
- [232] K. J. Larsen and Y. Zhang, “Integration-by-parts reductions from unitarity cuts and algebraic geometry,” *Phys. Rev. D* **93** (2016) no. 4, 041701, [arXiv:1511.01071 \[hep-th\]](#).
- [233] K.-T. Chen, “Iterated path integrals,” *Bull. Am. Math. Soc.* **83** (1977) 831–879.
- [234] S. Müller-Stach, S. Weinzierl, and R. Zayadeh, “Picard-Fuchs equations for Feynman integrals,” *Commun. Math. Phys.* **326** (2014) 237–249, [arXiv:1212.4389 \[hep-ph\]](#).
- [235] L. Adams, E. Chaubey, and S. Weinzierl, “Simplifying Differential Equations for Multiscale Feynman Integrals beyond Multiple Polylogarithms,” *Phys. Rev. Lett.* **118** (2017) no. 14, 141602, [arXiv:1702.04279 \[hep-ph\]](#).

- [236] E. Remiddi and J. A. M. Vermaseren, “Harmonic polylogarithms,” *Int. J. Mod. Phys. A* **15** (2000) 725–754, [arXiv:hep-ph/9905237](#).
- [237] A. B. Goncharov, “Multiple polylogarithms, cyclotomy and modular complexes,” *Math. Res. Lett.* **5** (1998) 497–516, [arXiv:1105.2076](#) [math.AG].
- [238] J. Broedel, C. Duhr, F. Dulat, and L. Tancredi, “Elliptic polylogarithms and iterated integrals on elliptic curves II: an application to the sunrise integral,” *Phys. Rev. D* **97** (2018) no. 11, 116009, [arXiv:1712.07095](#) [hep-ph].
- [239] D. J. Broadhurst, J. Fleischer, and O. V. Tarasov, “Two loop two point functions with masses: Asymptotic expansions and Taylor series, in any dimension,” *Z. Phys. C* **60** (1993) 287–302, [arXiv:hep-ph/9304303](#).
- [240] J. Broedel, C. Duhr, F. Dulat, B. Penante, and L. Tancredi, “Elliptic symbol calculus: from elliptic polylogarithms to iterated integrals of Eisenstein series,” *JHEP* **08** (2018) 014, [arXiv:1803.10256](#) [hep-th].
- [241] P. A. Baikov, “Explicit solutions of the multiloop integral recurrence relations and its application,” *Nucl. Instrum. Meth. A* **389** (1997) 347–349, [arXiv:hep-ph/9611449](#).
- [242] H. Frellesvig and C. G. Papadopoulos, “Cuts of Feynman Integrals in Baikov representation,” *JHEP* **04** (2017) 083, [arXiv:1701.07356](#) [hep-ph].
- [243] M. Argeri, S. Di Vita, P. Mastrolia, E. Mirabella, J. Schlenk, U. Schubert, and L. Tancredi, “Magnus and Dyson Series for Master Integrals,” *JHEP* **03** (2014) 082, [arXiv:1401.2979](#) [hep-ph].
- [244] R. N. Lee, “Reducing differential equations for multiloop master integrals,” *JHEP* **04** (2015) 108, [arXiv:1411.0911](#) [hep-ph].
- [245] J. Vollinga and S. Weinzierl, “Numerical evaluation of multiple polylogarithms,” *Comput. Phys. Commun.* **167** (2005) 177, [arXiv:hep-ph/0410259](#).
- [246] C. Duhr and F. Dulat, “PolyLogTools — polylogs for the masses,” *JHEP* **08** (2019) 135, [arXiv:1904.07279](#) [hep-th].
- [247] S. Foffa, P. Mastrolia, R. Sturani, and C. Sturm, “Effective field theory approach to the gravitational two-body dynamics, at fourth post-Newtonian order and quintic in the Newton constant,” *Phys. Rev. D* **95** (2017) no. 10, 104009, [arXiv:1612.00482](#) [gr-qc].
- [248] Y. Brychkov, O. Marichev, and N. Savischenko, *Handbook of Mellin Transforms*. 10, 2018.

- 
- [249] I. Gonzalez, “Method of Brackets and Feynman diagrams evaluation,” *Nucl. Phys. B Proc. Suppl.* **205-206** (2010) 141–146, [arXiv:1008.2148 \[hep-th\]](#).
- [250] B. Ananthanarayan, S. Banik, S. Friot, and T. Pathak, “On the Method of Brackets,” *Phys. Rev. D* **108** (2023) no. 8, 085001, [arXiv:2112.09679 \[hep-th\]](#).
- [251] C. Meyer, “Algorithmic transformation of multi-loop master integrals to a canonical basis with CANONICA,” *Comput. Phys. Commun.* **222** (2018) 295–312, [arXiv:1705.06252 \[hep-ph\]](#).
- [252] C. Dlapa, J. Henn, and K. Yan, “Deriving canonical differential equations for Feynman integrals from a single uniform weight integral,” *JHEP* **05** (2020) 025, [arXiv:2002.02340 \[hep-ph\]](#).
- [253] H. Frellesvig, “On epsilon factorized differential equations for elliptic Feynman integrals,” *JHEP* **03** (2022) 079, [arXiv:2110.07968 \[hep-th\]](#).
- [254] C. Dlapa, J. M. Henn, and F. J. Wagner, “An algorithmic approach to finding canonical differential equations for elliptic Feynman integrals,” *JHEP* **08** (2023) 120, [arXiv:2211.16357 \[hep-ph\]](#).
- [255] Maplesoft, a division of Waterloo Maple Inc., “Maple.” <https://hadoop.apache.org>.
- [256] N. Arkani-Hamed, S. He, T. Lam, and H. Thomas, “Binary geometries, generalized particles and strings, and cluster algebras,” *Phys. Rev. D* **107** (2023) no. 6, 066015, [arXiv:1912.11764 \[hep-th\]](#).
- [257] L. F. Alday, E. I. Buchbinder, and A. A. Tseytlin, “Correlation function of null polygonal Wilson loops with local operators,” *JHEP* **09** (2011) 034, [arXiv:1107.5702 \[hep-th\]](#).
- [258] O. T. Engelund and R. Roiban, “On correlation functions of Wilson loops, local and non-local operators,” *JHEP* **05** (2012) 158, [arXiv:1110.0758 \[hep-th\]](#).
- [259] O. T. Engelund and R. Roiban, “Correlation functions of local composite operators from generalized unitarity,” *JHEP* **03** (2013) 172, [arXiv:1209.0227 \[hep-th\]](#).
- [260] L. F. Alday, P. Heslop, and J. Sikorowski, “Perturbative correlation functions of null Wilson loops and local operators,” *JHEP* **03** (2013) 074, [arXiv:1207.4316 \[hep-th\]](#).
- [261] N. Arkani-Hamed, J. Henn, and J. Trnka, “Nonperturbative negative geometries: amplitudes at strong coupling and the amplituhedron,” *JHEP* **03** (2022) 108, [arXiv:2112.06956 \[hep-th\]](#).





# Acknowledgments

Firstly, I would like to express my gratitude to my supervisors Paolo Benincasa and Johannes Henn. Coming out of the masters and with the vast landscape of interesting topics in theoretical physics, it was hard to grasp the best path that would lead me to a happy career in physics. They introduced me to the research in scattering amplitudes, cosmology and its connection with new mathematical ideas in physics, such as positive geometries. To Paolo I am thankful for giving me the freedom to tackle the problems we encountered in my first projects, the encouragement to think for myself, to discuss physics as a peer, and ultimately to become an independent researcher. I will always cherish our 8 AM blackboard discussions in the old MPP building. To Johannes I am thankful for providing me with every opportunity I could ask for to further develop myself as a physicist and researcher. For introducing and teaching me several ideas in the study of Feynman integrals, namely the topic of differential equations, which ultimately led me to develop my first more independent project with another student.

Then I would like to thank Nima Arkani-Hamed for our collaboration, and for his support in the later stages of my Ph.D. His unwavering enthusiasm for physics at all hours is inspiring, and the couple of weeks in Princeton leading up to the Cosmohedron were among the most memorable experiences of the past three years. For this I am also thankful to Carolina Figueiredo. But mainly for being a great friend and collaborator, who introduced me to these ideas that became the focus of much of my work during the final year of my Ph.D. Then I would like to thank Giacomo Brunello with whom I developed my first more independent work. I would also like to thank Daniel Baumann for hosting me in Taiwan for a month visiting his group, for his support, and whose several fantastic lecture notes in cosmology provided me a great introduction to this topic. Finally, I would like to thank Giulio Salvatori for many interesting discussions while sharing an office for most of my Ph.D.

I am also thankful for the several friends I met these three years, namely Julian Miczajka, Antonela Matijašić, Wojciech Flieger, Martin Lagares, Anders Schreiber, Prashanth Raman, Shun-Qing Zhang, Ana Fernandes Alexandre, Jungwon Lim, Elia Mazzucchelli, Luc Schnell, William Torres Bobadilla, Darren Scott, Sara Ditsch, Subramanya Hegde, Facundo Rost, Aaron Hillman, Kamran Salehi Vaziri, Nick Early, Francesco Calisto, Jonathan Gräfe, Maximillian Haensch, Dimitri Corradini, Paola Cappellazzi and Matteo Bevilacqua.

Then, I am very grateful for my friends Sérgio Carrôlo, Matilde Fonseca, Diogo Ribeiro and Pablo Morales who made my life in Munich far more enjoyable.

I am grateful to my wife Francisca for her love, and unconditional support as I pursue a career in physics. Her encouragement has been invaluable, not only during my move to Munich for my Ph.D, but also as we look forward to the future stages of our life together.

Finally, to my parents Aida and Rui, and my brother João, I am eternally grateful for all of their love and support, and for always providing me with best possible environment for me to achieve my goals.

Then I would like to express my gratitude to the Max Planck Institute for Physics where I did my Ph.D. And also to the European Union which funded the projects *Novel structures in scattering amplitudes* (grant agreement No 725110), and UNIVERSE+ (ERC, UNIVERSE PLUS, 101118787) .